

Design Synthesis Exercise - Final Report

Swarm of Hybrid MAVs

Faculty of Aerospace Engineering

25 - 06 -2013

Tutor:
Bart REMES

Coaches:
Chris VERHOEVEN
Linfeng CHEN

Authors:
Jakko DEKEN
Yvonne FERRIER
Malte FUCHS
Nimrod GOLDBERG
Andreas MAKUS
Maarten NIESSINK
Anne PRONKER
Elisabeth VAN DER SMAN
Robbin SUIKER

Morpheus

Preface

This is the final report of the Design Synthesis Exercise (DSE), which concludes the bachelor curriculum in Aerospace Engineering at Delft University of Technology. The group was assigned to design a swarm of hybrid micro air vehicles to compete in the IMAV 2013 outdoors competition. The swarm should be able to perform several mission elements and cooperate within the swarm.

The group would like to give special thanks to ir. Bart Remes, dr. ir. Chris Verhoeven and ir. Linfeng Chen for their guidance and advise during the project, Erik van der Horst for his knowledge and experience in MAV production and Paparazzi programming and ir. Hann Woei Ho for his knowledge in QR-Code recognition. Furthermore, the group would like to thank Dirk Dokter for his knowledge in Paparazzi and image processing, Freek van Tienen for his help in MAV production and Paparazzi programming, MSc Shuanghou Deng for his knowledge in CFD modelling and Ewoud Smeur for his knowledge in transition mechanisms.

Versioning

Version	Date	Done by	Description
0.01	10 - 06/ 24 - 06 - 2013	All	Generate Report
0.02	18 - 06/ 24 - 06 - 2013	Andreas	Quality Check
0.03	20 - 06/ 24 - 06 - 2013	Maarten	L ^A T _E X Structuring
1.00	25 - 06 - 2013	All	Final Report

Contents

Preface	ii
List of Figures	vii
List of Tables	ix
Nomenclature	ix
List of Symbols	x
Summary	xiv
1 Introduction	1
2 Mission	2
2.1 Competition Description	2
2.1.1 Automatic Take-Off	3
2.1.2 Drop Zones	3
2.1.3 Flight Performance	3
2.1.4 Target Detection and Recognition	3
2.1.5 Urban Corridor	3
2.1.6 Precision Landing	4
2.2 Competition Strategy	4
2.2.1 Endurance and Range	4
2.2.2 Swarm Technology	4
2.2.3 Autonomous Take-off and Landing	4
2.2.4 Strategy	4
2.3 Functional Breakdown Structure	5
2.4 Functional Flow Diagram	5
2.4.1 Pre-Operational Inspection (1.0)	5
2.4.2 Take-Off (2.0)	5
2.4.3 Fly Mission (3.0)	5
2.4.4 Land (4.0)	6
2.4.5 Maintenance (5.0)	6
2.4.6 End of Life (6.0)	6
2.5 Equipment of MAV Groups	6
2.6 Design Speed	7
2.7 Requirements	7
3 Conceptual Design	9
3.1 Conceptual Concepts	9
3.1.1 Concept 1	9
3.1.2 Concept 2	9
3.1.3 Concept 3	9
3.2 Trade-Off	10
3.2.1 Aerodynamics	10
3.2.2 Stability and Control	10
3.2.3 Structure and Materials	11
3.2.4 Propulsion and Power	11
3.2.5 Operations	11

3.2.6	System Integration	12
3.3	Concept Selection	12
4	Detailed Design	13
4.1	Aerodynamics	13
4.1.1	Airfoil Selection	13
4.1.2	Wing Design	14
4.1.3	Wing Characteristics	19
4.1.4	Verification and Validation	20
4.2	Control and Stability	21
4.2.1	Equations of Motion	21
4.2.2	Natural Static Stability	23
4.2.3	Dynamic Stability of the MAV	24
4.2.4	Unity Negative Feedback Loop and Frequency Analysis	26
4.2.5	Feedback Loop Using a PID Controller	29
4.2.6	Conclusion and Further Research	30
4.3	Structures and Materials	30
4.3.1	Load Case	31
4.3.2	Structural Design	34
4.3.3	Structural Analysis	38
4.3.4	Verification	39
4.3.5	Finite Element Analysis	40
4.3.6	Materials	42
4.3.7	Designed Structure	44
4.4	Propulsion	44
4.4.1	Components of the Propulsion System	44
4.4.2	Constraints	46
4.4.3	Design Approach	46
4.4.4	Subsystem Selection	47
4.4.5	Verification and Validation	48
4.5	Power Supply	49
4.5.1	Type of Battery	49
4.5.2	Sizing the Battery	49
4.5.3	Verification and Validation	50
4.6	Guidance and Navigation	50
4.6.1	Autopilot	50
4.6.2	GPS	50
4.6.3	Verification and Validation	51
4.7	Communication	51
4.7.1	Requirements	51
4.7.2	General Overview of the System	53
4.7.3	Data link	54
4.7.4	Safety Link	56
4.7.5	Video Link	57
4.7.6	Link Budget	59
4.8	QR-Code	60
4.8.1	Localization of Drop Zones	62
4.8.2	Further Approach, Verification & Validation	64
4.9	Ball Dropping System	64
4.9.1	Working Principle	64
4.9.2	Complexity and Solution	65
4.9.3	Solution by Using Micro-Controller	65
4.9.4	Testing the Circuit	66
4.9.5	The Complete Design and Components	66
4.9.6	Releasing the Ball	67
4.10	Ground Station	68
4.11	Design Integration	68
4.11.1	Hardware Configuration	68
4.11.2	Electrical Layout	70
4.11.3	Data Handling	71
4.12	Manufacturing & Assembly	72

4.12.1	Manufacturing	72
4.12.2	Assembly	72
4.13	Sensitivity Analysis	73
4.13.1	Size	73
4.13.2	Mass	73
4.13.3	Flight Speed	74
4.13.4	Autonomy Level	74
4.13.5	Vertical Take-off and Hovering	74
4.13.6	Efficient Horizontal Flight	74
4.13.7	Sensitivity of Major Parameters	74
4.14	Performance Analysis	75
4.14.1	Endurance	75
4.14.2	Range	76
4.14.3	Turning Performance	76
4.14.4	Climb Performance	77
4.14.5	Flight Speed	78
4.15	Resource Allocation and Budget Breakdown	78
5	Paparazzi	80
5.1	Software Architecture	80
5.1.1	Airframe	80
5.1.2	Flight Plan	80
5.1.3	NPS Simulator	80
5.1.4	Modules	81
5.1.5	Ground Control Station	81
5.1.6	Communication Flow Diagram	81
5.2	Transition	81
5.2.1	Control	82
5.2.2	Empirical Model	83
5.2.3	Tuning Gains	83
5.2.4	Implementation for Autonomous Flight	84
5.2.5	Conclusion	84
5.3	Swarming	84
5.3.1	Swarm Communication	84
5.3.2	Flight Plan	85
5.3.3	Collision Avoidance	86
5.3.4	Verification and Validation	86
5.4	QR-Code Detection	86
5.4.1	Communication Protocol	87
5.4.2	Paparazzi Codes	88
5.5	Drop Ball Module	90
6	Verification and Validation	91
6.1	Verification	91
6.2	Validation	92
6.3	Compliance Matrix	92
7	Operations	94
7.1	Pre-Mission	94
7.2	Mission	94
7.2.1	Vertical Take-Off and Hover	94
7.2.2	Transition	95
7.2.3	Horizontal Flight	95
7.2.4	Mission Elements	95
7.2.5	Presentation	96
7.2.6	Landing	96
7.3	Post Mission	97

8 Risk Assessment	98
8.1 Risk Analysis	98
8.2 Reliability, Availability, Maintainability and Safety	99
8.2.1 Reliability	99
8.2.2 Availability	100
8.2.3 Maintenance	100
8.2.4 Safety	100
9 Sustainability Analysis	101
9.1 MAV Design	101
9.1.1 Benefits of Design	101
9.1.2 Life Cycle	101
9.2 Swarming	102
10 Market Analysis	103
10.1 MAV Properties	103
10.2 Market Segment	103
10.2.1 Security and Military Applications	104
10.2.2 Civilian Applications	104
10.2.3 New Market Segments and Forecast in Europe	104
11 Post DSE	106
11.1 Project Design and Development Logic	106
11.2 Gantt Chart	106
11.3 Cost Breakdown Structure	106
12 Conclusion and Recommendations	107
12.1 Conclusion	107
12.2 Recommendations	108
Bibliography	109
Appendix	113
A Competition Analysis	113
B Functional Breakdown Structure	115
C Functional Flow Diagram	116
D Drive Calculator	120
E Telemetry	120
F Technical Drawing Structure	121
G Flight Plans	122
H Drop Ball Module	126
I QR-Code Module	129
J Post DSE Functional Flow Diagram	131
K Gantt Chart	132
L Cost Breakdown Structure	134

List of Figures

2.1	MAV Mission Overview [1]	2
2.2	Front view of the Urban Corridor's entrance [1]	3
3.1	CATIA Renderings of the Preliminary Concepts	10
4.1	Airfoil nomenclature [5]	13
4.2	Airfoil Characteristics	14
4.3	Impact of propeller slipstream on C_L and C_D as a function of wingspan position [8]	15
4.4	Elliptical Wing Analysis	16
4.5	Lift distribution per unit span [9]	16
4.6	Top view of the wing planform	17
4.7	Schematic of different velocity components acting on the wing.	18
4.8	Schematic of the morphed wing showing the tilted ribs at the wing tips	18
4.9	Boundary layer flow interaction	19
4.10	Generated mesh for the analysis in FLUENT, the control volume on the left and the wing on the right	19
4.11	Lift curve and drag polar of the wing	20
4.12	3D results from CFD analysis at 6 degrees angle of attack	20
4.13	Comparison of lift and drag curves from different programs	21
4.14	Control of the MAV	22
4.15	Static natural behavior of the MAV	24
4.16	Symmetric responds for step pitch input	25
4.17	The effect of C_{m_α} on the dynamic behavior	25
4.18	Asymmetric response for initial bank angle	26
4.19	Control Methods	26
4.20	Root Locus for Pitch Control	27
4.21	Frequency Response for Unity Feedback Control	28
4.22	Response for a Unit Step	28
4.23	PID controller in a negative feedback loop	29
4.24	PID controller diagram for pitch	29
4.25	PID controller diagram for roll	29
4.26	Response for a Step Input Using a PID Controller	30
4.27	Reference Frame	31
4.28	Free Body Diagrams	32
4.29	Internal Shear, Moment and Torque Distribution	34
4.30	Stresses on the Beam [Pa]	36
4.31	Wing Body	36
4.32	Wing Tip Reinforcement	37
4.33	Deflection of the Wing and the Twist of the Beam	39
4.34	Mesh	40
4.35	Finite Element Analysis, Loads, Midsection	41
4.36	Finite Element Analysis, Equivalent (von-Mises) Stress, Midsection	41
4.37	Attachment of the Landing Sticks to the Body	43
4.38	Working of a propeller	45
4.39	Difference between the brush and brushless motor [34]	45
4.40	Load Diagrams, the Green Points Represent the Design Points	48
4.41	General overview of the communication subsystem	54
4.42	ZigBee	54
4.43	DigiMesh Node Types [49]	55
4.44	XBee865/868LP [50]	55

4.45	Turnigy 9XR Transmitter Mode 2 , [56]	57
4.46	Orange Rx R110X [57]	57
4.47	Example QR-Code	60
4.48	Functional diagram for ZBar decoder [69]	62
4.49	Camera view of QR-Code	62
4.50	QR Position Determination	63
4.51	Drop Ball System Description	64
4.52	Ball Dropping System Principle	65
4.53	Micro Controller	65
4.54	Reaction Measurements	66
4.55	Drop Ball Circuit Board	66
4.56	Ball drop circuit schematic	67
4.57	Hardware Configuration Top View	69
4.58	Hardware Configuration Bottom View	69
4.59	Structural Integration	70
4.60	Lisa/M Pinout	70
4.61	Electrical Diagram	71
4.62	Overview of the data handling	72
4.63	Exploded View	73
4.64	Endurance ratio versus angle of attack	75
4.65	Turning performance for 50km/h	77
4.66	Climb Speed	78
5.1	Paparazzi Communication Flow Diagram [79]	81
5.2	Transition	82
5.3	Attitude loop for yaw, pitch and roll angle [80]	82
5.4	Attitude loop for yaw, pitch and roll rate [80]	83
5.5	Guidance loop for hovering [80]	83
5.6	Communication Flow Diagram	85
5.7	GCSs	86
5.8	SPI bus	88
5.9	Hardware	88
5.10	Timing Diagram SPI [86]	88
5.11	Connection Caspa VL, Overo FireSTORM and Lisa/M v2.0	89
5.12	Coordinate System Transformation	89
6.1	Prototype	91
6.2	Test setup	92
7.1	Side view of the vehicle in take-off and landing position	95
10.1	UAV Market Increases	104
10.2	UAV Applications	104
10.3	Barriers and challenges to using UAV's as a common vehicle [97]	105
10.4	Forecast for future UAV missions [97]	105
A.1	Overview of the competition and the location of the different mission elements	114
A.2	Functional Breakdown Structure	115
A.3	Legend for Functional Flow Diagram	131
A.4	Project Design and Development Logic	131
A.5	Cost Breakdown Structure	134

List of Tables

2.1	Flight Speed Estimations	7
2.2	List of Requirements	8
3.1	Final Trade-Off	12
4.1	MAV design properties	23
4.2	Dimensionless derivatives for the MAV	23
4.3	Eigenvalues of symmetric and asymmetric state space system	24
4.4	Close Loop Properties	27
4.5	Final results for a PID controller for pitch and roll	30
4.6	Load Locations	32
4.7	Finite Element Analysis Loads	40
4.8	Finite Element Analysis Results	41
4.9	Material Properties SLS Materials (x/y/z)	42
4.10	Summary Material Properties [24], [31], [28]	44
4.11	Constraints for the Propulsion System	46
4.12	Specification of One Motor at Maximum Thrust and Cruise	48
4.13	Capacity required	49
4.14	Specifications of Turnigy 1300mAh 3S 20C Lipo Pack	49
4.15	Lisa/M v2.0 with Aspirin IMU specifications [43]	51
4.16	Analog Camera selection	58
4.17	Video Transmitter and Receiver Specifications	58
4.18	Ground station antenna specifications	59
4.19	Hardware Selected for Image Processing	61
4.20	Selected Camera	61
4.21	Resource Allocation and Budget Breakdown	79
4.22	Mass Contingencies [%]	79
4.23	Power Consumption Contingencies [%]	79
5.1	Trade-Off Communication Protocol	87
6.1	Compliance Matrix	93
8.1	Risk Map: Consequence vs. Likelihood	99
A.1	Point Distribution of the Seperate Mission Elements	113

Nomenclature

<i>Abbreviation:</i>	<i>Explanation:</i>	<i>Abbreviation:</i>	<i>Explanation:</i>
<i>3DP</i>	Three-Dimensional Printing	<i>LiPo</i>	Lithium-ion Polymer
<i>AFA</i>	Automatic Frequency Agility	<i>LOM</i>	Laminated Object Manufacturing
<i>Ap</i>	Autopilot	<i>mAh</i>	Micro Ampère Hour
<i>BEC</i>	Battery Eliminator Circuit	<i>MAV</i>	Micro Air Vehicle
<i>CG</i>	Center of Gravity	<i>MCU</i>	Multipoint Control Unit
<i>CSMACA</i>	Carrier Sense Multiple Access Collision Avoidance	<i>MJM</i>	Multi-jet Modeling
<i>DOT</i>	Design Option Tree	<i>Mol</i>	Moment of Inertia
<i>DSE</i>	Design Synthesis Exercise	<i>MS</i>	Mission Statement
<i>DSSS</i>	Direct Sequence Spread Spectrum	<i>NPS</i>	Advanced Rotorcraft Simulator
<i>ESC</i>	Electronic Speed controller	<i>NS</i>	Need Statement
<i>ETSI</i>	European Telecommunication Standard Institute	<i>PCB</i>	Printed Circuit Board
<i>FBS</i>	Functional Breakdown Structure	<i>PCM</i>	Pulse Code Modulation
<i>FDM</i>	Fused Deposition Modeling	<i>PLT</i>	Paper Lamination Technology
<i>FDM</i>	Flight Dynamic Model	<i>PPM</i>	Pulse Position Modulation
<i>FEA</i>	Finite Element Analysis	<i>PSL</i>	Plastic Sheet Lamination
<i>FFD</i>	Functional Flow Diagram	<i>QPSK</i>	Quadrature Phase-Shift Keying
<i>FHSS</i>	Frequency Hopping Spread Spectrum	<i>RAM</i>	Random-Access Memory
<i>GCS</i>	Ground Control Station	<i>RC</i>	Radio Controlled
<i>GPS</i>	Global Positioning System	<i>RF</i>	Radio Frequency
<i>ID</i>	Identity	<i>RFP</i>	Rapid Freeze Prototyping
<i>IEEE</i>	Institute of Electrical and Electronics Engineers	<i>RP</i>	Rapid Prototyping
<i>IMAV2013</i>	International Micro Air Vehicle Conference and Flight Competition	<i>RPM</i>	Rounds per minute
<i>IMU</i>	Internal Measurement Unit	<i>RPSMA</i>	Reverse Polarity subMiniature version A
<i>JSBSim</i>	Flight Dynamic Model	<i>SCS</i>	Solid Creation System
<i>KV</i>	Rounds per minute per voltage	<i>SLA</i>	Stereolithography Apparatus
<i>LBT</i>	Listen Before Talk	<i>SLS</i>	Selective Laser Sintering
		<i>TCAS</i>	Traffic Collision Avoidance System
		<i>USAR</i>	Urban Search and Rescue Missions
		<i>VRLA</i>	Value Regulated Lead-Acid

List of Symbols

Roman

<i>Symbol:</i>	<i>Explanation:</i>	<i>Unit:</i>
A	Area cross-section	[m ²]
AR	Aspect Ratio	[-]
b	Wingspan	[m]
b_c	Width cross section	[m]
c	Chord Length	[m]
\bar{c}	Mean aerodynamic chord	[-]
C	Capacity	[mAh]
C_d	Drag coefficient (2D)	[-]
C_D	Drag Coefficient (3D)	[-]
C_{D_0}	Zero-Lift Drag Coefficient	[-]
C_l	Lift coefficient (2D)	[-]
$C_{l_{max}}$	Maximum lift coefficient (2D)	[-]
C_{l_p}	Effect of roll on roll stability	[-]
C_{l_r}	Effect of yaw on roll stability	[-]
C_{l_β}	Effect side slip on roll stability	[-]
C_L	Lift coefficient (3D)	[-]
$C_{L_{des}}$	Design Lift Coefficient	[-]
$C_{L_{max}}$	Maximum Lift Coefficient (3D)	[-]
$C_{m_{ac}}$	Aerodynamic Moment Coefficient	[-]
C_{m_α}	Effect of angle of attack on the moment in Y direction	[-]
$C_{m_{\dot{\alpha}}}$	Effect of the change in angle of attack on the moment in Y direction	[-]
C_{m_u}	Effect of velocity on the moment in Y direction	[-]
C_{n_β}	Yaw natural lateral stability	[-]
C_{n_p}	Effect of roll on yaw stability	[-]
C_{n_r}	Effect of yaw on roll stability	[-]
C_{x_α}	Effect of angle of attack on the force in x direction	[-]
C_{x_q}	Effect of angle of pitch in Y direction	[-]
C_{x_u}	Effect of velocity on the force in x direction	[-]
C_{z_α}	Effect of angle of attack on the force in z direction	[-]
$C_{z_{\dot{\alpha}}}$	Effect of the change in angle of attack on the force in z direction	[-]
C_{z_u}	Effect of angle of velocity on the force in z direction	[-]
dy	Distance centroid shape to centroid cross-section	[m]
D	Drag	[N]
D_c	Dimensionless derivative	[-]
D_i	Inner diameter beam	[m]
D_o	Outer diameter beam	[m]
e	Oswald Factor	[-]
E	Young's Modulus	[Pa]
E_{batt}	Energy stored in battery	[Wh]
E_{spec}	Specific Energy	[Wh/kg]
f_{usable}	Depth of discharge ratio	[-]
F	Point force	[N]
g	Gravitational acceleration	[m/s ²]
G	Shear Modulus	[Pa]
I	Moment of Inertia	[m ⁴]

I	Current	[A]
K_t	Torque constant	[Nm/A]
l	Length from center beam to location on beam	[m]
L	Lift	[N]
L	Length of beam	[L]
L	Volume	[m ³]
m	Mass	[kg]
m	Number of point loads	[-]
\dot{m}	Mass flow	[kg/s]
M	Moment load	[Nm]
M_{ac}	Moment around AC	[Nm]
M_{prop}	Reaction moment propeller	[Nm]
n	Load factor	[-]
n	Number of distributed loads	[-]
n_{cel}	Number of cells	[-]
n_{ult}	Maximum loading factor	[-]
p	Roll rate	[rad/s]
P	Point force on tip	[N]
P	Power	[W]
P_{batt}	Battery Power Needed	[W]
P_{thrust}	Power for thrust	[W]
q	Pitch rate	[rad/sec]
q_s	Shear flow	[N/m]
$q_{s,0}$	Shear flow at cut	[N/m]
r	Yaw rate	[rad/s]
R	Resistance	[Ω]
Re	Free stream Reynolds Number	[-]
R_{turn}	Turning radius	[m]
S	Wing Surface	[m ²]
SF_{Thrust}	Safety factor on thrust	[-]
t	Thickness	[m]
T	Thrust	[N]
T	Torque	[Nm]
U	Voltage	[V]
v	Deflection	[m]
V	Velocity	[m/s]
V	Shear Load	[N]
V_e	Exit velocity	[m/s]
V_∞	Free-Stream Velocity	[m/s]
\hat{u}	Dimensionless velocity	[-]
T_p	Thrust for pitch maneuvering	[N]
T_r	Thrust for roll maneuvering	[N]
T_y	Thrust for yaw maneuvering	[N]
w_i	Distributed load	[kg/s ²]
W	Weight	[N]
W	Watt	[J/s]
Wh	Watt-hour	[J]
\bar{W}_{TO}	Take off weight	[N]
x_{ac}	Aerodynamic location	[m]
x_{cg}	Center of gravity location	[m]
x_{F_j}	Distance force to root	[m]
x_1	First limit of the wing section	[m]
x_2	Second limit of wing section	[m]
y_b	Distance of beam to leading edge	[m]
y_{F_j}	Distance of point forces to leading edge	[m]
y_{w_i}	Distance of distributed load to leading edge	[m]

Greek

<i>Symbol:</i>	<i>Explanation:</i>	<i>Unit:</i>
α	Angle of attack	[rad]
β	Side slip angle	[rad]
δ_a	Aileron deflection	[rad]
δ_e	Elevator deflection	[rad]
δ_r	Rudder deflection	[rad]
η_{prop}	Propeller efficiency	[-]
θ	Pitch angle	[rad]
μ_c	Weight factor	[-]
μ_∞	Dynamic Viscosity	[Ns/m ²]
ρ	Air density	[kg/m ³]
ρ_∞	Free-Stream Density	[kg/m ³]
σ	Wind gradient	[rad]
σ_x	Bending Stress	[Pa]
τ_V	Shear stress due to force	[Pa]
τ_T	Shear stress due to torque	[Pa]
ϕ	Twist angle	[deg]
ϕ	Bank angle	[rad]
ω_n	Natural frequency	[Hz]

Summary

The demand for autonomous micro air vehicles (MAV's) is rapidly increasing for commercial, military, research and government purposes. The International Micro Air Vehicle Conference and Flight Competition (IMAV2013) is an event which aims to bring researchers and developers of MAV's together to present their results. A system of multiple MAV's capable of flying in a swarm is designed to win the outdoor flight competition of IMAV 2013.

In order to complete the mission with the highest score possible, a swarm of MAV's is set up and divided into three groups, performing different mission tasks at different times. While group 1 and group 3 have an emphasis on locating and decoding QR-Codes, group 2 will perform mission elements that give a high score, such as dropping balls and flying through a corridor.

When designing the aerodynamics of the wing an analytical model was made and CFD calculations were performed using TORNADO, XFLR5 and FLUENT. The control and stability of the vehicle was modelled numerically in state space format. When designing the structure an analytical model was used and this was verified by a finite element analysis in ANSYS 13. To size the propellers and select the engines a program used Drive Calculator was used. Literature studies were performed to select the communication hardware, autopilot, sensors, battery and cameras. The working of a QR-code search and recognition system was investigated and the working of the circuit to operate the ball drop system was simulated and tested using a micro-controller. The Paparazzi software suite was used to simulate autonomous swarming.

The final design consist of an autonomous swarm of micro air vehicles able to take-off and land vertically and transition to efficient horizontal flight. The designed MAV has a rectangular, morphing wing with two tip propellers. It has a cruise speed of 50 km/h and an endurance of 28 minutes. It is capable of dropping balls at specified targets and of recognizing a QR-code. The structure will be 3D printed, has an elastic skin and is produced and operated in a sustainable way.

Chapter 1

Introduction

The demand for micro air vehicles (MAV's) is rapidly increasing. There is a rising interest in the development and design of highly autonomous small unmanned air vehicles driven by commercial, military, research and governmental purposes. The International Micro Air Vehicle Conference and Flight Competition (IMAV2013) is an event which aims to bring researchers and developers of MAV's together to present their designs.

The objective of this project is to design a system of multiple MAV's capable of flying in a swarm to win the outdoor flight competition of IMAV 2013. Besides performing several mission elements, emphasis is put on two different aspects of the MAV's for this competition, namely the level of autonomy and the size of the MAV's. In order to impress the jury innovative solutions like transitioning between horizontal and vertical flight and a morphing wing structure will be implemented. The selected project group, consisting of nine students of the TU Delft, will put their engineering skills into practice by designing the entire system to conclude their bachelor study program at the Faculty of Aerospace Engineering.

The purpose of this report is to present the final design for the system and to describe the analysis and design activities performed to comply with the requirements. A prototype of the MAV is produced and will be used for testing. After optimization the final design will be assembled, tested and used to participate in the IMAV 2013 competition.

The structure of this report is as follows. First, the mission is analyzed and based on this a strategy to win the IMAV 2013 competition is determined in chapter 2. A functional breakdown structure is used to determine the different functions that the MAV's have to perform and a flow diagram shows the function sequence in time. Based on this the final system requirements are set and a division is made between key and driver requirements.

Chapter 3 gives an overview of the preliminary design phase. Three concepts are analyzed and a trade-off is made to decide on the final design based on technical performance. Trade off criteria are aerodynamics, stability and control, structures and materials, propulsion, power and operations.

For the final design all subsystems are designed in detail and described in chapter 4. The integration of all subsystems and manufacturing techniques are discussed to ensure the product will be able to be produced. Furthermore, the sensitivity of design solutions to changes in major design parameters is discussed in a sensitivity analysis. The performance of the vehicle is analyzed based on endurance, range, turning radius, climb rate and flight speed. The resource allocation and budget breakdown shows the mass, power and cost of each component.

An overview of the used software suite Paparazzi and how it is used to perform this particular mission is given in chapter 5. The software architecture is described and the implementation of transition from horizontal to vertical flight, swarming algorithms, QR-code detection and a ball dropping system is discussed.

Chapter 6 gives an overview of the verification and validation process. The verification method of subsystems and the complete system is explained. Requirements, models and the final product are validated to ensure the product fulfils its purpose.

Chapter 7 discusses the operations of the MAV system before, during and after the mission. The steps necessary to start the mission, the way the mission elements and flight modes are performed and the round up after the mission is described.

However, there is more to designing a system besides hardware and software. A risk analysis is performed and described in chapter 8 to investigate the technical risks the project is exposed to and their consequences on the overall success and ability to fulfil the performance, schedule and cost requirements. A sustainability analysis is performed in chapter 9 to ensure the environmental footprint is minimized. chapter 10 describes a market analysis in order to establish the competitive cost and volume of the market for the product and for the services the product can provide.

Finally, the phase between the final review and the IMAV 2013 competition is analyzed and a schedule is made including the activities still to be performed in chapter 11. A conclusion is drawn in the final chapter on the designed system.

2.1.1 Automatic Take-Off

The automatic take-off mission is indicated with a number one in the competition overview. This is the point at the team zone where the ground station is positioned. Therefore, all MAV's start at this position. For the score it is important to know what the requirements are for the competition. The following requirements were given. The MAV can be hand-launched, and the take-off is considered automatic as long as the safety pilot does not transmit any commands (except the mission start signal).

2.1.2 Drop Zones

This mission is indicated with number two and consists of four drop zones that are scattered around the flight area. The drop zones are indicated in the overview with the black white squares surrounded by an orange line. The goal of this element is to fly towards the coordinates of the drop-zone and drop a ball as close as possible to the QR-code which lies in the center of the drop zone. Points are awarded based on the distance from the center. Since the competition is based on autonomous operation and teamwork an extra element is added to be able to show the performance. This extra element added to this mission means that one of the four coordinates provided at the competition is within 20 meters of the actual coordinates which means that all the coordinates should be checked with a visually before dropping the ball. The requirement for the ball is that it should have a diameter between 15 mm and 20 mm and that it has a flag behind it of 1 cm width and 20 cm length.

2.1.3 Flight Performance

The flight performance mission is indicated with number three and its goal is to show the endurance, top speed and turning performance of the MAV. The red points in the overview indicate two cones around which laps can be flown. There is a starting point indicated in the overview with a rectangular filled with white and black squares. This is the point where the measurements of the amount of laps made per MAV are started. Points will be given when the start sign is crossed again and the MAV has flown around the two cones. The distance between the two poles is 330 meters that gives a total distance of more than 660 meters.

2.1.4 Target Detection and Recognition

The target detection mission consists of a large area with two visual land markers. It is indicated with number four in the overview. The goal of this mission is to find the markers and decode them as autonomously as possible. The flight area is 230 by 120 meters containing two markers: one human readable and one QR-code. To ensure autonomous operation the QR-code should be detected and decoded on board of the vehicle. The visual mark is only for vehicles which cannot decode the QR-code.

2.1.5 Urban Corridor

The urban corridor is 100 meters long and has a maximum width of 6 meters. It is indicated with number five in the overview. The goal is to enter the area between two conical shaped poles, fly through the end of the corridor while staying between the 6 meters width and finally to leave the area again between the two identical poles at the end. The poles have a conical shape which means that the width of the corridor is larger at higher altitude. In Figure 2.2 the front view the cones are shown with the dimensions. More points are awarded if the MAV flies at low altitude between the cones.

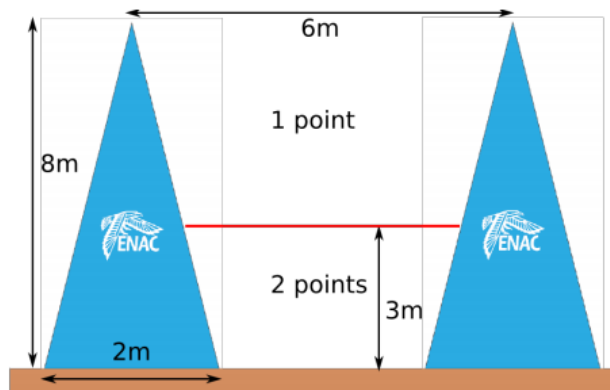


Figure 2.2: Front view of the Urban Corridor's entrance [1]

2.1.6 Precision Landing

All MAV's must land within a time slot, otherwise all mission points since the last take-off will be discarded for the specific MAV. Points are awarded for landing the MAV and the landing is classified in three categories that determine the points awarded. The category with most points is precision landing. The vehicle will have to land on a H-shaped platform and the precision of the landing needed for maximum points depends on the size of the vehicle. The second category is a normal landing that is still on the same platform as the precision landing but with less accuracy. Finally, there is a field landing that can be performed anywhere but it is not rewarded with points. An important part to pay attention to is the ability to take-off again and fly higher than 5 meters to score more points. When the MAV has a rough landing the capability to land should be shown to the jury afterwards. When the vehicle is not capable to land properly no points will be awarded.

2.2 Competition Strategy

There are many different strategies to win the competition and there is a second goal needed for the mission performance. An Excel file is used to compute the competition points that can be awarded and the different factors which influence the final score with different strategies. In section A the detailed point distribution of the competition elements is given. While analysing several strategies a few simple strategies were discovered which resulted in a large amount of points. For example, a train consisting of many MAV's flying circles around the poles deliver a large amount of points while they can be developed very cheap, since the design will be simple. Another example is, when a large amount of MAV's fly through the corridor, land and take-off again. Because of easy and straightforward solutions, the goal to impress the jury with an innovative and creative design is added. This will be accomplished by showing the efficiency of hybrid vehicles (endurance and range), demonstrating state of the art of swarming, autonomous landing/take-off and the ability of the vehicle to perform each element of the competition. In this section first the focus points of the strategy are elaborated individually and in the end the final strategy used will be explained.

2.2.1 Endurance and Range

Since the whole mission needs to be completed in 30 minutes, all the vehicles should be designed to fly for 20 minutes, because the mission time includes setting up the software, some time to make sure they land in time and some time to disassemble everything. If the MAV is able to fly for more than 20 minutes, the design needs to be iterated to increase its endurance, for example by decreasing the battery weight/capacity. The design should score points on the flight performance elements at least once to show the benefits of a hybrid concept (Mission 3).

2.2.2 Swarm Technology

In order to demonstrate the swarming technology of the MAV system, the MAV units need to cooperate while performing the mission. This can best be demonstrated by employing a group of MAV units in the target detection and recognition task (Mission 4). Flying together in an optimal path will decrease the time needed to detect the code, leaving more time to perform other mission elements to increase the competition score. Another good element to show swarming technology is the target area dropping, because one of the four coordinates is not precisely given and it is not efficient to search for them independent of each other. So one vehicle will have to search for the exact locations and communicate these with the others, if this algorithm is written well the time efficiency of the different missions is increased significantly.

2.2.3 Autonomous Take-off and Landing

To present the MAV's ability to perform an entirely autonomous landing, MAV's will be assigned to perform this mission element. When other MAV groups have completed their mission tasks, they will be assigned to perform a landing as well in order to increase the competition score.

2.2.4 Strategy

From the competition analysis it was concluded that the focus should be on the ball dropping mission element, flying through the corridor and autonomous take-off and landing. Performing these mission elements will result in the best score. The flight performance mission will only be executed when time is left or when the QR-codes from the ball dropping mission element is not yet found by other MAV's. The search and recognition of the QR-code will take a lot of time and will not grant a lot of points. Therefore, this mission element is not that important. However, it will be executed by one or two MAV's to increase the number of MAV's in the swarm.

There will be three groups of vehicles participating in the competition, all performing different tasks. While doing this, they will communicate their status and cooperate. This strategy is chosen because swarming capabilities can

be shown with a high level of autonomy. The tasks that each vehicle will perform is stated in the section functional flow diagram, see section 2.4.

2.3 Functional Breakdown Structure

In this section the Functional Breakdown Structure (FBS) will be discussed. The FBS is an AND-tree in which the functions the system has to perform are stated. The functional breakdown structure that will be presented in this section specifies high level functions for the system and shows only the essential functions, and can be viewed in Appendix B. From this structure the functional flow diagram is made in which specific functions are called to which the design should comply. It is therefore a good design tool to construct all the functional requirements of the system.

The most essential functions to perform the mission are listed on the first level of the functional breakdown structure. The system has to provide power which also includes dividing power between subsystems and including a low battery warning. It also has to provide payload capability; this includes a ball dropping system, camera, sensors and a on board processor. Since the vehicle should be able to fly the function 'to perform flight' is an important one. The vehicle must provide lift, stability, control and propulsion. Since it has to be hybrid as stated in the DSE requirements, the vehicle must also be able to perform transition from vertical flight to horizontal flight and vice versa. Different solutions can be found to transition between horizontal and vertical flight. This will be further explained in section 5.2. Other important functions the system or subsystems have to perform are providing guidance & navigation, communication, structural integrity and data handling.

2.4 Functional Flow Diagram

The Functional Flow Diagram (FFD) shows the tasks that are identified in the functional breakdown structure in a logical time-sequenced order. The blocks describe the functions that the system must perform and are connected by arrows. The first level diagram is identical for all the MAV's. The entire life cycle is represented by the first level. Each block can be expanded to a series of functions that are different depending on the flight mission. In many cases even a third level is needed to explain all the functions that the system has to perform. In the following paragraphs the various phases will be described in detail. The functional flow diagram can be found in Appendix C. A detailed description of all functional blocks is given in chapter 7.

2.4.1 Pre-Operational Inspection (1.0)

The first step in the diagram is the pre-operational inspection. This phase consists of a list of system tests that has to be checked before taking part in the competition and before every flight section 7.1. The pre-operational inspection will ensure everything is working as intended.

2.4.2 Take-Off (2.0)

The next phase is the take-off of the MAV. The MAV shall take-off vertically and autonomous. A detailed descriptions can be found in section 7.2.

2.4.3 Fly Mission (3.0)

This phase is different for every mission and will be described separately for the three groups of MAV's. Details on the execution of different functional blocks can be found in section 7.2.

MAV Group 1

The main mission element of MAV Group 1 is to search for a QR-code and scan it. After take-off, the vehicles need to ascend to a height where they can transition to horizontal flight. In horizontal flight the vehicles can achieve a high speed to fly as quickly as possible to the target area. The MAV's can now start searching for the QR-code. To demonstrate the capabilities of a swarm the two MAV's will work together during the search. They will fly horizontally the optimal flight path to minimize the time necessary to find the target. The search consists of making pictures of the ground and looking for signs of a QR-code. If the QR-code is found the MAV will communicate to the rest of the MAV Group 1 that the task has been completed, so the other MAV will immediately stop searching. After the QR-code is decoded the MAV's from Group 1 will estimate the time left for other mission elements. Depending on the time left, the MAV will join MAV Group 2. If time is limited than the MAV will fly to the landing area and perform a precision landing or a normal landing. In that case the mission is ended and block 4 of the functional flow diagram will be performed.

MAV Group 2

Group 2 performs the main tasks to score a lot of points. The number of MAV's in this group is limited by the production cost and time. The MAV will take-off vertical autonomously and will hover directly to the landing spot. At the landing spot the MAV will perform a precision landing within the appointed area and take-off after 10 seconds staying still. After vertical take-off the MAV hovers towards the first arches of the corridor. The MAV will fly through the corridor and once the MAV passes through the second arch the mission element has been completed. The MAV will receive GPS coordinate information about the drop zones from MAV Group 3. If the position coordinates are checked for a drop zone, the MAV will calculate the optimum flight path to the drop zones and start performing the ball dropping mission elements. The MAV will descent to lower altitude and drop the ball. This is not very accurate, because the GPS has an error of a few meters, however the balls will be dropped within 10 meters at least. If the MAV does not get information at all from Group 3 it will start performing the flight endurance test and keeps flying rounds until a certain time where they still have enough time to drop all four balls at the locations given from the competition. In this case one of the balls will not be dropped correctly since one of the drop ball zones is not at the given location. However, a lot of points can still be scored by dropping balls on the other three drop zones. Note that the order of doing the precision landing and the corridor can be changed if there are not enough landing spots (this is not yet clear in the competition regulations).

MAV Group 3

MAV Group 3 will assist MAV Group 2 by checking the exact GPS coordinates of the ball dropping zones. This group will consist of one or two MAV's depending on the total number of MAV's. The coordinates of four drop zones are given, however one of them will deviate by around 20 m. After take-off the MAV will use a camera to find the QR-codes at the given coordinates. The MAV will fly in horizontal position over each drop zone, determine the position and drop the ball. If there is no QR-code at the given GPS coordinates, the MAV will start searching the area of 20m for the QR-code. Once a drop zone is checked the MAV will communicate the coordinates to MAV Group 2 and MAV Group 3. If time allows the MAV will perform a precision landing and fly rounds around the poles. Otherwise the MAV will end the mission.

2.4.4 Land (4.0)

It is a competition requirement that all MAV's should land before the end of the mission time. If time is running out all MAV's will abort their mission and land. Since MAV Group 2 starts with the landing and restart element they will not receive points for this landing and it will not be important to make a precision landing within the landing area. Therefore, they will land in either horizontal flight or vertically on a nearby landing spot.

2.4.5 Maintenance (5.0)

Maintenance is also an important aspect in the life of a MAV system. Scheduled maintenance will be performed after each flight as will be explained in section 8.2. Unscheduled maintenance is performed in case of any damages and after flight maintenance will be performed after each flight as well, for example cleaning the camera and the airframe.

2.4.6 End of Life (6.0)

The life of the system will end one day by for example an unexpected (crash) or by wear and old age. In both cases sustainability is an important aspect. When the MAV is too old to operate, it can be disassembled, sorted and recycled as is shown in the FFD.

2.5 Equipment of MAV Groups

In MAV Group 1 there will be two vehicles that will show swarming capabilities and will detect and read the QR-code as fast as possible. In MAV Group 3 there will be one MAV that locates the ball drop coordinates and communicates these to the others. These two groups need a visual processing unit to detect and read the QR-codes. Since this visual processing will increase costs, the amount of visual processing units should be kept as low as possible. However, using more vehicles will increase the chance to win. Therefore, Group 2 will operate without the use of a camera. To ensure MAV Group 2 will perform as planned MAV Group 3 should be replaced intermediately by an MAV from Group 1 in case of failure.

To conclude there will be three groups of MAV's flying in the mission. MAV Group 1 will consist of 2 vehicles with a camera and processor to see and read QR-codes. They will also be equipped with a ball drop system to have the possibility to score extra points when finished early. MAV Group 2 will consist of many vehicles that only have

the ball drop system with an autopilot which will guide them through all the mission elements. MAV Group 3 will consist of one MAV with a camera and processor to detect the ball drop coordinates. Since this is an important part of the mission they will communicate their status with Group 1. For the three live video streams, three MAV's from Group 2 will be equipped with a camera.

2.6 Design Speed

The flight speed for which the system will be optimized is part of the mission strategy. Since the most important MAV group is Group 2 and because this group will perform most of the mission elements the flight speed will be based on this group. An Excel sheet was made to calculate the total mission time with estimated time per mission elements. The distances between the mission elements were estimated using Google Maps. Since the group will consist of multiple MAV's that will perform the same mission, a time interval of one minute between the MAV's was chosen to create some space between them. All MAV's within the group should be able to finish the mission in time. The time left will be used for the flight performance mission element. The number of MAV's in Group 2 was estimated to be five and the total range between the mission elements was estimated to be 3850 m. The time to complete the mission elements and the time between the MAV's was subtracted from the mission time of 20 minutes. Furthermore, a safety factor was applied to the time left to cover this range to account for collision avoidance. Also it was taken into account that the distance between the elements is a few hundred meters. Since the MAV has to accelerate and decelerate between the elements it is not useful to have a very high design speed since the MAV will probably not have the time to reach it. The number of flight performance laps was estimated to be around three. With this information the average speed between the mission elements was estimated to be 50 km/h and the speed during the flight performance around 60 km/h depending on the time and power left (Table 2.1). This analysis probably overestimated certain time spans, but it ensures that the mission will be completed sufficiently.

Table 2.1: Flight Speed Estimations

Total time [s]	1200	# MAV's	5	Mission Speed [km/h]	50
Time between MAV's [s]	300	Range [m]	3850	Flight performance speed [km/h]	60
Time for mission elements [s]	660	Safety factor	1.1		
Time between mission elements [s]	264				

2.7 Requirements

The list of requirements is shown in Table 2.2 [1][2]. The requirements regard design constraints and functionalities of the system. The requirements are categorized and indicated with labels. Also, a number is assigned to each requirement in the same category. The following labels are used:

- **DesCon:** Design constraints
- **CompCon:** Competition constraints
- **DevCon:** Development constraints
- **FHD:** Flying with a hybrid design
- **AF:** Autonomous flight
- **SI:** Structural integrity
- **SW:** Swarm operation
- **MT:** Perform mission tasks

The last columns in the table indicate whether the requirement is a key or driver requirement. A key requirement is a requirement that is of primary importance to the customer. It can be a killer or driving requirement or known to be a risk item. A driving requirement is a requirement that drives the design more than average and a killer requirement is a requirement that drives the design to an unacceptable extent [3]. Since there are no requirements that drive the design to an unacceptable extent there are no killer requirements for the system.

Table 2.2: List of Requirements

ID	Requirement	Key	Driver
HyMAV-Sys-DesCon-01	The MAV shall weigh 2 kg or less.	✓	
HyMAV-Sys-DesCon-02	The MAV shall have a size of less than 50 cm.	✓	✓
HyMAV-Sys-DesCon-03	The MAV system shall cost less than budget available.		
HyMAV-Sys-DesCon-04	The MAV system shall communicate using one of the authorized frequencies and power.		
HyMAV-Sys-CompCon-01	The MAV shall fly below a height of 50 m.		
HyMAV-Sys-CompCon-02	The MAV shall fly within the boundaries of the competition area.		
HyMAV-Sys-CompCon-03	The MAV shall be able to detect a QR-code.		
HyMAV-Sys-CompCon-04	The entire system shall be able to finish the mission in 30 minutes.		
HyMAV-Sys-CompCon-05	Each MAV shall have a clear distinction from the other MAV's .		
HyMAV-Sys-CompCon-06	Each MAV shall have a flight endurance of at least 20 minutes.		
HyMAV-Sys-CompCon-07	The MAV system shall be completely autonomous.	✓	✓
HyMAV-Sys-CompCon-08	The MAV system shall be able to operate in light rain.		
HyMAV-Sys-CompCon-09	The MAV system shall be able to operate in winds of up to 5 bf.		
HyMAV-Sys-CompCon-10	The MAV system shall be able to operate in gusts of up to 6 bf.		
HyMAV-Sys-CompCon-11	The MAV system shall allow for communication between all units.		
HyMAV-Sys-CompCon-12	The MAV system shall have at least three video streams.		
HyMAV-Sys-DevCon-01	The MAV system shall be developed within the 10 weeks of the DSE project.	✓	✓
HyMAV-Sys-DevCon-02	The MAV system shall not produce any waste.		
HyMAV-Sys-FHD-01	The MAV shall have a vertical take-off capability.	✓	✓
HyMAV-Sys-FHD-02	The MAV shall have an efficient horizontal cruise mode.	✓	✓
HyMAV-Sys-FHD-03	The MAV shall be able to hover.	✓	✓
HyMAV-Sys-FHD-04	The MAV shall be able to transit between hover mode and cruise flight mode.	✓	✓
HyMAV-Sys-FHD-05	Each MAV shall maintain positive control in all stages of flight.		
HyMAV-Sys-FHD-06	The MAV system shall provide power for continuous operation of all electrical components.		
HyMAV-Sys-FHD-07	The MAV shall fly stable.	✓	
HyMAV-Sys-FHD-08	The MAV shall provide lift.		
HyMAV-Sys-FHD-09	The MAV shall be able to provide enough thrust for each flight mode.		
HyMAV-Sys-AF-01	The MAV shall be able to perform a vertical landing.		
HyMAV-Sys-AF-02	The MAV shall be able to report its position.		
HyMAV-Sys-AF-03	The MAV shall have a search and recognition capability.		
HyMAV-Sys-AF-04	The MAV shall have a integral signal processing capability.		
HyMAV-Sys-AF-05	The MAV system shall be capable to make decisions fully autonomously.	✓	✓
HyMAV-Sys-SI-01	The MAV shall provide structural integrity to carry all aerodynamic loads.		
HyMAV-Sys-SI-02	The MAV shall provide structural integrity to survive a fall on a hard surface from 1 m.		
HyMAV-Sys-SI-03	The MAV materials shall allow for MAV production within one day.		
HyMAV-Sys-SW-01	The MAV system shall be able to cooperate to complete a mission.		
HyMAV-Sys-SW-02	The MAV system shall be able to avoid in-flight collisions.		
HyMAV-Sys-SW-03	The MAV system shall provide for a human interface.	✓	
HyMAV-Sys-SW-04	The MAV system shall allow for control of each unit at all times.	✓	

Chapter 3

Conceptual Design

During the conceptual design phase of this project sixty different concepts were analyzed on their performance and a trade-off was made after a preselection by means of a feasibility and weakness analysis. This resulted in three different concepts which were analyzed in detail during the preliminary design phase. The technical performance of these three concepts was discussed and compared in a second trade-off. The result of the second trade-off is a concept which is designed in detail for the IMAV competition and allows for improvements. This chapter describes the preliminary design phase in which the three concepts are analyzed. Trade-off criteria will be discussed and the result of the trade-off will be shown. Details about the trade-off grades and about the conceptual designs can be found in the midterm report [4].

3.1 Conceptual Concepts

In this section the three concepts, resulting from the conceptual design process, are discussed and visualized.

3.1.1 Concept 1

Concept 1 is a low aspect ratio wing with an elliptical front shape and straight rear. This results in a varying chord along the relatively short span. The design is propelled by two contra-rotating propellers attached to the nose. These contra-rotating propellers will prevent rolling of the MAV by counterbalancing their torque. Furthermore two elevons attached to the back of the MAV will stabilize and maneuver the MAV. Transition to horizontal flight is performed by using the elevons to induce a moment, which will rotate the body of the MAV to a horizontal flight state. Figure 3.1a shows the general layout of this design concept.

3.1.2 Concept 2

Concept 2 is a flying wing with a relatively high aspect ratio, compared to Concept 1, to which sweep and taper can be applied if desired. A tail or landing support system can be attached to the wing center, that can also act as vertical stabilizer and rudder for the control and stabilization of the MAV. Two counter-rotating propellers are attached to the wing tips of the MAV. These will reduce wing tip vortices due to the rotating flow they create. The propellers can be tilted to control the attitude of the MAV and to ensure stability. The transition to horizontal flight is done by tilting the propellers to induce a moment which will rotate the MAV body to a horizontal flight state. The general layout is shown in Figure 3.1b.

3.1.3 Concept 3

Concept 3 is a concept where the body does not rotate, but remains horizontal. The wing has a high aspect ratio and has sweep and taper. This concept features two propellers, attached to the nose with two small rods, for propulsion during horizontal flight, and one propeller in the back for vertical take-off and landing. The two propellers in the front are able to rotate in pitch, but the back propeller is fixed horizontally and can be optimized for vertical flight. The combination of the three propellers will create all the possible moments of the MAV and thus provide control and stability. The transition to horizontal flight is done by rotating the two front propellers and shutting down the back propeller. The layout of the horizontal flight mode is shown in Figure 3.1c.

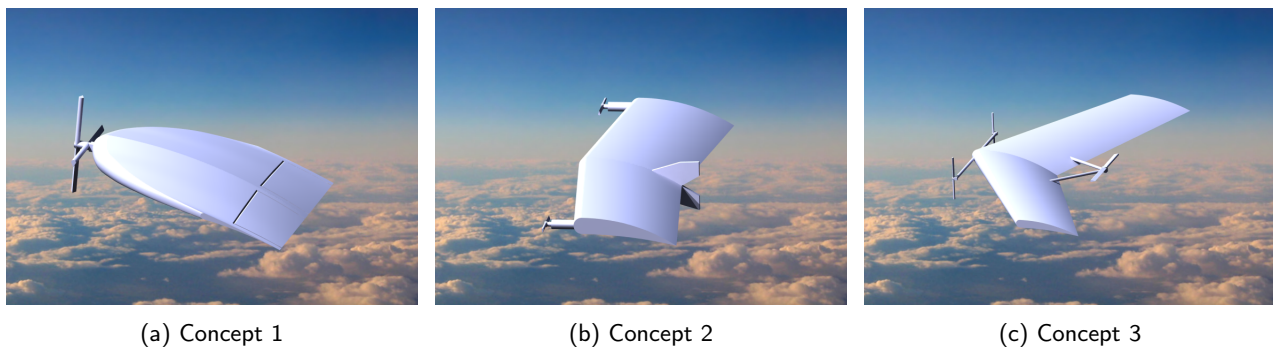


Figure 3.1: CATIA Renderings of the Preliminary Concepts

3.2 Trade-Off

In this section the criteria used to trade-off the preliminary concepts are discussed. The following aspects were investigated for the trade-off: Aerodynamics, Stability & Control, Structure & Materials, Power & Propulsion, Operations and Integration. Grades were given for each criterion according to the performance of the concepts. The grades vary from 1 to 3, where 2 means the concept performs average compared to the others, 1 below average and 3 above average.

3.2.1 Aerodynamics

The aerodynamic performance of the MAV is an important criterion in the selection process since it influences the endurance of the aircraft and the time it will take to finish the mission. To compare the three concepts the Aspect Ratio, Reynolds number and effect of the propellers were analyzed. After analysis the following conclusions were drawn.

Concept 1 has the benefit that the propeller slipstream affects a large section of its lifting surface, generating a considerable amount of extra lift. It does suffer, however, from a relatively low aspect ratio, increasing the induced drag as compared to the other concepts. Two points are awarded to this concept for the Preliminary Design Trade-Off.

Although Concept 3 has a high Aspect Ratio, no significant amount of additional lift is generated since the propeller slipstream affects only a negligible section of the lifting surface. Furthermore its third propeller creates unwanted drag in horizontal flight. For these reasons the concept is also given 2 points for the trade-off.

Concept 2 has a high Aspect Ratio and propellers at the wing tip, which counteract the tip vortices. This concept is the clear winner with respect to aerodynamic efficiency, and is awarded three points for the trade-off.

3.2.2 Stability and Control

Although the MAV's will be controlled by an autopilot and therefore designing a naturally unstable MAV is allowed, the power consumption due to its unstable nature will be higher, as well as the weight. This is mainly because of the actuation of lifting surfaces and propellers at a higher rate and the increased frequency at which the auto-pilot operates.

For those reasons there is a high interest in balancing the MAV's as much as possible in order to increase its flight performance. The following criteria were used for the trade-off between the three concepts:

- **Natural Longitudinal Stability** - This criterion examines the natural behaviour of the MAV's design in the longitudinal direction.
- **Natural Lateral Stability** - This criterion examines the natural behaviour of the MAV during side slip, roll and yaw.
- **Transition** - The MAV has to be hybrid and therefore be able to switch from vertical to horizontal flight and vice versa.
- **Manoeuvrability** - The manoeuvrability of the MAV is an important performance parameter and is directly related to the turning capabilities of the MAV.

Each concept has its own advantages and disadvantages and it is therefore rather hard to state which of the concepts is the best. However, one can notice that Concept 2 has good gliding properties due to high aspect ratio. Control wise, Concept 3 has good and simple transitioning performance. Furthermore, Concepts 2 and 3 have an advantage when considering manoeuvrability due to the rotating propellers. From the analysis it was concluded that the natural

stability of the MAV will increase when a small sweep angle and a vertical stabilizer are applied. If Concept 2 could have a small sweep angle it would have both advantages. For stability and control Concepts 2 and 3 are the desired ones in terms of stability and control while Concept 1 is considered less suitable.

3.2.3 Structure and Materials

This subsection describes the differences in structural integrity of the different concepts. Since no load cases and precise dimensions were available in this project phase the structure will be judged base on the number of critical points, the production complexity and the structural weight.

Weight is a main factor in the design process since it drives most subsystems. The amount and type of critical points is considered the most important next to the weight, since critical points drive the weight and the time to design the structure. Designing critical points in the structure will take a lot of time and is therefore inconvenient regarding the time span of this project. Also the probability of failure increases due to critical points. The production complexity is the least important consideration, since the production process itself is not known yet and it does not influence other subsystems. However it drives the design, time and effort required to build the structure. Finally, the concepts can be ordered, Concept 1 has the best options in terms of structural integrity, then Concept 2 and finally Concept 3.

3.2.4 Propulsion and Power

This subsection describes the trade-off of the three concepts for the propulsion and power subsystem. The criteria of the trade-off are the efficiency of the propellers, the weight of the subsystem as well as the reliability of the concept. The propulsion and power subsystem trade-off contains only the power of the propellers since the other subsystems that use power are similar for all concepts in this preliminary design phase. These systems include the the autopilot, the camera and communication subsystem.

The weight is mainly related to the number of propellers in the concept. Concept 1 has two propellers, two engines and two servos. Concept 2 also has two propellers, both placed in different locations, so there need to be two different engines to control these propellers. To roll and pitch, the propellers need to rotate separately, so there need to be two servos to control these. Concept 3 has three propellers on different locations, so it needs three engines. It also needs an extra servo to rotate the two engines in the front. It is concluded that Concept 2 together with Concept 1 require less weight than Concept 3.

When considering reliability the following conclusions were drawn. Concept 1 does not have tilting engines, only elevators to control pitch and roll. There is a low risk of failure in case one engine fails because the elevators can adapt the rotating moment. However, Concepts 2 and 3 both have tilting engines and if one engine fails their are not elevators to counteract the moment. So Concepts 2 and 3 have a low reliability compared to Concept 1.

The different criteria differ in terms of importance. Efficiency of the propeller is the most important criterion followed by the weight of the propeller system and the reliability. Reliability seems to be an important issue, however, since the mission is conducted in a swarm, the failure of one MAV does not have a huge impact since other units can take over its mission task. Concept 3 is the best design for the propulsion system and Concept 1 scores least.

The power needed is considered as a combination of the weight, the propeller efficiency and the aerodynamic efficiency. In terms of aerodynamic performance Concept 3 is considered less suitable, because of the extra weight caused by the extra motor during cruise and the extra amount of drag due to the larger area at the back. Concept 1 is preferred because of the smaller propeller area and straighter flow over the wing. The second propeller uses the wasted energy of the first one and straightens the flow which reduces drag. However, Concept 2 counteracts tip vortices and creates extra lift at the wing tips which is also beneficial for the power performance. Concluding, Concepts 1 and 2 are best in terms of power and Concept 3 is less suitable.

3.2.5 Operations

In order to compare how well a certain concept operates, supporting possibilities during take-off and landing and maintenance are compared between the three concepts. Swarming is also considered part of operations, however this is programmed in Paparazzi and will not significantly differ between the concepts. Therefore, swarming is not considered for the trade-off between the three concepts.

For operations the take-off and landing possibilities are considered more important than maintenance. This is because maintenance is not a distinguishing factor between the three concepts. Concept 3 has the best landing performance, because it does not need to transition the body. Concept 2 is preferred over Concept 1, because the center of gravity will be closer to the ground during landing, which reduces the chance on tip-over.

3.2.6 System Integration

For design integration important aspects that were considered are the space and positioning possibilities available for payload and subsystems, required cabling and interference between subsystems.

Concept 1 has the lowest aspect ratio of all concepts and offers a lot of space for the required payload. The different components can be placed close together which makes cabling and access for maintenance easy. The only drawback of this concept is the relatively high risk of interference due to the proximity of the different receivers, transmitters and the propulsion system. The design was therefore graded highest among the concepts.

Concept 2 is a higher aspect ratio wing with a smaller chord and smaller maximum airfoil thickness and therefore offers less space for the payload. The small thickness also limits the possible placements of the different components and might cause difficulties in achieving the desired position of the center of gravity. The integration of the tiltable engines introduces further difficulties.

The swept wing and high aspect ratio of Concept 3 leave the least payload space, which is further reduced by the mechanical attachments of the three propellers. The three motors of which two are tiltable increase the complexity of the systems and make the cabling and payload placement more difficult. These reasons make the concept least favourable for system integration.

3.3 Concept Selection

For the selection of the final concept some trade-off criteria were considered more important than others. The criteria with the lowest weight are system integration and operations. The system integration is mainly about fitting the hardware and payload on the body. Since this depends heavily on the aerodynamic design it is not considered an important criterion for this trade-off. For operations only the take-off and landing system is considered and therefore a weight factor of 0.05 was appointed. The most important criteria are aerodynamics and power, because these criteria will influence the performance and efficiency of the vehicle to a large extent and depend heavily on the chosen concept. Control and stability also has a high weight factor, because it determines mainly how well the MAV will perform its mission. From these three aerodynamics was considered slightly more important, because it determines the overall efficiency the most. Structures and materials is considered less important since it does not differentiate that much between the concepts.

The final trade-off including all the weight factors and points for each concept can be found in Table 3.1. The concept with the most points was Concept 2 and the concept with the least points was Concept 1. The difference between the concepts is considered large enough to lead to a final decision. The concept chosen for the detailed design phase is Concept 2.

Table 3.1: Final Trade-Off

Criteria	Weight	Concept 1	Concept 2	Concept 3
Aerodynamics	0.25	2	3	3
Control & Stability	0.20	2	3	3
Structures & Materials	0.15	3	2	1
Operations	0.05	1	2	3
Propulsion	0.10	1	2	3
Power	0.20	3	3	2
System Integration	0.05	3	2	1
Total	1	2.25	2.65	2.4

Chapter 4

Detailed Design

After selecting the final concept, the system can be designed in detail. The following main subsystems in the MAV are distinguished which are designed in detail: aerodynamics, control and stability, structure and materials, propulsion, power supply, guidance and navigation and communication. Some small subsystems are discussed afterwards, these are: QR-code, ball dropping and the ground station.

All these subsystems are designed in parallel and discussed separately and combined in the design integration. After designing the complete system, the building process is elaborated. The sensitivity of design solutions to changes in major design parameters is discussed in a sensitivity analysis and the performance of the vehicle is assessed. Finally, a resource allocation and budget breakdown for the system is made.

4.1 Aerodynamics

This section deals with a detailed analysis of the aerodynamics of the selected MAV design and includes design choices with regard to its airfoil shape and wing planform. Before the wing is designed, the airfoil is selected and its characteristics are described. Next, several parameters and their influence on the wing design are discussed and the design solution is given along with its characteristics. At the end of this section, the results are verified and the necessary steps to validate the results are explained.

4.1.1 Airfoil Selection

The wing profile is a very important factor with regard to the MAV's aerodynamic performance. This is why the selection of the airfoil must be done carefully, analyzing many different shapes each having different parametric values. The parameters that affect the shape of the airfoil, as seen in Figure 4.1, include:

- Airfoil camber
- Maximum thickness
- Thickness position
- Leading edge shape

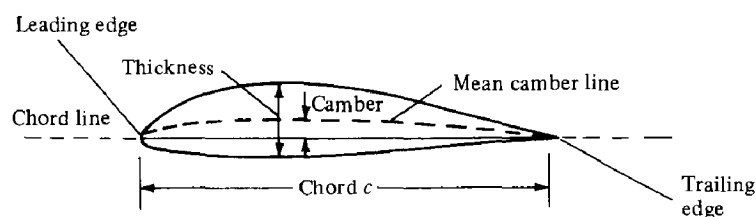


Figure 4.1: Airfoil nomenclature [5]

In order to choose the most appropriate airfoil shape, the influence of these characteristics on aerodynamic performance should be investigated. This is why some selection criteria are established and compared for each airfoil shape that fulfils the requirements. The criteria include:

- Maximum lift coefficient $C_{l_{max}}$
- Maximum endurance ratio $C_l^{3/2}/C_d$

- Aerodynamic moment coefficient $C_{m_{ac}}$
- Stall characteristics

The first selection criterion is the maximum lift coefficient $C_{l_{max}}$ of the airfoil. The $C_{l_{max}}$ is very important for the aerodynamic performance of the MAV since it determines the minimum speed at which the aircraft can operate in horizontal flight. At a lower speed extra thrust is needed to account for loss in lift in the transition regime, which decreases efficiency. A higher $C_{l_{max}}$ is therefore favorable. The design lift coefficient $C_{l_{des}}$ also needs to be taken into account. If this coefficient is close to the $C_{l_{max}}$, the probability of stall during cruise flight increases since even small gusts can increase the angle of attack of the wing beyond its stall limits. Because wing stall has several adverse implications such as loss of lift and increased drag which increases the required power significantly, this situation must be avoided by choosing an airfoil with a large enough margin to the maximum lift coefficient.

The second selection criterion is the maximum $C_l^{3/2}/C_d$ -ratio, which determines the optimum lift-to-drag ratio for maximum endurance flight for electrical vehicles. For the derivation of the endurance ratio see subsection 4.14.1. When optimizing the aerodynamic design for this ratio, this allows the MAV to operate at an airspeed that gives the longest time in the air in order to perform all missions.

Another criterion by which the airfoil is selected is the aerodynamic moment coefficient $C_{m_{ac}}$. Since no elevators are used in the design, the natural stability of the aircraft in longitudinal direction strongly relies on the airfoil shape and CG position. The airfoil can be shaped to have a reflexed trailing edge pointing slightly upward.

This negative camber causes the airflow to induce a low pressure at the bottom side of the aft part, creating a positive moment which is needed for stability of a flying wing.

The stall characteristic of the airfoil is an important point to consider. It describes the way that the airflow separates from the airfoil when the critical stall angle is exceeded. An abrupt stall can cause a sudden drop in lift causing an inefficient recovery, which is particularly undesirable in autonomous flight where the autopilot must correct the unusual flight behavior. This is why it is preferable to select a wing with a relatively smooth stall transition, where flow separation can be countered more effectively.

After comparing several potential airfoil shapes, the *MH-60 Airfoil* is chosen for the MAV design, which can be seen in Figure 4.2a. This airfoil displays a relatively high $C_{l_{max}}$ of 1.16, shown in Figure 4.2b, a high maximum endurance ratio of 57.1, as well as good stall characteristics. The big advantage of the airfoil is its large drag bucket, which allows for efficient operation across a large velocity regime, and its slightly positive $C_{m_{ac}}$ makes it possible to stabilize the vehicle naturally.

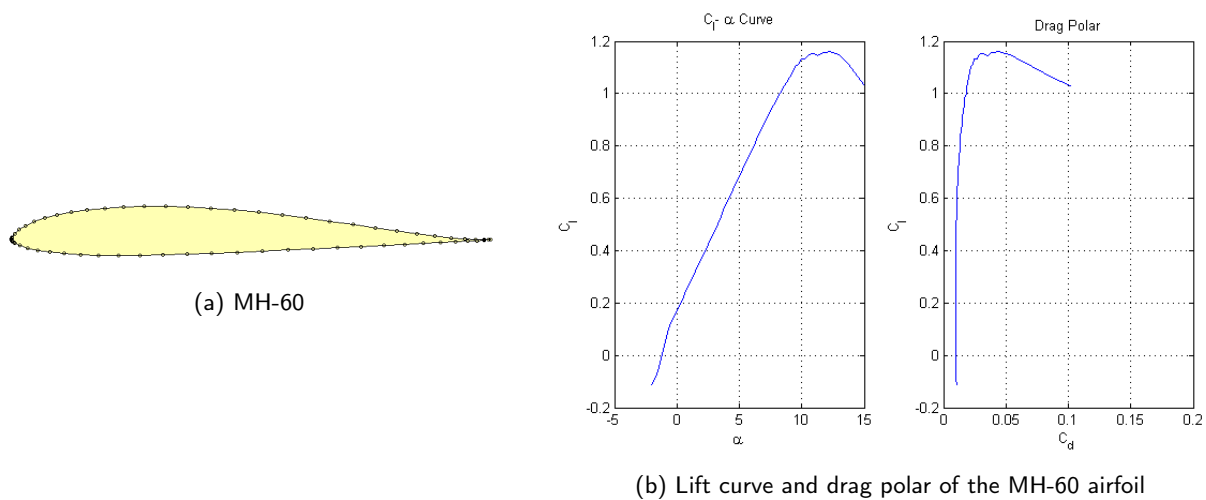


Figure 4.2: Airfoil Characteristics

4.1.2 Wing Design

Now that the airfoil of the wing is selected, the wing design can be elaborated on in more detail. There are several design choices to be made that have great effects on the lift distribution and drag generation, both positive and negative. The design specifications considered in this subsection include:

- Propeller placement
- Wing sweep
- Wing taper and planform
- Wing dihedral
- Attitude control mechanism
- Reynolds number

Propeller Placement

Propeller placement is an important factor for the MAV design. Many implications arise from the propeller placement, some of which will be discussed in this section. From an aerodynamic point of view, an innermost placement of the propellers seems to be desirable because of the effect of the propeller slipstream on lift generation over the wing. The more area is affected by the slipstream the higher the gain in lift, which benefits the MAV's performance. However, the opposite is suggested in the paper by Veldhuis [8]. As the propeller is moved from the wing root towards the tip, the increased aerodynamic effect of propeller swirl increases, having a considerable impact on aircraft performance when placed at the tip. As can be observed in Figure 4.3, the lift coefficient increases and the drag coefficient decreases as the propeller, which is rotating inwards up, is moved towards the tip. This behaviour is attributed to propeller swirl, counteracting the induced tip vortices and hence reducing induced drag and increasing overall performance.

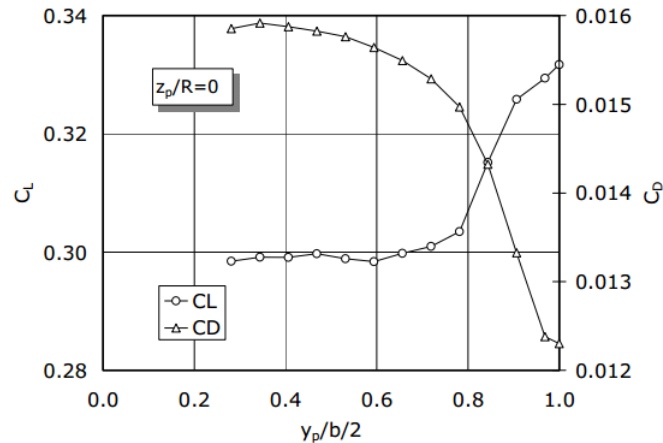


Figure 4.3: Impact of propeller slipstream on C_L and C_D as a function of wingspan position [8]

The placement of the propellers at the wing tips in order to limit the formation of wing tip vortices is a very important consideration, as the paper by Sathaye [9] suggests. Due to the low Reynolds Number at which the low Aspect Ratio wing is operating, non-linear behavior caused by wing tip vortices has a dominant effect on the wing characteristics. Preventing these vortices from developing is therefore of high importance for aerodynamic performance.

Another important aspect of propeller placement is the maneuverability and controllability of the MAV. The further the propeller is placed outwards, the longer its moment arm, and the less energy is needed to perform a roll or yaw maneuver. Because of the positive effect on aerodynamic performance and maneuverability, the propellers are positioned at the wing tips.

Wing Taper and Planform

The taper ratio of a wing is defined as the ratio between the tip chord and the root chord length. Wing taper affects the distribution of lift along the wingspan because it decreases the lift generation along the span as the chord length decreases. This means the wing tips have to carry smaller loads, reducing structural weight.

Taper also influences the aerodynamic performance by decreasing the tip vortices. The less lift is generated at the tip, the smaller is the pressure difference between upper and lower wing surface, which decreases span wise airflow and therefore limits the generation of tip vortices [5]. This in turn decreases induced drag generated by the wing, improving its effectiveness.

With an Oswald Efficiency Factor of almost one, an elliptical planform as shown in Figure 4.4a has the most ideal lift distribution. As can be seen in Equation 4.1, the Oswald Factor is important when calculating induced drag, minimizing it when being close to one.

$$C_D = C_{D_0} + \frac{C_L^2}{\pi A R e} \quad (4.1)$$

Conventional aircraft have an Oswald Efficiency Factor of around 0.8 [10]. However, elliptical wings are difficult to produce with conventional production techniques and are therefore not often designed. Since these production restrictions do not apply to MAV design, because of limited size and because production methods like rapid prototyping are applicable, an elliptical wing planform is a promising option.

However, it has to be taken into consideration that the wing has a low Aspect Ratio and operates at low Reynolds Numbers, which exposes it to non-linear effects from tip vortices. The paper by Sathaye shows a slight advantage of an elliptical shaped wing planform in aerodynamic performance when flown at low Reynolds Numbers and low

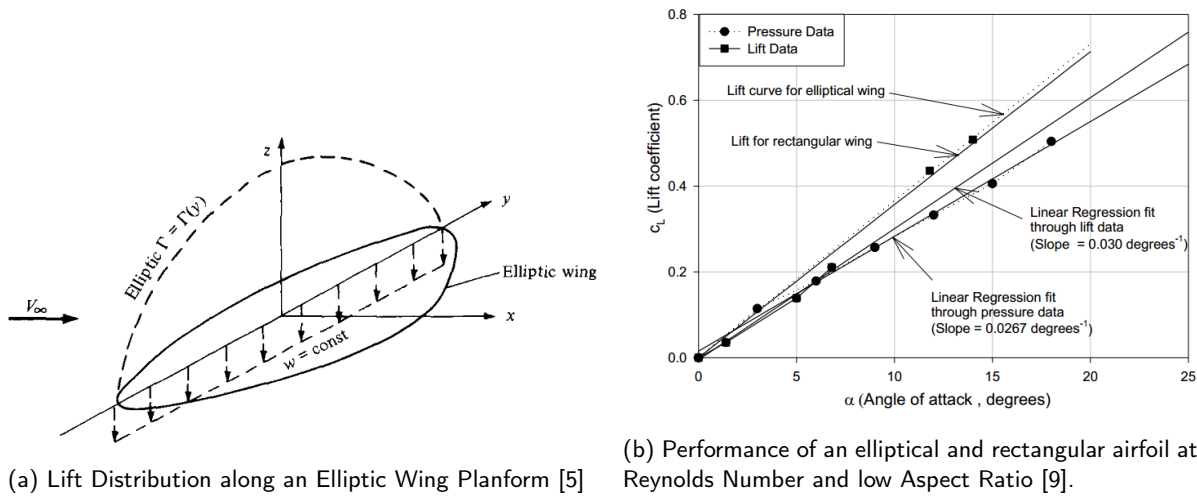


Figure 4.4: Elliptical Wing Analysis

Aspect Ratios as seen in Figure 4.4b [9], however it is assumed that the wing is exposed to free-stream airflow. This MAV design includes wing tip propellers that accelerate the incoming airflow. This accelerated airflow can provide a considerable increase in lift if a rectangular wing shape is used, since it has an increased area inside the slipstreams as compared to an elliptical wing.

Assuming that the propeller does not add any considerable drag, the accelerated velocity of the slipstream is calculated to be $V_e = 14.6$ m/s using Equation 4.2.

$$D = T = \dot{m} (V_e - V_\infty) \tag{4.2}$$

This increases the lift generation with 10% over the area within the slipstream. If propeller drag is also considered, this gain will increase even more.

Another interesting phenomenon observed by Sathaye at low Reynolds numbers and for low Aspect Ratio aircraft describes a positive influence of the tip vortices on the generation of lift [9]. Although the tip-mounted propellers will limit the induction of tip vortices, they can not completely erase them. Depending on the angle of attack, these vortices can energize the airflow in the vicinity of the wing tips and increase the local lift coefficient as seen in Figure 4.5.

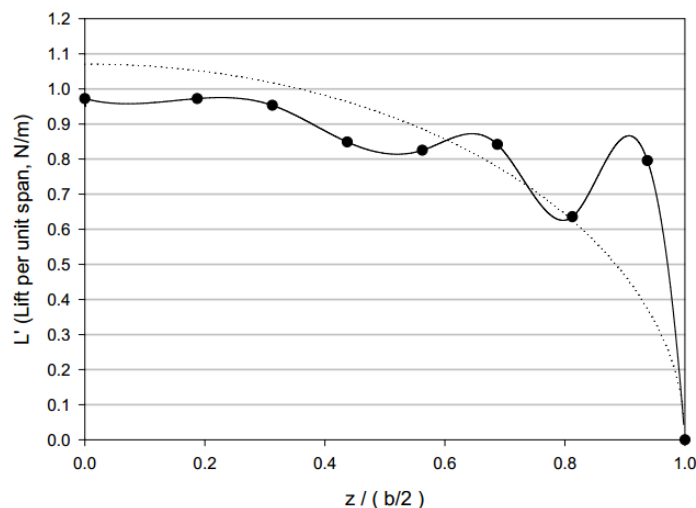


Figure 4.5: Lift distribution per unit span [9]

This effect can be used to generate extra lift by employing a rectangular wing, since the lifting surface affected by the vortices is larger than for an elliptically shaped planform. Moreover, this effect can be advantageous with respect to the stability of the MAV as described in a paper by Torres et al [11]. It is said that, as the vortex effect increases lift generation near the wing tip, it particularly affects the aft part of the wing, moving the aerodynamic center backward. This backward movement increases the margin between center of gravity and aerodynamic center, increasing the stability of the MAV.

After analyzing the advantages and disadvantages of both the elliptical and the rectangular wing shape, the rectangular shape is preferred over the elliptical shape and is therefore implemented in the design. The top view of the wing planform can be seen in Figure 4.6.

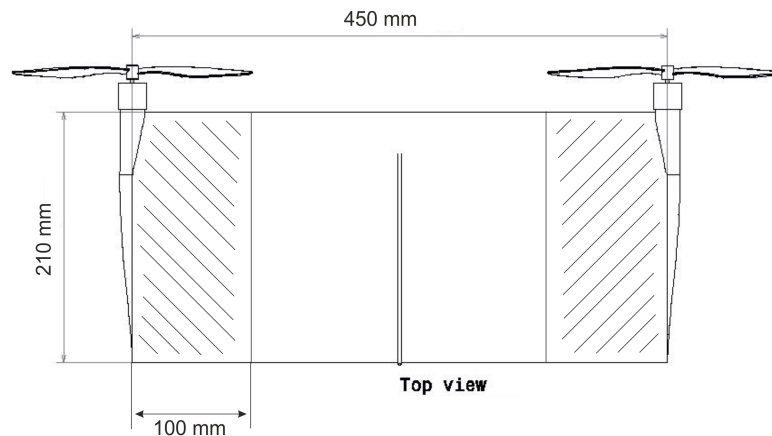


Figure 4.6: Top view of the wing planform

Wing Sweep

The sweep of the wing is the angle between the quarter-chord line along the wing and the line perpendicular to the longitudinal axis of the aircraft. Wing sweep decreases the free stream velocity component that the airfoil "sees" [12], decreasing its lift generation and the lift-to-drag ratio. Wing sweep is usually implemented in high-speed flight in order to increase the critical Mach Number of the wing [12], which is not necessary in for the flight regime that the MAV will operate in.

Wing sweep can also be implemented for stability reasons. Swept wings generally move the aerodynamic center rearwards, increasing the distance to the CG of the aircraft and therefore giving more longitudinal stability [13]. Roll stability is similarly affected by wing sweep, increasing stability with an increase in sweep. This is caused by the fact that the wing which is exposed to a positive side slip angle experiences a larger angle of attack, creating a counteracting moment that will decrease side slip [13].

However, sweep can also work in the opposite direction. Forward sweep for example increases aerodynamic effectiveness of the wing [5], but decreases longitudinal stability by moving the aerodynamic center forward. The forward movement of the aerodynamic center can be limited by using less forward swept wing surface, allowing to mount the engines in a more forward position which benefits both stability and maneuverability.

In order not to compromise on aerodynamic effectiveness of the wing and because the MAV is able to stabilize itself using thrust vectoring, an unswept planform chosen as can be seen in Figure 4.6.

Wing Dihedral

Wing dihedral is defined as the angle between the wing along its span and the aircraft's horizontal plane. It has no aerodynamic benefits and is normally employed for stability purposes. As already indicated, any disturbances will be counteracted by thrust vectoring, which is why dihedral will not be considered in this design.

Attitude Control

The attitude control of the MAV is being done by incidence morphing the outer parts of the wing and therefore changing the pitch of the propellers which are attached to the wing tips. The morphing parts of the wing span the outer 10 cm, the length of a propeller blade as can be seen in Figure 4.6 as the shaded area.

Although it seems to be disadvantageous to rotate an entire wing section in order to change the pitch of a propeller, because a larger mass has to be shifted. However, elevators will not be employed due to their ineffectiveness in pitch and roll, making it difficult to control the aircraft in gusty conditions. The alternative of just deflecting the propellers for maneuvering has its drawbacks as well.

If, for example, the MAV should roll to the left, the propeller must be tilted upwards on the right wing. The increased propeller pitch causes the slipstream over the wing to deflect downwards, reducing the angle of attack on the wing section that is exposed to the slipstream. This decrease in angle of attack causes a decrease in lift over the affected section and has an adverse effect on the roll maneuver, as it induces a roll tendency to the right. This effect can also have a great effect on the endurance of the MAV since the propellers constantly induce a decrease in lift when pitching up, forcing the wing to fly at a higher angle of attack and therefore generate additional drag. If, however, the entire wing section is rotated to increase the pitch of the propeller, this problem can be avoided.

When looking at a pitching maneuver, tilting propellers provide an advantage in terms of controllability. Considering a pitch-up of the vehicle, the propellers have to increase the pitch angle to provide a positive pitch moment. The increase in propeller pitch leads to a decrease of angle of attack over the wing, causing an additional positive moment about the CG.

When wing morphing is employed, this effect has very little influence. Assuming that the morphing proceeds in a linear fashion along the span, the effect of the decreased angle of attack due to the propeller slipstream is offset by an increase in angle of attack by the free-stream airflow over the morphing part, as seen in Figure 4.7. An upwards deflected wing tip causes the propeller to induce a steady decrease in angle of attack towards the wing root, whereas the deflection itself causes an increase in angle of attack towards the tip. Since the slipstream and free-stream velocities are almost equal due to the low amount of required thrust, as can be calculated with they effectively cancel each others moment-inducing effects.

$$T = \dot{m} (V_e - V_\infty) \quad (4.3)$$

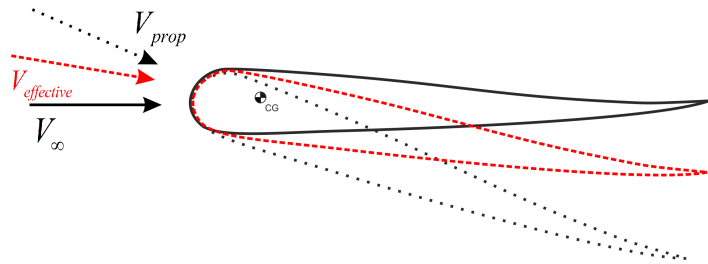


Figure 4.7: Schematic of different velocity components acting on the wing.

To summarize the above, it can be said that a tilting propeller has an advantage in pitch, but a disadvantage in roll and in lift generation due to the decrease in angle of attack caused by the propellers, whereas a morphing wing has neither advantages nor disadvantages in either of these aspects. A morphing wing is highly innovative, and its implementation could lead to new ways of providing control, which is why the morphing wing is chosen for the MAV design.

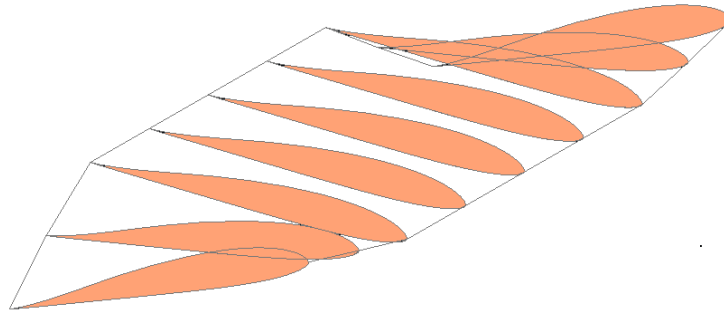


Figure 4.8: Schematic of the morphed wing showing the tilted ribs at the wing tips

Reynolds Number

Another important quantity for airfoil and consequently wing performance is the Reynolds Number. The Reynolds Number is a measure of inertia forces to viscous forces in a flow [5] and can be an indicator for the type of flow within the boundary layer. A low Reynolds Number is associated with laminar flow whereas a high Reynolds Number can indicate turbulent flow. Since it is a function of free-stream velocity and chord length, as seen in equation 4.4.

$$Re = \frac{\rho_\infty V_\infty L}{\mu_\infty} \quad (4.4)$$

Since the MAV will perform its flight at a relatively low Reynolds Number of 194,000 the phenomenon of the separation bubble has to be accounted for. This "bubble" usually develops on the upper surface of an airfoil exposed to a low Reynolds Number airflow and can cause an adverse pressure gradient leading to a reduction in lift and an increase in drag [6]. The separation bubble forms when laminar flow separates from the lifting surface due to an increase in angle of attack and the associated adverse pressure gradient. This separation causes the airflow to become turbulent, adding energy to the airflow and causing the turbulent flow to re-attach to the wing as seen in Figure 4.9a.

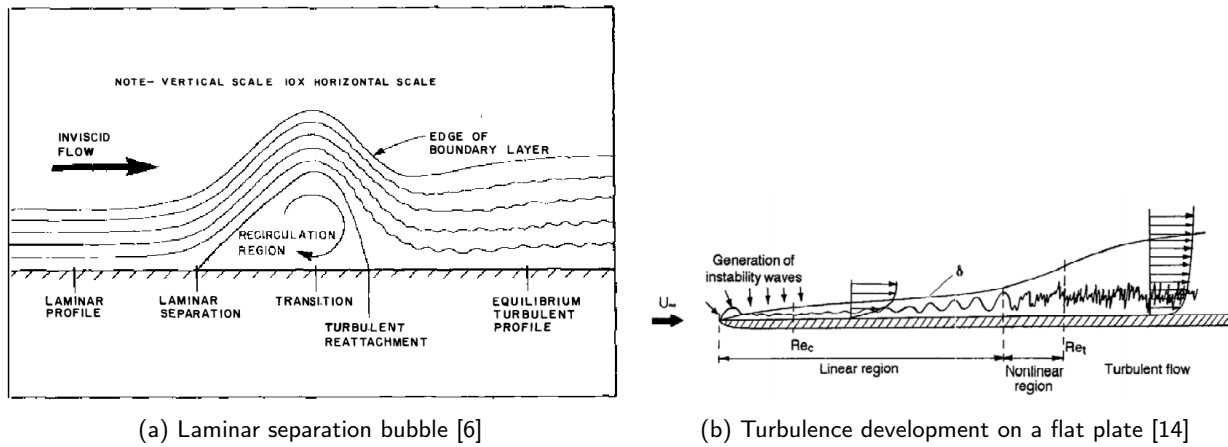


Figure 4.9: Boundary layer flow interaction

An area on the upper surface of the wing will not provide lift, which has a detrimental effect on aircraft performance. As the angle of attack is increased, the laminar separation occurs at an earlier stage, increasing the size of the bubble. In some instances, an increase in angle of attack can cause this bubble to burst [14], leading to large performance decrease and possibly to an abrupt stall. In order for the separated flow to re-attach to the surface, a certain chord length is required. This required length can be expressed by the critical Reynolds Number, which is about 70,000. At numbers below that re-attachment is unlikely to occur, whereas the opposite is true for Reynolds Numbers above this value [6].

There are different techniques to avoid the onset of a laminar separation bubble on the upper surface of the wing. Most of them are based on the principle of disturbing the airflow to increase its tendency to stay attached [14]. This however leads to an increase in drag because of the fact that turbulent airflow in the boundary layer has a higher drag as compared to laminar flow [12].

As the paper of Slangen [14] suggests the so-called zigzag tape is a very efficient way to turbulate the airflow, which is why this type of transition device will be employed in the design. Its working principle can be seen in Figure 4.9b. However, it is very difficult to determine the optimal position for the tape, and wind tunnel tests have to be performed in order to find it.

4.1.3 Wing Characteristics

All the design choices stated above have an impact on the aerodynamic performance of the wing. The Computational Flow Dynamics (CFD) program FLUENT was used to describe the characteristics by determining the lift curve and drag polar. A three-dimensional mesh was created for the computation as seen in Figure 4.10, where a control volume was defined around the half-span of the wing using triangular meshing.

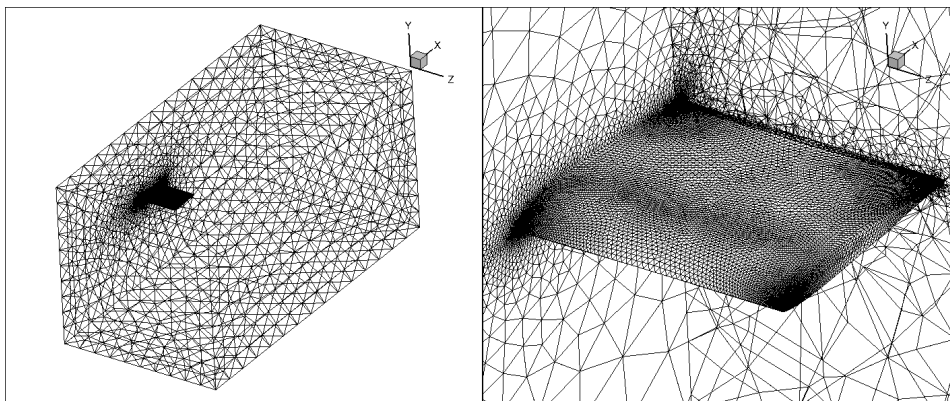


Figure 4.10: Generated mesh for the analysis in FLUENT, the control volume on the left and the wing on the right

The control volume has the size of 1.2x0.5x1 m in order to ensure that the entire airflow affected by the wing is taken into account in the calculations. The wing is fixed to the wall using only its half-span and a symmetric boundary condition is applied to that wall to make calculations more efficient. The wing was modeled without the propellers as this would increase the difficulty of the calculations immensely, and not add a lot of valuable information to the results. Wind tunnel tests will be conducted to measure the propeller effect on aerodynamic performance.

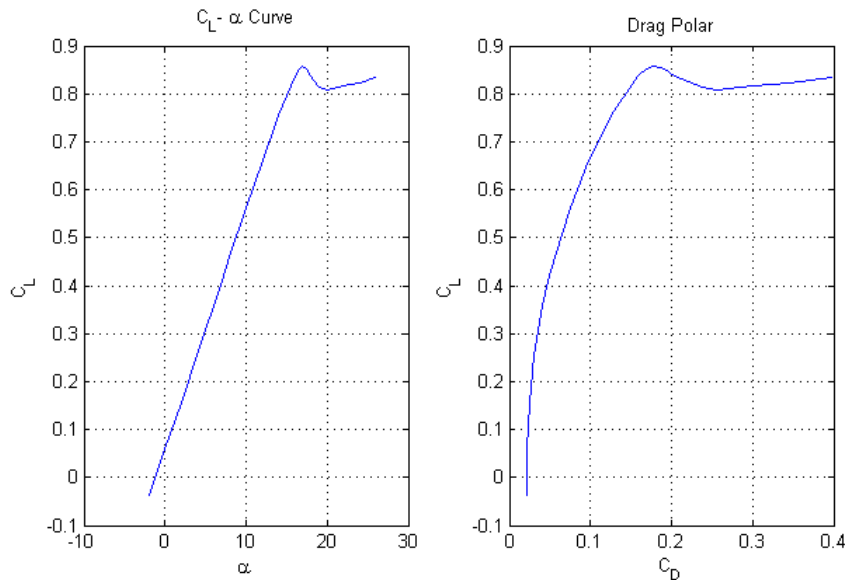


Figure 4.11: Lift curve and drag polar of the wing

Once the mesh has been generated, the lift curve and drag polar were generated, as shown in Figure 4.11. Here, it can be seen that the wing stalls at an angle of attack of approximately 17 degrees, with a $C_{L_{max}}$ of 0.859. This leads to a minimum flight velocity of 8.9 m/s (32 km/h) in horizontal flight. Using the lift equation Equation 4.5, the $C_{L_{des}}$ is determined to be 0.35 at an angle of attack of 6 degrees, leaving enough buffer to the stall regime.

$$L = \frac{1}{2} \rho V^2 C_L S \quad (4.5)$$

It can be observed that a slight kink in the $C_L - \alpha$ -slope occurs at an angle of attack of approximately 7 degrees. This kink indicates the onset of the laminar separation bubble, which leads to a slight performance decrease. In order to prevent it, a zigzag tape will be employed in the design in case the surface roughness is not sufficient enough to avoid it.

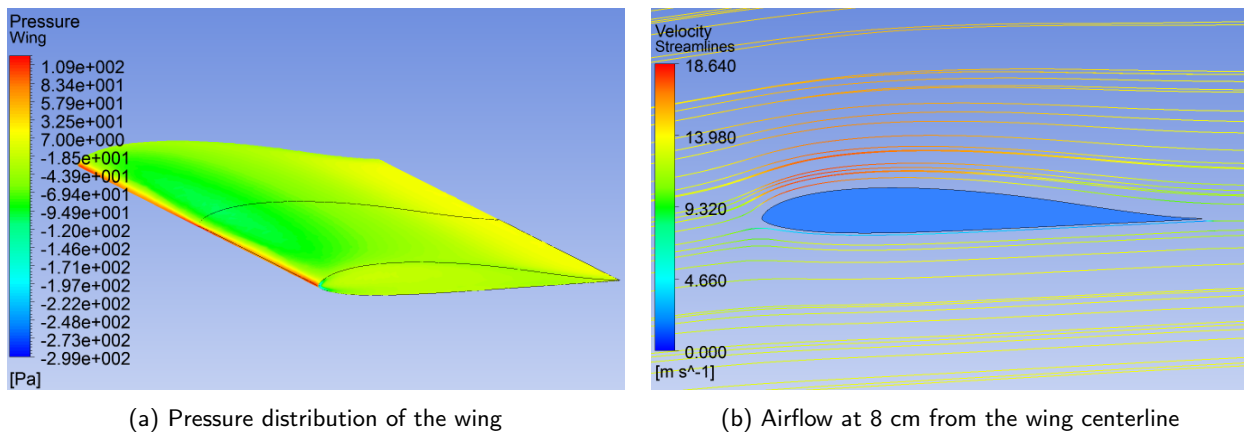


Figure 4.12: 3D results from CFD analysis at 6 degrees angle of attack

Figure 4.12a and Figure 4.12b show the pressure distribution and the airflow around the wing at an angle of attack of six degrees, respectively. The pressure distribution shows a high pressure at the bottom side of the leading edge, with a low pressure peak at within the first third on the top skin where the airflow accelerates to its highest velocity. The effect of the tip vortices due to the low aspect ratio can be seen in the pressure increase near the tips. The pressure increases towards the aft, showing a positive pressure near the trailing edge due to the reflexed airfoil shape. The behavior of the wing is as expected.

4.1.4 Verification and Validation

In order to verify the accuracy of the generated plots, it must be verified using results that were derived analytically. Several programs, such as XFLR5, TORNADO, and FLUENT, have been used to determine the lift and drag of the

wing, and the results can be seen in Figure 4.13.

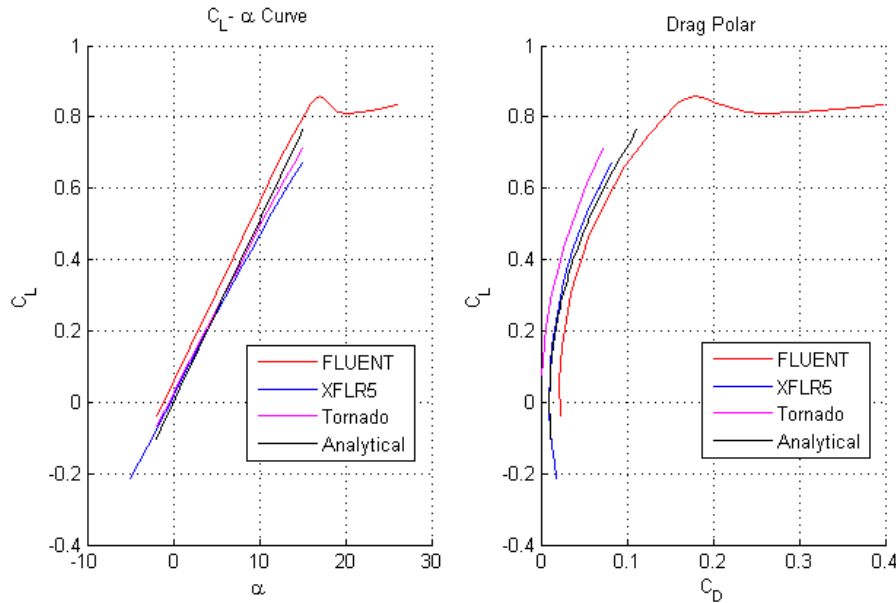


Figure 4.13: Comparison of lift and drag curves from different programs

The plots show the lift curve on the left side and the drag polar on the right. Looking at the lift curve, it is evident that the programs have slightly different results for the linear part, which are especially obvious between FLUENT and TORNADO/XFLR5. This has to do with the fact that both TORNADO and XFLR5 use the Vortex Lattice Method (VLM) for their calculations, which has its limitations with low Reynolds Numbers and Aspect Ratios, and large angles of attack due to the increased influence of viscosity [15][16]. However, when comparing the calculated slopes of the three programs, it can be seen that the difference between them is relatively small. This is also true for the drag polars.

The analytically determined lift slope is very close to the ones determined computationally, which verifies the eligibility of using TORNADO and XFLR5 for slope calculations in the linear regime. FLUENT's results can only be properly verified for the linear part since it is very difficult to estimate the $C_{L_{max}}$ for a wing, but the calculated values are very realistic when compared to similar wing designs.

In order to validate the results for the wing, wind tunnel tests measuring lift and drag forces have to be performed and their results compared. However, since time was limited no wind tunnel tests could be performed within the time set for the project. It is advised that these tests take place before the competition, since they not only will shed light on the validity of the results, but also can be used to optimize the design with regard to propeller efficiency and zigzag tape placement.

4.2 Control and Stability

In this section the complete static and dynamic stability of the MAV will be modeled mathematically using the equation of motion of the MAV. In order to analyze the stability and control behavior of the MAV the model will also be simulated. After analyzing the complete natural stability of the MAV the control method will be described and discussed.

4.2.1 Equations of Motion

In order to model the stability and control of the MAV it is important to first derive the equation of motion of the MAV. The general equation of motion for a conventional airplane is given in [13], where symmetric flight is given by Equation 4.6 and asymmetric flight by Equation 4.7.

$$\begin{bmatrix} C_{X_u} - 2\mu_c D_c & C_{X_\alpha} & C_{Z_0} & C_{X_q} \\ C_{Z_u} & C_{Z_\alpha} + (C_{Z_{\dot{\alpha}}} - 2\mu_c) D_c & -C_{X_0} & C_{Z_q} + 2\mu_c \\ 0 & 0 & -D_c & 1 \\ C_{M_u} & C_{M_\alpha} + C_{M_{\dot{\alpha}}} & 0 & C_{M_q} - 2\mu_c K_Y^2 D_c \end{bmatrix} \cdot \begin{bmatrix} \hat{u} \\ \alpha \\ \theta \\ \frac{q\bar{c}}{V} \end{bmatrix} = \begin{bmatrix} -C_{X_{\delta_e}} \\ -C_{Z_{\delta_e}} \\ 0 \\ -C_{M_{\delta_e}} \end{bmatrix} \cdot \delta_e \quad (4.6)$$

$$\begin{bmatrix} C_{Y_\beta} + (C_{Y_{\dot{\beta}}} - 2\mu_b) D_b & C_L & C_{Y_p} & C_{Y_r} - 4\mu_b \\ 0 & -\frac{1}{2} D_b & 1 & 0 \\ C_{l_\beta} & 0 & C_{l_p} - 4\mu_b K_X^2 D_b & C_{l_r} + 4\mu_b K_{XZ} D_b \\ C_{n_\beta} & 0 & C_{n_p} + 4\mu_b K_{XZ} D_b & C_{n_r} - 4\mu_b K_Z^2 D_b \end{bmatrix} \cdot \begin{bmatrix} \beta \\ \phi \\ \frac{pb}{2V} \\ \frac{rb}{2V} \end{bmatrix} = \begin{bmatrix} -C_{Y_{\delta_a}} \\ 0 \\ -C_{l_{\delta_a}} \\ -C_{n_{\delta_a}} \end{bmatrix} \cdot \delta_a + \begin{bmatrix} -C_{Y_{\delta_r}} \\ 0 \\ -C_{l_{\delta_r}} \\ -C_{n_{\delta_r}} \end{bmatrix} \cdot \delta_r \quad (4.7)$$

However, since the MAV has no elevators, ailerons or rudder, their respective coefficients can be taken out of the equation of motion. The MAV uses wing rotation and thrust increments for controlling the attitude. Figure 4.14a, Figure 4.14b and Figure 4.14c show the control method for pitch, roll, and yaw of the MAV respectively. In order to pitch the aircraft, both rotors will be tilted in the same direction which creates a rotation around the Y-axis. For roll control, the rotors will be tilted in opposite direction, generating a moment couple around the X-axis, and for yaw the thrust of the motors increases or decreases depending on the required yaw rate.

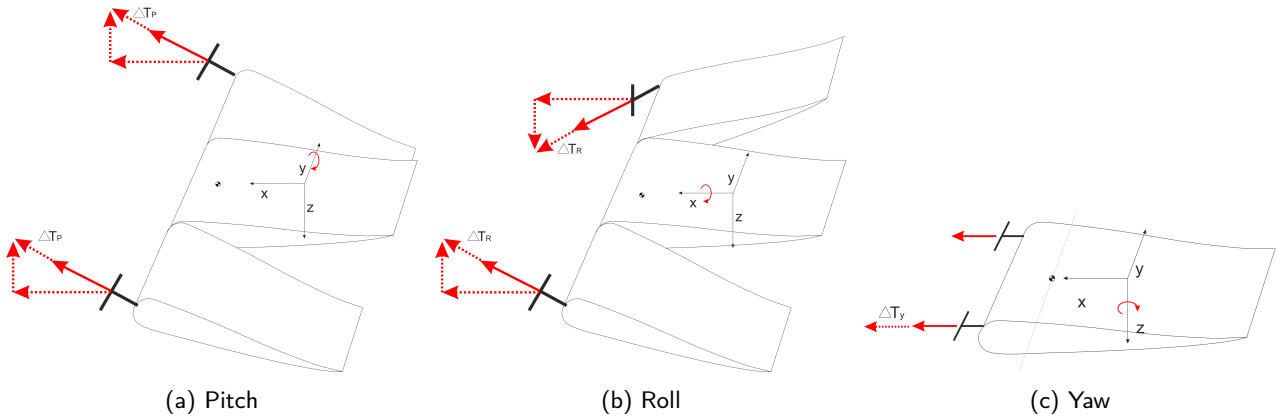


Figure 4.14: Control of the MAV

In order to implement these control methods in the equation of motion the following assumptions need to be made:

- To control the MAV in pitch and roll, the wingtips rotate to a constant angle of 10deg first.
- The thrust will then increase while the angle of attack remains constant.
- Each of the control methods is decoupled from one another.

The reason for making these assumptions is because tilting the wing at the same time as increasing the thrust causes the system to become non-linear. This type of system is difficult to model, and can even be impossible. However, one should keep in mind that in real life a small error in attitude can be adjusted by just increasing or decreasing the wing tip deflection. If the above described control method (first increasing the angle, then the thrust) will not be sufficient to generate the desired result, the MAV design has to be modified. Using the above simplifications and assumptions, the symmetric equation of motion can be calculated as shown in Equation 4.8, where d is the moment arm from the thrust vector to the center of gravity. The asymmetric equation of motion are stated in Equation 4.9.

$$\begin{bmatrix} C_{X_u} - 2\mu_c D_c & C_{X_\alpha} & C_{Z_0} & C_{X_q} \\ C_{Z_u} & C_{Z_\alpha} + (C_{Z_{\dot{\alpha}}} - 2\mu_c) D_c & -C_{X_0} & C_{Z_q} + 2\mu_c \\ 0 & 0 & -D_c & 1 \\ C_{M_u} & C_{M_\alpha} + C_{M_{\dot{\alpha}}} & 0 & C_{M_q} - 2\mu_c K_Y^2 D_c \end{bmatrix} \cdot \begin{bmatrix} \hat{u} \\ \alpha \\ \theta \\ \frac{q\bar{c}}{V} \end{bmatrix} = \begin{bmatrix} -\cos(10^\circ) \\ \frac{1}{2} \rho V^2 S \\ -\sin(10^\circ) \\ \frac{1}{2} \rho V^2 S \\ 0 \\ -\frac{d \sin(10^\circ)}{\frac{1}{2} \rho V^2 S \bar{c}} \end{bmatrix} \cdot \Delta T_p \quad (4.8)$$

$$\begin{bmatrix} C_{Y_\beta} + (C_{Y_\beta} - 2\mu_b)D_b & C_L & C_{Y_p} & C_{Y_r} - 4\mu_b \\ 0 & -\frac{1}{2}D_b & 1 & 0 \\ C_{l_\beta} & 0 & C_{l_p} - 4\mu_b K_X^2 D_b & C_{l_r} + 4\mu_b K_X Z D_b \\ C_{n_\beta} & 0 & C_{n_p} + 4\mu_b K_X Z D_b & C_{n_r} - 4\mu_b K_Z^2 D_b \end{bmatrix} \cdot \begin{bmatrix} \beta \\ \phi \\ \frac{pb}{2V} \\ \frac{rb}{2V} \end{bmatrix} = \begin{bmatrix} 0 \\ 0 \\ -\frac{b \sin(10^\circ)}{\frac{1}{2}\rho V^2 S b} \\ 0 \end{bmatrix} \cdot \Delta T_r + \begin{bmatrix} 0 \\ 0 \\ 0 \\ \frac{b}{\frac{1}{2}\rho V^2 S b} \end{bmatrix} \cdot \Delta T_y \quad (4.9)$$

Using CATIA and some results from section 4.1 the MAV properties were found as shown in Table 4.1 and used in the equations of motion as $\mu_c = \frac{m}{\rho \bar{c} S}$, $\mu_b = \frac{m}{\rho b S}$, $K_x = \frac{I_{xx}}{mb^2}$, $K_y = \frac{I_{yy}}{mc^2}$, $K_z = \frac{I_{zz}}{mb^2}$ and $K_{xz} = \frac{I_{xz}}{mc^2}$.

Table 4.1: MAV design properties

S=0.0945 [m ²]	m=0.4 [kg]	b=0.45 [m]
$I_{xx} = 7.55 \cdot 10^{-4} [kgm^2]$	$I_{yy} = 0.006 [kgm^2]$	$I_{xz} = -8.785 \cdot 10^{-6} [kgm^2]$
$I_{zz} = 0.007 [kgm^2]$	e=0.85[-]	

The coefficients in the equations of motion can be calculated by hand or they can be found using CFD programs. The coefficients and the derivatives for the MAV are calculated using the program TORNADO, which has been verified before, and are shown in Table 4.2.

Table 4.2: Dimensionless derivatives for the MAV

$C_{m_{ac}} = 0.006$	$C_{Y_\beta} = 0$	$C_{Z_q} = -3.1816$	$C_{m_{\dot{\alpha}}} = -0.7232$
$C_{L_{\alpha}} = 2.6472$	$C_{Y_{\dot{\beta}}} = 0$	$C_{Z_u} = -0.7038$	$C_{m_q} = -0.7823$
$C_{x_0} = 0.0428$	$C_{Y_p} = 0$	$C_{l_\beta} = -6.0798e - 13$	$C_{m_u} = 0$
$C_{x_{\alpha}} = -0.2662$	$C_{Y_r} = 0$	$C_{l_p} = -0.2199$	$C_{n_\beta} = 4.3492e - 15$
$C_{x_{\dot{\alpha}}} = 0$	$C_{Z_0} = -0.3483$	$C_{l_r} = 0.0014$	$C_{n_{\dot{\beta}}} = 0$
$C_{x_q} = -0.3201$	$C_{Z_{\alpha}} = -2.6472$	$C_{m_0} = 0.006$	$C_{n_p} = 0.0083$
$C_{x_u} = -0.0864$	$C_{Z_{\dot{\alpha}}} = -1.2679$	$C_{m_{\alpha}} = -0.0641$	$C_{n_r} = -2.5869e - 5$

Those coefficients that are not mentioned here are equal to zero. It is still important to verify and check if these derivatives are compatible with the theory. Looking at the derivatives with respect to the Y-axis (lateral), for example, reveals that the equation is depending on the vertical tail as seen in Equation 4.10 [13]. In fact, all lateral equations with respect to the Y-axis are dependent on the vertical stabilizer and for that reason it is expected to be equal to zero since there is no vertical stabilizer in the MAV design. Looking at Table 4.2 one can see that indeed all the derivatives with respect to Y-axis are zero.

$$C_{Y_\beta} = -C_{Y_{v\alpha}} \left(1 - \frac{d\sigma}{d\beta}\right) \left(\frac{V_v}{V}\right)^2 \frac{S_v}{S} \quad (4.10)$$

The equation of motion, being an important part of the mathematical model for the dynamic behavior of the MAV, is now fully derived. Before diving into the dynamic behavior of the MAV it is important to take a look on the static behavior of the MAV which will effect the dynamic behavior as well.

4.2.2 Natural Static Stability

Static stability is defined by the aerodynamic center location x_{ac} of the wing and the center of gravity location of the MAV design. The following equations given in this subsection can be referred to [13]. The longitudinal static stability of the MAV can be described with Equation 4.11.

$$C_{m_{\alpha}} = C_{N_{\alpha}} \frac{(x_{cg} - x_{ac})}{\bar{c}} < 0 \quad (4.11)$$

In order for the this equation to hold, the center of gravity location x_{cg} must be smaller than $\frac{1}{4}\bar{c}$, measured from the leading edge, since this is where the Aerodynamic Center is located. Another important point is that $C_{m_{ac}}$ must be positive in order to achieve a trimming condition. The CG is located 4 cm from the leading edge. Using the program TORNADO, $C_{m_{\alpha}}$ is found to be -0.06 and the $C_{m_{ac}}$ of the corresponding wing profile is found to be 0.006. Figure 4.15 describes the natural static stability of the MAV in order to achieve the optimal C_L for maximum

endurance. As one can see, the slope of the $C_{m\alpha}$ is negative which guarantees a static natural stability, however the slope of the curve is very shallow. This is a point to keep in mind since it affects the dynamic stability of the MAV which will be discussed in the next section. A question that arises from this section is why not to shift the CG closer to the leading edge and thereby increasing the natural stability of the MAV. There are a multiple reasons for this:

- The trimming of the MAV should be at the angle of attack where C_L is optimized for maximum endurance.
- Shifting the CG to the leading edge decreases the arm to the wing hinge, decreasing pitch rate when trying to control the MAV.
- The CG movement is restricted due to the wing profile shape and the integration of all the parts into the wing.

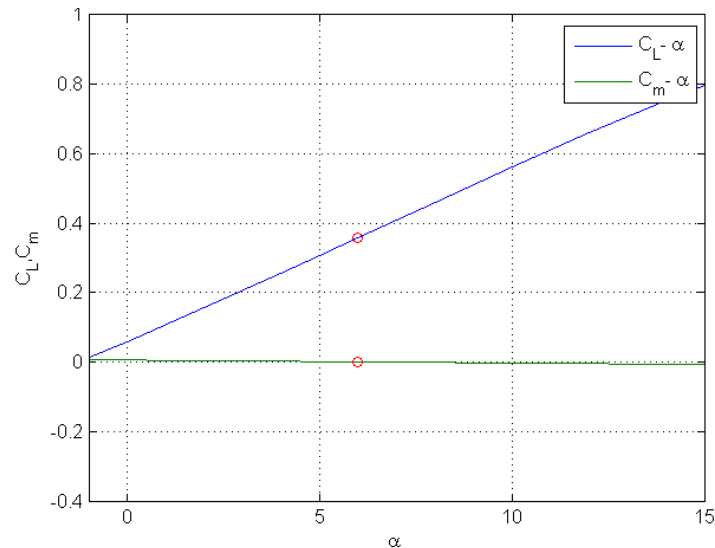


Figure 4.15: Static natural behavior of the MAV

The static stability of the MAV can be summarized by saying that the MAV is just slightly statically stable which has an influence on the dynamic behavior of the MAV. However, as will be discussed in the following sections, this problem can be solved by implementing the right control method.

4.2.3 Dynamic Stability of the MAV

Returning to the derived equation of motion, it is possible to analyze how the MAV will behave when encountering a step input in symmetric or asymmetric motion. For example, it is assumed that the MAV is flying at a trimmed condition and encountering a gust of wind which increases the angle of attack. Because the MAV is statically stable one can assume that the MAV will tend to decrease the angle of attack due to a negative moment coefficient. The question is if the MAV will return to the trim angle of attack and will stay there. In order to answer this question the equation of motion should be rearranged into state-space form. After rearranging the equation of motion the state-space is formed which can be described as: $\dot{x}(t) = A(t)x(t) + B(t)u(t)$ and $y(t) = C(t)x(t) + D(t)u(t)$. Now the full dynamic behavior of the MAV can be analyzed using the program MATLAB. The eigenvalues for symmetric and asymmetric equation of motion have been summarized in Table 4.3.

Table 4.3: Eigenvalues of symmetric and asymmetric state space system

Symmetric motion	Asymmetric motion
$0.0003 \pm 0.0101j$	-0.6543
$-0.0696 \pm 0.0298j$	0.000009
	± 0.0000003

Eigenvalue Interpretation

Table 4.3 is an important result. Looking at the eigenvalues for symmetric flight, one can see two different motions, which are described as phugoid and short period. The eigenvalue $0.0003 \pm 0.0101j$ is an unstable eigenvalue and will cause a system which is not damped. Figure 4.16 shows the symmetric reaction of the MAV for a pitch step input at an initially trimmed flight condition. Figure 4.16 shows an important result. As expected, due to the unstable eigenvalues the MAV does not return to equilibrium. The MAV interchanges the kinetic energy with potential energy

(as velocity increases, pitch angle decreases). Clearly the first behaviour of the MAV is to return to initial condition (due to a static stability) however the motion is not damped and will continue to increase.

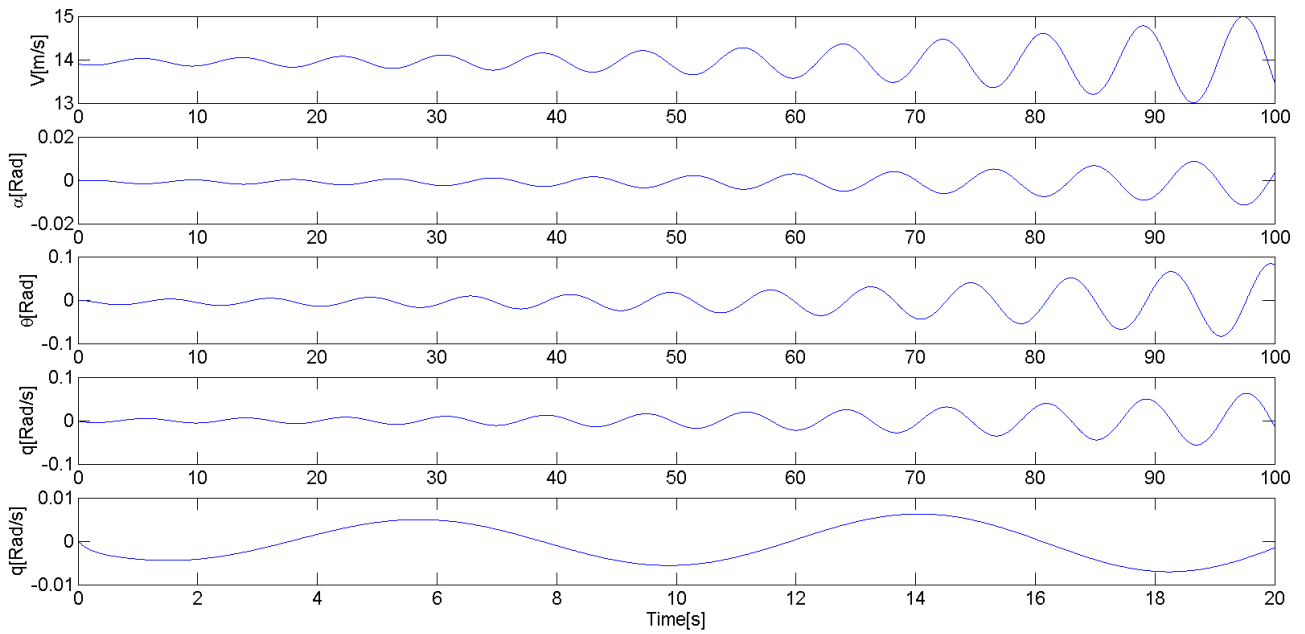


Figure 4.16: Symmetric responds for step pitch input

In subsection 4.2.1, the statically stability of the MAV was analyzed. The value of C_{m_α} was found to be -0.06 which gives a very shallow slope. The question when considering dynamic stability is what effect the slope has on the dynamic behavior of the MAV.

Figure 4.17 shows two different cases for a unity step input on the pitch motion. C_{m_α} in the first case is -0.5 which is a usual moment coefficient (Cessna Citation). The second design has a $C_{m_\alpha} = -0.06$ as in the MAV design. It can be clearly seen that when $C_{m_\alpha} = -0.5$, the motion will get damped while when $C_{m_\alpha} = -0.06$ will not.

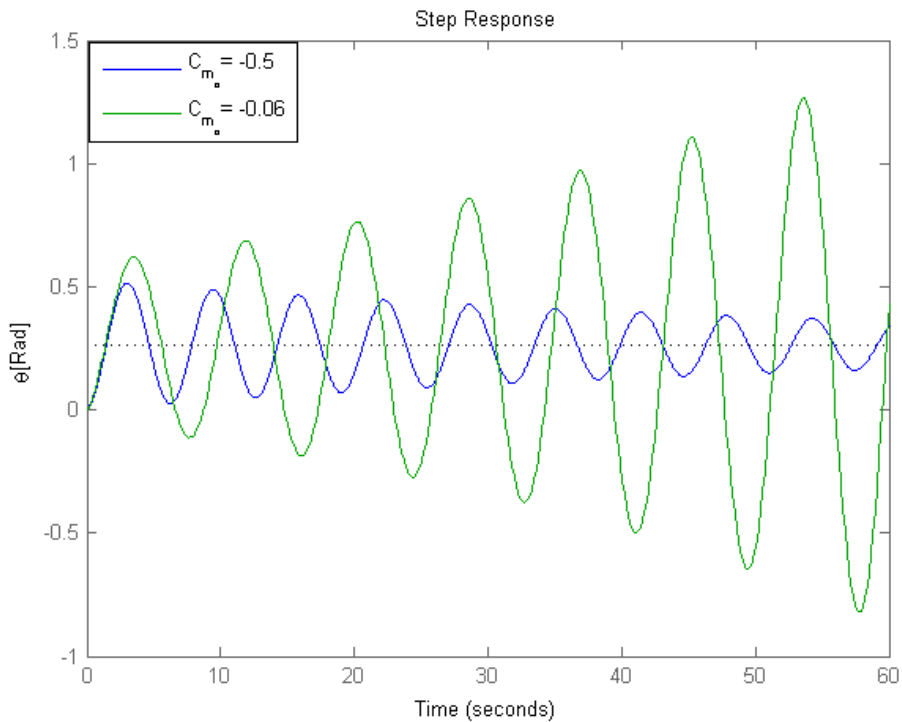


Figure 4.17: The effect of C_{m_α} on the dynamic behavior

The asymmetric motion can be analyzed in the same manner. Figure 4.18 shows the MAV behavior for initial bank angle. As expected the MAV has no damping surfaces such as a vertical stabilizer. This means that the MAV will continue to rotate without the rotation being damped.

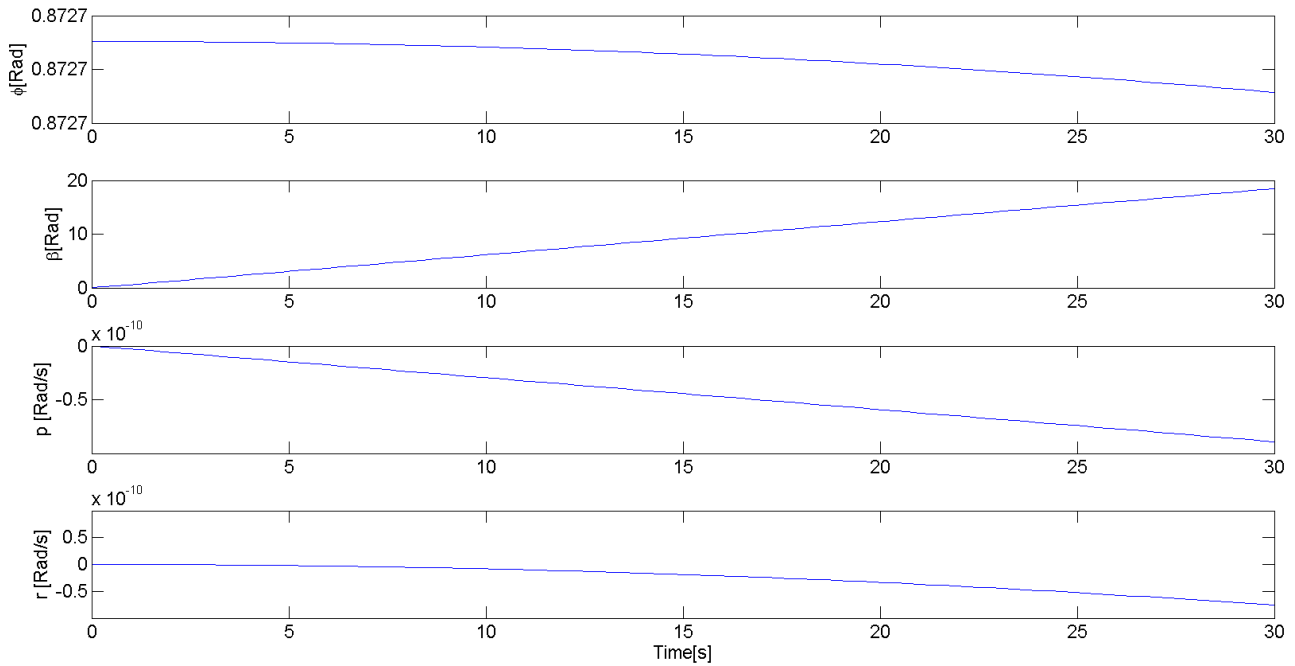


Figure 4.18: Asymmetric response for initial bank angle

The natural dynamic behavior can be summarized by saying that the MAV has no natural dynamic stability. However, when looking at Figure 4.16 and Figure 4.18, it can be seen that the MAV is not extremely unstable and the change in each one of the motions is rather small in a short amount of time. Implementing the right control theory might solve the stability problem.

4.2.4 Unity Negative Feedback Loop and Frequency Analysis

So far the reaction of the MAV has been analyzed using a step change in the input and the corresponding output response of the MAV. Figure 4.19a shows an example in pitch motion for this control. However, the MAV seems to not have a natural stability and is not damped to equilibrium in that case. Because of this a different control theory has to be applied. Figure 4.19b describes a different control method for controlling pitch, which is called Unity Negative Feedback Control. In this case the sensor always senses the current pitch angle, compares it to the desired one and uses thrust to correct the error. The disadvantage in this control method is that the autopilot will constantly have to work, which consumes power.

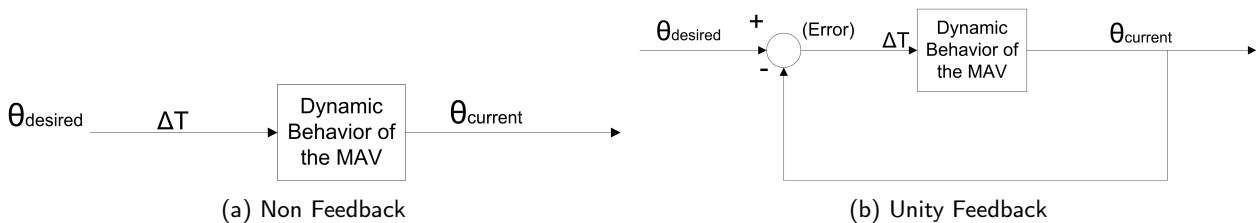


Figure 4.19: Control Methods

Using Unity Feedback the eigenvalues (corresponding to the poles and the zeroes) will change to closed loop poles and zeroes which will change the MAV responses. In this section the analyses will be given for pitch and roll motions since these are the most critical control motions of the MAV, however the method can be applied to all the motions.

Figure 4.20 shows the pitch control root locus. It describes the open and closed loop poles of the system. Clearly, the open loop poles are located at the positive real axis. Recall that the Fourier transform between frequency to time domain for each poles can be represented by Equation 4.12 [17].

$$e^{(\xi \pm \mu i)t} = e^{\xi t} (\cos \mu t + \sin \mu t) \tag{4.12}$$

This equation states that the poles closer to the origin (on the real axis) will dominate the motion (the exponential expression will be damped slower) and so the system without feedback will not be damped. It is also possible to see that the closed loop poles for a unity feedback is slightly negative. In fact, the exact location and properties of

the closed loop poles are given in Table 4.4a. Another interesting point in Figure 4.20 is that by increasing the gain of the feedback the design control properties of the MAV will change as well. This will give flexibility in the MAV control behavior.

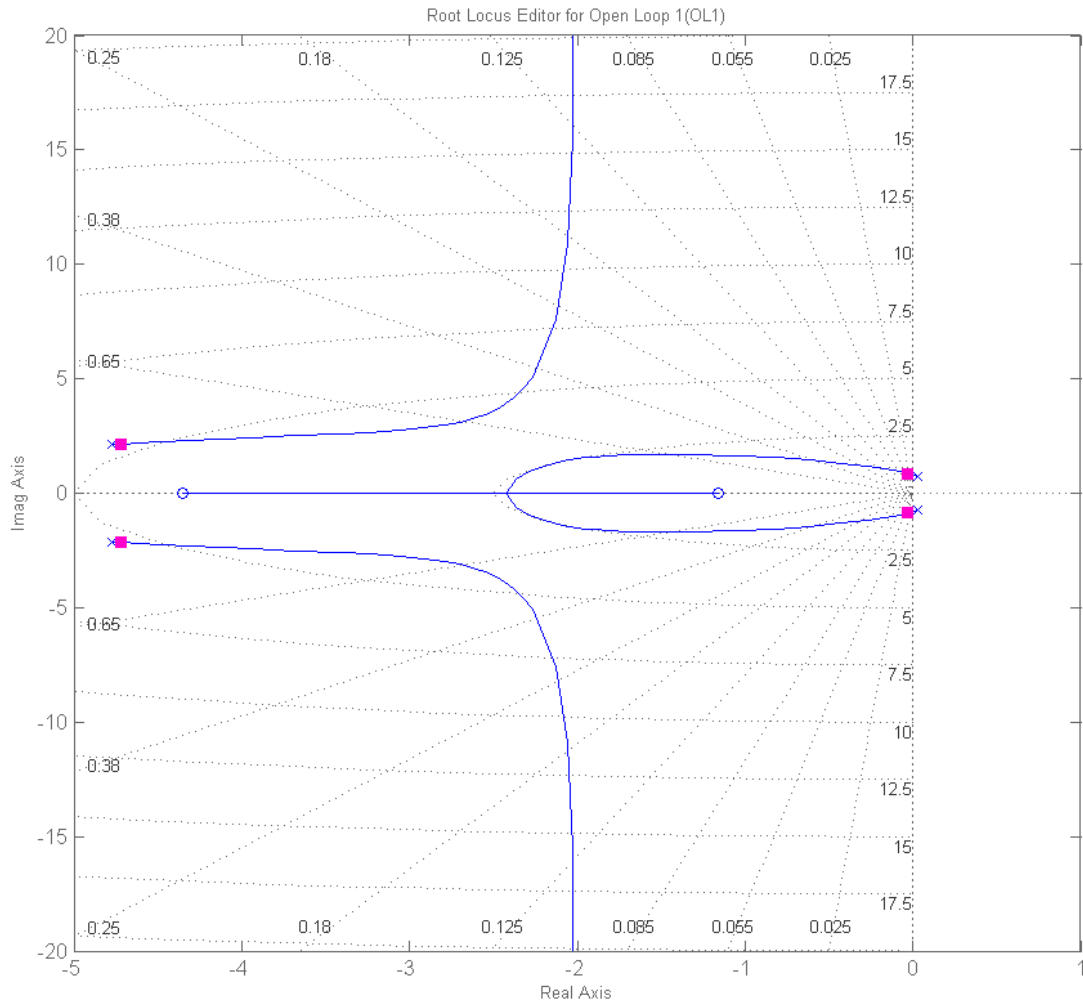


Figure 4.20: Root Locus for Pitch Control

Figure 4.21 shows the frequency response using a Bode Plot. The magnitude and the phase are shown below each other. It is possible to see the critical value where the feedback will not give the desired results and the system will become uncontrollable. The gain margin (the gain in the feedback where the system will become uncontrollable) is found to be -6.14 dB and the corresponding frequency is 0.803 rad. The phase margin is found to be 16.5 deg at a frequency of 0.865 rad. The same approach can be used for roll. The closed loop poles for roll are given in Table 4.4b.

Table 4.4: Close Loop Properties

(a) Pitch			(b) Roll		
Pole Value	Damping	Frequency	Pole Value	Damping	Frequency
$-5.12 \pm 2.26j$	0.915	5.59	-21.9	1	21.9
$-0.0376 \pm 0.853j$	0.044	0.854			

Table 4.4a and Table 4.4b are important results, they state that it is possible to control the system using Unity Feedback (all the poles are negative on the real axis). The question here is whether this approach performs well or not (in terms of final error, settling time, rising time etc). Figure 4.22a and Figure 4.22b show the behavior of the MAV for a step unity input in pitch and roll motion.

It is possible to see that the motion will be damped but the settling time and the final error clearly need to be reduced. This section can be summarized by saying that the system will be controllable, however the responses are not as fast as they should be. This can improve by using a Proportional-Integral-Derivative (PID) controller.

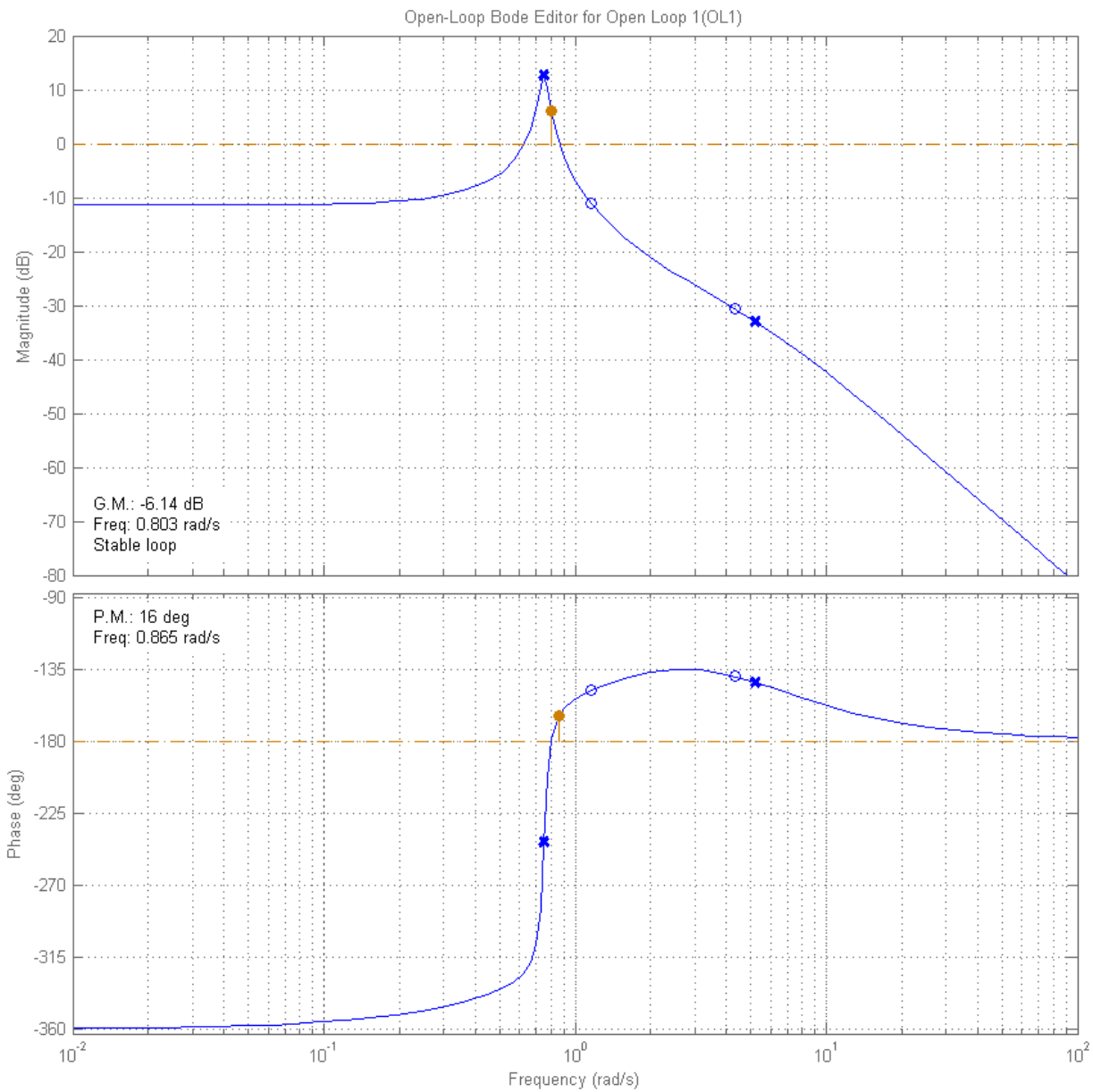


Figure 4.21: Frequency Response for Unity Feedback Control

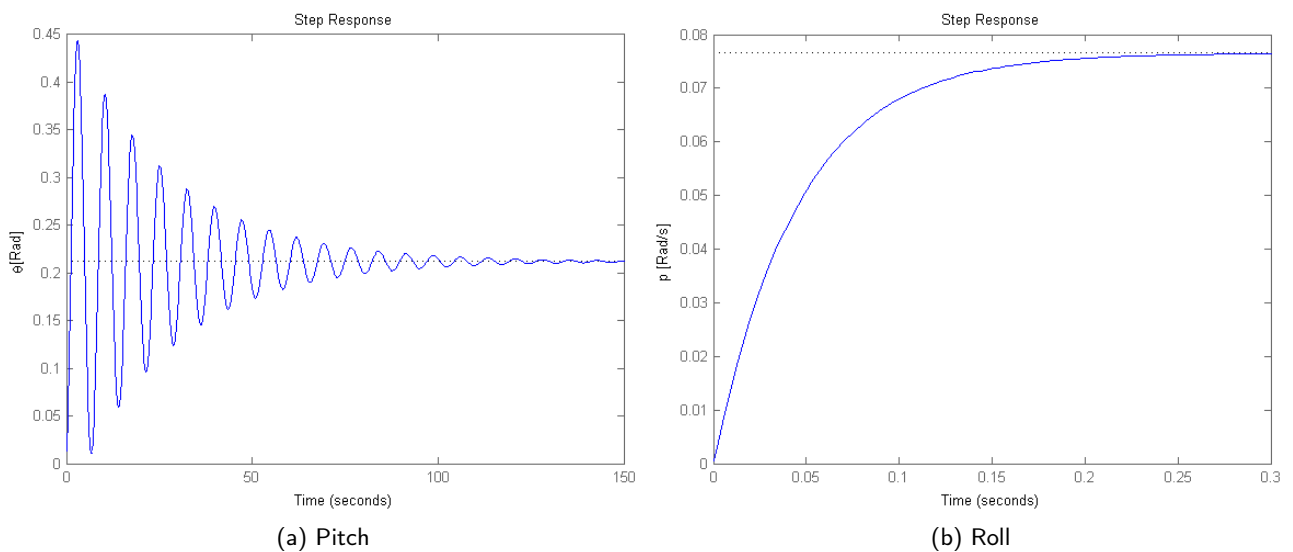


Figure 4.22: Response for a Unit Step

4.2.5 Feedback Loop Using a PID Controller

A PID controller is a common controller which is implemented in PAPAARAZZI as well as in other programs. The controller improves the results by using a proportional gain differentiation and integrator to the feedback error. Generally speaking, a PID controller is working in the following way. A zero (proportion differentiate) is added to the system which decreases the settling and the peak time. In order to decrease the final value error a pole located at the origin and a zero located just to the left of the pole needs to be added to the system (this adaption is named a proportion integrator). Figure 4.23 shows the control theory behind the PID controller.

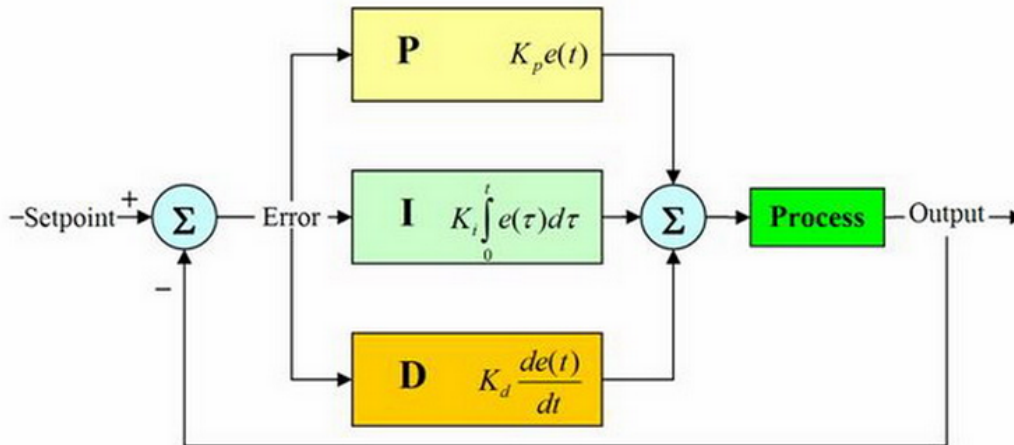


Figure 4.23: PID controller in a negative feedback loop

The complete way to find the PID controller coefficients can be found in [17]. In this section only the final results will be given. Using SIMULINK, which is subprogram inside MATLAB, the PID controller coefficient can be found. Figure 4.24 and Figure 4.25 are the final results of the PID controller coefficients for pitch and roll, respectively. The changes in the MAV control during pitch and roll unity step can be seen in Figure 4.26a and Figure 4.26b. Clearly the the final error has been reduced as well as the settling time. The complete results can be found in Table 4.5.

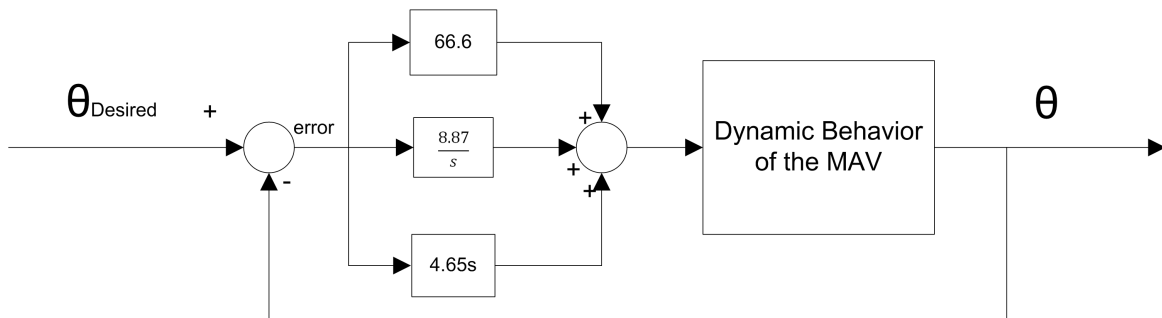


Figure 4.24: PID controller diagram for pitch

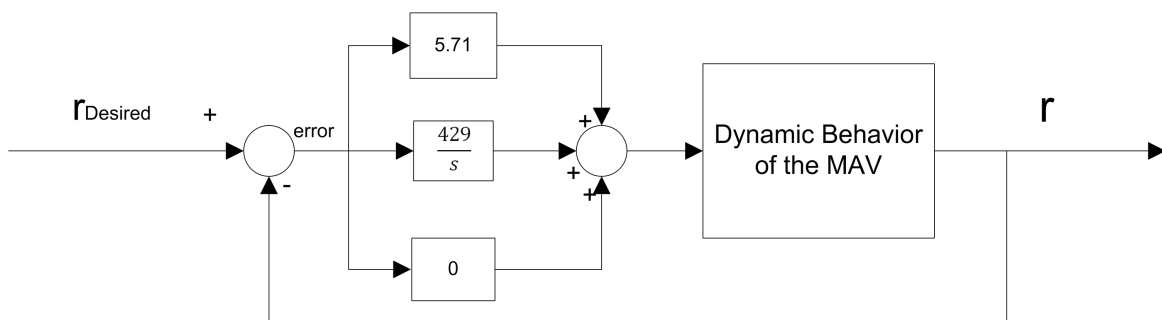


Figure 4.25: PID controller diagram for roll

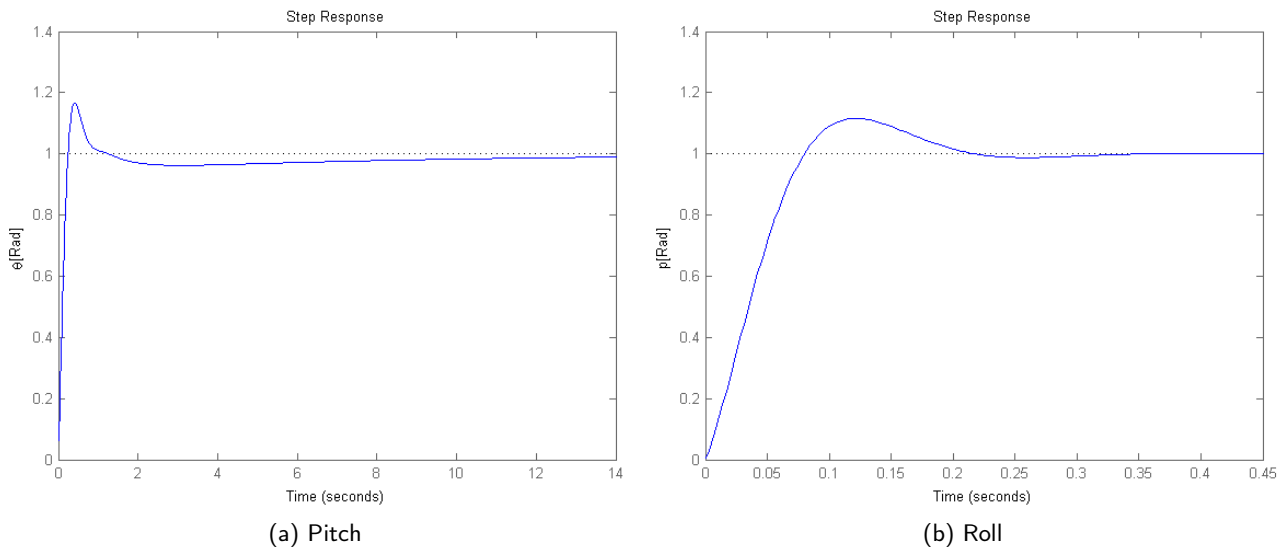


Figure 4.26: Response for a Step Input Using a PID Controller

Table 4.5: Final results for a PID controller for pitch and roll

	PID pitch control	PID roll control
Final Error [Rad]	0	0
Settling time [s]	8.31	0.196
Rise time [s]	0.18	0.0587
Peak time [s]	0.419	0.121
Peak amplitude [Rad]	1.17	1.12
Overshoot [%]	17.3	11.6

4.2.6 Conclusion and Further Research

The method to control the MAV was given in this section. The MAV is expected to be controllable, where the reaction and damping time for pitch seem to be slower than for roll. This was expected due to the limited moment arm of the MAV design. In this section a few assumption have been made in order to approach and model the MAV. In practice, those assumptions can not be neglected. The pitch, roll and yaw control methods will not be decoupled and a real test, measurement and comparisons will have to be performed to guarantee and validate a control stability of the MAV.

4.3 Structures and Materials

This section describes the detailed design for the structure of the MAV. The structure has demands it needs to meet, it needs to carry the loads acting on it, the payload needs to be integrated in the design in a way for easy access, the wing tips need to morph, it needs to be lightweight, easy to produce and cheap. When designing the structure of the MAV first several use cases are distinguished. The use cases are very important for the determination of requirements for the load case. The most important use cases for the MAV's are:

- Horizontal flight
- Vertical flight
- Hover
- Vertical landing (on different grounds)
- Crash
- Production and maintenance
- Transportation, usage and storage

It is also important to take the different environments the MAV's are exposed to into account. The most important environmental conditions are listed below.

- Direct sunlight
- Hot weather (up to 40°C)
- Rainy weather

- Sand, dust and dirt
- Heat from components inside the vehicle

The interfaces the structure has with the different components are also important to identify beforehand. Interfaces include attachments to the structure and the external influences on the MAV.

For the detailed design a literature study is performed to analyze all aspects of the design. The outcomes are documented here; first the load cases will be discussed consisting of the aerodynamic forces, handling loads and impact loads. Then the design of the structure will be explained including the morphing wing and the wing body. After the structure is designed the deflection, twist, airfoil shape control and fatigue are analyzed. A finite element analysis (FEA) is performed to verify the calculations. Knowing the stresses from the FEA, different materials will be investigated and selected. Finally, the complete structure is summarized in the last subsection.

4.3.1 Load Case

The loads acting on the MAV originate from different situations. During horizontal and vertical flight the MAV experiences aerodynamic loads. The MAV is exposed to impact loads when it is dropped or it crashes and when the MAV is roughly handled the structure needs to cope with handling loads. These loads are all analyzed in this subsection.

Assumptions

The detailed design of the structure implies a lot of calculations and to simplify these calculations assumptions are made. The reference frame used in this section is right handed and is shown in Figure 4.27. The origin is located in the center of the MAV on the leading edge, with the x-axis in span wise direction, the z-axis upward and the y-axis along the airfoil. The assumptions made are stated below:

- A1: The lift is distributed elliptically along the span.
- A2: The area behind the propeller generates constant lift.
- A3: The center of the MAV is clamped.
- A4: The weight of the structure is equally distributed.
- A5: The component weight are point loads acting in the center of the corresponding component.
- A6: The lift acts in the aerodynamic center.
- A7: The aerodynamic center is placed on the quarter chord.
- A8: The shear, moment and torque loads are perfectly carried through the hinge points on the structure.

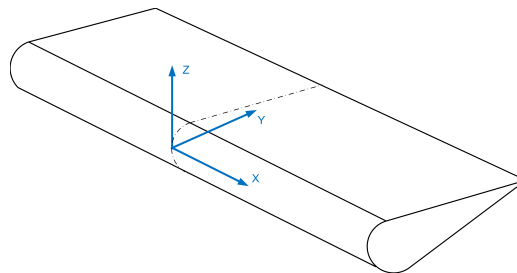


Figure 4.27: Reference Frame

These assumptions create a difference between the calculated loads and the actual loads. The elliptical lift (A1), till the point where the propeller effects the flow will only deviate slightly from reality. Implying that the area behind the propeller creates constant lift (A2), will induce small deviations, since the vortices at the tip will effect the flow over the wing. The actual lift will be lower than estimated. Since the modelled forces are higher than in reality the beam will be strong enough to cope with the actual forces, which makes the assumption valid.

Assuming the center of the MAV is clamped (A3) simplifies the calculation of internal forces on the MAV. In reality the MAV will be able to move freely. This assumption creates higher forces in the wing, which also makes the beam stronger and heavier. Having a constant structural weight along the span (A4), will not cause large deviations since the wing is rectangular. Assumption 5 will simplify the weights of the subsystem by changing them from distributed loads to point loads. The internal shear, moment and torque will deviate along the span, but the maximum values will still be the same. Assumption 6 states that the lift acts in the aerodynamic center, adding a constant moment around the aerodynamic center will make this assumption valid. Assumption 7 states the aerodynamic center is placed on the quarter chord. Since the MAV has a constant chord and no sweep the actual aerodynamic center will be close to this location, so this assumption is also valid. Finally, assumption 8 allows the loads to have a perfect transition from the morphing wing to the wing body. This does not have a large effect since no extra loads are added there, only same load concentrations are neglected.

Load Factors

The load factor, which is defined as the lift to weight ratio of the aircraft, represents the loads to which the MAV structure is subjected. For normal flight and manoeuvring a load factor of 4 is assumed, which is quite high to ensure agility. However, this is not the highest load case the MAV will encounter since impact and handling should be taken into account too. During impact the g-force the MAV experiences is estimated to be 10 [18]. This factor is applied to the weight of the complete structure on the most critical impact points, the tips. For handling loads a large load factor is assumed to allow for rough handling of the MAV. This load factor is applied on the aerodynamic forces since these forces resemble the handling forces most. For the handling loads a load factor of 15 on the aerodynamic forces is applied.

Aerodynamics & Handling Loads

During horizontal and vertical flight several forces act on the MAV. The maximum load case is a combination of the two flight cases. The load case consists of horizontal flight loads with maximum thrust applied on the tips, where the lift has the load factor of 15 included. The forces acting on the MAV during flight consist of the lift, the structural weight, the weight of all components, the thrust, the moment around the aerodynamic center, the reaction moment of the engine and the resulting forces in the center of the MAV. These loads in z- and y-direction are shown in the free body diagrams in Figure 4.28a and Figure 4.28b. Only the positive x-direction of the wing is shown, since the point loads of the subsystems are very similar to the negative x-direction. The only difference is that the weight of the camera and remote controller are changed with the weight of the GPS, XBee and antenna.

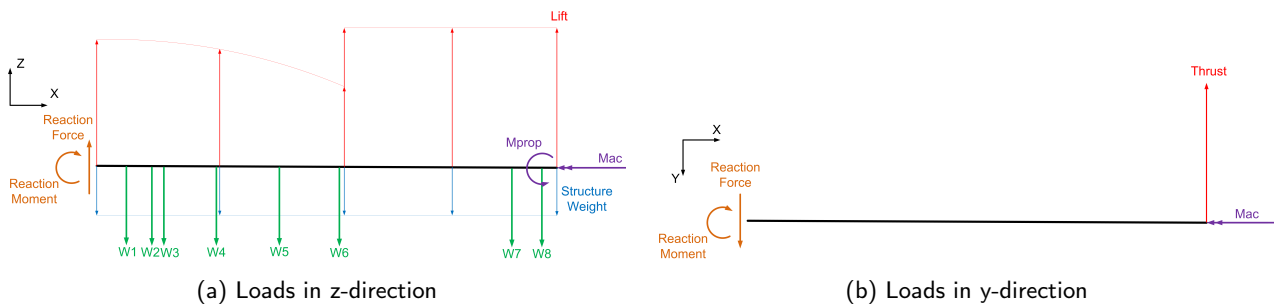


Figure 4.28: Free Body Diagrams

Table 4.6: Load Locations

Label	Description	x [mm]	y [mm]	Mass [g]
W1	Lisa M	± 15	60.5	5.4
W2	Battery 1	± 18.75	58	17.8
W3	VPU	± 19.05	94	6.1
W4	Battery 2	± 37.5	26.94	35.6
W5	Balls	± 63.6	49 & 73	2.5 each
W6 Right	Servo, Camera and RC	98	31.5, 79 & 89	10, 23 & 3.7
W6 Left	Servo, GPS, XBee and Antenna	-98	31.5, 79, 79 & 89	10, 13.5, 4 & 4
W7	Motor Controller	± 198	29	9
W8	Engine with Propeller	± 210	-22	35
Structural Weight	Distributed Structural Weight	-225 to 225	64.5	80
Label	Description	x [mm]	y [mm]	Force [N]
Lift	Distributed Lift	-225 to 225	52.5	Equation 4.13
Thrust	Propeller Thrust Force	± 210	-22	Equation 4.14
Label	Description	x [mm]	y [mm]	Moment [Nm]
M_{ac}	Moment around the AC	-225 to 225	-	Equation 4.15
M_{prop}	Reaction Moment from the Engine	210	-	Equation 4.16

Table 4.6 shows the different subsystems with the corresponding labels in the free body diagram, the mass, force or moment, and position. Subsystems W1 to W4 are located in the center of the MAV, these weights are split up and placed on both wings. The weight is then halved and it is located in the middle of the cut part. The values are taken from section 4.11. In one wing there are one and a half batteries cell, two balls, one servo, one motor controller and

one engine with propeller. Of all other components only one half is present, since these are located in the center of the MAV.

As can be seen in the free body diagram the lift is distributed elliptical till the point where the propeller is positioned. From there on the lift is constant and a factor higher then the elliptical distributed lift. This factor is caused by the increase in velocity due to the propeller slipstream, and is calculated in section 4.1. The total lift is calculated with Equation 4.13, where W is the total weight of the MAV and n the load factor. The total thrust is calculated with Equation 4.14, where SF_{Thrust} is a safety factor set to 1.5.

The moment around the aerodynamic center can be calculated by Equation 4.15 [12], where ρ is the air density, V is the airspeed, S the surface area, c the chord length and C_{mac} the moment coefficient around the aerodynamic center of 0.006, obtained from section 4.1. The reaction moment of the engine is shown in Equation 4.16, where K_t is the torque constant of 0.659 Ncm/A, and I the current through the engine of 12.6 A, both obtained from section 4.4. Finally, the point loads are equal to the mass times the gravitational constant for each subsystem and the structural weight is distributed equally along the span.

$$L = W \cdot n \quad (4.13)$$

$$T = 2 \cdot W \cdot SF_{Thrust} \quad (4.14)$$

$$M_{ac} = \frac{1}{2} \cdot \rho \cdot V^2 \cdot S \cdot c \cdot C_{mac} \quad (4.15)$$

$$M_{prop} = K_t \cdot I \quad (4.16)$$

Knowing all the forces and their locations (Table 4.6), the internal shear, moment and torque distributions can be calculated using Equation 4.17, Equation 4.18 and Equation 4.19 respectively [19]. The beam is separated in parts, where each part has a different load case. The parts are split up at the root, tip, point loads and the point where the propeller starts to alter the flow. The internal shear, moment and torque distribution are calculated, where the distributed loads are denoted by $w_i(x)$, the number of distributed loads by n , the forces by F_j , the number of forces by m and the distance of the force to the root by x_{F_j} .

To calculate the torque the distance in y direction needs to be known. y_{w_i} defines the y position of the distributed load from the leading edge, y_b the position of the load carrying structure from the leading edge and y_{F_j} the position of the forces from the leading edge. y_b has a value of 8.5 mm. x_1 and x_2 define the boundaries of the section. The number of distributed loads and forces at the boundaries are defined by n and m respectively. The shear, moment and torque distributions for the aerodynamic and handling loads are shown in Figure 4.29.

$$V(x) = - \int_{x_1}^{x_2} \left(\sum_{i=1}^n w_i(x) \right) \cdot dx - \sum_{j=1}^m (F_j) \quad x_1 \leq x \leq x_2 \quad (4.17)$$

$$M(x) = - \int_{x_1}^{x_2} \left(\sum_{i=1}^n w_i(x) \right) \cdot x \cdot dx - \sum_{j=1}^m (F_j \cdot (x_{F_j} - x)) \quad x_1 \leq x \leq x_2 \quad (4.18)$$

$$T(x) = - \int_{x_1}^{x_2} \left(\sum_{i=1}^n w_i(x) \cdot (y_{w_i} - y_b) \right) \cdot dx - \sum_{j=1}^m (F_j \cdot (y_{F_j} - y_b)) \quad x_1 \leq x \leq x_2 \quad (4.19)$$

Impact Loads

Now the aerodynamic loads are discussed, it is time to have a look at the impact loads. Impact loads are hard to determine, but "Gulf Coast Data Concepts, LLC" recorded flight data of a crash landing of a RC plane. The plane crashed in a tree and the experienced load cases were recorded during this crash. The maximum load factor measured on this RC plane during the crash was 8 g [18]. Since this is a similar vehicle the maximum loading on the MAV is estimated slightly higher at 10 g, which is applied to the total weight.

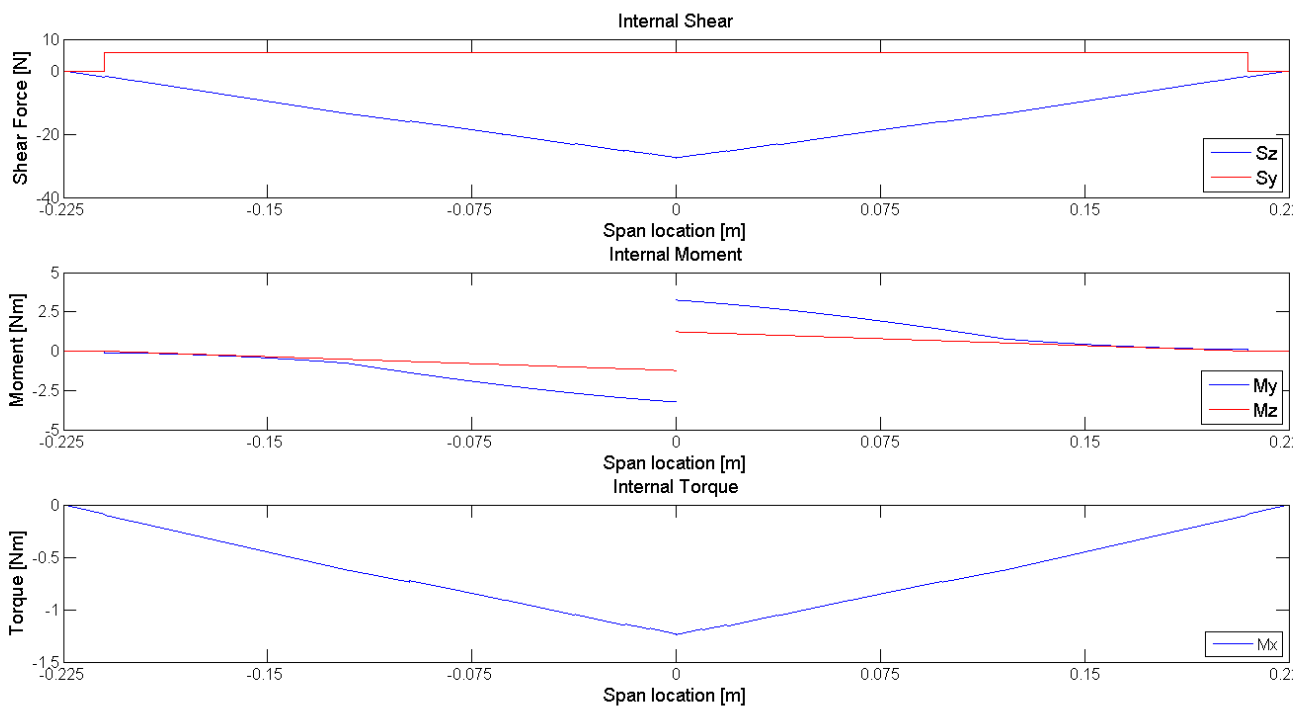


Figure 4.29: Internal Shear, Moment and Torque Distribution

4.3.2 Structural Design

Knowing the loads, the structure can be designed to cope with these loads. The total structure exists of three parts, the wing body and two morphing wings. First, the morphing wing will be discussed.

Morphing Wing

The morphing wing is a complex part of the structure, the wing needs to have active twist without breaking or plastic deformation and it also has to carry the other loads. Several design options were considered and when selecting on weight and complexity one option remained. This design reduces the number of gears and other extra materials such that the weight and complexity are minimized.

Mechanism

The mechanism consists of multiple parts, the main part is the beam in the leading edge of the airfoil that carries the loads and functions at the same time as the hinge axis. At the tip of the beam an airfoil shaped web is attached and fixed, so the beam and the web rotate simultaneously. Between the body and the last web multiple airfoil shape webs are attached to the beam, but are not fixed, these webs are free to rotate around the beam. An elastic skin is stretched over all the webs to create the surface of the morphing wing.

When a torque is applied on the beam, the beam with the tip web will rotate a number of degrees, the elastic skin will stretch and pull the webs in between with it. This way all webs will rotate with a different angle and the wing is morphed. The airfoil shape is maintained since the webs keep the skin in the correct form. The loads acting on this part are all carried by the beam in the tip of the wing.

Attachment

The wing is attached to the body and runs through two webs in the body with bushings. This way the vibrations in the beam are reduced. The beam is attached to a servo with gears. The space in the body did not allow for placement of the servo directly on the beam, so several gears are needed to control the morphing. By attaching the beam this way bending loads will be carried through the webs into the body instead of acting on the servo. The only load the servo needs to withstand is the torque in the beam.

This torque is calculated similar as before, but now using only the aerodynamic load factor, since the servo does not need to withstand the torque during handling. With this load factor included, the servo can still control the morphing when the MAV is in a turn with a load factor of four. The moment around the x-axis at the morphing

location on both wings is equal to -16.1 Ncm. Hence, the servo needs to withstand a torque of 16.1 Ncm to be able to rotate the wing and keep the wing from rotating.

Beam Design

The beam needs to withstand the loads acting on it and be able to rotate. The latter requirement reduces the choice of the cross section to circular shapes. Knowing the shear loads and moments in y- and z-direction and the torque, the shear and bending stresses on the beam can be calculated.

The direct bending stress with two moments acting on the beam is calculated with Equation 4.20 [20]. Knowing that the Moment of Inertia (Mol) of the beam is constant along the y-axis and I_{yz} is zero due to symmetry, the equation can be simplified to Equation 4.21. The z and y coordinates are related by the common equation for a circle. The Mol of the circular beam in the yz plane is shown in Equation 4.22, where D_o is the outer diameter and D_i the inner.

$$\sigma_x = \frac{I_{yy} \cdot M_z - I_{yz} \cdot M_y}{I_{yy} \cdot I_{zz} - I_{yz}^2} \cdot y + \frac{I_{zz} \cdot M_y - I_{yz} \cdot M_z}{I_{yy} \cdot I_{zz} - I_{yz}^2} \cdot z \quad (4.20)$$

$$\sigma_x = \frac{M_z \cdot y + M_y \cdot z}{I} \quad (4.21)$$

$$I = \frac{1}{64} \cdot (D_o^4 - D_i^4) \quad (4.22)$$

Knowing the z and y coordinates of the beam, the distributed bending stress along the entire beam can be calculated, since the bending moment differs along the x-position. This can be seen in Figure 4.30a.

The shear stress consists of two parts, resulting from the shear force and from the torque. Since the force and torque are already known the shear stress can be calculated. The shear forces can be combined easily since the cross section is constant along the y-axis. Adding the two shear force vectors and calculating the shear stress with one shear force will be sufficient. The shear flow is calculated using Equation 4.23 [20]. Applying the same simplifications as for the bending stress and knowing the shear flow is zero at a cut at the shear center the equation is simplified to Equation 4.25. Where l is the distance, parallel to the resulting shear force, from the center of the beam to the location on the beam.

$$q_s - q_{s,0} = -\frac{I_{yy} \cdot V_y - I_{yz} \cdot V_z}{I_{yy} \cdot I_{zz} - I_{yz}^2} \cdot \int_0^s t \cdot y \cdot ds - \frac{I_{zz} \cdot V_z - I_{yz} \cdot V_y}{I_{yy} \cdot I_{zz} - I_{yz}^2} \cdot \int_0^s t \cdot z \cdot ds \quad (4.23)$$

$$q_s = -\frac{V}{I} \cdot \int_0^s t \cdot l \cdot ds \quad (4.24)$$

Solving Equation 4.25 results in a shear flow along the beam that changes along the x-axis due to a shear force that changes along the span. Knowing that the thickness is constant along the beam the shear stress distribution due to shear force can be calculated. The distribution is shown in Figure 4.30b.

$$\tau_V = \frac{q_s}{t} \quad (4.25)$$

The shear stress due to torsion is calculated using Equation 4.26 [20], where A is the enclosed area of the cross section and t the thickness. The distribution of this stress is plotted in Figure 4.30c. All the stresses acting on the beam are calculated. However, the stresses can interfere and the combined maximum stress is therefore calculated with Von Mises. The simplified version of this equation is shown in Equation 4.27 [20].

$$\tau_T = \frac{T}{2 \cdot A \cdot t} \quad (4.26)$$

$$Y = \sqrt{\sigma_x^2 + 3 \cdot (\tau_V + \tau_T)^2} \quad (4.27)$$

Finally, knowing the size of the beam from the payload integration section 4.11, the maximum stresses can be calculated. A beam with a diameter of 5.5 mm and a thickness of 1 mm will have a maximum stress at the root of 68.5 MPa. Including a safety factor of 1.5 the material should withstand stresses of 137 MPa. The plot of the resulting Von Mises stress is shown in Figure 4.30d.

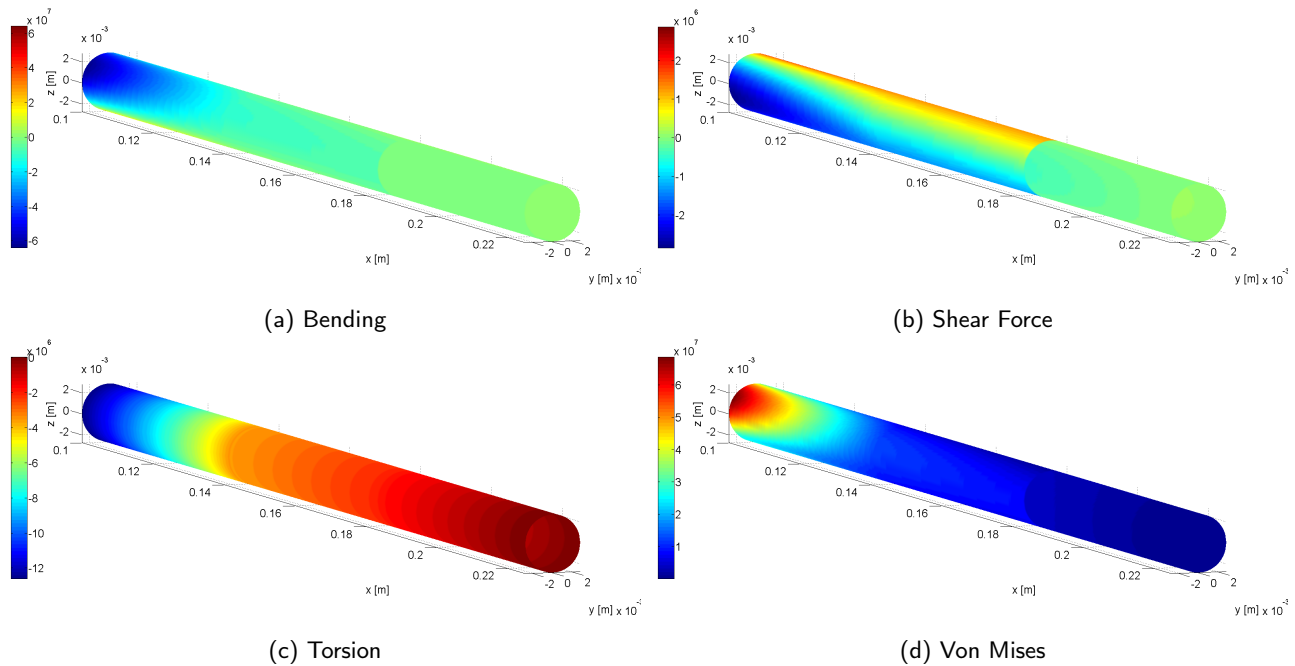


Figure 4.30: Stresses on the Beam [Pa]

Wing Body

This section will discuss the design of the main body. For the main body, it is important to take the payload into account. In fact, the whole mid-section is designed around the payload.

The morphing wing tips are connected to the midsection through the hinge axis. The torque on the axis due to the aerodynamic loading will be carried by the servo that actuates the morphing section. This torque is hence introduced at the location where the servos are mounted (the rectangular hole in the rib, see Figure 4.31a). The rotational axis is pushed through the two holes one can also see in the figure below. All other forces and moments will be carried by the two webs. The hanging structure that can be seen at the right side of the figure is meant for the battery, but more on this will be explained in section 4.11.

In Figure 4.31b the left half side of the mid-section is shown. Note that the material at the trailing edge is solid. This is done, because the sharp edge will otherwise puncture the skin and it will increase the moment of inertia around the z-axis. It will also make the trailing edge section a lot stiffer and it will define the airfoil shape better.

Also near the leading edge, some extra material is added. This part will also give the structure more stiffness by increasing the moment of inertia around the y- and z-axis and it is designed to carry all the (bending) loads. Besides this, the 3D-printed structure is rough. Extending the surface over the top side of the vehicle hence increases the aerodynamic performance as has been discussed in section 4.1. This extension of the skin over the top side of the vehicle will also allow for integration of a payload bay. Once the skin material is wrapped over the skeleton of the structure, it is hard to remove it again. For this reason a hole has been made in the elongated 3D printed skin and a 3D printed hatch can be clicked in, closing the hole again after all payload has been placed inside the structure.

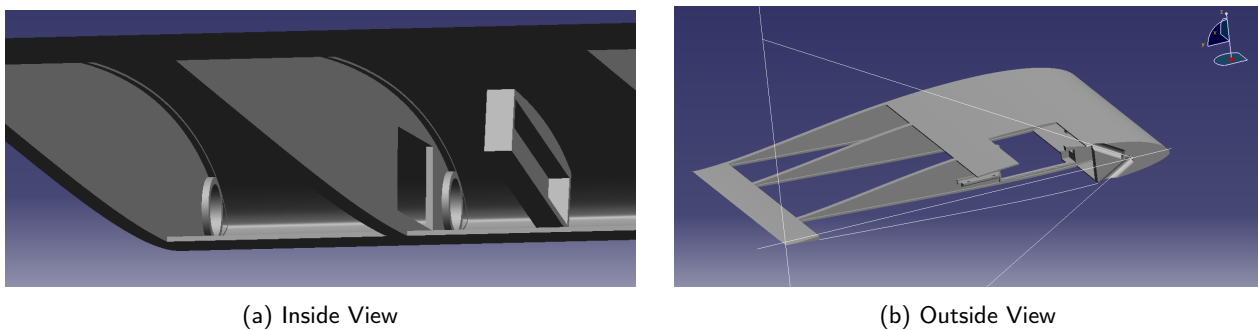


Figure 4.31: Wing Body

The white lines in Figure 4.31b indicate the geometry of the landing structure. Near the leading edge, extra material is added to increase the stiffness and to deal with the landing forces. The two lines indicating the landing sticks intersect above the center of gravity. They also intersect the line parallel to the y-axis. This is the line that goes

through the center of gravity. In other words, no moment is created. More about the landing structure will be discussed in the next section.

Landing System

The landing system for all MAV's consist out of two structural external rods and a landing structure integrated in the morphing wing tips. First, the design of the landing structure integrated in the morphing wing tips will be discussed and after this the design of the external rods will be discussed.

Wing Tip Reinforcement

The planform and the CG position of the MAV are now fixed. From simple trigonometry, the tip-over angle was calculated to be 53 degrees, see Figure 4.32a. This means, not taking into account any rotational velocity, that the maximum landing angle for the MAV is 53 degrees. This angle is defined to be reasonable and this is the maximum landing angle the MAV is designed for.

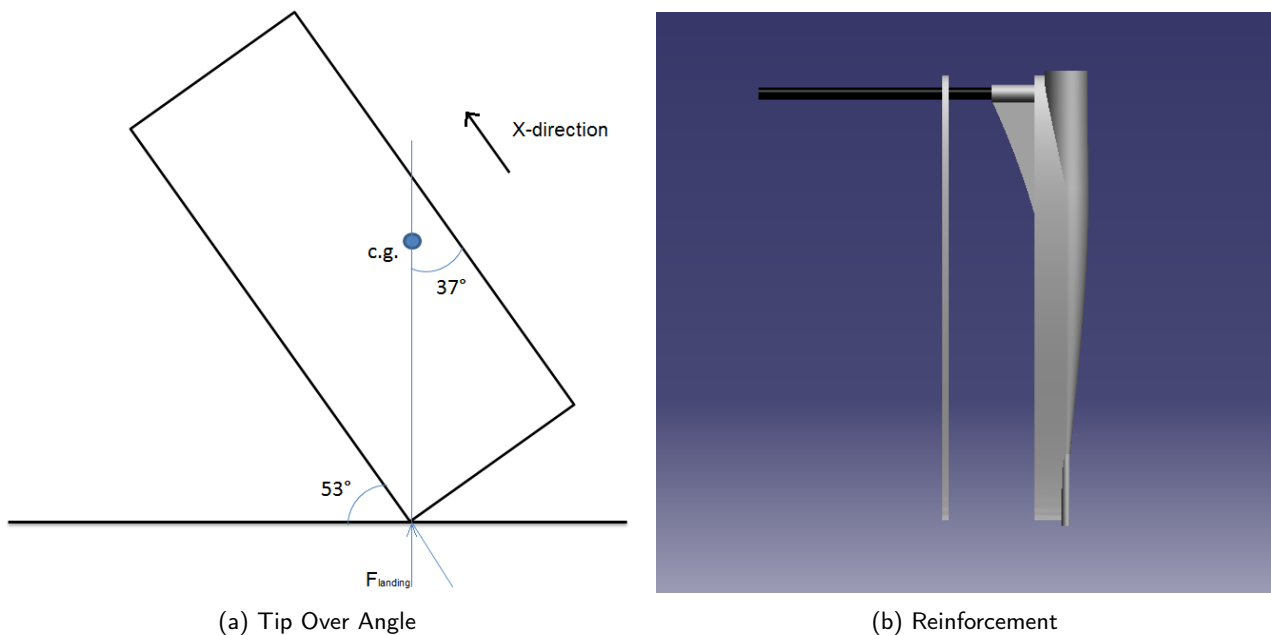


Figure 4.32: Wing Tip Reinforcement

Having an impact on the tip in this manner can cause deformations of the tip, which will deform the entire MAV. To counteract this deflection during impact a extra structure is added, as can be seen in Figure 4.32b. This extra structure will prevent the wing tip from deforming too much and in this manner the wing will not fail due to deformation. When the structure drops on the tip as described above the deformation will not be permanent.

Landing Sticks

To stabilize the MAV in landing, some constraints are set to prevent rotation around the x-axis and hence to prevent the MAV from tip-over in this direction. In a worst case scenario, the MAV will land on one of these sticks during a rough landing. The sticks stick out of the airframe and to increase the ease of transportation, it has been decided to make them detachable. This will also be useful when assembling the hardware inside the airframe. After all, the stick is in front of the opening. Because the sticks point out of the airframe and hence generate drag, it has been decided to make them as thin as possible. This means the stick will be solid and the stick is allowed to brake during a very hard landing (>3 g). The structure is capable of landing with 10 g, but decreasing the load case for the landing stick allows for smaller stick sizing and the sticks are easy to replace due to the implemented mechanism.

For a long and thin rod like this, buckling is important to take into account. The Euler formula for buckling is shown in Equation 4.28, where $K=2$ for a beam that is fixed on one end and free on the other end. With a diameter of 3 mm and a length of 204 mm (from CATIA), the buckling force is 11.78 N. The maximum landing angle in this direction is defined to be 60deg. When the MAV lands with 3 g exactly on the stick, the maximum normal force will be 11.77 N. With this load, the stick will be on the edge of buckling. However, in this case (on side clamped, the other side free), when the stick buckles it will still be able to carry a part of the loads.

$$F = \frac{\pi^2 \cdot E \cdot I}{(K \cdot L)^2}, \quad (4.28)$$

When evaluating the normal stresses due to normal and bending loads ($S_N = \frac{F_N}{A} + \frac{My}{I}$) and shear stresses, it has been concluded that a 3 mm pultruded carbon fiber landing stick is able to carry all loads that can occur during a landing up to 3 g.

4.3.3 Structural Analysis

Knowing the general layout of the MAV the structural characteristics of the MAV can be analyzed. Some characteristics are not acceptable and will change the design. The deflection of the entire wing, the twist of the beam, vibrations of the beam, the ability to maintain the airfoil shape and fatigue will be discussed.

Deflection

Due to the forces on the wing, the wing will deflect. The deflection must not be too large, since it will effect the generation of lift on the wing, it will tilt the resultant lift vector inward, losing upward force. The calculation of the deflection is done by splitting the wing in two sections, from the root to the morphing part and the morphing part itself. For the deflection in z-direction the moment curve is integrated twice and divided by the Young's Modulus (E) times the Mol (I). Boundary conditions are set to find the deflection curve of each section using Equation 4.29 [21]. For simplification it is assumed that the beam is fixed at the root and fixed at the hinge location of the beam. The maximum deflection of the first part is added to the second part. The Mol is different in the two sections, in the morphing part the beams Mol is calculated with Equation 4.22 and for the midsection the Mol's are taken from the CATIA model.

$$v(x) = \frac{1}{E \cdot I} \cdot \iint M(x) \cdot dx \cdot dx \quad x = 0; v = 0 \quad v' = 0 \quad (4.29)$$

For the deflection in y-direction Equation 4.30 is used [21] with the maximum thrust at the tip, where P is the force at the tip and L the beam length. Again the beam is split up in two parts and both roots are fixed. The Mol's are again calculated with Equation 4.22 and taken from CATIA.

$$v(x) = \frac{-P \cdot x^2}{6 \cdot E \cdot I} \cdot (3 \cdot L - x) \quad (4.30)$$

The deflections are calculated with the beam as defined above with an aerodynamic load factor of 4 and with the SLS material PA 2105. This results in a deflection in z-direction of 10.8 mm and in y-direction of 28.1 mm. A deflection of 3 cm is too much, since the thrust will be misaligned and stability will become difficult. The size of the beam can not be increased due to payload integration issues. That is why a carbon beam is included in the calculations, the deflection in z-direction of carbon is 0.17 mm and in y-direction only 0.39 mm. When considering the deflection it is better to have a carbon beam instead of a printed beam, but the body can be made from PA 2105 without a problem. The results are shown in Figure 4.33.

Twist

The twist of the beam in the morphing section is completely dependent by the torque. Since the torque distribution is calculated earlier the twist can be calculated using Equation 4.31 [21], where T(x) is the distributed torque, L the length of the beam, G the shear modulus and J the polar Mol calculated for a beam with Equation 4.22 [19]. For a load factor of 4 and PA 2105 and carbon as materials this results in the twist angles shown in Figure 4.33. The twist using PA 2105 is 14.3 degrees and using carbon 0.43 degrees. This means that in order to have a wing that will not morph when its flying normally a carbon beam must be implemented.

$$\phi(x) = \frac{\int_0^x T(x) \cdot dx}{G \cdot J} \quad 0 \leq x \leq L \quad (4.31)$$

Vibrations

Knowing the behaviour of the wing is helpful for understanding the effects the MAV will experience. A part of this behaviour is related to the natural frequency of the beam. Using Equation 4.32 [22], the natural frequency can be determined. The beam is modelled with the engine, propeller, motor controller and web weight at the tip. By summing these weights and substituting them in the equation the natural frequencies can be determined.

$$\omega_n = \sqrt{\frac{3 \cdot E \cdot I}{m \cdot L^3}} \quad (4.32)$$

The natural frequencies for the PA 2105 beam as described above will give a natural frequency of 110.6 Hz and for the carbon beam the natural frequency will become 941.7 Hz. Knowing these values helps understanding the system.

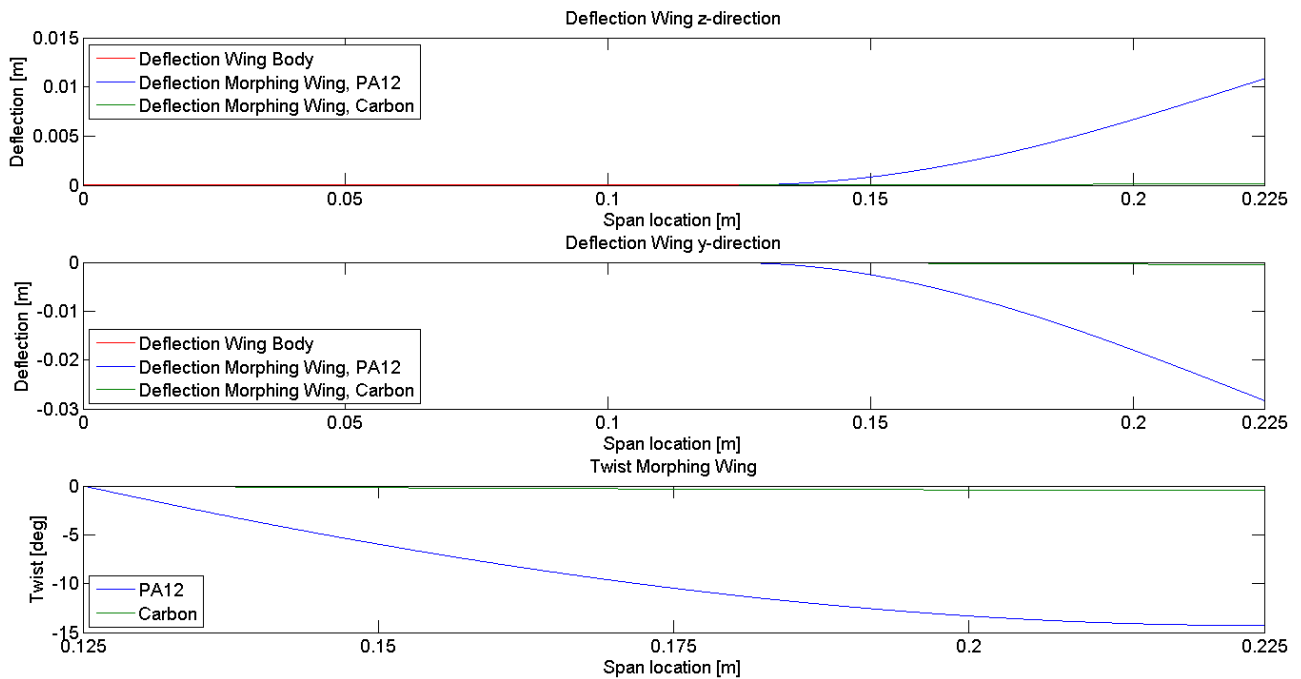


Figure 4.33: Deflection of the Wing and the Twist of the Beam

Airfoil shape

The airfoil shape should be maintained during the flight phase to keep the characteristics of the MAV stable. Using a flexible skin to implement the morphing will make this difficult. The analysis on how the skin will behave during morphing is too far fetched for this design and it will be checked during the actual morphing. Knowing that the maximum rotation of the beam during the control will be small results that it will not be too difficult to maintain the shape. One web in the middle of the morphing part should be sufficient, but this will be made out in the testing of the design itself, it is not hard to implement more freely rotating webs on the beam. For the body itself the number of webs described in the wing body design are more than sufficient for the maintainability of the airfoil shape, since the body itself will not deform actively.

Fatigue

Fatigue is not as important for the design since we will not design the MAV for a long lifespan and in case something does break, the parts can be replaced. Breaking of the parts will most likely not be caused by fatigue but by impact or handling for example. Since the MAV is designed for one mission the probability that failure due to fatigue will occur is minimal. The fact that a carbon beam is used and the maximum stresses are 100 to 150 MPa fatigue will not cause issues. However, when the design is used for mission with a longer lifespan fatigue can be further investigated.

4.3.4 Verification

The models of the loads, stresses and deformations need to be verified to know that the values are reliable. To do this the models are checked analytical. When any unreasonable results appear the code is checked for any errors and inconsistencies. Errors can be caused by using wrong units, programming errors and rounding errors.

For the load calculations the largest value for the shear stress is checked by summing all forces by hand, the moment is estimated by summing the forces multiplied with the arms and the maximum torsion is checked analytical to verify the model. Furthermore, the position of the jumps in the plots caused by component weights are checked for verification.

The model for the stresses is verified analytical as well. The model was simplified by using forces on a beam with a simple cross section. The plot is checked by looking if the jumps are in the right places. A large increase in the stresses on the point of the engine shows that the thrust acts on the right location. Multiple positions are checked to ensure that the model is working as intended.

The deformation model is checked by having a similar load on the tip of a beam and calculating the deflection and twist. The actual deflection and twist should be lower but close to this calculated value since the loads are distributed along the span instead of working on the tip. Also, a unit check is performed to prevent incorrect values.

4.3.5 Finite Element Analysis

To verify the calculations on the structures, a Finite Element Analysis (FEA) is performed. For this analysis ANSYS 13.0 is used. The CATIA model of the structure was exported as a step file and imported again in ANSYS. The 3D-printed material, PA-12, does not exist in the Engineering Data folder of ANSYS, so the material was added manually. It is assumed that the material is a homogeneous isotropic linear elastic material (directional dependencies negligible). The material properties are, in reality, due to their layer-by-layer production, to some extent direction dependent [24]. The elastic properties of a homogeneous isotropic linear elastic material is uniquely defined by any two moduli and all other elastic moduli can be calculated with basic formulas. The material density is 950 kg/m³ and the Young's Modulus is 1850 MPa according to EOS. The Poisson's Ratio is estimated to be 0.4 [23], and together with the Young's Modulus, the material properties are now defined.

The next step in the FEA is to mesh the structure. The method that was chosen in the analysis is the 'Hex Dominant Method' and the element size has been set to 1 mm and after that to 0.5mm. The second step with the smaller element size was performed in order to check whether the converged solution was found or not. The results didn't deviate that much, so for preliminary sizing a 1 mm element size is good enough. Analysing the structure with this larger mesh is significantly faster. In Figure 4.34 the mesh with element size 0.5mm can be seen. The right side of the figure shows a part of the mesh in more detail.

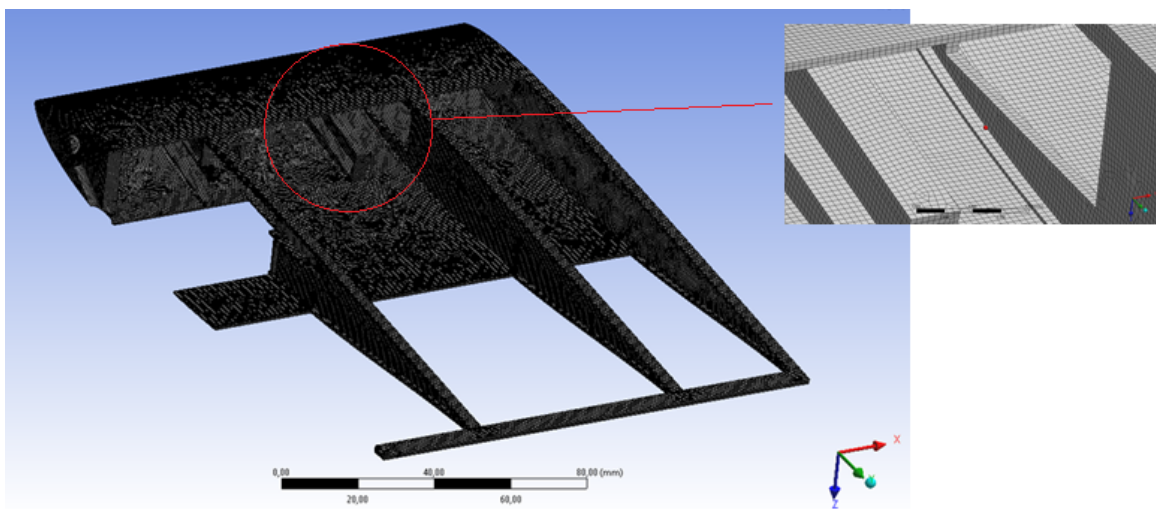


Figure 4.34: Mesh

Now the mesh has been generated, it is time to apply the correct loadings. An overview of the loadings can be found in Figure 4.35. Table 4.7 gives a more detailed overview of the magnitude and orientation of the loads. The magnitude of the loads are determined earlier. All loads and attachment points are taken very conservative in order to make sure that the calculated stresses are worst-case scenarios. The final result can be found in Figure 4.36 and Table 4.8. The maximum stresses are well within the capabilities of the material (45 MPa). Also note that the maximum stresses occur at the root and at sharp corners/cutouts. The stresses can be reduced somewhat by applying fillets and smooth transitions. The maximum deflections are acceptable. It must however be noted that the attachment of the lift for the mid-section was at the trailing edge as can be seen in Figure 4.35. The moment of inertia is very small at the root and the pressure distribution over the airfoil causes the actual lift to apply more at the front of the airfoil. This value will therefore be quite a lot higher than in reality.

Table 4.7: Finite Element Analysis Loads

Label	Load	Direction	Magnitude [N]
A	Fixed support	-	-
B	Tip lift moment	z	14
C	Tip lift moment	-z	14
D	Gravitational acceleration	-z	
E, F, G	Battery weight	-z	1 each
H	GPS, XBee/Camera weight	-z	1
I	Tip lift	z	4
J	Max thrust + moment contribution	-y	40
K	Max thrust - moment contribution	y	32
L	Mid-section lift	z	6

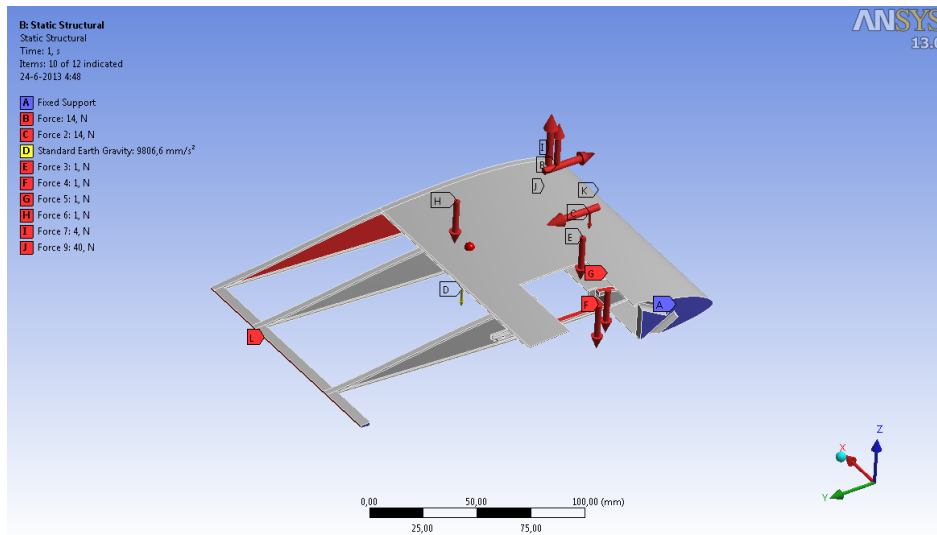


Figure 4.35: Finite Element Analysis, Loads, Midsection

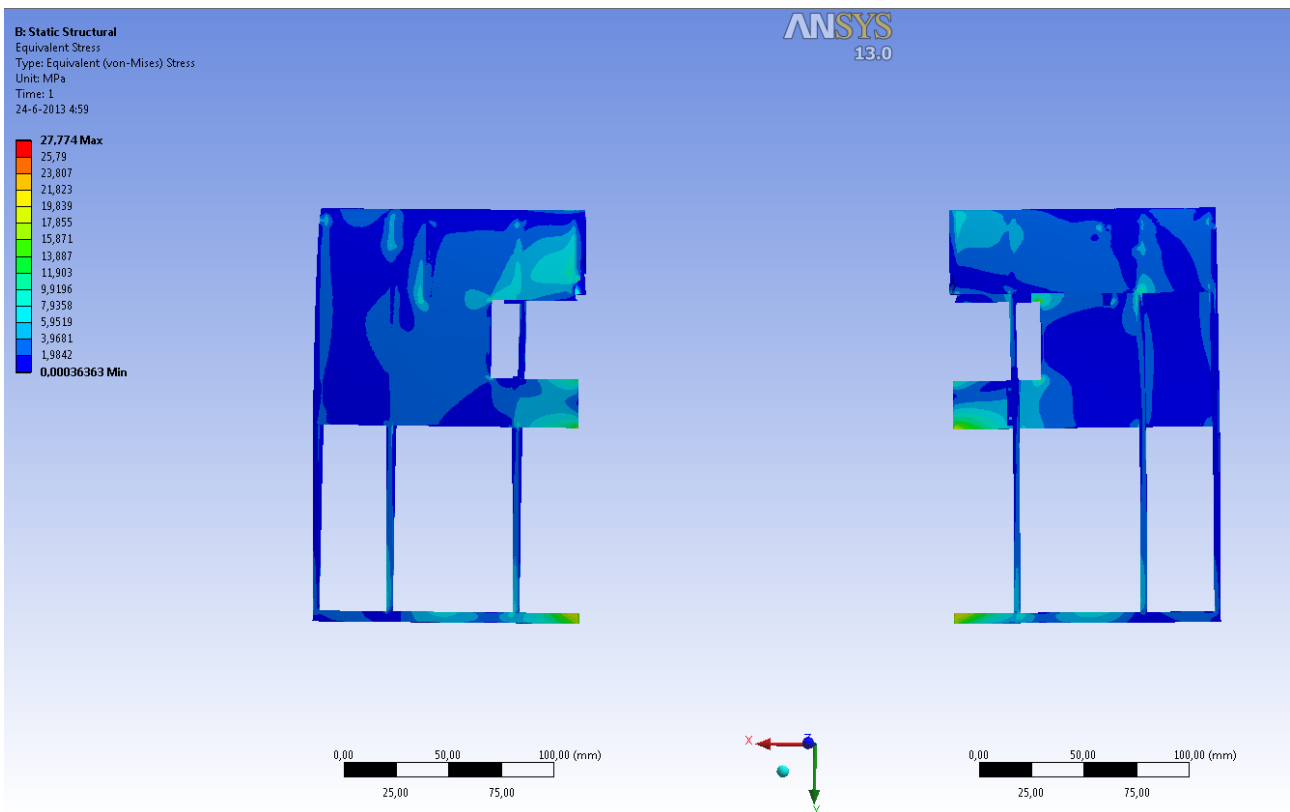


Figure 4.36: Finite Element Analysis, Equivalent (von-Mises) Stress, Midsection

Table 4.8: Finite Element Analysis Results

Solution	Value	Unit
Total Deformation	0.4558	[mm]
Directional Deformation (X/Y/Z)	0.0363/0.0261/0.4856	[mm]
Equivalent Elastic Strain	$0.391 \cdot 10^{-3}$	[mm/mm]
Principal Elastic Strain (min/max)	$2.81 \cdot 10^{-7}/0.445 \cdot 10^{-3}$	[mm/mm]
Maximum Shear Elastic Strain	$0.551 \cdot 10^{-3}$	[mm/mm]
Equivalent Stress	27.8	[MPa]
Principal Stress (min/max)	10.1/39.3	[MPa]
Maximum Shear Stress	14.7	[MPa]

4.3.6 Materials

As has been explained before, the structure will consist out of a 3D-printed skeleton and a skin wrapped over it. The MAV is designed to show swarming, which means that at least six MAV's have to be produced in a short time period since the competition starts on 17 September 2013. Therefore, 3D printing is ideal for this since it saves a lot of production time and it also allows the designer to design a more complex (efficient) structure. It also allows the designer to integrate all the payload in the structure. A disadvantage of 3D printing is that the structure can become relatively heavy because of its minimum printing thickness and its relatively heavy material (950 kg/m^3 for PA2105). The 3D printed skeleton will provide the required stiffness and strength to the structure and it will define the shape of the airfoil. However, due to the geometry of some parts of the structure, printed materials are not always able to meet the stiffness requirements as proved in the analysis section. In this case, carbon fiber tubes will be used because of their high stiffness (and strength) to weight ratio. A skin will be used to wrap over the 3D printed skeleton structure to save weight and allow for the morphing. This section will discuss the process of material selection for the structure and it will give an overview of the material properties. First the skeleton and then the skin will be discussed.

Skeleton Materials

For the skeleton, it is decided that the Selective Laser Sintering (SLS) method will be applied, since it allows for rapid production. For the SLS method only a couple of different materials can be used. The main provider of these materials is e-Manufacturing Solutions (EOS), and thus the list of SLS materials are obtained there [24], and is shown in Table 4.9.

Table 4.9: Material Properties SLS Materials (x/y/z)

Product	Polymer	Tensile Strength [Mpa]	Tensile Modulus [Mpa]	Strain at Break [%]	Density [kg/m^3]	Specific Strength [$(\text{Gpa} \cdot \text{m}^3)/\text{kg}$]
Alumide	PA12-MD(AI)	48/48/	3800/3800/	4	1360	35.3/35.3/
CarbonMide	PA12-CF	72/56/25	6100/3400/2200	4.1/6.3/1.3	1040	69.2/53.8/24.0
EOS PEEK HP3	PEEK	90/ /	4250/ /	2.8	1310	68.7/ /
PA 1101	PA11	48/48/48	1600/1600/1600	45/45/30	990	48.5/48.5/48.5
PA 2105	PA12	54/54/54	1850/1850/1800	20/20/15	950	56.8/56.8/56.8
PA 2200	PA12	48/48/48	1650/1650/1650	18/18/4	930	51.6/51.6/51.6
Balance 1.0						
PA 2200 Performance 1.0	PA12	50/50/50	1700/1700/1700	20/20/10	930	53.8/53.8/53.8
PA 2200 Speed 1.0	PA12	48/48/42	1600/1600/1550	18/18/4	930	51.6/51.6/51.6
PA 2200 Top Quality 1.0	PA12	52/52/52	1800/1800/1750	20/20/7	930	55.9/55.9/55.9
PA 2200 Top Speed 1.0	PA12	45/45/38	1500/1500/1500	18/18/3	930	48.4/48.4/40.9
PA 2201	PA12	48/48/	1700/1700/	15	930	51.6/51.6/0.00
PA 2202 black	PA12	50/50/48	1850/1850/1800	12/12/6	980	51.0/51.0/49.0
PA 2210 FR	PA12 FR	45/45/41	2500/2500/2300	5/5/3	1060	42.5/42.5/38.7
PA 3200 GF	PA12-GB	51/51/47	3200/3200/2500	9/9/5.5	1220	41.8/41.8/38.5
PrimeCast 101	PS	5.5/ /	1600/ /	0.4	770	7.1/ /
PrimePart r PLUS PA 2221	PA12	47/47/40	1650/1650/1600	16/16/4	930	50.5/50.5/43.0

The properties are, due to their layer-by-layer production, to some extent dependent on the direction. This has to be considered when designing the part and defining the building orientation. From this table, the material PA2105

is selected. This material has a high specific strength and specific stiffness. There are a couple of other materials that have higher specific properties, but the minimum printing thickness of 0.7 mm is too thick to use the materials optimally. These materials have a higher density and for the same volume, they will have a higher weight.

The diameter of the rotation axis of the morphing part can only be very small as has been discussed before. The reason for this was that the axis had to be mounted as much to the front as possible for controllability reasons. To prevent wearing out the 3D-printed material of the mid-section, it has been decided to use bushings. This however, reduces the maximum available outer diameter of the hinge axis to 5.5mm. To keep the response of the morphing structure predictable (no excessive deflection and rotation causes by aerodynamic loading), it has been decided to use a carbon fiber rod as hinge axis because of its high stiffness to weight and strength to weight ratio. The disadvantage is that the morphing part is not fully integrated. Now, a glued connection is necessary. For the glued connection, Scotch-Weld can be used with a shear strength of approximately 20 MPa [25].

As has been described above, the landing system should be detachable for transportation and operational reasons. The attachment to the airframe is made using a threaded connection into an adapter that is glued in the airframe. For the adapter, the same glue can be used as for the rotation axis of the morphing part. The threaded connection mechanism is designed as small as possible and it has been decided to use steel for these parts. The parts will be produced using a lathe. Tapping this size in steel is much easier than in, for example, Aluminum 7075-T6. Another reason for choosing steel is the fact that a threaded connection this small will easily fail on shear. It will already fail when one turns it too tight. The landing sticks itself will be 3 mm pultruded carbon fiber rods. The attachment can be seen in Figure 4.37 and the material properties of the materials in Table 4.10.

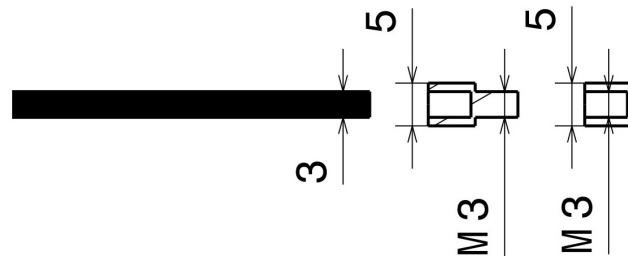


Figure 4.37: Attachment of the Landing Sticks to the Body

Skin Materials

Now that the material of the skeleton has been discussed, the material for the skin should be selected. Aircraft with morphing wings have been produced before. An example of such an aircraft is the X-53. This aircraft, however, still uses hinges and all the components are made of a solid material. Looking at the movement of the morphing wing of the MAV, it is evident that the material to be used has to be elastic and flexible. The flexibility of a structure is a function of the material and of the shape of the structure. When the 3D printing material discussed above is also used for the skin, the skin can be quite flexible, but the material itself is not elastic.

In order to pick a skin material, it is important to understand the exact movements of the morphing wing in order to determine the required characteristics of the material. The morphing of the MAV is basically a twisting motion since the cross-sections of the wing, the airfoil shape, remains the same during deflection. It will be a linear transition from the airfoil position at the edge of the midsection of the wing to the position of the airfoil at the tip of the wing (assuming the material is flexible). Also, the aerodynamic loads are acting on the wing skin. Combining all these requirements the important properties for the skin become [26]:

- Flexibility
- Elasticity
- Strength, strong enough to carry the aerodynamic loads
- Abrasive resistant, scratches/impacts the skin should be resisted
- Environmentally resistant, conform the environment described at the beginning of the chapter
- Tear resistant, able to have holes in the skin without tearing

The requirement that the skin has to be flexible is present because this is the only way linear morphing can be achieved. If the skin would be too stiff, the skin would behave as if it is clamped at the edges of the morphing part. The flexibility requirement is not difficult to achieve. As has been explained before, the flexibility of a structure is a function of the material and of the shape of the structure. Since the shape is a skin, the thickness is so small that actually almost all materials provide the required flexibility, even metallic ones.

The elastic requirement is the most important one for the selection of the skin material. It is important that no plastic deformation occurs. If this occurs, the skin will be permanently elongated and when it returns to its initial position, it will have excess material that will cause additional drag. Using simple trigonometry, it is calculated that

the skin has to elongate 3.17 mm, which comes down to 1.51 % elongation, for a morphing angle of 10 degrees. This maximum strain occurs at the trailing edge of the morphing wing. For many materials this strain is high and for materials with a high Young's modulus, this will also require a lot of force. This force has to come from the torque of the servo. Since the torque of the servo is limited and a higher torque requires a heavier servo and/or more power, it is important that this force is minimized.

Elastomer's are polymers with good elasticity properties, a low Young's modulus and a high failure strain. Especially the class of thermoplastic elastomer's called thermoplastic polyurethane (TPU) provide great morphing characteristics. "The Alliance for the Polyurethane Industry" describes TPU's as "bridging the gap between rubber and plastics", since TPU's offer the mechanical performance characteristics of rubber but can be processed as thermoplastics. This special niche of TPU's among other polymers and elastomer's imparts high elasticity combined with high abrasion resistance [27].

Three suitable skin materials are listed below. It is hard to choose on of them since the exact requirements for the skin are unknown, but Platilon U04 seems to be the lightest material with the required properties.

- Platilon U04, [28]
- SL200, SL700 or SL800, [29]
- Tecoflex 80A, [30]

4.3.7 Designed Structure

This section will conclude the structures and materials chapter. The final structure of all MAV's will consist out of a 3D printed skeleton using the Selective Laser Sintering method with the material PA12. Because PA12 is quite flexible it will deform under loads. For this reason, there has been decided to make the rod acting as the rotation axis for the morphing part from carbon fiber. To reduce the weight of the aircraft, the skin will be made out of a thin skin. For the skin a thermoplastic polyurethane called Platilon U04 has been selected. This foil combined the required flexibility and elasticity with good material properties.

An accurate load case with careful chosen safety factors has been setup and using this load case, some simplifications and elementary formulas a first estimation of the sizing of the structure and the landing system has been made. Using a more advanced program a Finite Element Analysis has been performed in order to verify the hand calculations and in order to make sure the structure does not fail under the exact (more complex) load case. The result of this analysis was that the current structure was capable of handling all loads. The landing stick is designed to be detachable and the stick will be a 3 mm pultruded rod. The table below summarizes the material properties. In Appendix F a technical drawing of the structure can be found.

Table 4.10: Summary Material Properties [24], [31], [28]

Material	Density [g/cm ³]	Young's Modulus [MPa]	Tensile Strength [MPa]	Strain at break [%]
PA12 (PA2105)	950000	1850	54	20
5.5mm pultruded carbon fiber rod	1.40 - 1.55	40000 - 60000	500 - 800	-
Thermoplastic Polyurethane film	1.17	-	6-7 (at 50% strain)	650

4.4 Propulsion

The propulsion system is an important factor in the design of the MAV since it provides the necessary thrust in horizontal and vertical flight. The system consist of a propeller, electrical motor, a controller which controls the speed of the motors and the battery. Since the total weight of the aircraft is largely affected by the propulsion system and the design of the system is based on an initial weight estimation, it will be a strongly iterative process. The propulsion system is discussed in this section, which is divided in several subsections. First, a brief explanation is given about how the propulsion system works and how the subsystems are all inter-related with each other. Then, the constrains for the design are discussed followed by the a description of the used design approach and the design choice.

4.4.1 Components of the Propulsion System

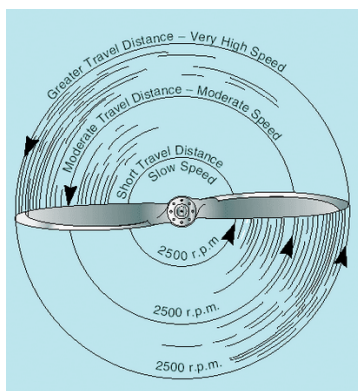
First, some general information about how the four systems of the propulsion system work and how they are interrelated, starting with the propeller theory, the working of the motor, the battery and finally the motor controller which plays an important role in the control of the aircraft.

Propeller

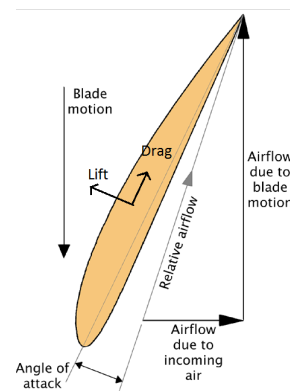
The working of a propeller blade is similar to a wing of an aircraft, producing both lift and drag. The higher the angle of attack of the propeller blade, the higher its generated lift and drag. With the propeller rotating around fast, the free-stream velocity component relative to the blade is not in flight direction but in the rotational direction, which creates lift in the direction of flight, also called thrust, as seen Figure 4.42.

Also seen in this figure the radial velocity at the tips is increased, which means that the relative velocity is directed almost completely in the direction of the rotational plane. In hover, for example, the flight speed is zero which means that the radial velocity determines the relative velocity. In horizontal flight, however, the relative velocity is more directed towards the velocity of the aircraft.

Just like the airfoil of an aircraft, the airfoil of the propeller blade will stall at certain angles of attack, depending on the speed it is flying at and the rotational speed of the propeller. This is due to the relative velocity which at the wing tips is mainly affected by the rotational motion and at the wing root by the flight velocity. The difference means that the airfoil angle should differ along the wingspan in order to avoid propeller stall. This difference in angles is called propeller pitch. If the pitch is changing along the chord it is called twist. In order to avoid propeller stall and have an efficient thrust generation, the propellers have a pitch and twist which are optimized for the specific flight conditions.



(a) Velocity Distribution over the Propeller [32]



(b) Side View of Propeller Showing the Relative Velocity [33]

Figure 4.38: Working of a propeller

Motor

The motor is the part that provides the power to rotate the propellers. Due to the given requirements, an electric motor is used which employs magnetic coils to turn the axis. The specifications of these motors are usually expressed in the amount of revolutions per minute per voltage (KV), the efficiency, the maximum amount of current it can draw and the weight. There are two different kinds of electric motors, brushed and brushless motors. They both make use of an alternating voltage but the brushed motor has coils on the axis and the brushless has poles on the axis with coils around it, seen in Figure 4.39. They both have advantages and disadvantages but the brushless motor is more efficient and is able to fly at all speeds (with rated load) which makes it more suitable for this design [34].

When selecting a motor, one should look at the KV value. With a high KV the coils have more/thicker windings which will carry a higher voltage at lower amps, producing a higher torque needed for bigger propellers. For low KV values it is the other way around and it is usually used for smaller propellers because of the lower torque requirement (low loads) and the high thrust requirements. This is dependent on the kind of propellers used and the battery voltage which influences the revolutions per minute (RPM).

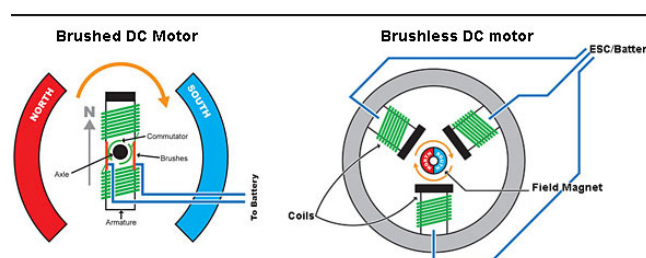


Figure 4.39: Difference between the brush and brushless motor [34]

Battery

The battery provides the entire system with power, but for the propulsion system it also determines how many RPM the motor can operate at. This depends on the voltage of the battery, which increases when more cells are added. This means that the voltage of the battery determines the maximum RPM that can be made. This number of RPM gives the static thrust, efficiency and power of the system and these are the main criteria for the design of the propulsion system

Electronic Speed Controller (ESC)

The disadvantage of the brushless motor is that it requires an electronic speed controller which determines the power translated to the motor. The motor controller has 3 connections: one towards the motor, one from the battery and one from the autopilot to the controller. It gets a constant voltage from the battery and the autopilot and motor determine what to do with it. This depends on the load on the motor (the larger the load, the more current it draws) and also on the required number of RPM from the autopilot and the actual amount of RPM. The voltage from the battery is converted in signals to the motors, the higher the frequency the more power is given.

The signal processing is complicated since it uses pulse width modulation which communicates the amount of power required with the width of the signals. For example, if the autopilot wants more thrust it sends a wider pulse which tells the controller to change the frequency of pulses to the motor. This method introduces the possibility to change the average voltage and let the motor run at different speeds. Since the autopilot gives signals at a frequency of 400 Hz the ESC should be able to handle these pulses.

A motor controller often has a battery eliminator circuit (BEC). It transforms the high voltage to a lower voltage by dumping heat. This unit is needed to power the other electric systems that are operating at lower voltage. Testing needs to be performed on how hot the units are going to be.

4.4.2 Constraints

Several constraints limit the design of the propulsion subsystem. These constraints are shown in Table 4.11 and result from earlier design decisions. The maximum propeller diameter results from the design lay-out and it depends on where the propellers are placed. If the propellers are placed in the middle of each half-wing the maximum dimension is 8 inches because of the minimum distance needed between them. However, placing them towards the tip increases the maximum dimension will be about 18 inches. This increases the size of the MAV significantly which reduces the points on the competition and has therefore be avoided.

It is important to not exceed the weight budget to much, because otherwise the design of the propulsion system should be iterated again. The weight of the total propulsion system is an important factor, but also the weight of the battery. The weight of the battery determines the capacity that can be used, which should not exceed the capacity of the propulsion system plus a buffer for all the other electrical systems. The capacity needed depends on the flight time of each flight mode, the efficiency of each flight mode and the amount of battery cells that are used. The buffer is taken to be 150 mAh that leaves 1150 mAh for the propulsion system since the weight of the battery will give 1300 mAh. In section 4.5 the buffer will be verified. The total weight of the propulsion system is estimated to be 90 grams.

Table 4.11: Constraints for the Propulsion System

System	Constraint
Propeller	Max dimension 16 inch
Weight	90 gram
Maximum capacity used during the mission	1150 mAh
Cruise speed(Drag)	13 m/s

4.4.3 Design Approach

In order to design the propeller for both vertical flight as horizontal flight and for a certain cruise speed it is important to get a feeling of the numbers for the parameters to perform a trade-off. For example, if a high cruise speed is preferred the diameter of the propeller should be kept small, whereas larger blades are required for more thrust during vertical take off. Due to the difference in velocities between cruise flight and vertical flight, the angle of attack of the propeller blade differs, which means that an optimal design can only be achieved with a variable pitch propeller. This, however, requires a heavier and more complex propeller, and is therefore not feasible. Because the pitch angle in vertical flight needs to be kept small while the it needs to be high in cruise flight, the propeller design has to be optimized for the least power consumption over the entire mission.

Since the design is optimized for endurance, the trade-off is based on the efficiency of both fly regimes. The efficiency of the propulsion system for a hybrid aircraft can be checked with the total energy required for the entire mission, expressed in mAh of the battery.

To calculate the total energy required for the propulsion system a combination should be made of power required for cruise and power required for vertical flight along with an estimation of flight times. First, an estimation for the thrust needed for both flight conditions is made with a rough indication of the time that the MAV spends in the respective mode. During cruise flight, the thrust is simply equal to the drag. However, to estimate the thrust needed for vertical flight, different opinions exist. For hovering flight, lift has to counteract the weight and the drag created by the propellers, but to ensure a stable climb more thrust needs to be provided (especially in this design where the rotors control the aircraft).

The MAV design therefore requires a thrust-to-weight ratio of two in order to ensure that the aircraft can climb at an acceptable rate in vertical flight [35]. Higher thrust to weight ratio's can be used to perform aerobatic flights, but this is not beneficial in this case because of the endurance requirement. To summarize, a thrust to weight ratio of 2:1 is needed in vertical flight and for cruise thrust needs equal to drag. An estimation of the drag is given in section 4.1 and does not take into account the drag developed by the engines. The time spend in each flight condition is assumed to be 8 % in hover, 4 % using max thrust, and 88 % in cruise. The following requirements need to be accomplished by the propulsion system:

- Able to provide 800 grams of static thrust
- Able to fly the cruise speed
- Should not be heavier than 90 grams
- Should not use more than 1150 mAh
- Propeller diameter should not overlap each other

When designing the propulsion subsystem the first step is to pick a propeller that is capable of providing the static thrust required, flying at cruise speed and is overall efficient for the mission. The propeller data itself is not enough to perform this calculation, because it also depends on the rotational speed of the motor and the voltage the motor is getting from the battery. This is because the motor has a big impact on propeller properties like pitch speed and static thrust. A program called Drive Calculator is used to select the appropriate propeller, taking the battery(voltage), motor, power regulator into account to compute the properties of the propulsion system (see Appendix D). It should be remembered that the behaviour of the propeller is non-linear and that it is really hard to predict the exact behaviour. The interaction of the propeller with the airflow is non-linear due to the highly unpredictable airflow and the changing blade properties over the chord. Therefore a classical blade-element/vortex formulation is used to calculate the desired properties with the use of the circulation of the flow [36].

Working with this program gives an insight in how the input parameters (size, weight, power, cruise speed) influence the design. Generally, the bigger the propeller the better the efficiency to provide static thrust but the lower the maximum speed. With a larger pitch the system is more efficient for high speeds whereas lower speed require a lower pitch angle in order to ensure that the propeller does not stall. The program also produces a graph which shows the thrust versus power versus efficiency to estimate the power required at different thrust settings. In Appendix D the layout of the program is shown.

The strategy for finding an appropriate propulsion system is to choose a propeller diameter and pitch with a comparable battery voltage, capacity and weight budget(1300 mAh, 80 grams) and a maximum motor weight of 40 grams each. This still gives a lot of results for the possible motors, but these are filtered on the main requirements for power, speed and static thrust which results in several combinations of propeller and motor. Some of these require less power for cruise and others less power for hover. Since hover requires approximately 10 times more power than cruise and a high propeller pitch increases the power required dramatically, the best hover propeller is chosen. One important factor to verify is how fast it can fly when the motor gets a lower voltage to fly at cruise, and what the top speed is going to be. This is especially important to consider since it is difficult to estimate the drag that is added by the propellers to the total drag of the wing.

4.4.4 Subsystem Selection

Using the Drive Calculator for analysis, a propeller with a diameter of 7 inches is chosen because at this dimension the static thrust is still high enough and only the power required is higher than when using larger diameters. A propeller pitch of 7 inch gives a good performance in cruise flight and still enough static thrust at a higher RPM. For the competition 1300 mAh is required with this specific combination which is just within the constrains. This together with the motor "Suppo 2804/14" gives the final results as shown in Table 4.12. These results are only for static thrust and one motor. With the big propellers it is hard to fly fast and provide a small amount of thrust and since the program calculates the pitch speed and not the cruise speed it is something that needs to be checked with the actual design. The torsional constant of the motor is 0.659 Ncm per Ampère and the KV is 1412.

The maximum current of the motor is 12.6 Ampères, so a motor controller (ESC) has to be able to handle at least 13 Ampères. However, as shown in Figure 4.40b, it can be slightly higher due to other loading on the propellers. This is why a re-programmable 18 Ampère motor controller with a reaction speed of 400 Hz is used.

Table 4.12: Specification of One Motor at Maximum Thrust and Cruise

	Maximum Thrust	Cruise
Power required(W)	132.7	11.4
Ampere(A)	12.6	2.9
Static Thrust(g)	384	76
Motor Weight(g)	30	30
Prop speed(RPM)	9968	4609

The final results for cruise and maximum thrust are shown in Figure 4.40a and Figure 4.40b containing the efficiency and power required at every thrust setting. The graphs change when the voltage is changed. This means that when there is more wind/drag the RPM drops and the current draw is larger. So first the thrust needs to be determined for the flight conditions which gives the voltage/RPM needed and then the current can be seen from the graphs. From this the power required is estimated. In the cruise condition the drag is estimated to be around 80 grams using a buffer of 1.5 which gives a power needed of 11.4 Watt during cruise. This power consumption should be checked with a prototype which will give us the velocity and the real thrust needed. The final design is a trade-off for both flight conditions since these requirements can only be fulfilled when the pitch and the diameter are high enough.

Weight

The selected controller is the "Turnigy Plush 18 A" with a weight of 19 grams for each engine. The propeller used is the Aeronaut E-Prop 7x7 with a weight of 2 grams and the motor as seen in previous section weights 30 grams. These values are only for one configuration and there are two so the total weight of the propulsive system is 102 grams.

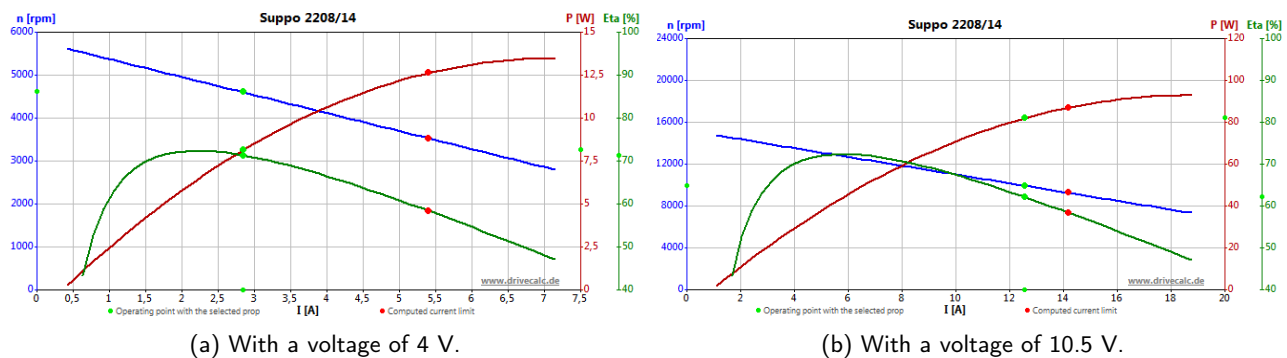


Figure 4.40: Load Diagrams, the Green Points Represent the Design Points

4.4.5 Verification and Validation

The propulsion system is a complicated system and therefore it should be checked if it works as expected. There are multiple points that need to be verified: The time it can fly in different modes when operating at the competition, the top speed of the vehicle and the thrust it can provide.

Verification

To verify the results a calculation will be performed to get a rough estimation of the thrust at different velocities. For this a configuration in the Drive Calculator is used where the propeller constants are already calculated or given by manufacturer. With the constants of the propeller the behaviour at different velocities can be estimated with a simple calculation. This results should comply with the outcome of the program.

Validation

For the validation a thrust set-up is made that shows the static thrust of the configuration. In this case a 400 grams wooden block with the motor attached to it. Finally, put maximum power on the motors and see if it is able to lift the block. With this set-up the motor controllers also are tested on the amount of heat they produce.

The top speed is checked with a prototype that is build from foam. This gives a rough estimation if the vehicle is able to fly at cruise speed and how fast it can go. This prototype is also used to test the power requirement for the competition flight plan.

4.5 Power Supply

One of the main requirements for the system was that enough electrical energy should be supplied. There are different types of batteries and the main criteria is the specific energy, since it will determine the mass of the battery for a certain power output. The current and average voltage during discharge, which is dependent on the circuit of the battery cells, are also important when selecting the battery. Another criterion is the energy density which influences how much size the battery needs depending on the power (Wh/L). The first section deals with the choice of the battery type and the second section describes its weight and size estimation.

4.5.1 Type of Battery

Since the specific energy is the most important criterion, a Lithium-ion polymer (LiPo) battery will be used. The LiPo battery is a rechargeable battery with a specific energy ranging from 130 to 200 Wh/kg and energy density ranging from 300 Wh/L. Shapes and sizes vary widely and can be chosen specifically for the system. The LiPo battery has a high open circuit voltage in a range of 3.2-3.7 V [37], which means a high amount of power can be supplied at low current. The LiPo battery is very often used in radio-controlled aircraft because the suitable characteristics, making it a reliable choice.

4.5.2 Sizing the Battery

To size the battery the needed capacity has to be known, enabling a weight and size estimation. The capacity of a LiPo battery is usually expressed in mAh and is dependent on drawn power, voltage and time. In section 4.4, a rough time estimation of the different flight conditions in the competition is given. The different flight times and the power required by the propulsion system and other subsystems are given in Table 4.13.

From this, the energy needed is derived and the capacity is calculated. Because a high voltage is beneficial for the propulsion system and for the capacity required, a LiPo battery with 3 cells is chosen. This will give a battery voltage of 11.1 V which was needed for the propulsion system and for the capacity required, see section 4.4.

The power required by the payload is estimated to be 5 W in section 4.15. This together with the power requirements for the propulsion system gives the total capacity needed for the mission that is calculated in Table 4.13. The total amount of capacity that need be provided by the battery is 1298 mAh. With these constraints there is still a lot of choice in battery dimensions, since the cell of a LiPo battery can have large differences in size and weight with the same amount of capacity. The placement of the three battery cells will be determined in the system integration.

The battery chosen for the design is the Turnigy 1300 mAh 3S 20C Lipo Pack. The battery is chosen due to the low weight and its small size. The specifications are listed in Table 4.14 [38].

Table 4.13: Capacity required

	Flight Time [s]	Power Required [W]	Capacity [mAh]
Maximum Thrust	45	265.4	301.6
Hover	100	96	242.4
Cruise	1055	22.6	602.1
Payload	1200	5	151.5
Total	2400	388.6	1298

Table 4.14: Specifications of Turnigy 1300mAh 3S 20C Lipo Pack

Feature	Value
Minimum Capacity	1300mAh
Configuration	3S1P / 11.1v / 3Cell
Constant Discharge	20C
Peak Discharge (10sec)	30C
Pack Weight	115g
Pack Size	81 × 36 × 21mm
Charge Plug	JST-XH

4.5.3 Verification and Validation

To verify the power supply system the compliance with the battery specification needs to be checked. It will be checked by visible investigation that the battery configuration is correct and that indeed three battery cells are connected in series. The dimensions of the battery are verified by measuring with a ruler and the weight is verified with a weighing scale. A voltmeter will be used to verify the voltage of the battery.

Because of the chemical reactions within the cells, the capacity of a battery depends on the discharge conditions such as the the current, the allowable terminal voltage of the battery and temperature [39]. The available capacity of a battery depends upon the rate at which it is discharged [40]. If a battery is discharged at a relatively high rate, the available capacity will be lower than expected.

To verify the capacity of the battery the battery will be discharged to an end point. For this a discharge resistor that takes at least one hour to discharge will be used. The minimum resistance can be calculated using Equation 4.33 [41].

$$R = (N_{cell} * 4000) / C \quad (4.33)$$

The resistor needs a resistance higher than this, but as close as possible, to decrease time to discharge the battery. The minimum resistor power needed can be calculated using Equation 4.34.

$$P = \frac{U^2}{R} \quad (4.34)$$

The battery voltage during the discharge is measured with a voltmeter. The resistor will be connected and a timer is started. The battery will be discharged to 3.2 V per cell, because the battery can be damaged by deep discharge [42]. The current is measured using an Ampé re meter and multiplying this with the time to discharge will give the capacity. The peak and constant discharge can also be found from these measurements.

The power supply subsystem is validated by proving the battery supplies enough power to all subsystems. This will checked by connecting all subsystems and investigating the power consumption.

4.6 Guidance and Navigation

This section describes the design of the guidance and navigation subsystem. The main devices of the guidance and navigation subsystem are the autopilot and the Global Positioning System (GPS), which are analyzed in the following subsections.

4.6.1 Autopilot

In order to have an autonomous MAV, it should be able to control itself independently. To make this possible, a control system (software) and associated hardware are required.

Because of the limited time of this project and to reduce complexity, it has been decided to use an open source, open hardware autopilot system. When comparing different open-source autopilot systems, it becomes clear that the right choice for this project would be Paparazzi. Paparazzi has a large professional community and it is one of the most advanced autopilots available. Furthermore, the Paparazzi system pays a lot of attention to safety and works for both rotorcraft and fixed-wing aircraft. On top of that Paparazzi is also used and developed within the faculty of Aerospace Engineering at the TU Delft and hence there is a lot of experience with Paparazzi within the faculty.

When selecting the autopilot hardware it must ensured that the autopilot runs on Paparazzi software. Computationally intensive tasks like video processing are not considered when selecting the autopilot, since none of the autopilots suffices to perform these tasks. Therefore, no real attention is paid to the microprocessor and its clock speed, flash and RAM. An additional processor board is included to deliver the needed computational power.

The Lisa/M v2.0 is selected as the autopilot for the MAV. The trade-off criteria used for its selection were availability, weight, size, type of MCU and the integration of the barometer and IMU. The Lisa/M has a newer STM32 series processor compared to other autopilots. Furthermore, it has been used by the university before, has an integrated aspirin IMU with magnetometers, an integrated barometer and has a small size with a weight of only 10.8 g with the Aspirin IMU mounted. The features of the Lisa/M v2.0 with Aspirin IMU are stated in Table 4.15.

4.6.2 GPS

In order to navigate around the terrain, the MAV should must know its position and the location of its destination. To ensure this, a GPS receiver will be integrated in the design since it is lightweight, more accurate than accelerometers and simple. The Lisa/M v2.0 board is able to process the data from the GPS receiver.

Many different GPS receivers exist on the market, and after carrying out some research it became clear that a U-Blox model is a good choice for the MAV system [43]. The U-Blox GPS receiver is chosen because of its plug-and-play capacity and offers a great performance on speed, size and accuracy (± 1.5 m 50% of the time). The selected

Table 4.15: Lisa/M v2.0 with Aspirin IMU specifications [43]

STM32 microcontroller STM32F105RCT6 datasheet with 256kB flash and 64kB RAM
Pressure sensor BMP085
7 x Analog input channels
3 x Generic digital in-/out-puts
2 x 3.3V TTL UART (5V tolerant)
8 x Servo PPM outputs (only 6 if second I2C (I2C1) bus in use)
1 x CAN bus
1 x SPI bus
1 x I2C bus (2 x when using only the first 6 Servo PPM outputs)
1 x Micro USB
4 x status LEDs with attached test point
10.8 grams (with Aspirin IMU mounted)
34mm x 60mm x 10mm
4 layers PCB design
3 Axis Gyroscope
3 Axis Accelerometer
3 Axis Magnetometer
Barometer MS5611

type among the U-Blox GPS receivers is the NEO-6Q reference board with an in-built Sarantel GeoHelix high gain antenna.

4.6.3 Verification and Validation

To verify the guidance and navigation subsystem the compliance of the chosen hardware with their specifications has to be proven. The dimensions will be verified by measuring the size and checking the mass with a weight scale. The layout of the hardware will be inspected visibly. The proper operation of the autopilot is determined by installing the Paparazzi software and performing flight tests with the MAV. The GPS accuracy is tested before integration in the final design by positioning it on known geographical coordinates and comparing them to the output position to measure the error. This needs to be done repeatedly since the accuracy within 2 m is only promised for 50 % of the time.

4.7 Communication

The communication subsystem is an essential component of the aircraft as it is necessary to achieve the mission objective of performing an autonomous flight by using swarming behaviour. Autonomy and swarming require data exchange between the MAV's for traffic coordination and mission task coordination. The system has to ensure that all the MAV's in the swarm can communicate with the other vehicles and if needed with the ground station. Furthermore, a video stream on board three different vehicles needs to be shown to the audience at the ground station. In this chapter the communication subsystem requirements will be analyzed and the final design will be explained.

4.7.1 Requirements

To reach the mission objective a series of requirements have to be met. Weight, power consumption, range, data rate, frequency, cost and reliability are parameters that will determine the communication system design.

Weight

The most important requirement is the weight as it has a major influence on the complete design process. A larger weight would cause a snowball effect that will make other components of the aircraft heavier such as the battery and the propeller. Therefore, the requirement is to choose a design that minimizes the weight.

Power Consumption

The power consumption influences the battery size and weight. The design should be optimized to reach the lowest possible power consumption to avoid a large battery size and to increase endurance.

Range

By analyzing the mission the range can be estimated. The mission will be performed in a region with maximum dimensions of 800x400x50m. The maximum distance between two MAV's can therefore be calculated as the diagonal of the box which has a length of approximately one kilometer.

Data Rate

The data that will be communicated between MAV's depends on the swarming algorithm used. The time between the tasks and the collaboration between MAV's will determine the frequency by which the task status will be communicated. The autopilot and the video streaming will be communicated over a different frequency range to ensure the lowest possible interference will occur. The autopilot should only focus on safe flight and not be overloaded by video information. Furthermore, separating the data will allow to optimize each link for a different data rate.

Paparazzi

In the section 4.6 the autopilot was chosen. The LISA/M autopilot uses the paparazzi system which has a very flexible message format [45].

In the paparazzi system the amount of parameters and the frequency can be tailored for the mission. The data of some messages can be decreased so that others can be increased. For example the period of the GPS data can be lowered when the speed is reduced and landing is initiated. For each different aircraft a different set of data can be selected depending on the mission profile.

For this mission the autopilot process is used. Therefore the process should be set to "Ap" (Autopilot). Each process will have a mode option. The mode determines the list of messages that will be sent and the period of each message. The mode can be changed during the flight plan. An example message is given below:

```
<process name="Ap">
  <mode name="default" >
    <message name="ATTITUDE" period="0.5" />
    ...
  </mode>
```

By analyzing the structure of each message more in depth it can be seen which information is actually sent. All the information is contained in fields. Each field will require a certain number of bits. If unit16 is specified this implies the length is 2 bytes. An example code is given below:

```
<message name="ATTITUDE" ID="6">
  <field name="phi" type="uint16" unit="deg"/>
  <field name="psi" type="uint16" unit="deg"/>
  <field name="theta" type="uint16" unit="deg"/>
</message>
```

In the header file "messages.h" the size of each variable can be found. In this file the size of the variables varies between 0 and 173 bytes. The message with the variable ATTITUDE given above has a length of 6 bytes as it is composed of three fields each of type unit16.

During the competition three different groups of MAV's will exchange information. The TCAS module (explained in section 5.3) will send information very often to avoid collision between aircraft whereas the Dropball module (explained in section 5.3) will only send information about the status and location of the waypoints. The location of the waypoints will only be communicated four times to each aircraft. Therefore, the Dropball module will not determine the data rate of the communication network.

The telemetry file for the mission contains the set of periodic messages that are sent over the downlink channel to the ground station. It will include the minimum amount of messages sent every minute. The messages differ between a rotorcraft and a fixedwing. For the final design the telemetry message based on a rotorcraft aircraft has been chosen as more information is required to analyze the performance during hover. An overview of this file is given in Appendix E. The data rate is the amount of bytes that each aircraft will send each minute. Most parameters are sent only once every second but the data regarding the flight plan, the GPS location and the integrated navigation system are sent four times each second as they are crucial for analyzing the flight parameters. Assuming that 10 aircraft will be used during the competition the total data rate will be of approximately 25 kbps.

Furthermore, it should be taken into account that a message sent by a modem device also contains additional information such as the sender ID and the message ID. If an XBee modem will be chosen the message will have the following format [46]:

```

XBee-message: ABCDxxxxxxxE
A XBEE_START (0x7E)
B LENGTH_MSB (D->D)
C LENGTH_LSB
D XBEE_PAYLOAD
  0 XBEE_TX16 (0x01) / XBEE_RX16 (0x81)
  1 FRAME_ID (0) / SRC_ID_MSB
  2 DEST_ID_MSB / SRC_ID_LSB
  3 DEST_ID_LSB / XBEE_RSSI
4 TX16_OPTIONS (0) / RX16_OPTIONS
5 PPRZ_DATA
  0 SENDER_ID
  1 MSG_ID
  2 MSG_PAYLOAD
  . DATA (messages.xml)
E XBEE_CHECKSUM (sum[D->D])

```

Previously the MSG_PAYLOAD data rate was analysed. It is estimated that the complete message will require on average at least one extra byte for each field adding 10 more bytes to the final message.

Video Streaming

One mission requirement is to show the audience three video streams of the flying aircraft. Video streaming requires a very high data rate. No requirements on the quality of the video are given therefore a low quality will be considered.

Frequency

During the competition a limited number of frequencies are allowed. The authorized frequencies can be found on the website of the competition and are the following [47]:

- 26 MHz, 41 MHz, 72 MHz: max power 100 mW
- 2.400 GHz to 2.454 GHz and 868 MHz: max power 100 mW
- 2.455 GHz to 2.483 GHz : max power 10 mW
- 5.8 GHz: 25 mW

Reliability

The system should be very reliable, thereby implying that the network should preferably be self-healing and send messages until they reach the destination. The network should not depend on one MAV as failure of this single aircraft would then cause the whole swarm to be inoperative.

Cost

Cost should always be considered when choosing a design option as it might affect the final feasibility of the project.

4.7.2 General Overview of the System

By analysing the mission requirements a basic overview of the system can be derived. The first characteristic of this system is that all communication will have to be wireless. The MAV's will communicate data about position, altitude, speed and waypoints to the other vehicles by using a bi-directional radio link. Furthermore, three video streams are required for the competition. For this purpose three aircraft will be equipped with a video transmitter and the ground station will have a video receiver. To participate in the competition and for testing the aircraft a radio controlled link is needed. This link is called safety link and data will be sent from the ground station to the aircraft. The basic overview is given in Figure 4.41. Each communication link will be analysed separately in the following subsections.

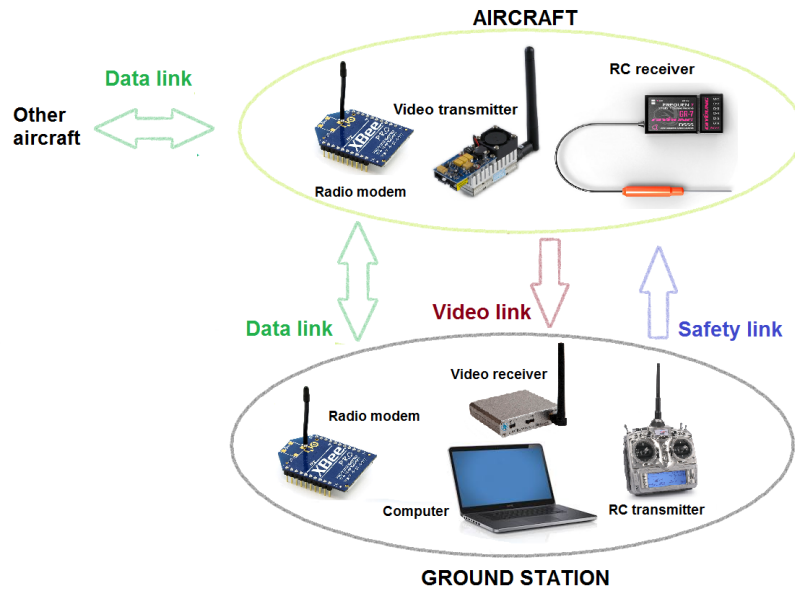


Figure 4.41: General overview of the communication subsystem

4.7.3 Data link

This link has to provide communication between the autopilots and the ground station. As multiple MAV's need to communicate at the same time this network will actually be quite complex. In the first part of this section the network topology and the network protocol will be explained.

Network Topology

The ideal option for swarming is a mesh network as it allows for connections between all nodes at all times. Mesh networking is used in applications where the range between two points may be beyond the range of the two radios located at those points. Intermediate radios are then used to forward on messages to and from the desired radios.

Network Protocols

For the mesh network topology a variety of protocols exists. In the following paragraph the ZigBee and DigiMesh protocols will be explained in detail.

ZigBee Protocol

ZigBee is a protocol that uses the 802.15.4 standard as a base and improves its features by adding mesh networking [48]. A useful feature of the ZigBee protocol is that the multiple radios will form a network automatically and will take care of a missing device as it has the ability to heal the network itself Figure 4.42a.

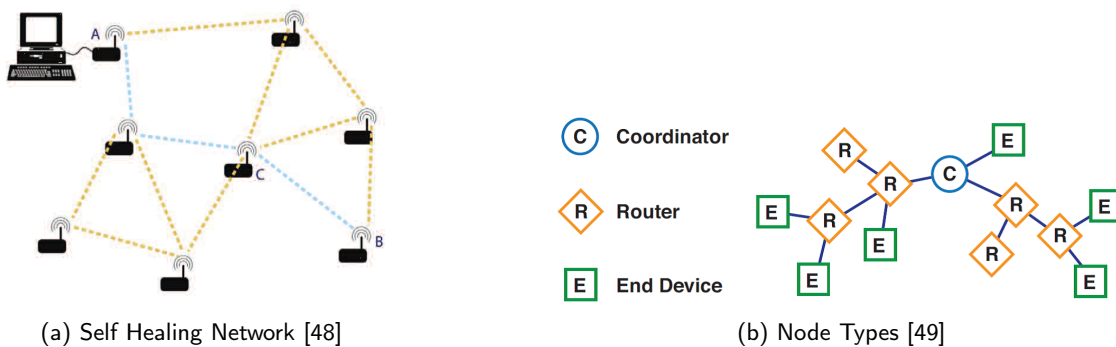


Figure 4.42: ZigBee

The ZigBee protocol is designed to ensure that if a number of different radios were deployed as in the figure above, the radios would automatically form a network without user intervention. If the radio at point C is removed in Figure 4.42b a new path will be created to route messages from A to B.

The ZigBee Protocol defines three types of nodes: Coordinators, Routers and End Device, with a requirement of one Coordinator per network [49]. The difference in roles is explained in the following section.

- Coordinators: There is only one coordinator in each network. It is the device that establishes the network originally and can store information about the network.
- Routers: act as intermediate nodes, relaying data from other devices.
- End Devices: can only talk to the coordinator and the routers and cannot relay data. It is therefore a device that has a low power consumption.

DigiMesh Protocol

DigiMesh is a homogeneous network with only one node type (see Figure 4.43) [49]. In this network there is no dependency between nodes. All devices can be configured to sleep when they are not in use reducing power consumption and thereby increasing battery life. DigiMesh is a more reliable solution as it does not depend on the coordinator. In this protocol if any point in the network fails another node will take over its task, making the network autonomous.

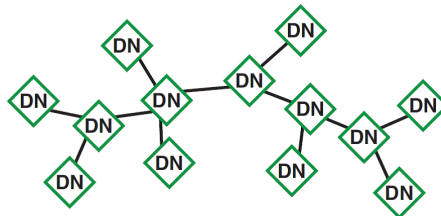


Figure 4.43: DigiMesh Node Types [49]

Design Choice

The XBee 865/868LP has been chosen as a radio modem for the MAV's. The modem characteristics will be explained in this section [50].



Figure 4.44: XBee865/868LP [50]

The weight of this device is approximately four grams. The maximum range of the network is up to 4 km if the low data rate mode is chosen. If all aircraft in the swarm are operating the data rate will be around 25 kbps therefore the high data rate has to be set decreasing the range. However this will not be a major issue as the required range is 1 km and a mesh network will be used. If a mesh network is used the maximum range will decrease as all nodes can relay data and act as intermediate beacons. Furthermore, the smaller the range the better as the signal strength which would allow for using a smaller antenna.

The XBee 868LP operates on the 868 MHz frequency band. This is ideal as it allows for transmitting the video streaming on the 2.4 GHz frequency. The XBee 868LP implements LBT (Listen Before Talk) and AFA (Automatic Frequency Agility) [50]. The advantage of using both LBT and AFA is that the radio can bypass the Duty Cycle requirement imposed by European Telecommunications Standards Institute (ETSI). Before transmitting the radio will listen to see if data is being sent over the channel. If the channel is in use then the radio will listen to be able to receive the data. After the radio transmits on a channel, it will not transmit on that channel again until the minimum transmitter off time has been met, which is greater than 100 ms. For this reason it is useful to have many channels, so transmissions are not delayed.

There is a requirement from the ETSI that only 100 seconds of transmission may occur over the period of an hour on 200 kHz of spectrum. This implies that the more channels are used the more transmission time is available. The effective duty cycle can be calculated based on the number of available channels enabled with the following equation:

$$\text{Effective Duty Cycle} = \frac{\text{Number of Channels} \cdot 100}{3600} \quad (4.35)$$

If all 30 channels of the XBee 868LP are used the Effective Duty Cycle would be:

$$EDC = 30 \cdot \frac{100}{3600} = 0.83 \quad (4.36)$$

This means that you can transmit 83% of the time in one hour. This implies a 100% duty cycle over a period of 30 minutes.

The XBee 868LP is also very reliable as it uses the the Carrier Sense Multiple Access Collision Avoidance (CS-MACA) [51]. This prevents radios from talking one over the other which would cause corrupted data. Before transmitting data the modem listens if the channels is free, if the channel is in use the modem will wait for it to be free before sending data. If a data packet does not get through, the modem will send it again up to three times. The XBee is also a very flexible modem, as more than one protocol can be used. Both the ZigBee and the Digimesh protocol are suitable for the competition.

Antenna

The antenna for the XBee 868LP modem has to comply with certain requirements given on the data sheet of the modem. On the data sheet it is specified that the outdoor range is up to 4 km with a 2.1 dBi antenna, up to 1 km with a PCB embedded antenna [50]. The antenna option are also given namely U.FL RF connector, RF pad, Embedded PCB antenna. It is important to notice that the Embedded PCB antenna is only approved with 10 kbps data rate and not with the 80 kbps data rate.

To achieve maximum range it is preferable to have a dipole antenna as this antenna can be connect to the U.FL and has a gain of 2.1 dBi. The chosen antenna for the XBee 868 series 8 is the Digi Antenna - 868 MHz, half wave, 2.1 dBi, RPSMA male, articulating (product: A08-HASM-560) [53]. The weight is 11 grams. However this weight can be decreased to approximately 4 grams by breaking the plastic casing around it and eliminating everything except the coaxial cable. Eliminating the casing will not have a major effect on the antenna performance.

An antenna with a vertical shape radiates perpendicular to the pointing direction meaning it will radiate across the horizon. During the system integration this should be considered. Also the location of the antenna should be carefully chosen as metal object might cause the signal to reflect reducing the antenna efficiency.

At the ground station a dipole antenna with a gain of 2.1 dBi, the same type as the on board antenna, will be used and tested initially. If the dipole antenna will not provide enough gain a patch antenna will be used as this type of antenna has a narrow bandwidth, a high gain and a large view angle.

4.7.4 Safety Link

The safety link should allow the operator from the ground to take control over the aircraft at any time. To guide the aircraft the operator has a radio transmitter and the aircraft is equipped with a receiver.

The safety link will operate on 2.4 GHz as this frequency allows to establish a unique connection between transmitter and receiver. On low frequencies such as the 72 MHz there are only a few channels available for transmission implying that only a few aircraft can fly at the same time without interference. At the competition multiple aircraft will be flying simultaneously. To prevent interference with other RC transmitters the 2.4 GHz frequency was therefore selected.

On the 2.4 GHz frequency spread spectrum technology can be used. This rather new development is based on embedding a digital signal on a frequency modulated radio wave and sending the signal over a broad spectrum [52]. Two modulation techniques can be applied to spread spectrum, namely Frequency Hopping Spread Spectrum (FHSS) and Direct Sequence Spread Spectrum (DSSS). The first technique sends the signal on a very narrow bandwidth and switches frequency very often, the second technique sends data on one selected frequency over a broad band. As the data is spread it is very difficult to intercept and the probability of transmitting on the same frequency channel becomes very low.

Radio Control Transmitter

The radio control transmitter has to provide control over at least five channels: roll, pitch, yaw, throttle and mode selector. The mode selector will be used to switch among the three paparazzi modes of Manual, Auto1 and Auto2. The transmitter that will be used during the competition is the Turnigy 9XR Mode 2 [54]. This transmitter operates on the 2.4 GHz frequency with 8 Channels. A special OrangeRX DSMX/DSM2 2.4 Ghz Transmitter Module has to

be connected to the transmitter to make it compatible with the DSMX protocol. DSMX technology is a wideband, frequency-agile 2.4 GHz signal protocol with advanced spread spectrum RC technology. It is an improvement of the DSM2 technology [55].



Figure 4.45: Turnigy 9XR Transmitter Mode 2 , [56]

Radio Control Receiver

The major design drivers for the receiver are low weight and small size. Furthermore, the receiver has to operate on the 2.4 GHz frequency and be compatible with the Turnigy 9XR transmitter. The selected Orange Rx R110X radio receiver complies with these requirements [58].

This device has a size of 27x19x10mm and a weight of less than 5 grams. It is compatible with the DSMX protocol and can be easily binded to the transmitter. This device is equipped with a short antenna with a length of 26 mm for transmission.

The binding process begins by inserting the bind plug into the battery socket and connecting the battery to one of the remaining sockets. As soon as the system is powered the led starts flashing to indicate the device is in binding mode. The transmitter bind switch can now be activated and the transmitter can be turned on. As soon as the led stays fixed the binding has been successfully completed.

The receiver has an UART output and can therefore be directly connected to the Lisa/M autopilot through one of the UART ports.



Figure 4.46: Orange Rx R110X [57]

4.7.5 Video Link

One of the requirements of the system of MAVs is to provide a live video link from at least three different aircraft. As this functionality is not essential for the successful completion of the mission but rather serves the entertainment of the audience and no quality requirements for the video are stated, the primary focus in the design of this subsystem was on low weight, small size and little interference with other subsystems.

The subsystem consists on the airborne side of an analogue camera, a video transmitter, an antenna and on the ground side of an video receiver with antenna and a computer or external screen to display the video. The integration of the subsystem is straight forward, as it operates independently of the other subsystem and does not require any adjustments. The different components simply have to be connected and the right channels selected. In the following a comparison of analogue and digital systems is given, subsequently the selected hardware is described in more detail.

Analogue vs. Digital

The main distinguishing characteristic of different video links is whether they use analogue or digital signals. The two signal types lead to different system properties that entail advantages and disadvantages. Digital video transmission

is significantly less sensitive to noise and greater ranges can be achieved. Furthermore, the signal can be encrypted to prevent unauthorized persons from accessing the video signal. Digital transmission usually requires more bandwidth than analogue transmission but compression methods can be applied to use the bandwidth more efficiently.

Analogue signals on the other hand, even when frequency modulated, are much more sensitive to noise and environmental influences, which reduces the range. However, analogue transmitters and receivers are less complex and are in production for a longer time at higher quantities. They are therefore available in smaller sizes at significantly lower cost and can be easier integrated into the system. The same is valid for analogue cameras.

Due to limitations in budget, development time and the better availability of analogue components in the required size, an analogue system was chosen.

Video Camera

Besides the requirement of an analogue output signal, the camera should also deliver a color video in order to visually please and entertain the audience during the competition. Other characteristics that positively influence the image quality are a high shutter speed, a high light sensitivity to prevent blurry images and a high image resolution. A large lens angle is also preferable as it gives the observer a better overview of the scene. Based on the weight, power consumption, availability and cost, the Mini Color CMOS Camera with Pinhole Lens was selected [59]. The camera characteristics are given in the table Table 4.16.

Table 4.16: Analog Camera selection

	Mini Color CMOS Camera
TV lines	380
Lux	1.5 at F1.2
Shutter	1/50-1/63000
Power	7-12V DC, 25mA
Dimensions (mm)	12 x 12 x 14
Weight (g)	3.3
View Angle (deg)	78

Video Transmitter

The analogue output signal of the camera is fed into the transmitter to be send down to the ground station via an antenna. The operating frequency should be in the 5.8 GHz frequency range, since the 2.4 GHz band is already used by the safety link and double assignment could cause interference. The maximum transmitting power is limited to 25 mW by regulations. Furthermore, the transmitter should have at least three channels such that three video streams can be operated simultaneously.

Due to its low weight and availability, the 200 mW 5.8 GHz A/V Transmitter distributed by FPV Hobby was selected [60]. The power output of the transmitter exceeds the allowed 25 mW but can be reduced using an attenuator or by alternating the transmitter hardware itself. The transmitter specifications are given in Table 4.17a.

Table 4.17: Video Transmitter and Receiver Specifications

(a) Transmitter

	200 mW 5.8 GHz A/V Transmitter
Frequency	5.8 GHz-8 channels
Tx power (mW)	200
Supply voltage (V)	3.3-5.5
Supply current (mA)	200
Dimensions (mm)	20 x 22 x 3
Weight (g)	2.2

(b) Receiver

	5.8 Ghz 8 Ch. A/V Receiver
Frequency	5.8 GHz-8 channels
Rx Sensitivity (dBm)	-90
Supply voltage (V)	12
Connections	Dual A/V output

Video Receiver

The requirements for the video receiver are based on the selected transmitter. It therefore needs to operate at a frequency of 5.8 GHz with at least three channels that match the ones of the transmitter. As the receiver is located on the ground its weight is only of minor importance and the focus in the selection process was put on price, availability,

receiver sensitivity and available connections. The 5.8 GHz 8 Ch. A/V Receiver from FPV Hobby is one option that fulfils all requirements [61]. Its specifications are given in Table 4.17b.

Antenna

Both sides of the video link require an antenna that is suitable for the used frequency of 5.8 GHz. The most important characteristics of the aircraft antenna are weight and an omnidirectional radiation pattern since the aircraft is constantly changing its orientation with respect to the ground station. Since the omnidirectional dipole antenna that is already connected to the transmitter fulfils these requirements and is light weight it will not be exchanged. The antenna is approximately 4.1 centimetres long and has a gain of 2.1 dBi.

As the transmitter is constantly in motion an antenna with a directional high gain will not be considered for the ground station. However, the gain of the ground antenna should be much larger than the aircraft antenna as weight is not relevant for the design. An important parameter is the view angle as the aircraft could be flying anywhere between the range specified by the competition area.

The antenna type which best matches these requirements at a frequency of 5.8 GHz is a patch antenna. This type of antenna has a narrow bandwidth, a high gain and a large view angle. The selected antenna is a 5.8 GHz 13 dBi Patch Antenna which features a relatively large viewing angle of 35 degrees and a suitable connector [62].

During operation the aircraft antenna and the ground antenna will constantly change their relative orientation. Since the use of linear polarized antennas, which are not aligned in one plane, results in significant losses, circular polarized antennas should be preferred. The use of circular polarized antennas on both sides of the link results in minimal losses. However, a circular polarized antenna will only be used on the ground. The small loss will be accepted by reason of the strong limitations on size and weight of the aircraft antenna.

Table 4.18: Ground station antenna specifications

	SpiroNet Circular 5,8 GHz Patch Antenna 13 dBi
Frequency range (MHz)	5740 - 5860
Antenna gain(dBi)	13
Beam angle vertical(deg)	35
Beam angle horizontal(deg)	35
Polarization	circular

4.7.6 Link Budget

The link budget aims to establish good network performance. Various parameters influence the range and the amount of data received, the major factors are the output power, the available bandwidth, the receiver sensitivity, the antenna gains, the radio technology and the environmental conditions. In this section the link margin will be calculated for the data communication link and the video link. For the data link the signal to noise ratio will also be evaluated to check whether the data can be decoded properly.

Assuming that the aircraft are always flying in line-of-sight the equation that describes the link margin is given by the Equation 4.37 [64] [63].

$$\text{Link Margin} = \text{Received Power} - \text{Receiver Sensitivity} \quad (4.37)$$

The received power includes the transmitted power, the gains and the losses (Equation 4.38) and is calculated using Equation 4.38.

$$\text{Received Power (dBm)} = \text{Transmitted Power (dBm)} + \text{Gains (dB)} - \text{Losses (dB)} \quad (4.38)$$

Combining Equation 4.37 and Equation 4.38 the link margin can be computed using Equation 4.39

$$\text{Link Margin} = \text{Transmitted Power} + \text{Gains} - \text{Losses} - \text{Receiver Sensitivity} \quad (4.39)$$

For in line-of-sight wireless applications the largest loss is caused by the free space loss which can be calculated using Equation 4.40.

$$\text{Losses (dB)} = -10 \cdot \log \left(\frac{4 \cdot \pi \cdot \text{Range} \cdot f}{c} \right)^2 \quad (4.40)$$

The Maximum Channel Noise depends on the modulation technique and the received power [64] and is given by Equation 4.41.

$$\text{Maximum Channel Noise} = \text{Received Power} - \text{Signal to Noise Ratio} \quad (4.41)$$

The Channel Noise depends on the operating temperature, the bandwidth and the noise figure of the receiver.

$$\text{Channel Noise} = \text{Thermal Noise} + \text{Noise Figure} \quad (4.42)$$

$$\text{Channel Noise} = k \cdot T \cdot B + \text{Noise Figure} \quad (4.43)$$

Where k is the Boltzman's constant ($1.38 \cdot 10^{-23} \frac{J}{K}$), T is the system temperature, assumed to be 290 K, B is the channel bandwidth (Hz), for QPSK: $B = 1 \cdot \text{Bit Rate}$. The noise figure for a low cost receiver is around 15 dB.

Data Link Budget

For the data link the losses were calculated to be -91.21 dB using Equation 4.40. The gains of the transmitter and receiver antenna were chosen to be 2.1 dB, the transmitter power of the XBee is 16 mW. Substituting these values into Equation 4.39 the link margin is calculated to be 25.98 dBm.

The link margin shows that the received signal strength is sufficiently above the receiver sensitivity. Fading of the signal due can be caused by interference of two waves travelling on different paths completely out of phase that cancel each other out. Other causes of fading might be misalignment of the antenna's and rainy weather conditions.

For the data link the minimum Signal-to-Noise Ratio is determined by the modulation technique. As the XBee 865/868LP uses QPSK [65], the Signal-to-Noise Ratio should be at least 13 dB if the bit error rate smaller than 0.0001 is necessary. A low bit error rate has been selected to prevent corrupted data. The maximum channel noise was calculated to be -88 dBm using Equation 4.41. The Channel noise was calculated to be -106 dBm using Equation 4.43.

This confirms that the channel noise is lower than the maximum channel noise, ensuring that the system has a good performance.

Video Link Budget

For the video link the losses are calculate using Equation 4.40 to be -107.7 dB. The link margin is calculated to be 11.4 dBm using Equation 4.39.

The link margin shows that the received signal strength is sufficiently higher than the receiver sensitivity for a range of 1 km.

4.8 QR-Code

In this section the subsystem used for the recognition of QR-Codes will be described, which forms an essential part of the mission as described in more detail in the chapter 2. In the following a brief introduction on QR-Codes will be given, followed by a description of the hardware being used. Furthermore, the decoding approach and the software used will be specified. The chapter is ended with an outlook on the further approach for the development and testing of the system.

A Quick Response Code (QR-Code) is a two-dimensional code. It consists of a quadratic matrix of black and white rectangular dots that present the contained information in a binary way. The size of the matrix is variable and ranges from 21x21 to 177x177 elements. The position of the QR-Code is indicated by three distinctive squares in the corners of the code, using a smaller square near the fourth corner to determine the size, orientation and viewing angle. The content of the code is protected by an error correction that depending on its level allows for restoring up to 30 percent of the data [66].

The QR-Code used during the competition has dimensions of 1 by 1 meters and is printed black over a white background. The size of the matrix is not specified and currently unknown. Given the example picture of a 25x25 elements code shown in Figure 4.47, it is assumed at this state that during the competition a similar code will be used.



Figure 4.47: Example QR-Code

Image Processing Hardware

Due to the limited computing power of the selected Lisa/M Paparazzi board a second processor has to be used to handle the QR-Code detection and decoding. This also reduces the risk of failure during operation as the critical flight control is separated from the ground station (Communication risks are avoided).

The video stream will be processed by a Gumstix Overo FireSTORM COM computer-on-module based on an ARM Cortex-A8 processor [67]. The Firestorm is very lightweight and small and offers enough processing power to allow for real time detection of the QR-Codes during flight. The specifications are given in Table 4.19. The FireSTORM computer-on-module will be mounted on a Pinto-TH, the smallest Gumstix expansion board for the Overo series. The expansion board offers a level shifter for the interface with the Lisa/M board and also allows for easy power supply. The FireSTORM communicates with the Lisa/M board via an SPI connection. A detailed description of the interface is given in section 5.4. For programming and testing a Gumstix Tobi expansion board is used, which offers an Ethernet and USB connection but is heavier than the Pinto-TH board.

Table 4.19: Hardware Selected for Image Processing

Hardware	Company	Model	Dimensions [mm]	Weight [grams]	Price [\$]	Power [V]
Vision Processing Unit	Gumstix	Overo FireSTORM COM	58x17x4.2	5.6	219	3.3
Expansion board	Gumstix	Pinto-TH	76.2x23	6.6	27.50	3.3

Camera

The selected Gumstix Caspa VL is a camera specifically designed for computer vision in combination with a board from the Over series. It is based on a Micron MT9V032 CMOS sensor with a resolution of 752H x 480V pixels at a rate of 60 frames per second [68]. The specifications of the camera are listed in Table 4.20. The camera features a filter for infrared light for better performance under standard light conditions. The camera has exchangeable optics and a fixed focus. Although the mission requires to detect objects from different distances, the fixed focus is not expected to cause any problems due to the small sensor size and the resulting large depth of field. The connection to the Overo FireSTORM is realized via the 27-pin connector (J5) on the top of each Overo.

Table 4.20: Selected Camera

Hardware	Company	Model	Dimensions [mm]	Weight [grams]	Price [\$]	Power
Camera	Gumstix	Caspa VL	39x25.7x20	22.9	75	3.3-4.2V

Detection and Decoding

As described in chapter 2 the recognition of the QR-Code will be performed in two steps. Since the QR-Code reading algorithm requires a relatively much processing power it can only be run at a low frame rate. For decoding the whole QR-Code has to be visible with an average of 3-4 pixels covering each of its elements which results in a low maximum ground speed of the MAV [69]. In order to cover a large searching area within a short time span, the position of the QR-Code first has to be estimated using different algorithms that can be run at a higher frame rate and image resolution. The first step is therefore to scan the whole area at a high speed and altitude. The resulting image stream will be processed using algorithms for color and corner detection, based on the known color and shape of the QR-Code which sets it apart from the background. Whereas the optimal algorithms still have to be determined and tested experimentally, the Open CV library offers a large selection and is proven and tested in combination with the Gumstix Overo boards [70].

If the QR-Code is detected and its location estimated as described in next section, the position can be approached and the surrounding area scanned at a lower altitude and speed. The image stream will then be processed using the ZBar decoder [69]. A schematic of the process is shown in Figure 4.48. The image stream from the camera is transformed into a linear stream of intensity samples by the image scanner. The linear scanner detects and measures the elements of the code, which is then searched for recognizable patterns and finally gets decoded.

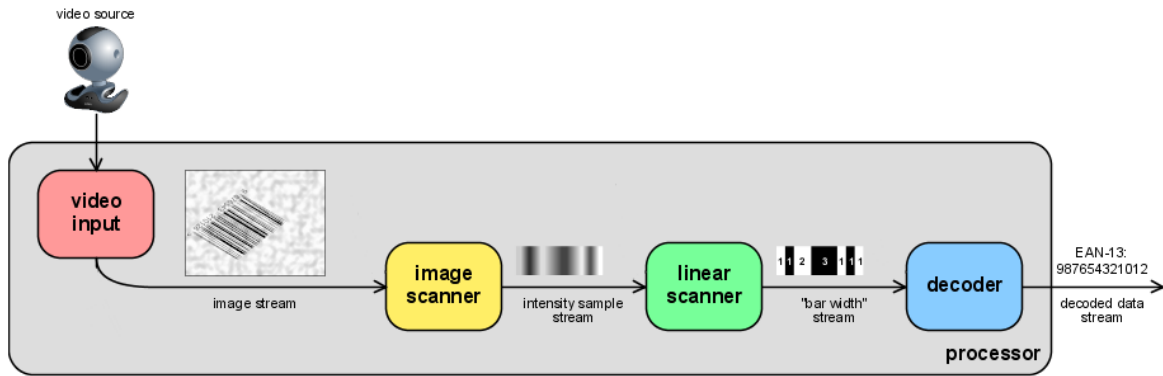


Figure 4.48: Functional diagram for ZBar decoder [69]

4.8.1 Localization of Drop Zones

The digital camera is used to scan the QR-Codes and to determine the locations of the 1x1m QR-Codes. These locations are needed since a ball will be dropped at those positions. As already mentioned in chapter 2, the localization of the QR-Codes needs to be as accurate as possible since more points are awarded for an accurate ball drop.

The ball drop positions are calculated by determining the relative distance from the QR-Code to the MAV. This relative distance can then be added to the current location of the MAV, which is assessed by the autopilot. The first step is to find the QR-Code by scanning the area near the given ball drop coordinates. When the digital camera recognizes the QR-Code, the current location of the MAV is noted. From the picture of the ground view and the QR-Code, the pixel distance from the center of the picture can be estimated. The relative distance of the QR-Code can then be calculated with Equation 4.44.

$$\frac{X}{x} = \frac{h}{f} \tag{4.44}$$

In this equation X is the distance of the center of the QR-Code to the MAV and x is the pixel distance of the QR-Code image to the center of the picture. The pixel distance is determined with the use of Figure 4.49 and calculated with Equation 4.45.

$$x = \sqrt{u^2 + v^2} \tag{4.45}$$

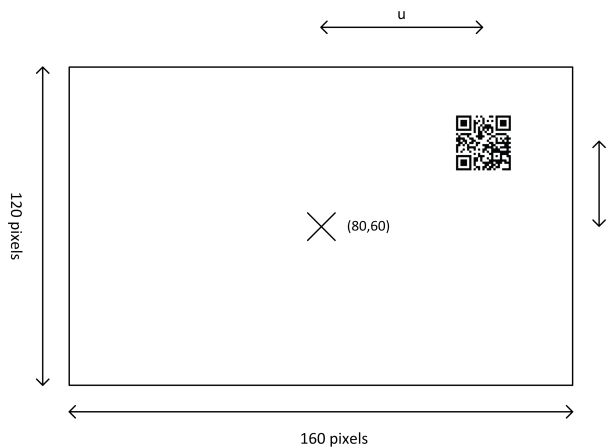


Figure 4.49: Camera view of QR-Code

The digital camera, the Caspa™VL, has an active imaging pixel array of 752Hx480V (360960 pixels). For this mission, the imaging pixel array will be downsized to 160Hx120V (19200 pixels). This downsizing of the pixel array is done to allow that more pictures can be processed within a set time and with less consumed power.

The focal length, f , of the Caspa™VL needs to be determined in pixels for Equation 4.44. In order to determine the focal length in pixels, a relation between the distance in pixels and in millimeters has to be established. This relation will be determined when testing the QR-Code module, described in section 5.4.

The height of the camera in Equation 4.44, h , is approximated to be equal to the height of the MAV. This height is determined by the GPS receiver and the barometer on the Lisa/M v2.0.

The distance of the center of the QR-Code to the MAV can be analyzed for two situations. The first situation is where the camera is always pointed vertically downwards. In the second situation the camera is fixed perpendicular to the frame of the MAV and the vehicle is tilted in horizontal flight. For both situations, an analysis is given in the following subsections.

Vertical Camera Position

An illustration of the QR-Code localization for the vertical camera position is given in Figure 4.50a. In this figure FOV represents the field of view, which is 97.5 degrees for the CaspaTMVL. The distance of the QR-Code to the MAV can directly be calculated from Equation 4.44 and Equation 4.45. In order to find the position of the QR-Code this relative distance is added to the position of the MAV.

Tilted Camera Position

For the tilted camera position, the angle of the camera with respect to the vertical position discussed above needs to be taken into account. See Figure 4.50b for an illustration of this situation. This rotation angle, α , is determined by the Attitude and Heading Reference System subsystem (AHRS). For this situation a variation of Equation 4.44 is needed. In order to determine the position of the center of the QR-Code to the MAV, L , the calculations in Equation 4.46 will be performed.

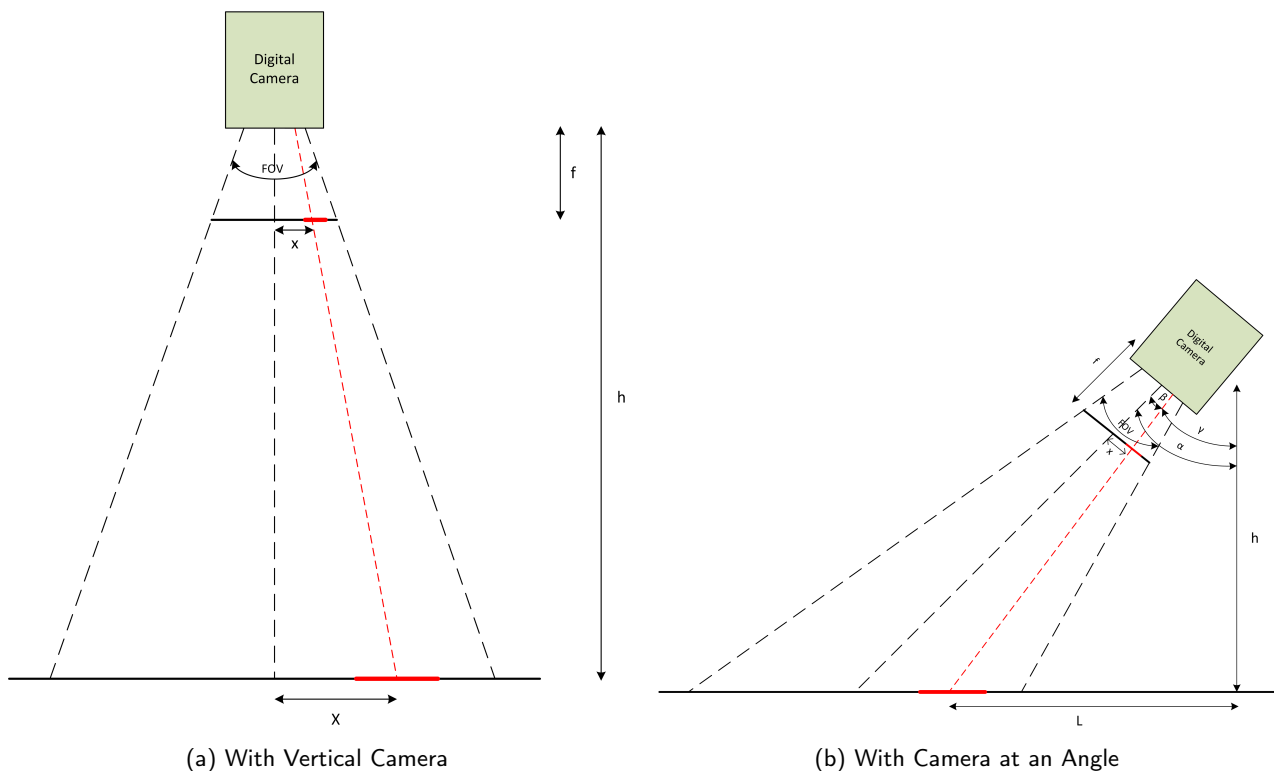


Figure 4.50: QR Position Determination

$$\beta = \tan^{-1} \left(\frac{x}{f} \right)$$

$$\gamma = \alpha - \beta \quad (4.46)$$

$$L = h \tan(\gamma)$$

For both situations the ground surface is assumed to be flat, however this is not necessary the case during the competition. Furthermore, inaccuracies in the position determination of the MAV due to the limited accuracy of the barometer and the GPS receiver can cause miscalculations in the QR-Code position determination. For this reason multiple pictures should be taken to improve the accuracy of the ball drop location. When the MAV detects the QR-Code for the first time, it will fly towards this position and consistently take pictures to update the most accurate location determination of the ball drop zone. The amount of images that can be taken has to be determined by

investigating the computational power that is needed for this process. When the MAV is at the drop zone location it will communicate the last determined location to the MAV's from group 2 and drop the ball.

4.8.2 Further Approach, Verification & Validation

The further development of the subsystem is mainly based on practical tests. As soon as the required hardware is available the different components have to be integrated. If the communication between the Overo FireSTORM, the Caspa camera and the Lisa/M work as expected, different algorithms for the QR-code detection can be tested and optimized. Using a test setup a first assessment of the subsystem performance independent of the platform can be carried out. The decoding time of the QR-code, the required resolution and possible frame rates can be determined. With these the maximum flight speed and altitude can be determined. With the test setup and finally the test during flight it is also possible to investigate the influences of vibrations and different light conditions on the reliability and performance of the subsystem. The implementation of algorithms for target detection based on their color also offers the possibility to use the system for obstacle avoidance during the urban corridor mission element. This solution would allow for a lower flight through the corridor, but has to be investigated in more detail in terms of development time and feasibility.

4.9 Ball Dropping System

The ball drop mission is an important mission element in the competition since it has a major effect on the acquired score. It was decided to put a lot of effort into scoring points by performing this mission element, mainly due to the high (and relatively easy) amount of points that the MAV can achieve by dropping the balls in the labelled zones. Failing in the ball-drop mission will have a dramatic effect on the group's performance in the competition.

To make the ball drop system efficient, it has to be light, accurate, consume a low amount of power and should not affect the general performance of the MAV. The ball drop system, which will be described in this section in detail, is the only subsystem which was fully developed and tested by the group during the DSE project.

4.9.1 Working Principle

As mentioned before, the drop ball system should fulfil the following requirements:

- Should be light.
- Should be accurate.
- Should have a low power consumption.
- Should not effect the general performance of the MAV.

Because of these restrictions, a mechanical system could not be implemented in the design. Mechanical systems require weight, space and therefore affect the aerodynamics of the MAV in one way or another. Therefore, an electrical system was chosen. The auto pilot can deliver power, which can be used to heat a resistor to burn a wire. This way the increase in weight and the required space of the system are minimal. Since the system is very small, the ball will almost completely be located inside the wing. To reduce the influence on the aerodynamic performance and to ensure a fast release, an elastic rubber will be used that covers up the hole once the ball is released. Figure 4.51 describes the functionality of the elastic rubber. A wire will hold the ball. At the moment that the wire will burn the rubber push the ball out of the MAV. The rubber will cover the hole to ensure a minimal aerodynamic effect.

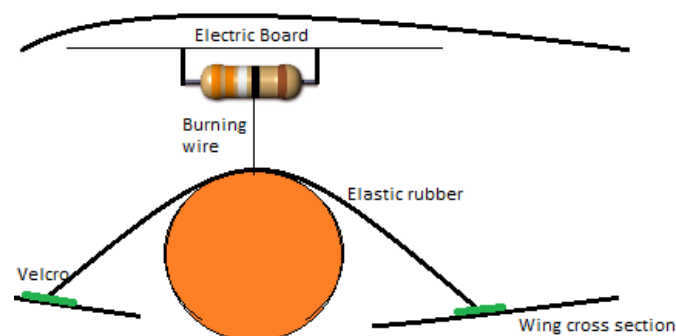


Figure 4.51: Drop Ball System Description

4.9.2 Complexity and Solution

Even though the idea sounds rather simple, the group encountered some problems during the making of this system. The first problem is that Lisa/M was given a limited Pulse-Width Modulation (PWM) amplitude. This limits the current through the resistor which will not be sufficient to burn a wire. To solve this problem, the resistor is connected to an outside voltage source (the battery) which will be controlled by a transistor. The transistor in turn is controlled by the autopilot.

Another problem is that Lisa/M has 8 servo outputs. Five of them are in use by the servos and the camera. This leaves 3 extra servo outputs available. However, each MAV should be able to control four balls, therefore missing one output. In order to solve this problem a servo chip is implemented. Figure 4.52 describes the method to solve this problem. As one can see the autopilot which is outside the ball drop system will generate different duty cycles. Using a potentiometer the chip will send a zero, a positive or a negative voltage difference to the output. The voltage difference will open the intended transistor according to the voltage difference sign.

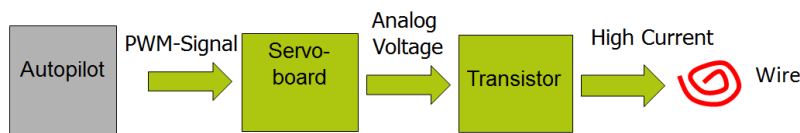


Figure 4.52: Ball Dropping System Principle

An electric circuit was successfully simulated and then built in order to test the performance of the ball drop system. However, the circuit did not behave in practice as expected. Due to the sensitive potentiometer the circuit behaved in an unpredictable way. Already a small change in the PWM signal could open one of the transistors, posing a difficulty since it consumed a lot of power from the system, which is unacceptable.

4.9.3 Solution by Using Micro-Controller

In order to solve the problem with the opening of the transistors at a low signal, an alternative solution has to be found for the servos chip. A component which will generate a safety margin and will guarantee a minimum loss of power from the battery when the system is not operational is needed. In order to solve this problem a micro-controller was implemented. Figure 4.53a shows the functionality of the micro controller. The advantage of the micro controller is the ability to program it to work exactly as the user wants it to work. Figure 4.53b describes how the micro controller is programmed in the drop ball system. The input pin is reading the pulse width from the autopilot's output. In case the pulse width is between 1 ms and 2 ms, the micro controller does not deliver power to the output. Using this method guarantees that the transistor is kept closed even when the pulse width is just above or below 1.5 ms. When the pulse width increases beyond 2 ms one transistor will open while the other will stay closed. The same is true when the pulse width is below 1 ms.

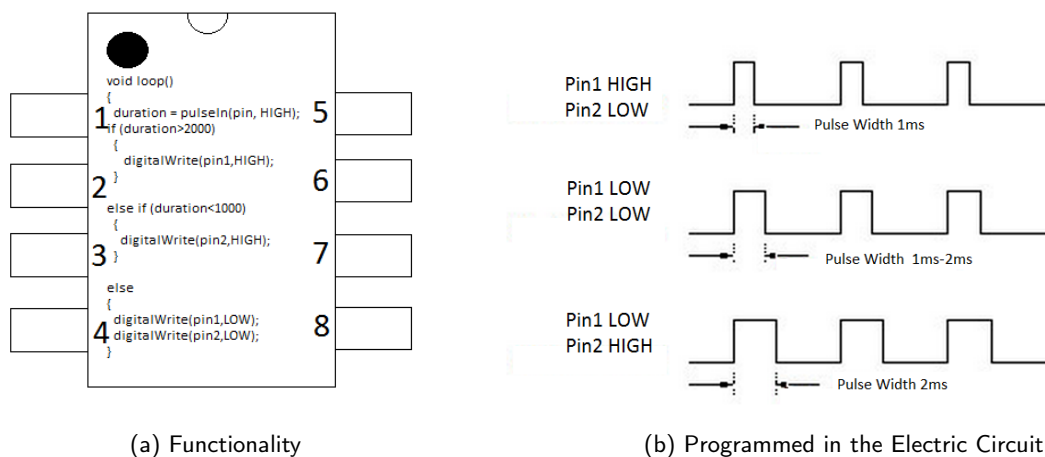


Figure 4.53: Micro Controller

4.9.4 Testing the Circuit

After simulating and testing the circuit with the micro-controller it is concluded that circuit behaves as expected. The transistors are closed through a high range of duty cycles and there are no more power consumption problems. However, the resistance of the resistor still needs to be decided. On one hand, as the current increases the wire will burn faster, on the other hand the transistor is limited in current and can not carry high current unless the size of the resistor increases, which is undesirable.

Another question is how fast the ball will be dropped after the autopilot send the signal to perform the drop. Since the MAV flies at cruise velocity, a difference of one second can lead to the ball missing the drop zone.

For this a series of measurements have been conducted. A pen weighing 30 grams replaced the ball in order to model the ball with the elastic rubber force acting on it. This is a first order approximation which makes the experiment easy to perform. The pen itself is connected to an electric wire back to the micro controller. When the nylon wire is burns through the pen falls and opens the circuit. Figure 4.54a, Figure 4.54b and Figure 4.54c show the experiment method. First, the pen is tied to the resistor with no current running through the resistor (PWM around 1.5 ms). Then, the PWM signal increases at once and the micro controller program reads the time that the pin turns to HIGH. The wire is burned, releases the pen and turns the Pin to LOW (the program takes a time measurement when the pin is LOW). The time from the moment the pin is HIGH till the moment the pin is LOW measures the delay time which is required to burn the resistor. To ensure accuracy, the voltage and the pen were documented on film. Using slow motion it is possible to see how many frames there are between the voltage turning to high and the pen falling. This experiment has been repeated four times, and the average delay time was found to be 0.3 seconds.

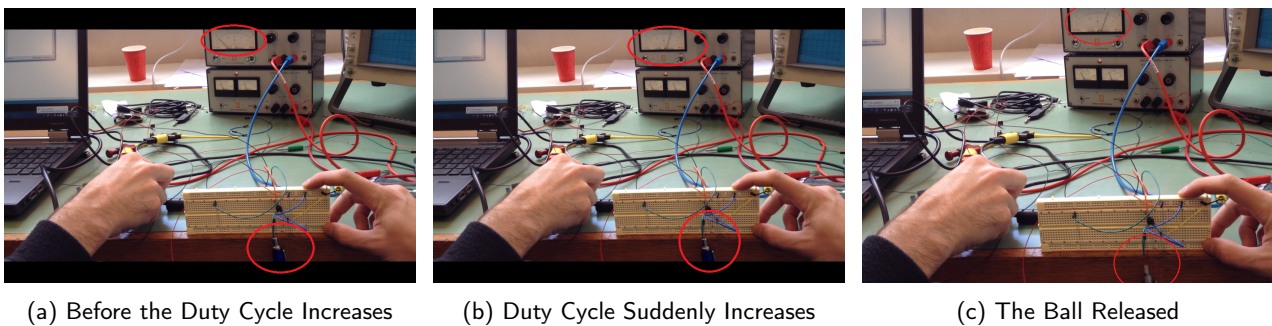


Figure 4.54: Reaction Measurements

4.9.5 The Complete Design and Components

After testing the circuit, the complete circuit was designed using the program EAGLE. Figure 4.56 shows the complete schematic drawing of all components. A resistor of 1 K ohm was added in order to limit the current to the micro controller and the autopilot. Another capacitor and resistor were added before the micro controller to prevent noise and unexpected behaviour of the micro controller. The printed board is given in Figure 4.55a with the bottom side of the board shown on the left. Notice that the printed wires where a high current is expected are thicker than the others. This board is the complete product which is now ready for production.

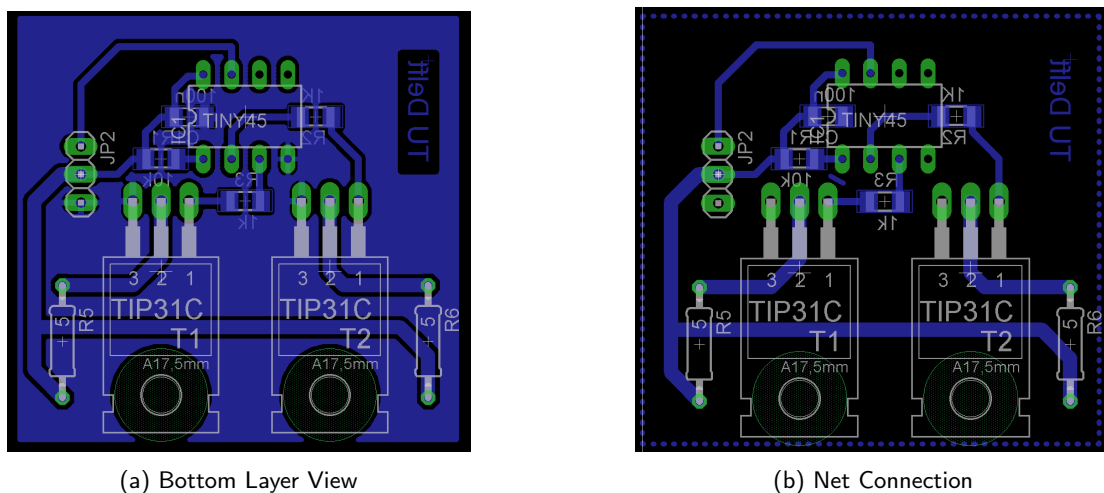


Figure 4.55: Drop Ball Circuit Board

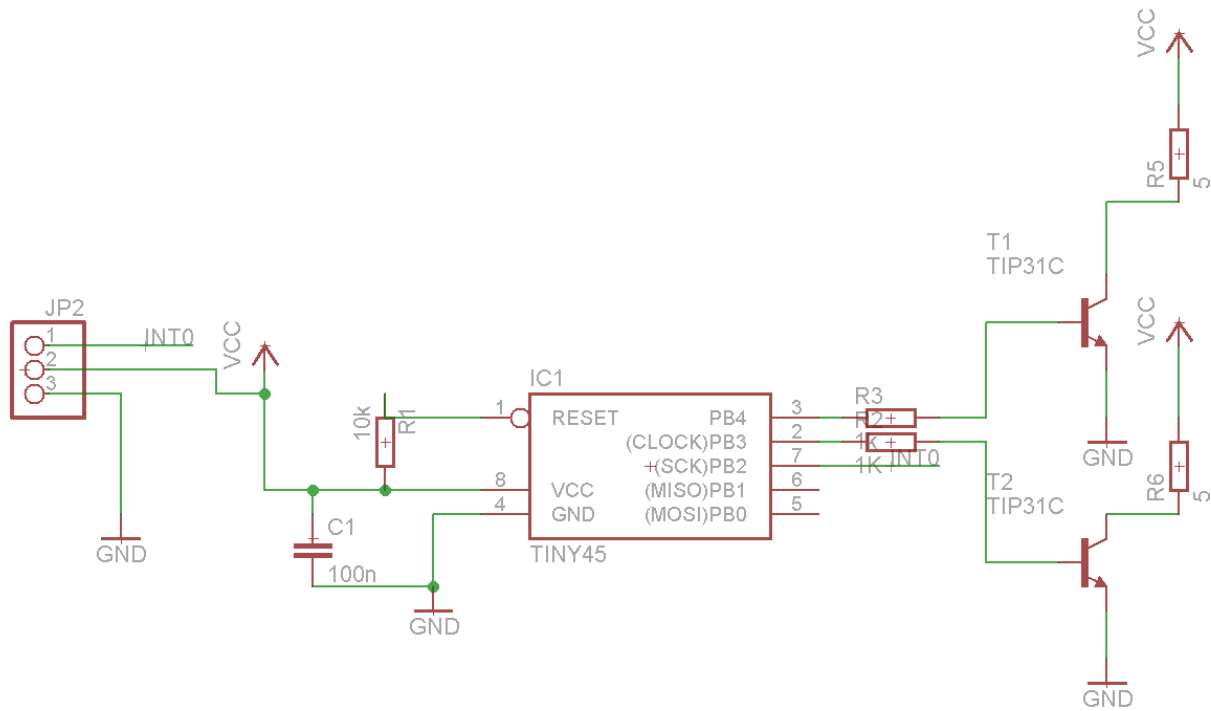


Figure 4.56: Ball drop circuit schematic

4.9.6 Releasing the Ball

The complete subsystem has been designed and verified. The delay time has been found and now the only thing left to determine is the ball release during flight. The balls will be dropped in horizontal flight at the design velocity of 13.9m/s . Furthermore, the flying altitude is estimated to be around 1 m. The lower the distance from the ground, the better the accuracy because the ball is affected less by the wind. Due to inaccuracies of the barometer a height of 1 m is reasonable distance. Using simple dynamic equations the following can be calculated:

$$y = V_{0y}t + \frac{1}{2}gt^2 \quad (4.47)$$

As explained before, the rubber will push the ball out with an initial velocity. In order to calculate the initial velocity, recall that the pen was weighting 30 grams which is a force of about 0.3 N. Using the relations from Equation 4.48, Equation 4.49, and Equation 4.50 the initial velocity can be calculated and is found to be 2.68 m/s using the assumptions that the ball has a mass of 1 gram and that the rubber will stretch a distance of about 12 mm.

$$F = ma \rightarrow a = \frac{F}{m} \quad (4.48)$$

$$a = \frac{dx}{dt} \frac{dv}{dx} = v \frac{dv}{dx} \rightarrow adx = vdv \rightarrow \int_{x_0}^x adx = \int_{v_0}^v vdv \quad (4.49)$$

$$ax = \frac{v^2}{2} \rightarrow v = \sqrt{2ax} \quad (4.50)$$

Using Equation 4.47 the time for the ball to reach the ground is estimated at 0.2534 seconds. Using Equation 4.51

$$x = V_{0x}t \quad (4.51)$$

the horizontal distance before dropping the ball is determined to be 3.52 m. However this is only a first approximation. The ball is light and will have an effect from the wind. In Paparazzi the delay of dropping the ball is set to 0.3 seconds. This delay call gives a command to the output servo a 0.3 s (or 3.52 m) before the MAV is at the specified distance. The cause for this delay is the time it takes to burn the wire. The system will be tested and adapted to different wind velocities later on in the design process.

4.10 Ground Station

The Ground Control Station (GCS) is essential when flying with Unmanned Air Vehicles as it provides a human interface for configuration, monitoring and control. The ground station has the following functions:

- Configure the vehicle
- Run a simulation
- Log data
- Provide communication

The Paparazzi Ground Control Station software has many different features and can be configured to meet different requirements. The most relevant features for the competition are given in the list below [71].

- Simultaneous flying multi UAS support
- Support of multiple protocols and autopilots/projects by writing a IVY Plugin
- 2D Map capable of displaying Google Satellite, OpenStreetMaps Images and Microsoft Satellite Maps
- Mission planning
- Realtime movable waypoints
- Realtime flightplan adjustments if needed
- System status overview
- Realtime Airframe in air tuning and calibration
- Supports rotary and fixed-wing

To set up the Paparazzi Ground Control Software a computer with Linux installed will be used at the competition. Furthermore three different computers will be present to receive the video streamings. A big screen with beamer will also be installed to show the presentation. To make the presentation interactive a more complex option will be considered post DSE, namely installing a router that sends the video streaming over a wireless network from the ground station to the audience. The audience will be able to access the wireless network and watch the live video streams from their mobile telephones and Ipad's.

4.11 Design Integration

Up to now, the detailed design phase has resulted in design solutions for each subsystem. Amongst these choices are aerodynamic choices, structural choices and payload choices. This section will discuss how everything will be integrated. The next section will elaborate on the manufacturing and assembly of the MAV's. The hardware configuration, the electrical block diagram and the data handling block diagram will be discussed.

4.11.1 Hardware Configuration

In this subsection, the hardware configuration will be discussed. Hardware in this case means all physical parts of the MAV. The hardware configuration can therefore be seen as the vehicle layout. This section will only give the final result, but it must be noted that the hardware integration is a highly iterative process. In Figure 4.57, a top view of the packaging can be found. Figure 4.58 shows the same configuration from the bottom. For clarity, the mid-section has been hidden. The vertical white lines indicate the edges of the mid-section.

The red balls in the pictures are the balls to drop on the QR-codes (including flag). The white board above it is an electric board to which the balls are mounted, but more on this will be explained in Equation 4.11.1. The yellow part is the GPS receiver, the brown part next to it the XBee modem. From the XBee modem, an antenna (thin wire) will run to the trailing edge of the vehicle and will hence not interfere with the GPS.

The green blocks in the morphing parts of the wing (near the motors and propellers) are the motor controllers. They are placed as close to the motors as possible, which means they are far away from for example the Lisa/M and other electrical hardware components. This will decrease the interference. It is expected that this position will be far enough. If this is not the case, blocking foil can be wrapped around it.

The motors and propellers are mounted as much to the tip as possible to increase the stability performance. The servos (black) will rotate the rotation axis (also black) of the morphing part. The connection from the servo to the rotation axis is not shown, but will consist out of gears. The gear ratio (or speed ratio) will be as small as possible. The servo has a range of approximately 180 degrees. The morphing part is estimated to rotate by at most 10 degrees. With a low gear ratio, one has more control over the position of the wing tip and it will reduce the effect of play. The vertical black sticks in the middle of the vehicle are the removable landing sticks and the three brown rectangular boxes are the three battery cells. The autopilot, ball drop and camera subsystems are discussed in more detail below the figures.

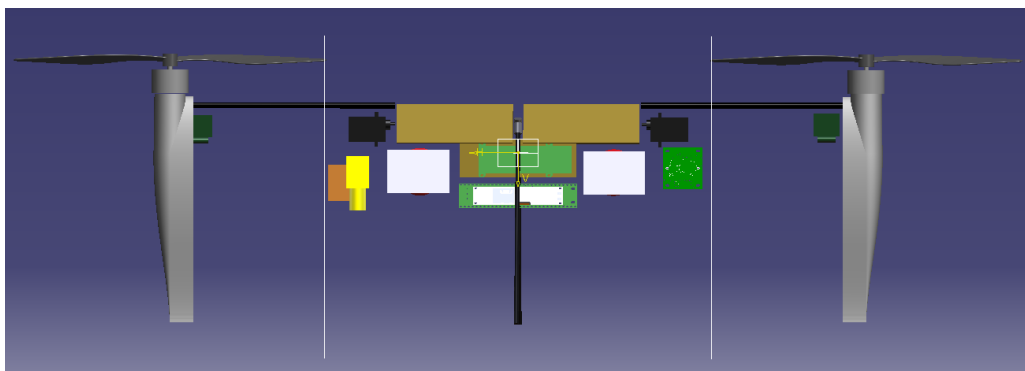


Figure 4.57: Hardware Configuration Top View

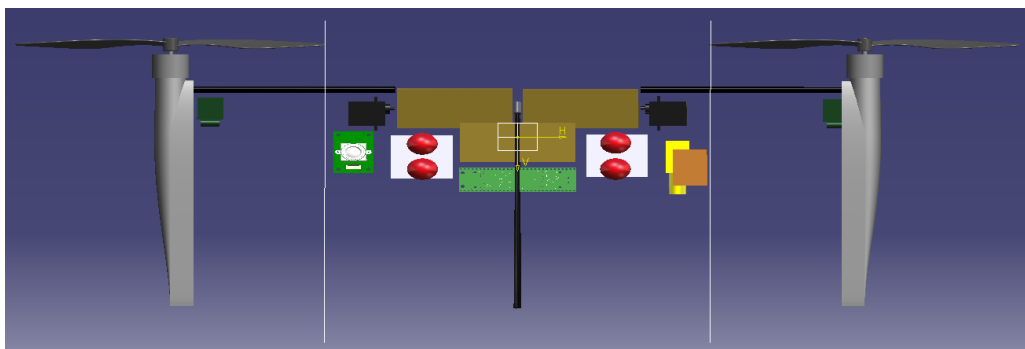


Figure 4.58: Hardware Configuration Bottom View

Autopilot

As autopilot, the Lisa/M board will be used. On this board, a 10 DoM IMU will be mounted to the body. To increase the quality of the measurements, it has been decided to mount the Lisa/M on the battery. The battery is heavy, and hence decreases the vibrations of the autopilot:

$$f_n = \frac{1}{2\pi} \sqrt{\frac{k}{m}} \quad (4.52)$$

Since November 2012, the barometric pressure sensor is not mounted on the board itself any more, but it is included on the Aspirin v2.2 10 DoM IMU. This IMU is mounted to the bottom side of the Lisa/M and this side will be attached to the battery cell as has been discussed before. Attention must be paid to this connection, since the sensor must still be able to sense the air and provide a good pressure measurement. This means that the Lisa/M cannot be directly mounted to the battery cell. It should also be taken into account that a venturi effect can be created where the air is accelerated between the battery and the IMU and the sensor measures air with increased velocity and hence with a lower static pressure which results in a higher altitude than in reality.

Ball Dropping

The ball drop system is given in Figure 4.51. It is composed out of an electric board, burning wire, ball, velcro and an elastic rubber. The way the system will integrate in the the design is as follows. There will be a cover on top of the wing where the electric board can push in or out of the wing. The burning wire will be fixed to the resistor which will be part of the electric board and the electric board will push back and close the cover. The elastic rubber can be taken apart of the wing or attached to the wing using velcro from the bottom side of the wing. The burning wire then will be attached to the ball and the elastic rubber will stretch to push the ball.

Camera for QR-Code Detection

The camera described in section 4.8 has to be rotatable to allow for detection of the QR-code in horizontal flight as well as in hover. It will therefore be mounted on a servo driven tilting mechanism. During horizontal flight the camera is counter-sunk in the wing and the whole around the lens is covered with foam to reduce drag. During transition it is then rotated around a hinge fixed to its rear side. The connection to the Overo board is realized via a flexible 27-core ribbon cable and the servo is connected to one of the available servo ports of the Lisa/M.

Structural Integration

In Figure 4.59, a part of the structure can be found. This picture shows the great advantage of 3D-printing a structure: integration. As can be seen, the batteries are integrated in the structure by means of sliders. The idea is to lock all payload by means of clicking mechanisms. Whether this is possible has to be tested or discussed with a 3D-production company. Figure 4.59 also shows the location of the glued adapter to which the landing sticks are connected.

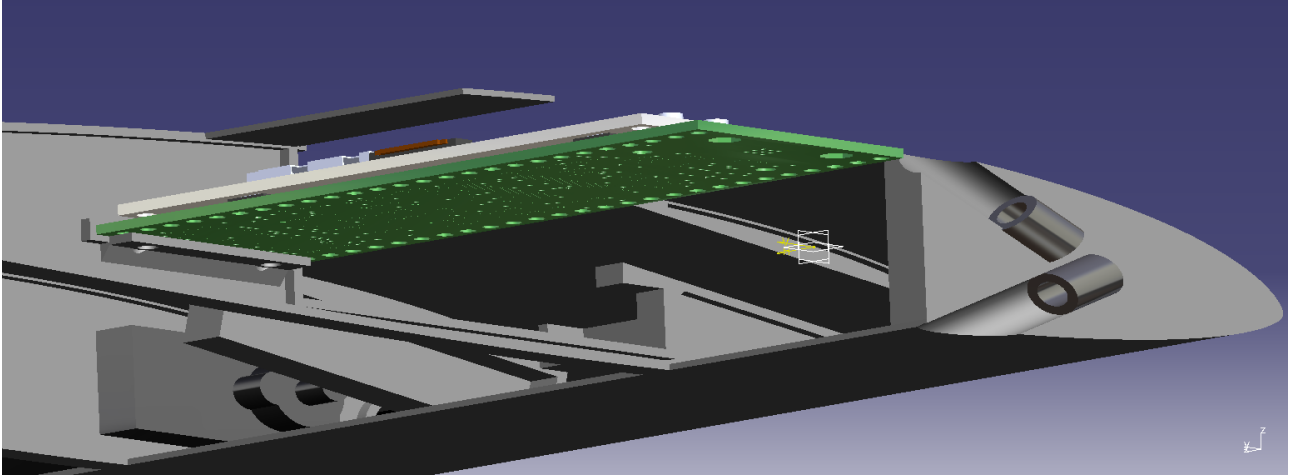


Figure 4.59: Structural Integration

Weight and Moment of Inertia Management

In the CATIA model the correct weights are added for all components. This allows the designer to control the location of the center of gravity and the moment of inertia. These values were monitored continuously and the correct values were forwarded to the control department. In the latest model, the center of gravity is located at 4 cm from the leading edge. This is the exact value that is required. It must however be taken into account that no wires, heat shrinks, and soldered connections are present in the CATIA model. These also have a weight and the exact c.g. position is therefore hard to predict. The influence will be minimal and it will be possible to compensate this with the position of other payload.

4.11.2 Electrical Layout

The previous section discussed the hardware configuration. Clearly, a lot of the hardware is electrical and they all need to be connected in order to communicate with each other. This section will therefore give an indication of how all the different components are connected. In Figure 4.60 the Lisa/M autopilot connections are shown and in Figure 4.61, the electrical diagram is displayed in a clear way.

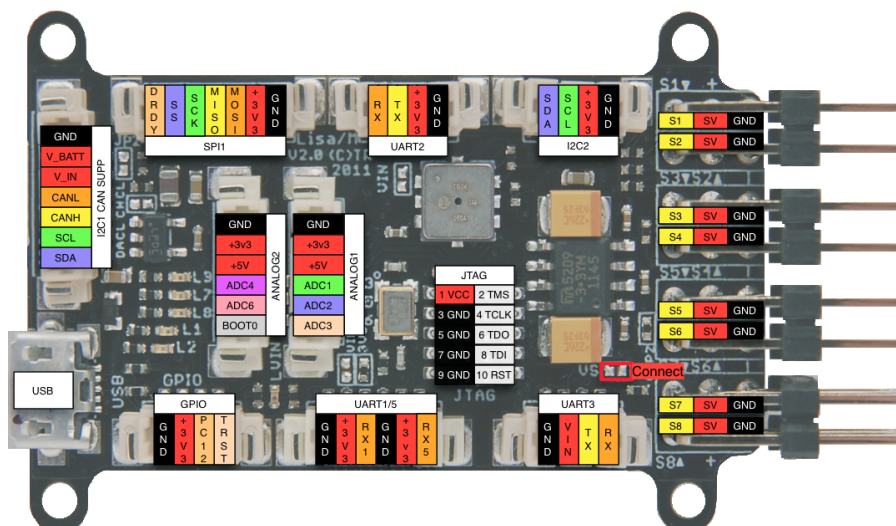


Figure 4.60: Lisa/M Pinout

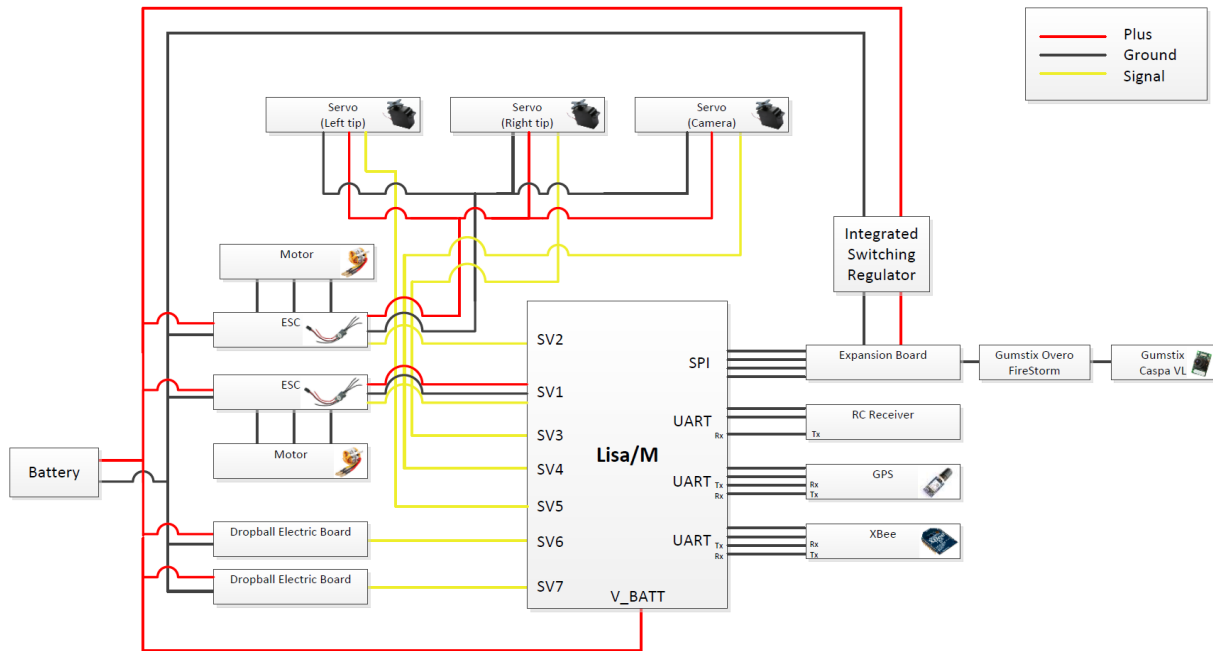


Figure 4.61: Electrical Diagram

At the left side of Figure 4.61, the battery is depicted. The battery powers all electrical components and it is connected to the two Electronic Speed Controllers (ESC's). The ESC's have a Battery Eliminator Circuit (BEC) that have an output voltage of 5 V and a maximum current of 2 A each. One of the two ESC's powers the Lisa/M and the other one powers the three servo's. Powering the Lisa/M via the ESC is possible via servo port 1 (SV1) when jumper one is soldered (see Figure 4.60). The PWM signal required to actuate the servo's come from servo ports on the Lisa/M. The motors are of course connected to the ESC's.

The drop ball subsystem also contains some electrical components. A self-designed electric board receives its power from the battery and a PWM signal will actuate the system as has been explained in section 4.9. Two balls are connected to one electric board and in total two electric board are carried by the MAV. The PWM signal for the two electric boards come from two servo ports on the Lisa/M autopilot.

Furthermore, some extra hardware is connected to the Lisa/M in order to fly autonomously: a RC receiver, a GPS receiver and a XBee modem. These three components will be connected to the UART ports on the Lisa/M. Important for this connection is that the transmitter ports (Tx) are connected with the receiver ports (Rx). If the Tx ports are connected with each other and the Rx ports too, components will burn.

For the detection of the QR-codes, video processing is required. For the video processing a Gumstix Overo FireStorm has been chosen as explained earlier. To connect the Overo FireStorm to the Lisa/M, it must be mounted on an expansion board. This expansion board is then connected via the SPI connection (as has been explained in section 4.8). The power will be drawn directly from the battery. The battery, however, delivers 11.1 V and this has to be reduced to 5 V for the expansion board. This is why the Integrated Switching Regulator is connected in between them.

The last connection is the one from the battery to the V_BATT port. This is done to measure the battery voltage during flight.

4.11.3 Data Handling

In a complex system it is important to understand how the data flows between the various components. From Figure 4.62 it can be seen which components receive and send data. The arrows indicate the direction of the data flow between components. The autopilot processor is the most important component of the system as it receives data from the sensors, the camera, the modem and the RC receiver. After processing the autopilot sends the data to the electronic speed controller and the actuators. Data does not only flow between the components on board of the aircraft but also between the aircraft and the ground station. The ground station is equipped with a modem to receive and send data to the modems on board of the aircraft with a laptop to receive the analogue video signal and with a transmitter to send data to the RC receiver.

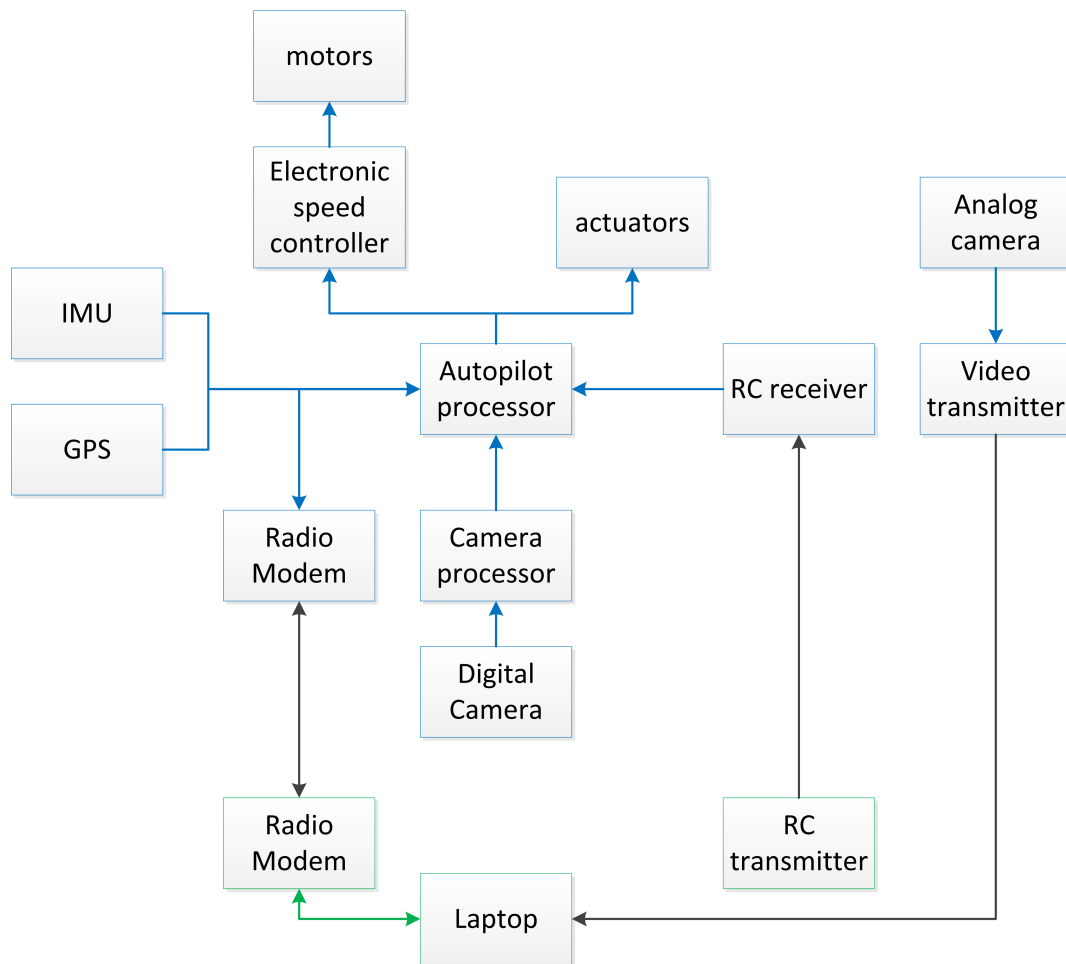


Figure 4.62: Overview of the data handling

4.12 Manufacturing & Assembly

The MAV's as described in this report, are being built. This section will describe the manufacturing techniques used.

4.12.1 Manufacturing

Because all MAV's have to be produced within a short period of time, there has been chosen for the rapid prototyping technique SLS (Selective Laser Sintering). Some advantages of rapid prototyping are: ease of fabrication, rapid fabrication, high part complexity and low set up costs. The SLS technique has already been described in the Mid-Term report and will hence not be described here again. The printing is done by a company and there is not much manufacturing for the group.

The carbon fiber rods used for the landing sticks and for the rotation beam of the morphing part will be pultruded. These pultruded rods can simply be bought. This will reduce manufacturing time significantly.

The adapters for the landing system can be made on a lathe. The parts are quite small and producing the parts will cost only a couple of hours.

All electrical components are of course soldered. For the ball drop system, a PCB has been designed by the group. The TU Delft has got some experience with manufacturing these boards and if possible they will be outsourced. If this is not possible, it is also doable to CNC it in the MAVLab.

4.12.2 Assembly

The assembling phase is divided into two parts: assembling the structure and assembling the electrical components. The structural assembly of the MAV is pretty straight forward. The skeleton is 3D printed by a company. In the structure, all connection points for the payload are already present and placing the payload is plug and play. Since the 3D-printed material could not provide the required stiffness for the rotation axis of the morphing part, a carbon fiber tube is used with bushings. This tube has to be glued to the 3D printed wing tip. At the same time the bushings can be placed in the midsection and when the morphing part is placed into the midsection, the gear has to be glued to

the rotation axis. After this, the servo can be mounted and the skeleton is finished. The last step is to wrap the foil around the airframe and to connect it with glue to the ribs. A sticker will be used to ensure all MAV's have a distinct colour. When this is all done, the structural part of the assembly phase is finished. In Figure 4.63, an exploded view can be found.

Concurrent, the electrical part of the MAV can be assembled. Assembling the electrical part basically consists of soldering everything together with connectors according to the wire diagram provided in subsection 4.11.2. Assuming all software has been written, it is now only a matter of connecting all connectors and flash it to the hardware components. When the structure is finished, all components can be plugged into the airframe and the MAV is ready to fly.

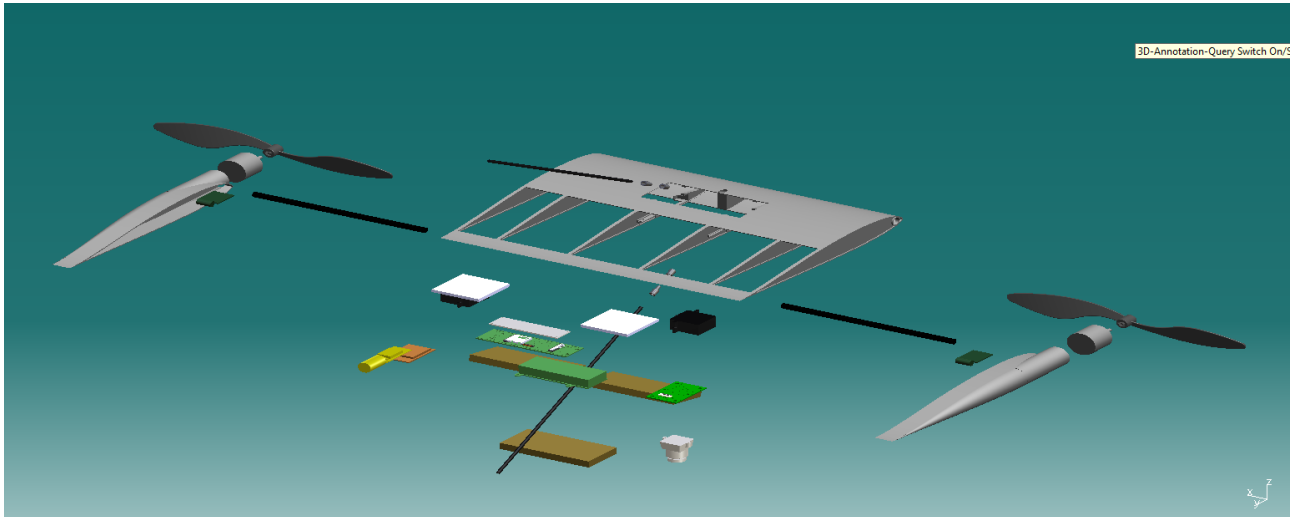


Figure 4.63: Exploded View

4.13 Sensitivity Analysis

This section describes the analysis of the sensitivity of the design solutions for a change in major input parameters. This analysis is carried out to investigate the robustness of the design.

4.13.1 Size

A requirement of 50 cm was given for the maximum size of the MAV which limits the aerodynamic design to low aspect ratio solutions. For the used flight envelope and a design point aimed to maximize the vehicle's endurance, it would be more efficient to have a higher aspect ratio concerning the aerodynamics of the MAV. The integration of hardware is also more difficult due to the size limit because the airfoil has to be thick enough to fit the hardware. For the chosen aspect ratio and airfoil the hardware fitted just inside the structure. Also, the morphing wing structure limits the space occupied by hardware. If the size constraint was higher, the design would have a larger aspect ratio and probably would have a fuselage with a blended wing body shape to integrate the hardware.

The size constraint does not influence the design solution of the propulsion system. The limiting requirement for the propulsion system is the cruise speed and not the size. The structural design of the system is able to carry all loads regardless the size limit. The control and stability is limited by the size since a further placement of the propellers will allow for an easier control in roll and yaw.

4.13.2 Mass

The mass constraint requirement for this system was set to 2 kg. However, to make a system with a size limit of 50 cm and hence a small lifting surface it was soon concluded that the design MAV of 400 g will have a large buffer. This mass limit might influence the hardware choices. However, the hardware should be as light as possible within the performance constraints and when the mass was allowed to be higher this would not have changed the decisions.

For the structural design a skeleton and skin solution was chosen to save weight. If the mass limit was higher this would not be necessary and the entire wing would be 3D printed apart from the morphing parts to reduce production complexity. The material choice and related production method was also influenced by the mass constraint. The chosen material (PA2105) had a lower specific strength as EOS PEEK HP, but was significantly lighter. If weight wasn't an issue EOS PEEK HP would also be a good choice.

4.13.3 Flight Speed

In order to complete the mission in a predetermined time span and based on the distances of the competition area a design speed of 50 km/h was estimated. The propulsion subsystem is mainly influenced by the design speed. A small increase in design flight speed will increase the frequency of rotations (rpm) of the propellers. This will increase the amount of power needed by the motors. The power needed will increase which might lead to a heavier battery. If the design flight speed is increased more, around 5 to 10 km/h, the propulsion system demands a higher propeller diameter.

If the design flight speed changes this will not highly influence the aerodynamic design as long as the Reynolds number is in the same range. However, small changes in the aerodynamic design will occur. Increasing the flight speed will increase induced drag. The required C_L will also change. This means the lift to drag ratio will change and a different airfoil should be chosen. A different option would be changing the wing surface. These changes influence payload integration in turn.

The structure of the system will not be influenced dramatically when the flight speed is changed in this flight regime. Changing the design flight speed will not influence the communication subsystem. The accuracy of the GPS system will not be affected by changing the flight speed in this speed range and therefore will not affect the guidance and navigation design solutions. The camera specifications are related to the flight speed, because it influence the clearness of the pictures. A larger shutter speed would be needed if the vehicle should fly faster.

4.13.4 Autonomy Level

If the level of autonomy is decreased to level 6 there are two options. Option one is autonomous target detection. In this case the data from the sensors and hardware is processed autonomously. This will not change the code for the sensors and payload in Paparazzi. Collision avoidance and target detection and recognition should still be working in Paparazzi. In this case there will be an operator which can change the flight plan from the ground station. The flight plan itself will not change, but the operator can move waypoints or activate different blocks. This means the messages sent based on the mission status will not be needed any more, since the operator can take over.

The second option is autonomous flight control. This means the flight plan and the decisions based on messages about the mission status are fixed, but the payload is operated from the ground station. In this case the code for target detection and recognition does not need to be programmed since it can be scanned by someone on the ground. Also the ball dropping can be activated by the operator. Therefore, a lot less programming is needed.

4.13.5 Vertical Take-off and Hovering

The fact that the MAV needs to take-off vertically and should be able to hover highly influences the design. For the aerodynamics subsystem the design does not much change, since it is mainly based on horizontal flight. The propulsive subsystem is designed for a compromise between hovering and horizontal flight. If the MAV does not need to hover it means the propulsion system will be optimized for horizontal flight. The propeller diameter will decrease and the propeller pitch should be increased. The rotational speed should be decreased?.

For the structure the main change is the take-off and landing support. If the vehicle should not land vertically the structure will change, because it has to withstand different impact loads. The landing sticks are not needed any more because the MAV will not land on its rear. The control of the system will be less complex, because the MAV will only fly in horizontal mode and does not need to transition. The ball dropping system is working in horizontal mode and the design solution will therefore not change. The camera should be able to rotate if the vehicle is not able to hover, because it needs to detect objects in front of it.

4.13.6 Efficient Horizontal Flight

Because it is required that the MAV should be efficient in horizontal flight, the choice is made to make a hybrid vehicle. Otherwise one could just as well design a quadrotor. The aerodynamic design is completely based on horizontal flight and therefore this is highly sensitive to this design parameter. The propulsion system would change significantly if efficient horizontal flight was not required as explained before and the control would be more easy. It is concluded that the entire design would change if the vehicle did not need to fly efficiently horizontally.

4.13.7 Sensitivity of Major Parameters

The most sensitive design parameters to changes considered are the requirement that the vehicle should be able to fly both horizontally and vertically and the size of the vehicle. These determine the total layout of the system and the size influences also the mass of the system. Changing the level of autonomy will influence only the programming complexity. Small changes in flight speed will not influence the design to a large extent, however large changes will.

4.14 Performance Analysis

This section describes the performance of the vehicle from a flight mechanics point of view, where endurance, range, climb and turning performance will be discussed.

4.14.1 Endurance

First, the endurance of the vehicle will be analyzed. The endurance indicates the maximum time the vehicle is able to fly and is highly depended on the flight mode. In hovering flight, the engines consume more power which decreases the endurance significantly. Therefore, the endurance for the vehicle will be analyzed for each flight mode separately.

Analyzing endurance for horizontal steady flight, it can be seen that the endurance for an electrical powered vehicle is calculated differently than for an aircraft running on fuel. The endurance for an electrical powered vehicle can be derived from the energy available from the battery and the power needed for forward thrust (Equation 4.53)[72].

$$Endurance = \frac{E_{batt}}{P_{batt}} \quad (4.53)$$

The power which should be provided by the battery is the thrust power divided by the propeller efficiency. Since power is equal to thrust multiplied by velocity for steady horizontal cruise flight and thrust is equal to drag and lift is equal to weight, Equation 4.54 can be derived for the battery power. Where the velocity is found from the lift equation and can be expressed as seen in (Equation 4.55).

$$P_{batt} = \frac{P_{thrust}}{\eta_{prop}} = \frac{TV}{\eta_{prop}} = \frac{DV}{\eta_{prop}} = \frac{W_{TO}V}{L/D\eta_{prop}} \quad (4.54)$$

$$V = \sqrt{\frac{2W_{TO}}{\rho C_L S}} \quad (4.55)$$

Substituting Equation 4.55 in Equation 4.54 and inserting the lift and drag coefficients for the lift-to-drag ratio gives Equation 4.56 for battery power. That can be further substituted with Equation 4.56 in Equation 4.53, and results in Equation 4.57. It can be concluded that the endurance is proportional to $\frac{C_L^{3/2}}{C_D}$.

$$P_{batt} = \frac{W_{TO}}{\frac{C_L}{C_D} \eta_{prop}} \sqrt{\frac{2W_{TO}}{\rho C_L S}} = \frac{W_{TO}}{\frac{C_L^{3/2}}{C_D} \eta_{prop}} \sqrt{\frac{2W_{TO}}{\rho S}} \quad (4.56)$$

$$Endurance = \frac{E_{batt}}{W_{TO}} \eta_{prop} \frac{C_L^{3/2}}{C_D} \sqrt{\frac{\rho S}{2W_{TO}}} \quad (4.57)$$

As seen in Figure 4.64, the endurance ratio at the operational angle of attack is not at its maximum value. There are several reasons for this design choice, which will be explained in the following.

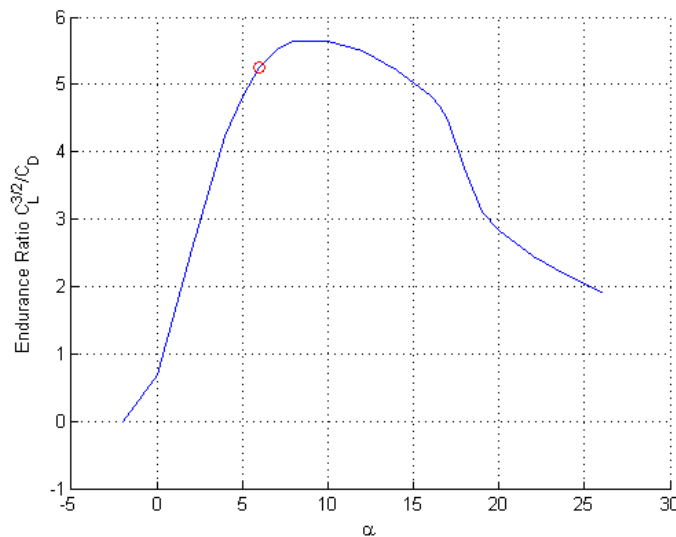


Figure 4.64: Endurance ratio versus angle of attack

In order to increase the endurance ratio of the vehicle, the design $C_L^{3/2}/C_D$ -ratio must be increased. This is achieved by decreasing the area and thereby increasing the design angle of attack and therefore the design lift coefficient. A decrease in area also leads to a lower drag coefficient since the Aspect Ratio increases, as can be seen in Equation 4.1. However, decreasing the area while trying to maximize the Aspect Ratio means that the chord length has to be reduced, which leads to a lower thickness of the wing. The wing thickness of the payload bay has a high priority because of component integration. Lowering its thickness is not possible because several components, such as the battery and autopilot, will not fit inside the bay or move the CG too close, or even behind, the neutral point of the vehicle, adversely affecting its longitudinal stability.

Another option is to only reduce the chord length of the morphing part of the wing where no components are stored in order to improve performance. This, however, also has an adverse effect on longitudinal stability and controllability. If taper is applied to the wing while keeping the leading edge in line for morphing purposes, and therefore applying forward sweep, the aerodynamic center moves forward, reducing its distance to the CG and worsening natural stability of the wing in longitudinal direction. In order to keep the same stability, which is expressed by C_{m_α} , the CG would have to move forward, decreasing its distance to the morphing hinge and thereby impairing pitch control.

Incorporating a fuselage, or a blended wing-body, would be a possibility, too. This way, the Aspect Ratio can be increased while having the ability to store all components in the payload bay. However, the aerodynamic characteristics over the affected part of the wing will suffer, making it less efficient, and the stability and controllability issues will still be present.

In order to account for these issues, a slightly more inefficient endurance ratio is accepted for the flying wing design by keeping the area slightly above and the Aspect Ratio slightly below optimum.

Having defined the endurance ratio and engine characteristics, the endurance can be calculated. Therefore it is necessary to know the energy in the battery and what influences it. The energy stored in the battery depends on the specific energy (E_{spec}), battery mass m_{batt} , efficiency (η_{batt}) and the depth of discharge ratio (f_{usable}). The depth of discharge, which is the ratio between the usable energy and energy stored, highly influences the endurance [72].

$$E_{batt} = E_{spec} m_{batt} \eta_{batt} f_{usable} \quad (4.58)$$

For cruise flight, the power consumed was determined to be 22.6 W from the propeller and engine characteristics and including the payload power consumption. This yields an endurance of 31 minutes for a fully charged battery. In vertical flight, the endurance depends on the power needed and the energy stored in the battery Equation 4.53. The thrust needed for hovering is equal to the weight and the power needed at this thrust setting is 96 W. Using Equation Equation 4.53, this gives a maximum endurance of 8.5 minutes. When flying at maximum thrust the power consumed is 265.4 W giving an endurance of approximately 3.2 minutes. Assuming that we fly at maximum thrust 4 % of the time, cruise 88 % and hover 8 %, a maximum endurance of around 28.2 minutes can be achieved, which is enough to complete the mission.

4.14.2 Range

The range that can be reached can be determined by multiplying the endurance with the ground speed (Equation 4.59)[72]. Range is calculated for straight cruise flight at a constant airspeed, and results in 32 km when flying at 50 km/h. A requirement for the mission was to be able to fly at a maximum wind speed of 5 bft. The wind speed will influence the ground velocity of the vehicle and therefore also affect the range. When flying at a flight speed of 50 km/h and with a headwind of 5 bft (35 km/h), the ground speed will be 15 km/h. This will decrease the range to 10 km. For a maximum tailwind of 35 km/h and a flight speed of 50 km/h the range increases to 52 km.

$$Range = \frac{E_{batt}}{W_{TO}} \eta_{prop} \frac{C_L}{C_D} \quad (4.59)$$

4.14.3 Turning Performance

The turning performance of the MAV for horizontal flight can be described from a flight mechanics point of view by using the airspeed and bank angle. From structural and agility considerations the load factor for maneuvering was set to a maximum of four. During a turn the lift is equal to the weight times the load factor by definition. For a steady horizontal turn the relation between the load factor and bank angle is than given by Equation 4.60[72].

$$n_{ult} = \frac{1}{\cos\mu} \quad (4.60)$$

This yields a maximum bank angle of 76 degrees. For a steady horizontal turn the turn radius can be calculated using Equation 4.61. The turning radius corresponding to each bank angle at a velocity of 50 km/h can be found in Figure 4.65, where it can be seen that the minimum turning radius at the maximum bank angle is computed to be 5 m. Equation 4.61 shows that the turning radius is proportional to the square of the velocity, hence for lower velocity the turning radius will decrease.

$$R = \frac{V^2}{g\sqrt{n^2 - 1}} \quad (4.61)$$

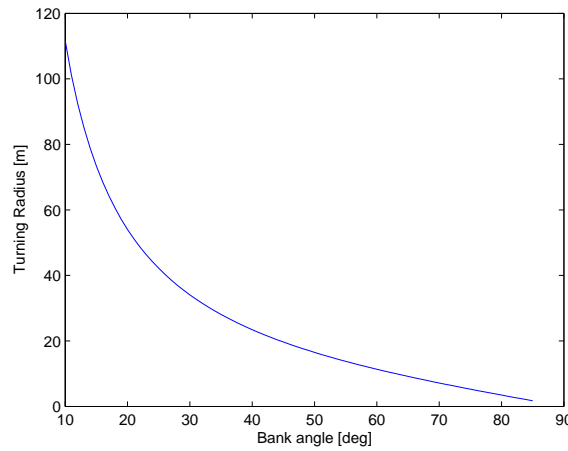


Figure 4.65: Turning performance for 50km/h

The drag during a steady horizontal turn is derived and show in Equation 4.62. The input power from the engine can be calculated using Equation 4.54. When combining this with Equation 4.62 the power consumed when turning at a maximum load factor is four times higher than in cruise flight. It can be concluded that turning often will affect the endurance, since significantly more power is consumed.

$$D = \frac{D}{L}L = \frac{C_D}{C_L}nW \quad (4.62)$$

The turning performance of this vehicle is considered sufficient for this mission. However, when really tight turns are necessary, as for example during the flight performance mission element, thrust can be increased on one engine in order to create a strong moment about the vertical axis. This moment can turn the vehicle around in a fraction of a second, changing its flight direction almost instantly. It has to be kept in mind, however, that this maneuver consumes even more power (adversely affecting endurance) and that the aerodynamic effect are very difficult to predict during the directional transition. Tests will be conducted to see whether this maneuver can be implemented when necessary.

4.14.4 Climb Performance

The climb performance of the vehicle can be determined for both hover mode and fixed wing mode. Analyzing the climb performance during hovering, Shkarayev et al.[73] suggests that the thrust required for a vertical climb speed in hover can be determined using Equation 4.63, where S_p is the wing surface affected by the propeller slip stream and V_0 the vertical climb speed.

The Equation was numerically solved and the results are shown in Figure 4.66a. The maximum thrust for hovering was set equal to two times the take-off weight, corresponding to a maximum climb speed of 11 m/s in hover. However, endurance decreases significantly because of the large amount of power needed. Up to a climb speed of around 3 m/s the amount of thrust and power needed is acceptable.

$$T - W + 0.5\rho \left[0.0305 + 0.0024 \left(\sqrt{V_0^2 + \frac{2T}{\rho\pi R^2}} - V_0 \right) \right] \left[S(V_0^2 + \frac{2T}{\rho\pi R^2} + (S - S_p)V_0^2) \right] = 0 \quad (4.63)$$

When flying in fixed wing mode, the rate of climb in steady flight is derived from the equations of motion and is shown in Equation 4.64.

$$RC_{st} = \frac{P_a - P_r}{W} = V \sin(\gamma) \quad (4.64)$$

For a flight speed of 50 km/h the climb speed and climb angle are found for different power settings (Figure 4.66b). The climb angle and speed are limited by the control system.

When comparing the required power of 101 W for hovering flight to the 14 W that are needed to accomplish a climb at a rate of 2 m/s, it can be concluded that climbing in fixed wing mode is much more efficient. Therefore, climbing in hover mode has to be avoided and should only be done at take-off reach a safe altitude for transition.

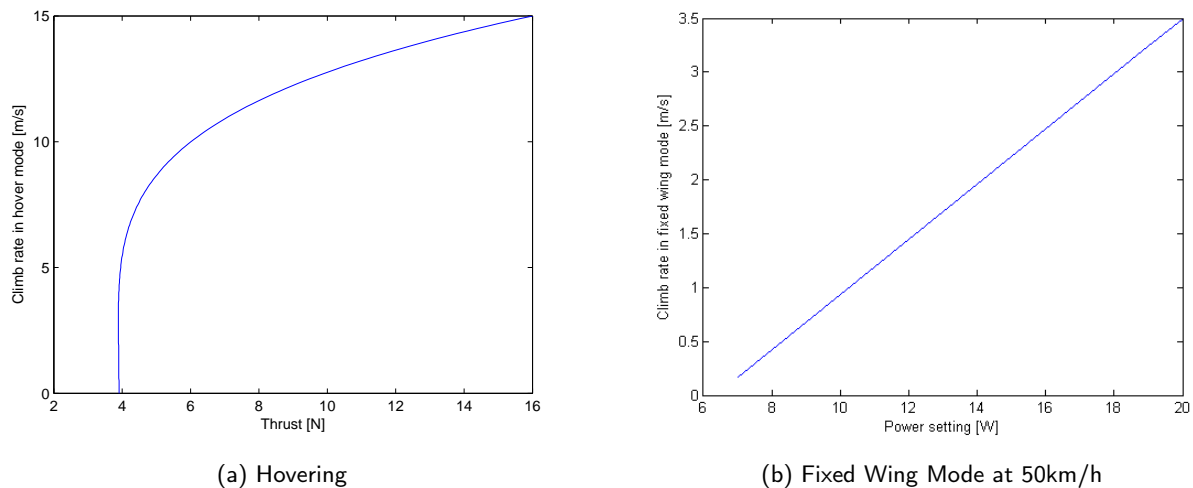


Figure 4.66: Climb Speed

4.14.5 Flight Speed

Since the vehicle is hybrid, it is able to decrease its flight speed to zero in hovering mode. The minimum flight speed in fixed wing mode corresponds to the maximum C_L and is calculated to be 32 km/h (8.89 m/s). Below this flight speed the vehicle will enter its transition regime. The maximum airspeed of the vehicle depends on the maximum power available. To find the maximum airspeed the required power should be equal to the power available. The maximum speed is then equal to the maximum power available for the engines divided by the drag. However, the maximum power available for the engines is depending on the power used by the payload and since this is not constant, the maximum airspeed remains unknown. Also, the drag at the maximum thrust setting is not known exactly. Therefore, the maximum airspeed will be found by testing the vehicle.

4.15 Resource Allocation and Budget Breakdown

Since all the subsystems are designed at this stage, the resource allocation is updated with the dimensions, weight and power consumptions of the final design choices. The resource allocation can be found in Table 4.21. In Table 4.21 also the budget breakdown is given. A section prototype is added to the budget breakdown table. This section contains all the components that are bought for testing the prototype, but are not used during the competition. From the resource allocation and budget breakdown it can be seen that the total weight of the MAV is 442.5g and the total cost for building and testing the MAV is €1348.

Contingency Management

Although the mass and the power consumption of the MAV parts are all determined and stated in Table 4.21, these properties can still change during the production of the MAV and the testing and competition phase. In order to decrease the risk that the properties will increase out of bound and will result in failure of the design, contingency management is applied to the mass and power consumption. Contingency management is the process of establishing and managing the technical resource budget.

For the contingency management the design is divided in subcategories. For each subcategory a contingency factor is determined, based on the stage of the design and the type of subcategory. The contingency factors for the mass and power consumption can be found in Table 4.22 and Table 4.23, respectively. If the mass and/or power inclines to reach out of bound, action must be taken to prevent this. Actions include multiple possibilities, for example modifying the design or the design approach.

Table 4.21: Resource Allocation and Budget Breakdown

Part	Dimensions (l x w x h) [mm]	Mass [g]	Power [W]	Cost [€]
Structure	470x210x21	95	-	200
Airframe	470x210x21	95	-	200
Control & Communications	-	34.6	1.92	314.53
Autopilot	60x34x10	11.5	1.7	184.00
GPS Receiver	50x18	10.1	-	63.14
RC Receiver (incl. antenna)	27x19x10	5	-	13.88
Wireless Modem	13.30x9.58x1.20	4	0.22	42.30
Antenna	20x20	4	-	11.21
Propulsion & Power	-	211.3	59.19	46.85
Propellers (2)	7x7 inch	4	-	4.55
Motor (2x)	27.5x26	72	59.19	20
ESC (2x)	45x24x11	38	-	12.74
Battery (3)	73.4x34.2x6.4	97.3	-	9.56
Payload	-	81.6	3.090	386.62
Digital Camera	39x25.7	22.9	0.320 (at max datarate)	59.50
Processor	58x17x4.2	5.6	1.320	204.10
Servo (3x)	23x12x30	30	1.125	5.49
Expansion Board	76.2x23	6.6	-	29.70
Analog Camera	12x12x14	3.3	0.300	60.57
Analog Video Transmitter	20x22x3	2.2	0.025	25.76
Balls (4)	20 (d)	4	-	1.50
Ball Drop System	40x40x3	7	-	-
Prototype	-	-	-	400
Total of MAV	-	422.5	64.2	1348
Ground Station	-	-	-	-
RC transmitter	-	1134	-	38.05
Transmitter Module	-	74	0.100	22.72
Video Receiver	76x64x18	90	33.30	-
Antenna	92x92x10	54	-	52.27

Table 4.22: Mass Contingencies [%]

	Structure	Actuators	Battery	Cabling	Autopilot	GPS	Communication
Production, Testing and Competition	5	5	5	2	2	5	2

Table 4.23: Power Consumption Contingencies [%]

	Sensors	Actuators
Production, Testing and Competition	5	5

Chapter 5

Paparazzi

This Chapter describes the software used for this system and implementation of the software for various purposes. First, an overview of the software architecture is given. The transition between horizontal and vertical flight will be discussed. The software implementation for autonomous swarming and the implementation of the ball drop system and QR-code detection will be described.

5.1 Software Architecture

This section describes the main files in Paparazzi which are used to achieve autonomous swarming. They include the airframe file, the flight plan, modules, the NPS simulator and the Ground Control Station.

5.1.1 Airframe

In the airframe file the aircraft configuration is outlined. It describes the used hardware, firmware, sensors, algorithms and configuration parameters [74]. For the hardware the autopilot, GPS, modem, radio control, IMU and others can be specified. Using control gains, trims and behavior settings the aircraft can be adjusted in the airframe file [74].

A distinction is made between rotorcraft and fixed wing vehicles. Although the MAV is designed for both hovering and flying with a fixed wing it is specified as a rotorcraft within the airframe file. This is done because a rotorcraft can be adjusted easily to a fixed wing aircraft by changing control gains, whereas the other way around is more difficult because of differences in control loops. It is important to keep this difference in mind, since all files from server to modules are specified specifically for either rotorcraft or fixed wing aircraft.

In the airframe file, the different attitude parameters are mapped on different vehicle motions in a motor mixing section before tuning the system. For example, for fixed wing mode an upwards deflection of the left throttle and a downwards deflection on the right throttle is coupled to the roll motion. This needed before trimming the aircraft as will be explained in section 5.2.

5.1.2 Flight Plan

The flight plan contains a navigation plan for the aircraft stored in the autopilot to achieve autonomous flight [78]. The flight plan consists of waypoints, sectors and blocks. Waypoints are geographical locations to specify navigation trajectories and routes. Sectors are geographical areas where the corners are marked by waypoints. Mission waypoints include the ball drop zones and corridor poles. Blocks are defined to describe mission units, for example flying from point A to B or flying around a waypoint. A sequence of blocks can describe a trajectory of different tasks. For MAV group 2 and 3 a separate flight plan is programmed which can be found in Appendix G. In order to let the separate MAV groups cooperate, changes in the flight plan can be communicated. This cooperation is discussed in (section 5.3).

5.1.3 NPS Simulator

NPS is the advanced rotorcraft simulator in Paparazzi. It uses sensor modules, JSBSim and FDM, which are flight dynamic models of the aircraft. This simulator is used to simulate the flight plan and swarming of the MAV groups, before testing it in reality.

5.1.4 Modules

Modules are used to add code with initialization, periodic and event functions without modifying the main autopilot loop [75]. Functions can be called in the flight plan or in the airframe file. Therefore, mission modules are available for transitioning, communicating, initiating the ball dropping system, QR-code scanning and recognition, and for collision avoidance.

5.1.5 Ground Control Station

The ground control station (GCS) is software to visualize and control unmanned aircraft during operations [76]. The control is not needed for autonomous flight, but the ground station will be used to monitor the MAV's during the competition.

5.1.6 Communication Flow Diagram

The communication between aircraft and the ground station is shown in Figure 5.1. The system consists of a MAV that is navigating autonomously and is controlled from the ground station. The ground control station provides a graphical user interface with telemetry data received by the link agent which manages the ground-based radio modem. The link agent distributes telemetry data across the network to the server and the messages. The server is an agent that logs, distributes, and pre-processes these messages for the GCS and other agents. The messages consists of a real-time numeric display of all telemetry data [79].

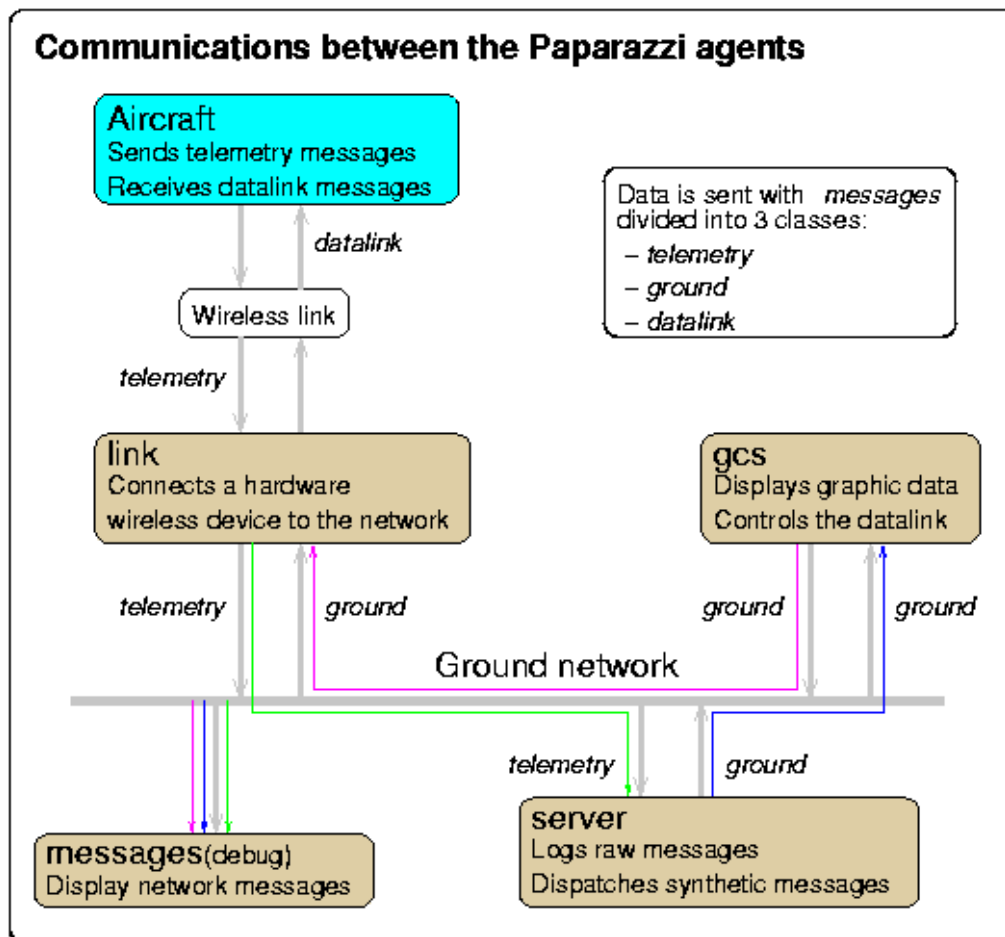


Figure 5.1: Paparazzi Communication Flow Diagram [79]

5.2 Transition

This section describes how the MAV can be stabilized for the flight transition manoeuvre from vertical to horizontal flight and vice versa. The transition is characterized by a change in pitch angle of 90 degrees and a change in the main lifting surface (section 5.2).

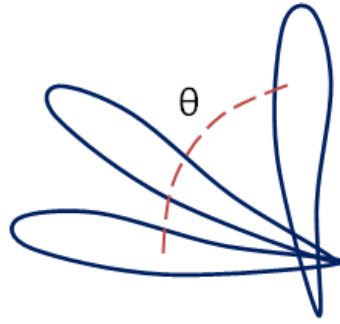


Figure 5.2: Transition

When transitioning, some issues arise which make it difficult to predict the systems behaviour. First of all, non-linear behaviour around the stall speed makes it hard to model the system stability. Second, the propeller slipstream will have a significant effect on the flow around the wing tips, in both vertical and horizontal flight. Also, the morphing wing tips change the angle between the body and tips which has effects on the stability during transition that are difficult to predict. Because of this, it is not easy to have an efficient transition between flight modes without deviating from the assigned altitude.

5.2.1 Control

The control of the system will be programmed in the airframe file in Paparazzi. Paparazzi uses PID control for stability and navigation [77]. A PID controller calculates the error between the desired output of the system and the measured output. The PID controller has the form of

$$u(t) = K_P e(t) + K_I \int_0^t e(\tau) d\tau + K_D \frac{d}{dt} e(t) \quad (5.1)$$

where $u(t)$ is the output and $e(t)$ the error. The gains (K_P, K_I, K_D) can be tuned to obtain the desired closed loop dynamics. If the system is well damped, the proportional gain can be adjusted. The integral gain counteracts long term errors and the derivative gain provides damping. To have a MAV flying on remote control the attitude of the MAV should be stabilized by adjusting the gains for the roll, pitch, yaw angle and yaw rate (Figure 5.3, Figure 5.4) [80].

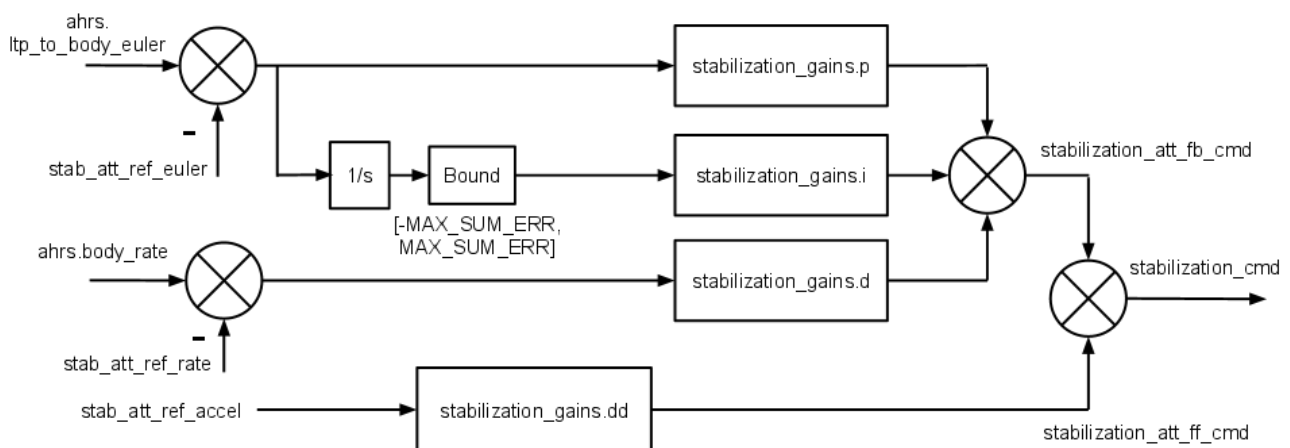


Figure 5.3: Attitude loop for yaw, pitch and roll angle [80]

To have an autonomous system flying the guidance has to be added in an outer control loop, where airspeed and altitude can be tuned (Figure 5.5) [80]. The guidance of the system is initiated by the flight plan.

Different flight modes can be included and an additional module might be needed to switch between those flight modes for transitioning depending on the pitch angle and flight speed. Several approaches for modeling the attitude control will be discussed in the following sections.

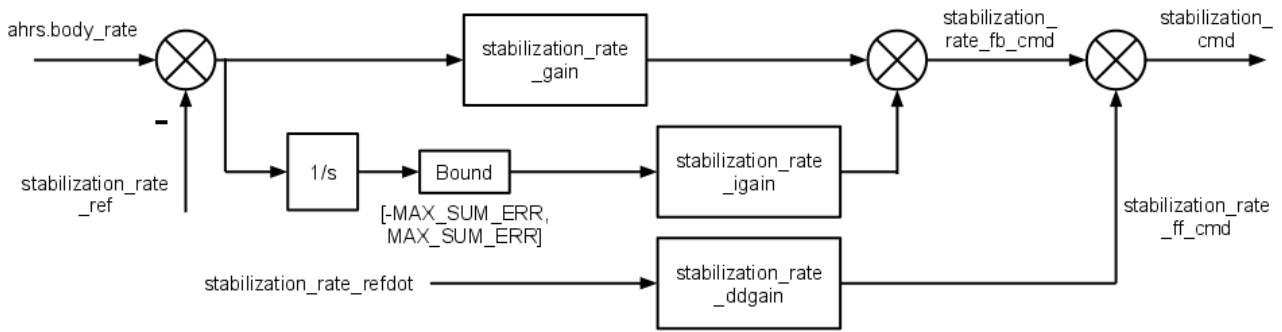


Figure 5.4: Attitude loop for yaw, pitch and roll rate [80]

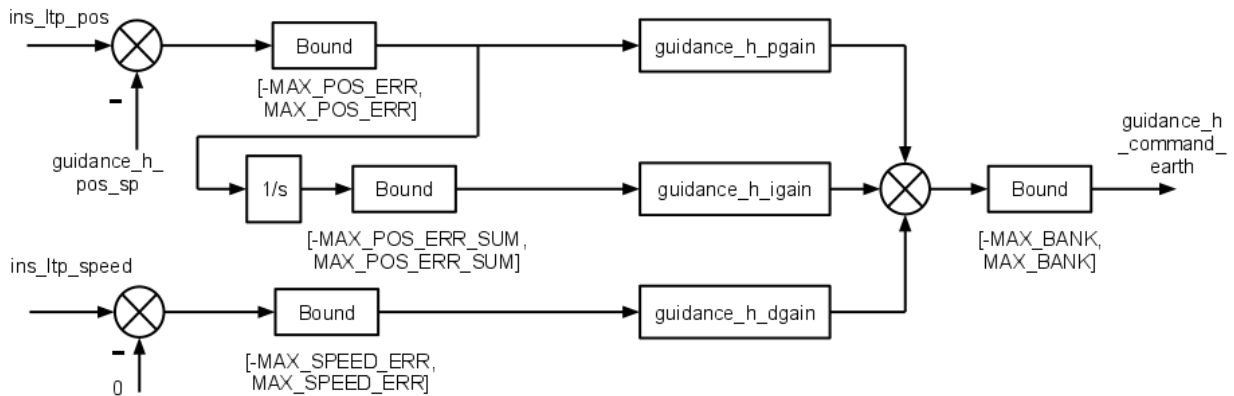


Figure 5.5: Guidance loop for hovering [80]

5.2.2 Empirical Model

Modeling the transition of the vehicle can be done by deriving equations of motion for the aircraft. Wind tunnel tests can be performed to determine the forces and moments and model them for the controller empirically [81]. The three different flight regimes can be distinguished as the pre-stall, stall and post-stall. Empirical formulas can be derived for the forces and moments as input for the model. In order to do so the state variables on which the forces and moments depend should be determined first. The lift, drag and moment coefficient depend on the angle of attack and flight speed whereas thrust is also dependent on the throttle setting [81]. Once the equations of motion for each transition regime are known, a state space model can be made. Because the model is based on testing the system in a controlled environment it will result in an accurate control model for the entire transitioning regime. However, testing the system in the wind tunnel, collecting the data and processing the data to set up the control model will take a lot of time and effort.

5.2.3 Tuning Gains

An easier way of dealing with stability is to trim the vehicle by iteratively optimizing the attitude gains. Two flight modes can be distinguished in the airframe file in Paparazzi, namely the horizontal and vertical flight mode.

Attitude Control

The gains to control the attitude of the MAV can be tuned for both flight modes during tests. A module can be made to implement switching from one flight mode to the other. First, an educated guess is made on the gains to control the attitude of the aircraft. This can be based on similar aircraft or simplified equations of motion. The system is tuned by holding it in the hand while small errors to the desired attitude can be applied as the attitude derivative and integral gains are adjusted in an iterative process to damp oscillations. Once the system is properly damped, the proportional control can be adjusted for each attitude gain. In reality, the system will not experience forces from someone holding it and therefore the iterative processes of tuning the attitude gains should be repeated while the system is flying on its own.

Guidance Control

Once the inner control loop gains are optimized, which means the system is able to stabilize its attitude, the system can be optimized for autonomous flight. This means the altitude and velocity gains can be optimized for inputs on

the throttle and pitch angle. Now the transition regime can be tuned to reduce the change in altitude.

A simple way of dealing with the transitioning problem is assuming the guidance gains to navigate the system vary linearly from horizontal to vertical flight. The guidance gains are first tuned for horizontal and vertical flight and an interpolation is performed to find the gains in the transition regime. This interpolation will be programmed in a module which will be included in the airframe file. In reality the gains will not vary linearly, because the moments and forces acting on the vehicle do not vary linear for the transition regime. Therefore, this method is not the most accurate and will result in less efficient flight performance. However, this method will not result in major changes in altitude [82].

A more accurate method is to tune the guidance gains by giving step inputs on the throttle and pitch angle and analyzing the response. The speed and altitude during the transition can be optimized in an iterative process. This can be done for different angle of attacks to cover the entire transition regime. Since the gains are known for each angle of attack for inputs on throttle and pitch, this method will result in a more accurate control of the flight speed and altitude. This method will require more testing time, but will result in more efficient transitioning, because altitude loss is limited.

5.2.4 Implementation for Autonomous Flight

Now that the methods to control attitude and guidance are discussed, the decision making of the MAV unit of when to transition from horizontal to vertical flight and vice versa during autonomous flight will be discussed. An easy approach to do this is to let the MAV decide the transition mode based on its position error, the difference between its current position and the destination. If the destination is more than 5 meters away from its starting point the MAV will make a transition to horizontal flight. As the position error becomes less than 5 meters the MAV will decide to switch to hover. This can be implemented in Paparazzi by using a module which uses information from the flight plan to activate the transition as described in the airframe file. However, if the destination where the MAV should hover is not the current waypoint, transition should be avoided. The ability to avoid transition should be added as an extra function which can be called by the flight plan.

5.2.5 Conclusion

Because of the limited amount of time, transition will be controlled by optimizing the gains. First the attitude will be stabilized by iteratively adjusting the gains for roll, pitch and yaw. Guidance gains for speed and altitude will be optimized for horizontal and vertical flight. If time allows this will be done for the entire transition regime. Otherwise the assumption will be made that the guidance gains vary linear between horizontal and vertical flight.

5.3 Swarming

A swarm is built up of individuals that interact with one another and with the environment. Within a swarm each individual has its own task, however through communication with the other members the individual will show intelligent behavior and the capacity to adapt to a dynamic environment. In case of a swarm there is no centralized control structure but the behavior is determined by local interaction among the individuals.

The IMAV2013 competition offers the perfect opportunity to show the strength of swarm behavior. The swarm of hybrid MAV's will cooperate by dividing the tasks and specializing in specific areas. In this context multiple sub-swarms instead of one standard swarm will be utilized. This framework will be used to find a good balance between exploration and exploitation. The exploration groups will focus on finding the QR-Code locations whereas the exploitation group will focus on obtaining the points for the competition by dropping the balls. When flying in a swarm collision avoidance is also taken into account to ensure safety for each unit.

The main characteristic of these swarms is that they maintain the information from the previously flown trajectories, meaning they will know which locations they have already explored and which still need to be checked.

To fly the optimal path the best solution needs to be constantly updated as they are operating in a dynamic environment. Group 3 which will drop the balls has a constantly changing optimum trajectory based on the number of QR-Code locations found and depending on the locations where the balls have already been dropped.

In this section first an overview of the communication between MAV's will be given. Secondly, the dynamically changing flight plan will be explained and finally an algorithm will be chosen to determine the dynamically changing optimal solution.

5.3.1 Swarm Communication

For communication between aircraft two types of messages will be sent, telemetry and datalink messages. As was already mentioned in the software architecture, the telemetry message is sent to the server by the aircraft whereas

the datalink message is sent to the aircraft by the server. To display the information at the ground station the server sends it to ground control which will display the information. To be able to send, receive and parse specific messages between aircraft a module has been created. In the module the parsing function is called.

Telemetry messages can be sent by using the command `DOWNLINK_SEND_x`. When the server receives a telemetry message it converts it to a datalink message. The data in the message is not changed but simply forwarded. There are two servers in paparazzi: a fixed wing server and a rotorcraft server. The fixed wing server contains all the standard messages, whereas the rotorcraft server will be used in case a message needs to be sent which only applies to rotorcraft. An overview of the communication for the ball drop system is given in Figure 5.6.

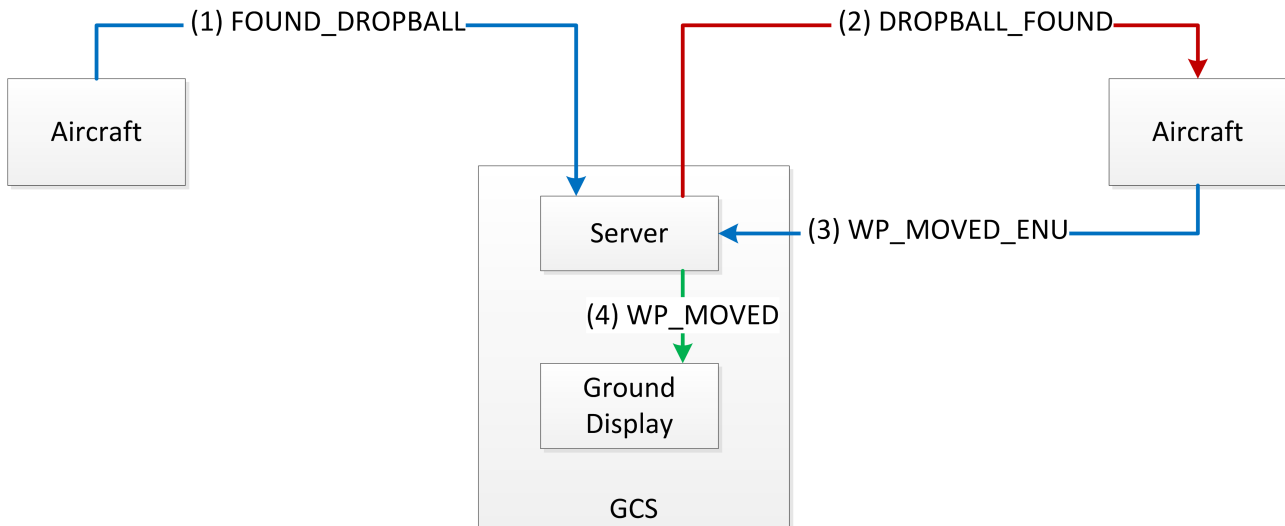


Figure 5.6: Communication Flow Diagram

The aircraft equipped with a digital camera will search for the ball drop zone. As soon as the location of the QR-Code has been determined a telemetry message named `FOUND_DROPBALL` containing the aircraft ID, the waypoint ID and the East, North and Up coordinates will be sent to the server. The server then forwards this message under the name `DROPBALL_FOUND` to the other aircraft. When the receiving aircraft detects an incoming datalink message with the name `DROPBALL_FOUND` it will call a parsing function. After successfully completing the parsing, the aircraft will send a telemetry message back to the server called `WP_MOVED_ENU`. This message was already present in paparazzi and is linked to the ground message `WP_MOVED` which will display the new waypoint location on the display at the ground station.

5.3.2 Flight Plan

The flight plan consists of a number of blocks for which the sequence was determined beforehand. To make the flight plan dynamically changeable with the environment the flight plan waypoints will be updated throughout the flight and blocks can be skipped if necessary. The location of the waypoints depends on whether the QR-Code was already found or whether the ball has already been dropped.

Traveling Salesman Optimization

To maximize the chances of winning the IMAV2013 competition, the maximum number of high-scoring mission elements should be performed within the time limit. As discussed in chapter 2 and subsection 5.3.2, the competition strategy and the flight plan are designed for this purpose. Due to changes in the location of one of the drop ball zones and the positions of the MAV's, the flight plan will be continuously optimized based on the traveling salesman optimization model.

The traveling salesman problem illustrates the problem of determining the most efficient route between points, where the points cannot be visited more than once. The goal of the optimization model is to find the minimum distance the salesman (or in this case: MAV) should cover to visit all the required points. The mathematical solution to this problem is given in equation 5.2. In this equation c_{ij} is the distance between the two points i and j and x_{ij} refers to if the path between i and j is selected.

$$\begin{aligned}
& \min \sum_{i \neq j} c_{ij} x_{ij} \\
& 0 \leq x_{ij} \leq 1 \quad \forall i, j \quad x_{ij} \in \{0, 1\} \\
& \sum_{i=0, i \neq j}^n x_{ij} = 1 \quad j = 0, \dots, n \\
& \sum_{j=0, i \neq j}^n x_{ij} = 1 \quad i = 0, \dots, n
\end{aligned} \tag{5.2}$$

For the MAV's of group 2 the optimization model is used to determine the sequence of the ball drop mission. Since the location of one of the ball drops will change, the MAV will update its flight plan after finishing each mission block. This process will start when the MAV's from group 2 receive the first message of group 3 about the drop zone location.

5.3.3 Collision Avoidance

When flying in a swarm multiple MAV's are flying in a restricted area, which raises the issue of collision. To ensure safety the MAV's should be able to change their trajectory to avoid collision, since the optimum flight paths as calculated using the traveling salesman problem have a possibility to intersect. Paparazzi includes a collision avoidance module which changes the flight altitude of the conflicted vehicles as minimal as possible. The TCAS is able to overwrite the control loop until the conflict is resolved. The TCAS module is continuously active during the flight and should be activated at the start of each flight. The module is now only available for fixed wing aircraft and will be rewritten before the competition to rotorcraft.

5.3.4 Verification and Validation

Verification and Validation are very important steps in the development of the swarming algorithms. For verification of the communication functions the flight plan was simulated several times to analyze if the new ball drop location was communicated. This analysis included the communication of the new drop ball location to the MAV from group 2, but also the updating of the drop ball zone in the MAV's (group 3) own flight plan. The traveling salesman optimization was verified by testing the model, with simplified numbers for the distances, on paper and with the program MATLAB. This test showed that the model succeeded in calculating the optimal flight path.

Validation of the swarming codes will be done by testing the swarm operations in practice. Special notice will be given to the adaption of the flight plans for the new ball drop zones. This tests will be performed after the termination of the official DSE project.

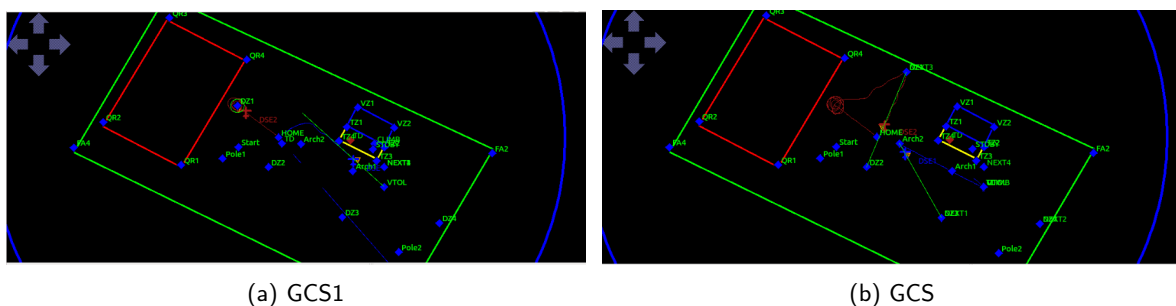


Figure 5.7: GCSs

5.4 QR-Code Detection

In order to apply the theory of the QR-Code detection, discussed in section 4.8, in practice, it has to be implemented in Paparazzi. This implementation brings several new considerations, for example which type of communication protocol is needed. In this section first the considerations in communication protocols are discussed. After this, the codes in Paparazzi for the QR-code detection, processing and communication are briefly analyzed. The implementation in Paparazzi of the QR-Code detection and the SPI communication will be tested in practice and also discussed together with further recommendations.

5.4.1 Communication Protocol

An efficient transfer of data between the Overo Firestorm and the Lisa/M v2.0 is subjected to rules and formats. This rules and formats are stated in a communication protocol. Several communication protocols are available for the interaction between the Overo Firestorm and the Lisa/M v2.0. For this reason, the applicable communication protocols will be discussed in this section.

Protocol Trade-Off

For the interaction between the Lisa/M v2.0, the Overo Firestorm and the CaspaTMVL a communication protocol had to be selected. Three protocols were briefly analyzed based on their transfer speed, implementation difficulty, the number of devices the protocol can support and the number of pins needed to implement the protocol [83]. The three protocol busses available at the Lisa/M v2.0 are the Serial Peripheral Interface, the Universal Synchronous Asynchronous Receiver Transmitter and the Inter-Integrated Circuit.

Serial Peripheral Interface

The Serial Peripheral Interface (SPI) has a four wire and three wire mode. SPI allows full duplex communication and contains one master and one or more slaves. The interaction between the master and a particular slave is possible by asserting the select line. The data is transferred by exchanging the data of the slave in its buffer and the data of the master in its buffer. Benefits of SPI are that no start and stop bits are required and the data is sent with the speeds of the masters' clock. Furthermore, the slave is only active when transmitting data, therefore a lower power consumption is allowed. Lastly the SPI protocol is relatively easy to implement.

Universal Synchronous Asynchronous Receiver Transmitter

Universal Synchronous Asynchronous Receiver Transmitter (USART) has a synchronous mode and an asynchronous mode. In asynchronous mode control bits, start and stop bits are needed. In synchronous mode the data is sent at a predetermined rate. A benefit of USART is that the data has a high level of accuracy.

Inter-Integrated Circuit

The Inter-Integrated Circuit (I^2C) allows both devices to act as the master and as the slave. The master send a start bit followed by an address to the slaves and the addressed slave returns an ACK bit. The biggest advantage of this protocol is that the slave acknowledges the message of the master.

To compare the protocols a trade-off was made of the above mentioned criteria in Table 5.1. The ranking was numbered from 1 to 3, with 3 being awarded for the best protocol of the specific criteria. SPI is the overall winner and the best choice for this implementation since transfer speed is of high importance.

Table 5.1: Trade-Off Communication Protocol

Protocol	Transfer Speed	Implementation Difficulty	# Devices	# Pins	Total
SPI	3	3	3	1	10
USART	1	2	1	2	6
I^2C	2	1	2	3	8

Serial Peripheral Interface Bus [84]

Some aspects and advantages of the SPI were already discussed above, however in this section the SPI bus will be analyzed in further detail. The SPI bus is a synchronous serial data link and uses a master/slave configuration. It can operate in full duplex mode and has complete protocol flexibility for the bits transferred. Furthermore, it has no maximum clock speed, allowing high throughput. A major disadvantage is that it has no master slave acknowledgment. For the interaction between the Lisa/M v2.0 and the Overo Firestorm, the Lisa/M v2.0 is the master and the Overo Firestorm acts as the slave. The link between them is illustrated in Figure 5.8. No addressing concept is needed for this communication. In the figure four logic signals are illustrated [84]:

- SCK : serial clock (output from master)
- MOSI: master output, slave input (output from master)
- MISO: master input, slave output (output from slave)
- SS: slave select (active low, output from master)

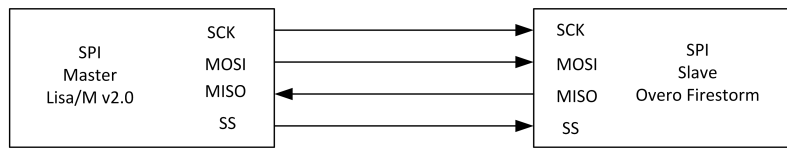


Figure 5.8: SPI bus

Before the data transmission can start, the bus master configures the clock with a frequency less or equal than the maximum frequency of the slave device. Since only one slave device is used, the ss pin can be fixed to active low. The master transmits the logic 0 to activate the communication. The SPI clock cycle then starts with the the full duplex communication, see Figure 5.9. These transmissions can be of any number of clock cycles. If the data transmission is finished, the master stops ends the serial clock.

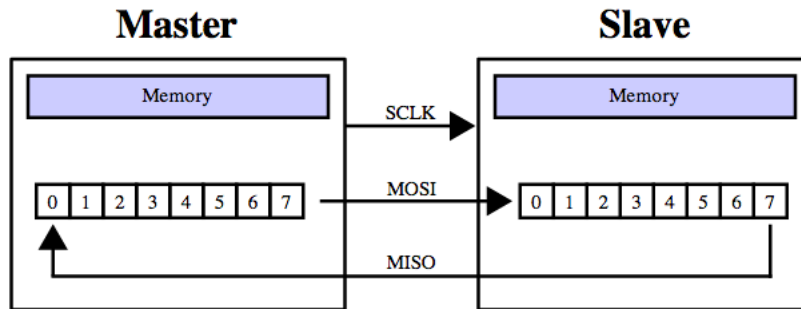


Figure 5.9: Hardware

With selecting the clock frequency, the master also sets the clock polarity (CPOL) and the clock phase (CPHA) with respect to the data. If CPOL is set to 0, the base value of the clock is zero. For CPOL = 1 the base value is one. CPHA is zero results in sampling on the leading edge, while when CPHA is set to one the sampling is done on the trailing clock edge. See Figure 5.10 for illustrations of the different possible modes.

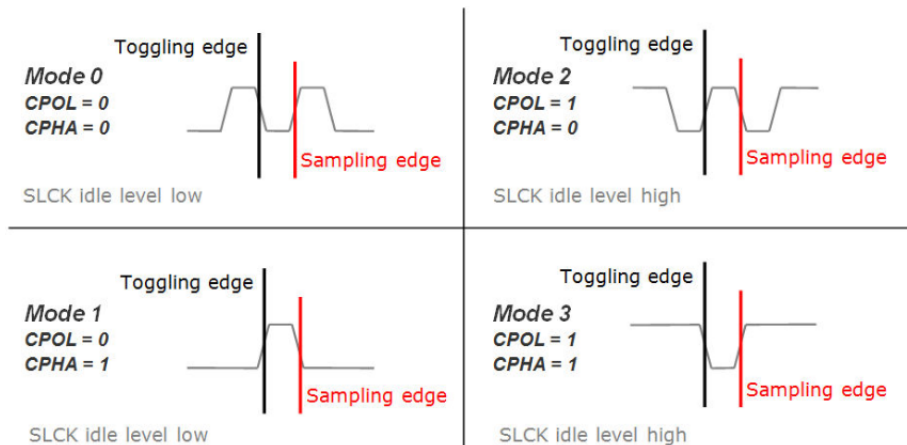


Figure 5.10: Timing Diagram SPI [86]

5.4.2 Paparazzi Codes

In order to take the image of the QR-Code, analyze the position relative to this image and send the location of the drop ball zone (DBZ), interaction between the Caspa VL, Overo FireSTORM COM and the Lisa/M v2.0 is needed. The theory of this QR-Code detection process is already discussed in section 4.8. In this section the implementation of the theory in Paparazzi will be discussed. This section will start with an explanation of the structure of the interaction. After this the modules in Paparazzi will briefly be analyzed. The section continues with a description of a test set-up for verification purposes. Finally, recommendations for further progress are given at the end of the section.

In Figure 5.11 the communication between the Caspa VL, Overo FireSTORM COM and the Lisa/M v2.0 is illustrated. The Caspa VL creates an image of the camera view when the QR-Code is detected. It then sends the

properties of the image to the gumstix Overo FireSTORM. The gumstix analyzes the image and determines the position of the QR-Code with the method explained in section 4.8.

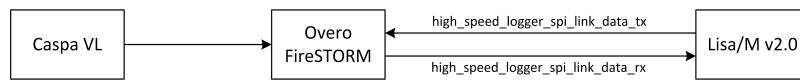


Figure 5.11: Connection Caspa VL, Overo FireSTORM and Lisa/M v2.0

As can be seen from Figure 5.11 the data between the Overo FireSTORM and the Lisa/M v2.0 is transferred with the structs *high_speed_logger_spi_link_data_tx* and *high_speed_logger_spi_link_data_rx*. These structs are part of the SPI communication module called *high_speed_logger_spi_link*.

The SPI communication module consists of a XML file, a header file and a source code file. This file represents the Lisa/M v2.0 side of the communication between the Lisa/M v2.0 and the Overo FireSTORM. The receiving struct (*high_speed_logger_spi_link_data_rx*) contains the id number, longitude and latitude of the detected QR-Code. This data is received from the Overo FireSTORM. The transmitting struct (*high_speed_logger_spi_link_data_tx*) contains the longitude, latitude and altitude of the MAV at the point of detection of the QR-Code. For further details, the reader is referred to the entire module in Appendix I. The attitude of the MAV, which is necessary for the determination of the DPZ for a tilted camera (see section 4.8), is excluded from the module since the camera is assumed to be positioned vertically during the entire mission.

The longitude and latitude of the MAV are determined in radians by the GPS. For a more accurate determination of the altitude, the barometer is used. A simple Kalman filter was applied to this altitude, increasing its accuracy. An illustration of the principle of the Kalman filter is given in Equation 5.3. The accuracy of the estimated altitude value is increased by the Kalman filter, since a weighted average with previous measurements is included [85].

$$\hat{X}_k = K_k Z_k + (1 - K_k) \hat{X}_{k-1} \quad (5.3)$$

Where \hat{X}_k is the current estimation, K_k is the Kalman gain, Z_k is the measured value and finally \hat{X}_{k-1} is the previous estimation. For this DPZ localization the ground is assumed to be flat. This will give an offset from the actual location, however this offset is estimated to be small due to the flat operational field during the competition.

As already mentioned earlier, the coordinates of the MAV position are determined in latitude, longitude and altitude. These parameters cannot be simply added to the coordinates of the QR-Code. For this reason the coordinates are transferred to the local north, east, up (ENU) coordinates. The relative position of the DPZ is also in ENU coordinates. These two positions can now be added to get the actual position of the DPZ. This position is then transferred again to longitude, latitude and altitude coordinates in order to send the data to the other MAV's. This process is illustrated in Figure 5.12. In the figure, the device in which the transformation or calculation is performed is highlighted.

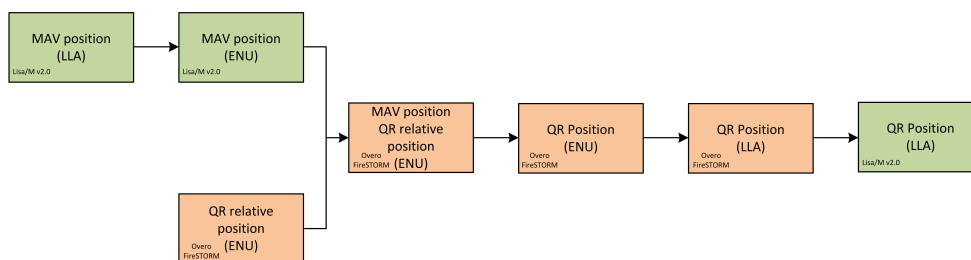


Figure 5.12: Coordinate System Transformation

For verification purposes, the SPI communication module can be tested with the use of an oscilloscope, a probe and a datalogger. The oscilloscope can detect the SPI communication since it observes constantly varying signal voltages. The probe is attached to the Lisa/M v2.0 and the oscilloscope to measure the voltages. The data logger records all the signals and can be programmed to decode the send signals. As a first step, the focus for this verification test will be on illustrating the SPI communication by displaying the voltage differences on the oscilloscope.

Further prospects in the development of the QR-Code module are image processing and QR-Code scanning. For the image processing the challenge lies in the autonomous distinction between the green grass and the black-and-white QR-Code. For the QR-Code scanning, the module has to be optimized for the minimal amount of images necessary to determine the position of the code as accurate as necessary. Finally the focal length, described in section 4.8, will be determined in pixels when the Caspa VLTM is optimized for the QR-Code detection.

5.5 Drop Ball Module

The Dropball module consists of a source code file, a header file and a xml file. In the header file the functions and variables are defined. The source code file determines all the steps and actions that need to be performed by using various functions. These functions include the ability to send messages, receive messages and determine the shortest route. The xml file is included in the flight plan and determines which functions should be called to parse data link messages. The code can be found in Appendix H.

In this section the functions used in the source code will be explained. The send message function receives information from the QR-Code module on the exact location of the QR-Code. This position is given in latitude, longitude and altitude coordinates. The position is converted to local East, North and Up coordinates (ENU coordinates) and then sent to the other aircraft.

The receiving aircraft will use the parsing function to update the location of the waypoint and change the status to detected. The waypoints have three characteristics in this module, namely id, detected and dropped. The id is a number and is unique for every waypoint. The detected and dropped characteristics can be set to either true or false.

The function used to determine the shortest route follows these steps:

- Determine how many waypoints have been detected and where the balls have already been dropped
- Determine the distance between all the drop ball waypoints
- Determine the distance from the start and end position to all the drop ball waypoints
- Find all possible routes using the lexicographic permutation algorithm
- Find the shortest route
- Move specifically defined waypoints to the optimal route sequence

The amount of waypoints that have been detected and dropped is determined by checking whether the status of the waypoints is true or false. If a waypoint has been detected the status will be true and the waypoint will be included in the flight plan route. However, if the status of dropped is set to true it implies a ball was already dropped on this location and it will not be included in the flight plan. The distance between two waypoints will be calculated in three dimensional space by using the North, East and Up coordinate system using Equation 5.4.

$$distance = \sqrt{\Delta x^2 + \Delta y^2 + \Delta z^2} \quad \text{where } \Delta x = |x_1 - x_2| \quad (5.4)$$

To determine all possible routes the waypoints will be stored into a vector and all the permutations of this vector will be computed. As all permutations will be stored into a matrix a non recurrent function should be used to prevent memory overflow. The algorithm that computes the next lexicographic permutation of a vector will be used [87]. This algorithm uses the following steps:

1. Store all the drop ball waypoints in vector $a[]$
2. Find the largest index k such that $a[k] < a[k + 1]$. If no such index exists, the permutation is the last permutation.
3. Find the largest index l such that $a[k] < a[l]$. Since $k + 1$ is such an index, l is well defined and satisfies $k < l$.
4. Swap $a[k]$ with $a[l]$.
5. Reverse the sequence from $a[k + 1]$ up to and including the final element $a[n]$.

To find the shortest route the distance between all waypoints of the route and the start and end point will be summed up. The sum will be compared with the value of the previously calculated minimum distance. After checking all routes the minimum distance route will be chosen for the flight plan. The waypoints will be moved to match this optimal order.

Chapter 6

Verification and Validation

This chapter describes the verification and validation of the complete system. To verify a system the compliance with the design solution specifications and descriptive documents should be proved. For validation it should be proved that the product accomplishes its intended purpose based on stakeholder expectations [89].

6.1 Verification

Verification of the product applied on several levels during the design process. Subsystems are verified based on their individual performance and requirements and the complete system will be verified based on system requirements. For every subsystem the verification method is discussed in the detailed design section of the specific subsystem.

System Verification

In order to verify the system a simplified prototype was build as can be seen in Figure 6.1. The prototype was cut out of foam and had the same dimensions and same CG location as the designed MAV. The morphing structure was simplified by splitting up the foam in three wing parts which could change their relative attitude using a hinge mechanism similar to the real design. The hardware excluding payload was glued or taped to the body.

The prototype will be used for initial testing of the stability, control and performance of the designed MAV. The working of the actuators and sensors will be verified and the stability gains will be trimmed as described in section 5.2 to make the airframe file working. After testing by hand the prototype can be tested using the setup shown in Figure 6.2 to prevent the MAV from crashing.

If the airframe file is working properly for the prototype it will be easy to update the airframe file for the 3D printed MAV. After testing the prototype, the final MAV design will be verified as well.

In order to verify the final MAV design it has to comply with the system requirements. The total weight of the vehicle will be measured with a weighing scale and the dimensions will be verified with a ruler. The hover and horizontal flight modes will be verified by testing the MAV on stability and performance as well as the transition. Also, precision landing and autonomous take off will be verified by testing. An outdoor test at rough weather conditions should be performed to verify the MAV is able to fly with wind speeds up to 5bft and gusts of 6bft and light rain. The

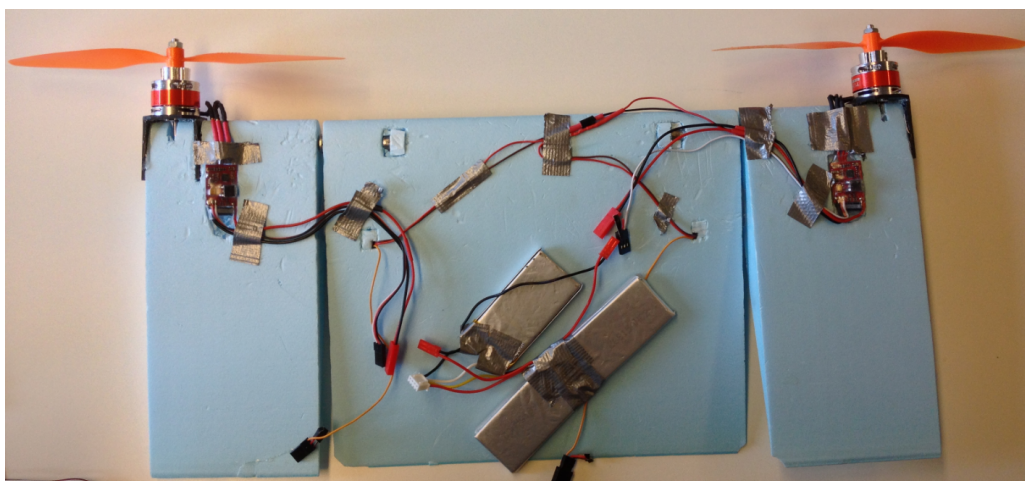


Figure 6.1: Prototype

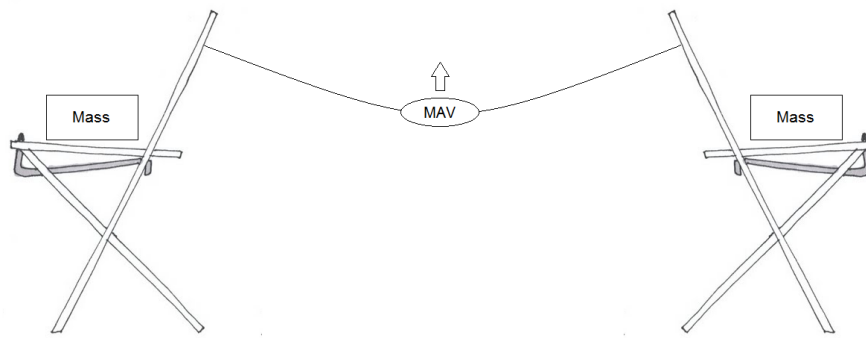


Figure 6.2: Test setup

wind speed will be measured with an anemometer. Furthermore, several autonomous flight tests will be performed to verify if the swarm is working properly. Collisions should be avoided and the MAV's should be cooperating when performing complex missions.

6.2 Validation

Validation takes place in multiple stages in the design process. All requirements were validated according to the following rules. The requirements should be verifiable (quantitative, objective), achievable (sufficient resources available), logical, integral (complete) and definitive (unambiguous) [89]. Furthermore, the models used to design the system were validated to develop objective evidence that the models reflect the real world as accurately as possible. Models were used for the structures, aerodynamic and stability and control subsystem. Also, software models were used for swarming and autonomous flight. All models were either validated by experience, analysis or by comparison in the detail design sections.

Finally, the product should be validated to prove that the product accomplishes its intended purpose based on stakeholder expectations. For this project this means ensuring the MAV is able to perform all mission elements autonomous and that multiple MAV's are able to cooperate in a swarm during the IMAV2013 outdoor competition. Therefore, the MAV's have to show their able to:

1. Perform an autonomous landing and take-off again
2. Drop the balls near the centre of the drop zone
3. Search and detect a QR-code in a large field
4. Fly through a corridor
5. Fly around two poles efficiently at a high speed and with a small turning radius
6. Cooperate in a swarm

6.3 Compliance Matrix

The compliance matrix states all requirements and if these are met, the compliance matrix is displayed in Table 6.1. As can be seen all requirements are met, the chapter number is given to show where the requirement is treated.

Table 6.1: Compliance Matrix

Requirement	Met	Chapter
The MAV shall weigh 2 kg or less.	✓	section 4.15
The MAV shall have a size of less than 50 cm.	✓	subsection 4.1.2
The MAV system shall cost less than budget available.	✓	section 4.15
The MAV system shall communicate using one of the authorized frequencies and power.	✓	subsection 4.7.3
The MAV shall fly below a height of 50 m.	✓	Appendix G
The MAV shall fly within the boundaries of the competition area.	✓	Appendix G
The MAV shall be able to detect a QR-code.	✓	subsection 4.8.1
The entire system shall be able to finish the mission in 30 minutes.	✓	Appendix G
Each MAV shall have a clear distinction from the other MAV's .	✓	subsection 4.12.2
Each MAV shall have a flight endurance of at least 20 minutes.	✓	subsection 4.14.1
The MAV system shall be completely autonomous.	✓	section 4.6
The MAV system shall be able to operate in light rain.	✓	subsection 4.3.6
The MAV system shall be able to operate in winds of up to 5 bf.	✓	subsection 4.14.2
The MAV system shall be able to operate in gusts of up to 6 bf.	✓	subsection 4.14.2
The MAV system shall allow for communication between all units.	✓	subsection 4.7.3
The MAV system shall have at least three video streams.	✓	subsection 4.7.3
The MAV system shall be developed within the 10 weeks of the DSE project.	✓	Report
The MAV system shall not produce any waste.	✓	subsection 9.1.2
The MAV shall have a vertical take-off capability.	✓	subsection 4.4.4, subsection 4.3.2
The MAV shall have an efficient horizontal cruise mode.	✓	subsection 4.1.2
The MAV shall be able to hover.	✓	subsection 4.4.4
The MAV shall be able to transit between hover mode and cruise flight mode.	✓	section 5.2
Each MAV shall maintain positive control in all stages of flight.	✓	subsection 4.2.6
The MAV system shall provide power for continuous operation of all electrical components.	✓	subsection 4.5.2
The MAV shall fly stable.	✓	subsection 4.2.6
The MAV shall provide lift.	✓	subsection 4.1.2
The MAV shall be able to provide enough thrust for each flight mode.	✓	subsection 4.4.4
The MAV shall be able to perform a vertical landing.	✓	subsection 4.4.4, subsection 4.3.2
The MAV shall be able to report its position.	✓	section 4.6
The MAV shall have a search and recognition capability.	✓	subsection 4.8.1
The MAV shall have integral signal processing capability.	✓	section 4.6
The MAV system shall be capable to make decisions fully autonomously.	✓	section 5.3
The MAV shall provide structural integrity to carry all aerodynamic loads.	✓	subsection 4.3.2
The MAV shall provide structural integrity to survive a fall on a hard surface from 1 m.	✓	subsection 4.3.2
The MAV materials shall allow for MAV production within one day.	✓	subsection 4.3.6
The MAV system shall be able to cooperate to complete a mission.	✓	subsection 5.3.1
The MAV system shall be able to avoid in-flight collisions.	✓	subsection 5.3.3
The MAV system shall provide for a human interface.	✓	section 4.10
The MAV system shall allow for control of each unit at all times.	✓	subsection 4.7.3

Chapter 7

Operations

Now that the MAV design is fixed, the operations of the MAV system before, during, and after the mission will be elaborated on. This section describes the steps necessary for the mission setup-up, how the mission elements and flight modes are performed, and the round-up during post-mission.

7.1 Pre-Mission

Before starting the mission, the setup of the MAV system needs to be completed. During this phase, all components need to be tested to make sure that they are operational. The following checklist needs to be completed step-by-step before the mission can be initiated:

- Inspection of all parts for intactness and possible damages caused by transportation.
- Check of the charging level of the batteries of the MAVs, ground station and safety link & recharging in case of low voltage.
- Assembly of the MAVs, including the attachment of the landing sticks and propellers.
- Set-up of the ground station computer.
- Connection of the receiver for video down link and the modem for data communication.
- Connection and alignment of the antennas.
- Selection of the flight plan and configuration files.
- Check of the flight plan for correct GPS location and adjustment of the reference point.
- Compiling of the autopilot software.
- Connection of the MAV to the ground station via FTDI USB cable.
- Upload of the autopilot software.
- Frequency check for the safety link transmitter & wireless modems.
- Setting the safety link switch to manual mode and power-on of the safety link transmitter.
- Power-on of the MAV.
- Start of flight session in the ground station.
- Check of the data link between ground station and the MAV.
- Functionality check of the servos and motors using the ground station.
- Placement of the MAV on the take-off position.
- Waiting for correct GPS signal.
- Execution of the flight plan and start of the mission.

7.2 Mission

Once the MAV system has been set up, the mission can be initiated, which is done by executing the flight plan in Paparazzi. This section describes the operations of the MAV units during the mission.

7.2.1 Vertical Take-Off and Hover

Before take-off is performed, the MAV stands vertically in take-off position with the propellers pointing upwards, while being supported by two rods on each side of the vehicle as seen in Figure 7.1. When the flight plan file is executed, the engines of the MAV unit are started, providing sufficient thrust to ascend to the desired altitude. Once the MAV has performed its take-off and a destination is included in the flight plan, it will try to move towards transition in

order to conserve energy. However, in some situations such as in the preparation for landing, the MAV unit needs to hover. While hovering, the flying wing is positioned vertically, with the motors pointing upwards. It is achieved when the propellers provide the same thrust force as the weight of the vehicle and the drag that is caused by the propeller slip streams. The system is, as in every flight mode, entirely controlled by wingtip deflections and thrust inputs.

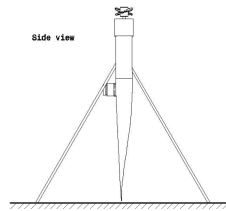


Figure 7.1: Side view of the vehicle in take-off and landing position

7.2.2 Transition

Once a safe altitude of 1.5 m has been reached, which is based on the assumption that a stable transition without considerable altitude loss can be achieved, the MAV switches flight modes from hover to horizontal flight. This is done to change the main lifting surface from propellers to fixed wing, saving energy and therefore increasing efficiency, as explained in subsection 4. The transition of the MAV is initiated by deflecting the wing tips to create a negative moment about the CG, while at the same time adjusting the thrust setting to account for attitude losses or gains. A more elaborate analysis of the transition maneuver can be found in section 5.2.

7.2.3 Horizontal Flight

Once the wing of the MAV reaches the linear region of the $C_L - \alpha$ -curve, it is considered to be in horizontal flight. For horizontal flight the MAV will fly approximately 50 km/h (13.9 m/s) and at an altitude of approximately 5 m, except for units that scan the ground for QR-Code detection. Stability and controllability in horizontal flight are mainly provided by deflecting the wing tips to induce correcting moments via thrust vectoring, as described in section 4.1 and section 4.2.

7.2.4 Mission Elements

Different mission elements have to be performed in order to score points at the IMAV2013 competition. These include the ball drop mission, QR-Code detection, corridor flight, and the flight performance mission. This section gives a detailed description on how each of these elements are performed at the competition.

Ball Drop

The ball drop mission is the most important mission element since it is the greatest potential point source. Each MAV has four balls on board that are dropped on the four target areas as seen in Appendix A. One of the target areas on the field is not located at its indicated position, which is why the MAV units have to first confirm their position by finding the QR-Codes of the drop areas. MAV Group 3 is therefore sent out to check the GPS coordinates of the target areas immediately after mission launch. Once the coordinates of the displaced target area are located, which is done with the use of the camera positioned on the bottom of the MAV's, each MAV is ready to drop their balls on the target areas.

The drop will occur in horizontal flight at the normal flight speed of 50 km/h and an altitude of around 1 m to account for winds, which could sweep the ball off away. The velocity has to be adjusted according the validation results of the ball drop system. Tests indicate a quick and predictable execution of the ball drop, which means that faster drop speeds are possible in the implementation. However, since the navigation fully depends on GPS signals, which can have a considerable error, the drop velocity will be determined after integrated testing has been performed.

QR-Code Detection

The QR-Code detection has two applications during the mission. The first one is during the target detection and recognition mission element, which is performed within a prescribed area where the location of a QR-Code needs to be determined and its message decoded. During this mission element, the MAV units of MAV Group 1 perform horizontal flight at a high altitude at a velocity of approximately 50 km/h, where the exact speed and height have

to be determined during testing. The MAV units fly an optimal pattern, depending on speed and altitude, in order to quickly recognize the QR-Code.

The recognition of the QR-Code itself is carried out in two steps. First, the QR-Code area is detected on the ground with the digital camera using a color algorithm. The MAV determines its relative direction and proceeds to fly towards the code while descending to a lower altitude. In the second step, the QR-Code is recognized, read and decoded as the MAV approaches and flies over it. Testing will determine the altitude and airspeed that are necessary for the camera to read the QR-Code. Once the code has been read and decoded, the decoded message is sent to the ground station and shown to the jury to receive points for the completed mission.

The second application of the code detection is during the ball drop mission. MAV Group 3 is sent out at mission start to scan the four QR-Codes on the drop zones to check whether these are at their indicated GPS coordinates. If the MAV unit can not find the QR-Code at its position, it initiates a pattern to look for the code in its vicinity. Once it has been found, the MAV communicates the new GPS coordinates to the other MAV units.

Corridor Flight

The corridor flight mission element is completed by flying between two cones of 8 m height that define the corridor, as seen in Figure 2.2.

In order to fly through the cones, the GPS system is used for navigation. Since the GPS coordinates of the cones are known, this mission element can be completed in the horizontal flight mode to make it efficient. As already mentioned, there are limitations to the precision of the used GPS system NEO-6, introducing constraints on the altitude that can be flown during the corridor flight. This means that flight at 3 m altitude through the cone is too risky, since the maximum distance between the two cones is only 4.75 m, meaning that a distance of only 2.37 m to each side of the MAV is available when flown through the center. In order to reduce this risk, an altitude of 7 m altitude is chosen to complete this mission element, keeping a distance of 2.87 m to each side. The score at this altitude, however, is reduced to one point per MAV. The mission will therefore be carried out at an altitude of 7 m and at cruise velocity of 50 km/h in horizontal flight.

Although a buffer of 2.87 m to each side of the MAV seems to be sufficient for using the GPS receiver as the means of navigation through the corridor, the possibility that it does not perform at the competition is always present and relies upon how many GPS signals can be received on the day of the competition. A way to circumvent this problem is to implement a function in the MAV that uses the camera to determine its position relative to the cones. This would affect MAV Group 1 and MAV Group 2 in particular.

In order to use the digital camera, the MAV has to switch to vertical flight and scan the cones, which are painted blue and could therefore be recognized using a color recognition algorithm. It hovers through the cones while staying central, and then switches back to horizontal flight to fly to the exit of the corridor. Here, it performs the same manoeuvre, switching to vertical flight, hover through the cones and continue its mission in horizontal flight. Since hovering flight is highly inefficient, its use has to be limited. This is why only the entrance and exit of the corridor relies on the camera, while the GPS is used to navigate the MAV through the main part.

Points are also scored when the MAV stays within the corridor boundaries for the entire duration, which means that this part of the mission element score is going to depend on the accuracy of the GPS receivers.

Performance Flight

The flight performance element is the least important element to be executed by the MAV units since it does not provide a high amount of points. As seen in Figure 2.1, the MAV's have to circle around two poles and cross the start/finish line to score points. This mission element is performed in horizontal flight at 50 km/h, at an altitude of 5 m. Collision avoidance in case of congestion is provided by an integrated TCAS module in Paparazzi that prompts affected MAV's to deviate from their current altitude to a safe altitude.

7.2.5 Presentation

The presentation of the mission performance is an important part of the overall score since it can add 10 % of the acquired points to the final count. Therefore, a presentation screen will be set up that shows the progress of the mission with the use of a high-lumen beamer. A speaker will comment on the progress while keeping the crowd entertained.

7.2.6 Landing

Once the landing coordinates have been determined and reached, the MAV unit must switch from horizontal to vertical flight in order to land. To perform the landing, it must position itself exactly above the landing spot while hovering, and reduce its altitude to approximately one meter. Due to inaccurate instrumentation, the altitude of the MAV can only be determined with an error, which can be as high 0.5 m as experiments from previous users of the

Lisa-M board have indicated. This is why a steady descent from one meter above ground level up to touchdown is performed.

In order to determine the horizontal position of the MAV, the GPS receiver is used. According to the technical spreadsheet of the NEO-6 GPS receiver [90], a precision of 2 m can be achieved during 50 % of the time. This does not allow for a precision landing, which is why MAV Group 2 performs a normal landing using GPS signals only. MAV Groups 2 and 3, however, have a tilting digital camera on board that can use existing color recognition algorithms to make a precise landing and thereby score extra points.

Measurements of the accelerometer indicate a high acceleration gradient at touchdown, which is recognized by the autopilot, switching the motors off. The rods on the sides of the MAV prevent it from flipping over upon landing, allowing a tilting angle of up to 30 degrees.

Wind is going to be an important factor when landing. Because of the MAV's ability to determine wind speed and direction during the mission, it will use this data to position itself for landing by turning sideways to the wind. This prevents the autopilot from doing unnecessary work and saves some energy that would otherwise be used for attitude corrections due to wind gusts. Landing sideways to the wind also ensures that the MAV does not tip over when on the ground, since the set requirements demand it to operate at high wind velocities.

The signal for landing is given when the battery power is low or the allocated mission time is about to expire. This means that the MAV units return to the starting point for landing in order to save time on collecting the MAV's, since the field needs to be completely cleared within the mission time.

7.3 Post Mission

After the mission is completed the MAVs have to be collected from their landing spots and turned off by disconnecting the battery. After a visual inspection for damages that might have been caused by the landing, the batteries can be removed for recharging. The MAVs can now be disassembled for transportation, which includes the removal of the landing structure and the propellers and the installation of a lens protection for the camera. The ground station will be shut down and the receivers and antennas disconnected.

Afterwards a post-mission analysis can be performed which is essential for further improvements of the system. A first general assessment of the mission gives an overview on which elements were performed satisfactory and which ones failed and need further improvement. The log files created during each mission contain all the telemetry data sent during flight and can be used for a more detailed analysis in order to optimize the different subsystems. The creation of a velocity profile for example is a good basis for the optimization of the propulsion system. In general the log files are a powerful instrument and will be used extensively for post mission analysis.

Chapter 8

Risk Assessment

This Chapter discusses the risks the project and product is exposed to and how is dealt with this risks. First, a risk assessment is performed identifying and analyzing risks. The reliability, availability, maintainability and safety of the system will be discussed in the second section.

8.1 Risk Analysis

The following section will give an overview and update of the different technical risks the project is exposed to and their possible consequences on the overall success and ability to fulfil the performance, schedule and cost requirements. The identification and assessment of risks will increase the awareness and will help to organize the design process in way to reduce risks and increase the chance of success of the project. The different risks are first described and afterwards classified according to their probability and consequences. The results are visualized in a risk map in Table 8.1.

1. **Unstable and uncontrollable MAV:** A critical aspect in the design of the MAV's is stability. The hybrid functionality requires stability during vertical flight, horizontal flight, hover and the transition phase, which significantly increases the complexity and likelihood of failure. As failing to achieve stability would have catastrophic consequences for the participation in the competition as well as the project itself, it is given highest priority in order to reduce the risk. Assumptions which can't be neglected in practice have been made in order to model the control of the MAV. Those will effect the real behaviour of the MAV.
2. **Swarming and communication:** The communication between the MAV's and the ground station is essential for operation. Failure of the communication subsystem will delay the development process and if occurring during the competition will drastically reduce the chances of a successful completion. The probability of a complete failure of the communication system is however relatively low.
3. **Power consumption exceeds budget:** A high power consumption may prevent the MAV's from achieving the minimum flight time specified in the requirements and therefore from completing their mission during the competition. Currently the design power consumption has been finalized and seems not to exceed the expected one.
4. **Exceeding size and weight limits:** As the size and weight limits are already known and the MAV will be designed according to them, the probability of exceeding them is very low. However, a failure to meet the requirements will have severe consequences as participation in the competition would not be possible. Currently the design has tendency to increase weight but not dramatically.
5. **Electronics and interference:** The risk of damaging electronic component during the project exists. The electronic components can be replaced and modified during the project. However, before the competition all the systems need to be maintained to prevent this during the competition.
6. **QR-code recognition and ball-dropping system fails:** This is when the MAV is stable and able to fly but a problem in the QR or the ball dropping system hardware and/or software withholds the MAV from completing its task. So far there are no problems or concerns and the QR code and the drop ball system have been already tested.
7. **Weather condition:** The weather condition has an effect on the competition preparation. In case of rain and strong wind testing should be done in a closed area or the MAV should be remodelled to that specific weather.
8. **Production:** Productions brings risks because of production delays and deficiencies in the product quality. This results in delays in the schedule. Since the design of the MAV is rather small the production line is expected to be rather simple. However, the group should still find a sponsor for 3D production. The group is continuously trying to find a company.

9. **Programming errors/bugs:** This is when an unexpected error is found in the code. It is common to have programming bugs however, those can be fixed on time. Due to unfamiliarity of the group with the Paparazzi software, fixing errors takes longer than expected. Due to this the risk will be higher.

Table 8.1 is the risk map analysis for each criteria. As one can see the most critical risk is in case of control and QR Code problems. In order to avoid delay in schedule some actions need to be taken. Those actions are:

- Take a time safety margin
- Allocate more people that will help and check the stability and control of the MAV as well as the QR code.
- Verify the results with other related designs
- Every critical decision should be consulted with an expert and well experience people

Table 8.1: Risk Map: Consequence vs. Likelihood

Very Likely		5		
likely		7	9	1
Unlikely			6,2,3	
Very Unlikely				4,8
	Negligible	Marginal	Critical	Catastrophic

8.2 Reliability, Availability, Maintainability and Safety

This section describes the reliability, availability, maintainability and safety (RAMS) characteristics of the system. Reliability and availability can be quantified based on component characteristics and test results. Since there was limited time for this project it was not possible to test the system to quantify the reliability and availability. However, during the design process reliability, availability and safety aspects are kept in mind. For maintainability an outline of scheduled and non-scheduled maintenance activities is given.

8.2.1 Reliability

Reliability is defined as 'the probability the system will perform in a satisfactory manner for a given period of time when used under specific operating conditions' [91]. It is important to keep in mind that reliability affects both availability, maintainability and safety. Reliability is equal to one minus the failure probability of the system, which is the integral over the failure density function. Hence, reliability decreases if the number of failure over time increases. Usually, the failure distribution over time is modelled as a negative exponential function, which means the reliability decreases over time for a constant failure rate [91]. The reliability is then derived as shown in Equation 8.1, where λ is the failure rate:

$$R(t) = e^{-\lambda t} \quad (8.1)$$

Each component and subsystem of the system has its own failure rate and reliability. The total reliability of the system can be modelled as a circuit of reliabilities. Critical components and subsystems are modelled as series within the circuit which means that if one fails the system will not be able to operate according to its requirements. The total reliability of a series of reliabilities can be calculated as:

$$R_{series} = e^{-\left(\sum_{i=1}^n \lambda_i\right)t} \quad (8.2)$$

Components or subsystems which are less critical when considering the overall system performance are modelled in parallel. Through active redundancy more components or subsystems can be placed in parallel which means reliability increases (Equation 8.3).

$$R_p = 1 - \prod_{i=1}^n (1 - R_i) \quad (8.3)$$

For this system the failure rates of the components are unknown, since no tests could not be performed because of the limited time span. However, each subsystem is considered crucial for the system to function according to the requirements. In order to improve reliability redundancy can be applied to critical components as a fail safe mechanism. Unfortunately, this will mean increasing weight which will have a negative affect on the design.

The reliability in accomplishing this mission can also be increased by increasing the number of MAV's within the swarm. If one MAV fails another one can take over its task and the mission can still be accomplished. Adding multiple MAV's will therefore increase reliability since this is modelled in parallel.

After the project is finished, specifically the airframe structure should be tested to quantify the reliability. For ordered components reliability is assumed to be within acceptable limits based on fabrication data sheets and user experience.

8.2.2 Availability

The availability of the system is defined as 'the degree, percent, or probability that a system will be available when required for use' [92]. Availability is affected by maintainability and reliability.

For this mission availability is important during test flights to practise for the competition and even more important during the competition. Since the MAV's are very small and light it is easy to transport the MAV to a preferable place for testing or practice. This means the system can be used at all times and places, however other issues like maintenance can decrease the availability.

Since the system consists of a swarm of multiple MAV's not only reliability but also availability is increased as the number of MAV's is increased. If for example one MAV requires maintenance the system is still able to operate as a swarm. In order to have the system flying autonomous however, also the ground station should be available. Therefore it will be ensured multiple laptops are available to function as ground station. The availability of a single MAV depends on the availability of components, maintenance and the charge of the battery.

All components should be available at all times during the period of practise and during the competition. Therefore, an inventory list of all the necessary components is made and continuously updated, ensuring that the right components are ordered on time.

During flight the battery will discharge and if the battery is fully discharged the MAV will not be able to perform any further mission elements. Therefore, the endurance of the battery will be long enough to fulfil all required mission elements. Furthermore, the battery will be fully charged before each flight test and before the final competition. However, for testing purposes longer endurance might be beneficial because when endurance is increased more test results can be acquired in the same session. A reserve battery can be used to increase the systems availability.

The maintenance of the vehicle will be discussed in the next section.

8.2.3 Maintenance

The maintainability of a system is defined as 'the ease with which a product can be maintained in order to maximize efficiency, reliability, and safety' [92]. As already shown in the functional break down structure maintenance consist of two separate parts: scheduled maintenance and unscheduled maintenance.

The scheduled maintenance is based on the chosen design solutions. Lifetime indications of all components should be considered when scheduling maintenance in order to keep the system working properly. The discharge rate over time of the batteries is logged for example. From this predicted failures of components can be prevented. For the maintenance a storage with equipment and working space is needed to execute the repairs and replacements. The MAV laboratory (MAVlab) of the TU Delft will provide this room and equipment.

Scheduled maintenance also consists of inspecting each MAV after flying or testing on damages. It is important to investigate damaged parts and decide on repairs or replacement in order to prevent future failures. Also, transport of the vehicles should be taken into account, since the vehicles should be transported to France. The components will be disassembled from the body and packed with a layer of bubble wrapping for safety. After transportation maintenance is scheduled which consist of inspecting each component on damages.

The unscheduled maintenance consists of repairing or replacing components for which failure was unforeseen. For example if an MAV crashes due to external influences. Unscheduled maintenance will decrease if reliability and safety increases. In the next section safety of the vehicle and operations is assessed.

8.2.4 Safety

The safety of a system is defined as 'the freedom from hazards to humans and equipment [92]. Safety needs to be provided for the system itself, including all MAV's and the ground station, other systems, humans involved and the environment. The safety of the system affects the reliability and also the maintenance, since damages can be prevented if safety is provided. Therefore, safety is increased by reducing hazards as much as possible.

During autonomous flying in a swarm safety will be provided by applying several measures. To avoid mid-air collisions a collision avoidance system called TCAS will override other functions to ensure the MAV's know each others positions and change flight paths if necessary. Also, MAV's will send status updates to check each others performance. A safety link will enable the operators to overrule the autopilot if necessary.

Furthermore, safety of the system will be provided during transportation by disassembling and packing the vehicle as explained before. When testing appropriate locations will be chosen to avoid crashes. Weather conditions will be checked beforehand to prevent the system from damages caused by environmental factors. Testing will always be performed by two or more people for safety of humans involved. Last but not least, scheduled maintenance will never be postponed in order to avoid structural failure of the vehicles.

Chapter 9

Sustainability Analysis

In this Chapter the sustainability of the design is analyzed and discussed. The sustainability is analyzed for a single MAV and for the complete system. The design part mainly consists of discussions on the sustainability of all aspects of the MAV, such as material selection and energy usage. The swarming part discusses the methods on how to operate a swarm in a sustainable way.

9.1 MAV Design

The sustainability of the design itself can be split up in two parts, the benefits of the design regarding sustainability and the life cycle of the MAV.

9.1.1 Benefits of Design

Since the size of the MAV is only 45 cm, the resulting footprint on the environment is small. However, the ecological footprint can always be reduced by implementing smart and sustainable solutions. Operating a swarm of these MAV's increases the footprint. Therefore, it is important to reduce the footprint of a single MAV.

One of the main characteristics of the MAV is its hybrid performance. This benefits the sustainability of the product, since the MAV is able to fly efficient horizontally while also keeping the ability to hover. The horizontal wing configuration is efficient during high velocity cruise and the hover flight is most efficient for precision landings and take-off. This will save energy and make the product more sustainable.

9.1.2 Life Cycle

A life cycle consists of pre-life, life and end-of-life. The pre-life phase regards the production, the life the operation of the vehicle and the end-of-life the disposal of the MAV.

Pre-Life

The MAV consists out of three main materials, the SLS material PA2105 consisting out of the polymer PA12, Carbon fiber and the elastic skin Platilon U04 consisting out of thermoplastics. Different processes are used to shape the materials. These processes have an impact on the environment and increase the footprint of the MAV.

Starting with SLS, the production method is generally very energy consuming but it has the advantage of low material waste. The product is created and the polymer powder left can be reused. However, not all material can be reused since it will be heated up, so the properties of the powder will degrade and after a while it can not be used any more. Several studies are performed to improve this aspect of the SLS technique and the sustainability of the technique improves [94]. Another benefit is that a smaller machine can be used, since the span is only 45cm and it can be printed in three parts, which decreases the energy usage and the material that can be lost. If the MAV is printed in one part a bigger machine is required which is more energy consuming.

Carbon fiber moulding is, depending on the method, either energy saving or very energy consuming. In general not much material is wasted during this production process. For this design a simple carbon rod can be bought and it does not need to be crafted separately. These rods are mass produced and the large number decreases the footprint of one rod immensely, decreasing the footprint of the MAV as well.

The Platilon U04 is mass produced as well, so the impact of the production of the elastic skin will not be very harming to the environment. The material can also consist out of recycled material, since it is a thermoplastic. The skin will be cut by hand to fit the design. Therefore, almost no material will be wasted when the cutting is done correctly and efficiently.

Assembly of component normally uses glue to fix components to each other, but by using SLS connections can be made such that components can be clicked in the design without need for other bonding materials. In this way less glue, which can be harmful to the environment, can be used to assemble the MAV resulting in a smaller footprint.

Life

Because the MAV is electrically powered this reduces the footprint, since it will not emit greenhouse or other hazardous gases. Having a rechargeable battery as energy source increases sustainability. The LiPo batteries used also have no leakage issues, preventing the chance of leaking hazardous materials in the environment.

Having a modular design will improve the life of the MAV, since broken parts can easily be replaced without having to build a completely new MAV. For example, if the video processing unit breaks the payload bay can be opened and the video processing unit can be replaced. All other parts can still be used, so the only footprint on the environment is the disposal of the video processing unit instead of the complete MAV. The parts that can have a large impact on the environment are then preserved and used in the fixed MAV.

The mission element of dropping balls requires to drop material in the environment. The size of these balls are very small, so needing to retrieve them can be quite difficult. Therefore a flag is attached to the ball to increase visibility and make the retrieval easier. Still, the ball can be lost entirely and this impacts the nature. This is why a biodegradable ball is used so the environment is not harmed when a ball is lost. The wire that will be burned in order to drop the ball is also left behind, but the size of this wire is so small that it will not harm the environment that much.

End-of-Life

The end of life consist out of the disposal of the components of the MAV. Most components, such as the engine, batteries and electric boards can be taken back to the factory to be reused or disassembled. However, some components cannot be reused and need to be recycled.

The SLS material PA2105 consisting of the polymer PA12 belongs in the recycle group 7 which is a group containing all plastics that usually are not recyclable [93] [95]. However, research is done on the recyclability of this plastic, decreasing the footprint of the MAV. Currently, the PA12 polymer has a big impact on the environment.

Carbon fiber is can not recyclable at the moment as well. Several studies are performed to make carbon available for recycling, but the properties of the recycled carbon are not as good as new carbon fiber. This cause by the function of carbon fiber, which is to last long and therefore it is not biodegradable at all [96]. However, this can benefit the footprint as well since the carbon rod in the MAV can just be reused in a new MAV, because the material does not degrade much. This way the carbon fiber rod can be recycled, in a new MAV or other functions the rod can have.

The Platilon U04 plastic can be recycled completely, since it is a thermoplastic. In the end of life phase of the MAV this plastic can be handed in and be reformed to another purpose.

9.2 Swarming

When having a swarm of multiple MAV they can be very unsustainable when the cooperation of the MAV's is not optimal. By increasing the efficiency of the flight plan this cooperation can be improved. The programming and planning of this flight plan should be as efficient as possible to increase the sustainability and footprint of the swarm on the environment. Performing all the task in a more energy saving manner will improve the performance of he swarm.

Sustainability is not only the impact on nature but also the noise the system produces. Operating multiple MAV's at the same time increases noise. However, the MAV's have rather small engines which result in a relatively low noise generation and the swarm will have a low noise output.

Though the swarm is developed to compete in the IMAV 2013 competition it can be used in environmental projects and studies to benefit the environment. These missions could be, for example, environmental reconnaissance missions. Having a low energy consuming hybrid swarm of MAV's performing an environmental reconnaissance mission will benefit the environment.

Chapter 10

Market Analysis

The hybrid MAV design has the potential to become a popular product among MAV consumers and penetrate the market in several industries. It has several innovative aspects that are not present on the market at the moment. This section gives a market analysis for the MAV. First, some unique properties of the design MAV will be given before the business and market opportunities will be analyzed to learn and understand in which direction and how fast the market develops.

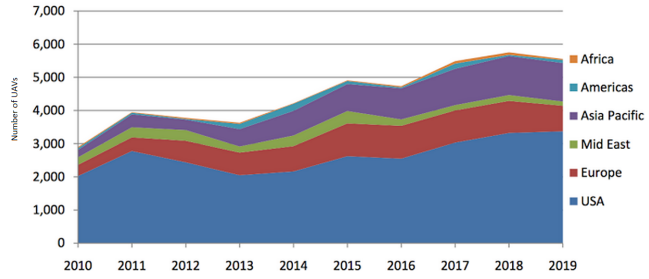
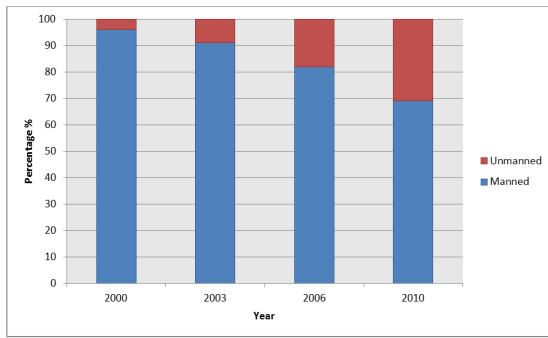
10.1 MAV Properties

The MAV design has some unique properties that could make it a desirable product for a wide range of consumers, its main properties are listed below:

1. **Hybrid:** The MAV can fly horizontally and vertically and can perform VTOL. This property allows the MAV to land, fly and take-off in various conditions and different environments. It can perform its tasks in highly populated areas as well as in more harsh surroundings.
2. **Autonomy:** The MAV is a completely autonomous vehicle. It can fly and perform its mission without any human interaction. Every repetitive activity can be done by the MAV without losing time and at minimum costs.
3. **Swarming:** A group of MAV's can work and perform a mission together to achieve a great and mostly efficient result.
4. **Video Streaming:** The MAV can deliver continuous images of its surroundings.
5. **Automatic Recognition:** The MAV is able to recognize and detect objects autonomously.
6. **Morphing:** The MAV uses an innovative technology which employs wing morphing and results in an efficient horizontal flight, which reduces consumer costs.
7. **Manufacturing:** The MAV is quick and easy to manufacture because the majority of the structure is 3D-printed.

10.2 Market Segment

The first important thing in market analysis is to look at the design product and compare it to competitive products on the market. By doing so, a conclusion can be made whether the product has a chance to generate profits. Figure 10.1a [97] shows that in the past few years there has been a rapid increase in the demand of unmanned vehicles with respect to manned vehicles. According to the forecast, half of the produced vehicles will be unmanned in 2024 [98], which means that in time more and more industries will use make use UAV's. Figure 10.1b [99] shows the continuous increase in UAV demand by region, indicating growth in every region of the world. Unmanned vehicles seem to be have a promising future. A deeper and more specific understanding of the markets that the MAV can be introduced to is needed to make meaningful decisions about the future of this project.



(a) Market Share, Manned vs Unmanned Vehicles [%]

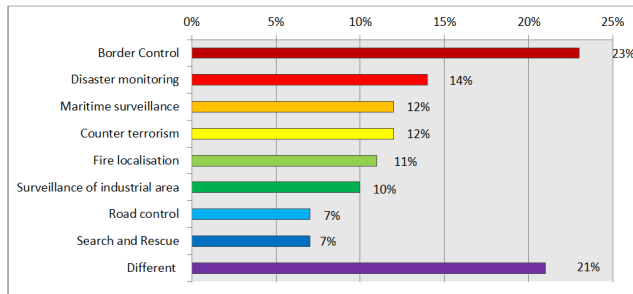
(b) Growing Markets for Unmanned Vehicle per Region

Figure 10.1: UAV Market Increases

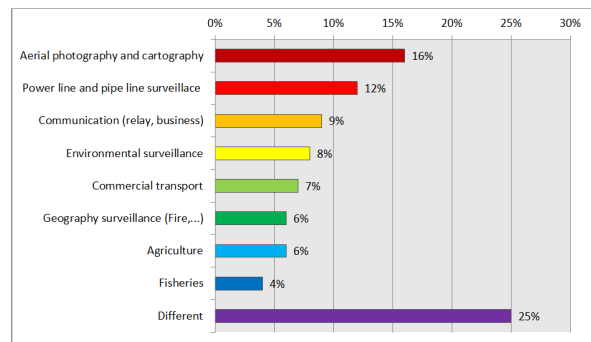
10.2.1 Security and Military Applications

The security and military industry is a relatively old market segment for MAV's. Looking toward the future, security missions and the demands for military MAVs will continuously increase. In fact, it is expected that investments in military MAV's will exceed 200 million US dollars in three years from now [100]. The increase in spending can be represented by the formula $y = 9.89e^{0.2843x}$ which predicts a rapid and continuous increase in this market. The MAV's currently in use are primarily launched by hand and not completely autonomous. The new MAV design does not only promise vertical take-off capabilities but also autonomous take-off, landing and mission completion. Wing morphing allows for more efficient operation even when different payloads are implemented.

Figure 10.2a shows the complete mission and investment area for which the MAV design has application potential [97]. These were analyzed and the corresponding segment distribution over the MAV market was found. The data was found by the European commission as part of the market analyses for UAV's. Due to the flexibility in landing and take-off, small size, efficiency in target detection and recognition due to swarming capabilities and a high efficiency, each of these industries are possible markets for the for the MAV design.



(a) Military and Security



(b) Civilian

Figure 10.2: UAV Applications

10.2.2 Civilian Applications

MAV's are getting more and more common in civilian applications. This is caused by the increase in performance and reduced costs of the MAV's. Nowadays, an average person can afford a MAV, as the large UAV community suggests. Future developments will make it more profitable to a company to send a group of MAV's to perform certain measurements than sending a team of workers. Figure 10.2b shows the MAV civilian applications and opportunities within the civilian MAV market [97]. These are analyzed and the corresponding segment distribution over the MAV market was found. Here again, each one of the industries is an opportunity to launch into the market.

10.2.3 New Market Segments and Forecast in Europe

As mention before, new markets can be opened due to the unique properties of the MAV. Those can be the food, flower and post delivery industry for example - the possibilities are endless.

Today, food and mail deliveries are mainly done using cars or motorbikes. Traffic, however, is really time consuming in populated areas where traffic jams and uncoordinated traffic lights dictate the norm. The roads are getting more

congested by the day and pollution becomes an issue. Imagine a group of students studying for exams or doing important projects which runs late. One click is needed and 5 minutes later the food is on the table. The same applies to mail delivery in busy cities, which are often made by bicycle couriers. The new MAV design has the perfect properties for deliveries. It can take-off and land at any location. It can detect the right location, drop the package using the drop ball system and manage the distribution process in the most efficient way. All this done autonomously.

However there are some barriers for these market segments. In 2008, the European commission did a research and a questionnaire about different aspects of UAV's and their place within society as a common vehicle [97]. It turned out that there are some barriers and challenges in the UAV's industry that need to be overcome at a social level. Figure 10.3 shows the barrier ranking on a scale from one to five [97].

As it goes in history it can be assumed that as time passes society will open up to technological changes which should not prevent the group from launching the product into the market. However the rules, regulation and legislation can prevent the group from going into these markets. However, since the use of UAV's becomes more common, the regulations are changing and opening new opportunities to penetrate more markets.

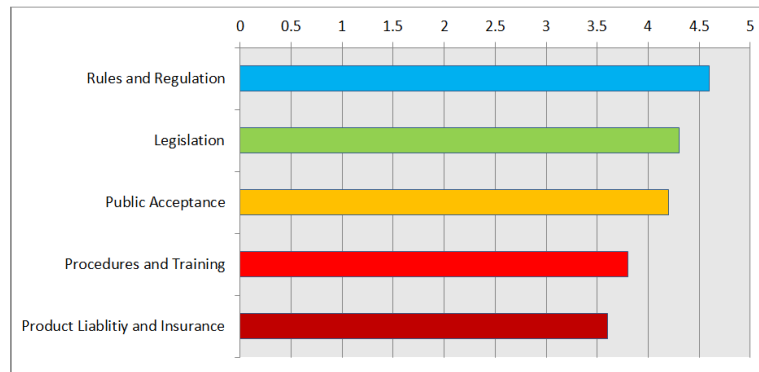


Figure 10.3: Barriers and challenges to using UAV's as a common vehicle [97]

Looking towards the future, it is necessary to have a feeling and be able to predict where the UAV is heading in order to develop guidelines for the group. This ensures a continuous update to keep track of ongoing developments in technology and a connection to future costumers. Figure 10.4 shows the mission forecast for future UAV applications. It can be seen that earth observation, coastguard and communication are expected to have the biggest segment in the market. For that reason the group will continuously develop the autonomy level, hybrid performances and swarming efficiency.

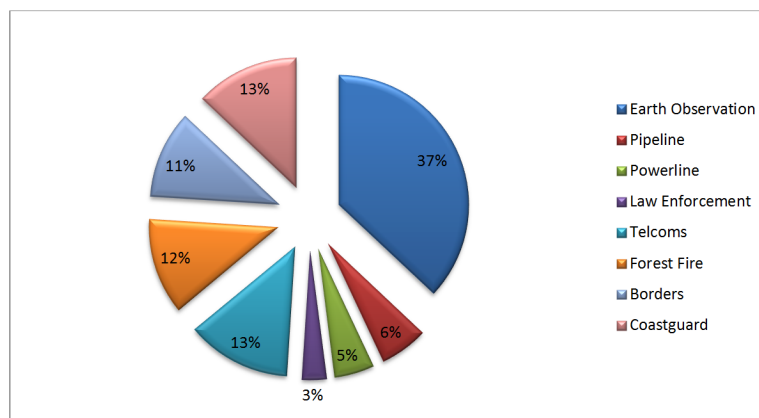


Figure 10.4: Forecast for future UAV missions [97]

Chapter 11

Post DSE

This Chapter describes the activities that need to be performed after the DSE. The project design and development logic after the DSE is shown with a flow diagram. A Gantt Chart is used to schedule the activities up to the IMAV 2013 competition.

11.1 Project Design and Development Logic

After the DSE there is still a lot to be done as preparation for the IMAV 2013 competition. A lot of tests should be performed to verify and validate the working of subsystems as well as each mission element. Also logistic and public relations tasks are identified. The flow diagram is subdivided in several tasks for clarification. The flow diagram after the DSE can be found in Appendix J.

11.2 Gantt Chart

From the flow diagram of the previous section a Gantt Chart is made which shows the schedule after the DSE is finished. The Gantt Chart is shown in Appendix K and is a good tool to monitor the progress of the project. With the time indications the projects current status, future activities and delays are presented. The time indications are rough estimations but include a safety margin to account for delays. The competition is held on 17-20 September 2013 and the project can be finished on the 15th of August in the same year, which means that there is enough time to develop the final product.

The post-DSE starts with software development, most of it is done during the DSE but improvements are necessary. Next, the assembly of all the subsystems starts. The prototype is already build and is tested, but the 3D printed model should still be assembled. In order to accomplish this parts need to be ordered and the competition elements should be tested, therefore a set-up should be made for the different competition elements.

Towards the end validation of the systems should take place. This takes time and continuous updating of the software is needed to eliminate errors. Finally, the complete mission test is done in the 6th of August.

11.3 Cost Breakdown Structure

In Appendix A.5 all costs of the entire Morpheus project are illustrated in the Cost Breakdown Structure (CBS). The CBS includes the costs made so far in building the prototype and testing the hardware, but also the future costs in optimizing the design, testing the design and the competing in the competition. For the prices of all the components in the Design section of the CBS the reader is referred to section 4.15.

Chapter 12

Conclusion and Recommendations

In this chapter the conclusion of the final report and some recommendations on what to improve are presented. First off is the conclusion, next the recommendations will be discussed.

12.1 Conclusion

The mission of the DSE project is to win the IMAV 2013 outdoor competition, for which an MAV system was designed. The result of the detailed design phase will be given in this section.

In order to complete the mission with the highest score possible, a swarm of MAV's is set up and divided into three groups, performing different mission tasks at different times. While Group 1 and Group 3 have an emphasis on locating and decoding QR-Codes, Group 2 will perform mission elements that give a high score, such as the ball drop or the corridor flight.

The aerodynamic performance is designed for a cruise flight speed of 50km/h with an endurance of 28 minutes while keeping the maximum size restriction of 0.5 m. The wing surface area needed was determined to be 0.0945 m^2 with a wing span of 0.45 m and a chord length of 0.21 m. The total weight of the system is 422.5 g. The wing itself is designed to operate at an angle of attack of 6 degrees and has a stall speed of 32 km/h. The engines are placed at the wing tip to counter-act tip vortices and provide highly reactive control of the MAV. Wing morphing is employed in the design to prevent discontinuities in the lifting surface and thereby increasing efficiency in forward flight.

Flight control is accomplished by deflecting the wing tips to which the propellers are attached. The wing tips are rotated by two servos around a hinge that is placed in front of the CG to ensure adequate pitch control. Although the aircraft has only marginal dynamic stability, positive stability will be ensured by using thrust vectoring with a PID controlled feedback-loop.

The chosen propulsive system consists of two propellers, two motors and two motor controllers, and has a maximum static thrust of 7.85 N, a maximum weight of 102 grams and a capacity of 1300 mAh. It is optimized for forward flight with a design speed of 50km/h resulting in a propeller diameter of 7 inches and a pitch of 7 inches. The power for the MAV will be supplied by a Lithium-ion polymer battery with three cells, which will also be used to damp engine vibrations on the autopilot.

To be able to take-off and land vertically while performing efficient forward flight, a hybrid design was developed. A separate transition phase will be used to change between the vertical and horizontal flight mode with a minimal loss in altitude. In order to take-off and land vertically two sticks are placed at the MAV body to avoid tip-over and cope with impact forces. Precision landing is performed by MAV Groups 1 and 3, using an on-board digital camera for positioning in vertical flight at low altitudes.

Since the IMAV regulations emphasize autonomous operation, the MAV was designed to perform all mission elements without any control input. In order to achieve this, a Lisa/M board was chosen as the autopilot with inputs from an IMU and a GPS receiver. The software used to run the autopilot is Paparazzi. Here, the airframe file and the flight plan is adjusted to control attitude and navigation. In order to perform the mission in the most efficient way using multiple vehicles, swarming is implemented. Swarming significantly increases the mission efficiency by assigning each individual unit its own task within the swarm, updating the flight plan based on information received from other MAVs. Communication with the other members of the swarm will also demonstrate intelligent behavior and the capacity to adapt to a dynamic environment.

For the communication subsystem the XB865/868LP modem was chosen with a 868 MHz dipole modem antenna. The RC receiver "Orange Rx R110X" is used as safety link to the MAV. A video link is needed to provide three video links to the ground station and the selected transmitter is the FTX-50 and the antenna the 2.4 GHz dipole.

The ball drop system consists of an electrical circuit that heats a wire, which is connected to the ball, when the signal to drop the ball is sent. This wire burns releasing the ball, and the ball is launched by a stretched rubber band. In order to detect and recognize the QR-code, the same camera that provides guidance during precision landing is used. A color recognition algorithm is used to scan a large area before the code is recognized and an approach towards it is initiated. When close enough, the QR-code will be read and decoded using a ZBar decoder.

In order to produce the MAV swarm within a short period, the production technique chosen is called selective laser sintering and is based on powder-based rapid-prototyping. This will allow for quick manufacturing and assembly, and is especially convenient when broken parts have to be replaced.

As shown in the report, a hybrid MAV system with swarming capabilities has been developed and verified. All requirements set for this project have been fulfilled resulting in a MAV with some unique features. Although the detailed design process is completed, the MAV will be further developed and optimized to compete in the IMAV2013, with an emphasis on the transition process and the swarming algorithm.

12.2 Recommendations

This section will discuss the recommendations. This report contains the work performed by 9 students in approximately 10 weeks. Although a lot has been done, there is also a lot of room for improvement. Below, some recommendations will be given for each subsystem.

Aerodynamics is obviously very important for a flying vehicle. A MAV like the one designed during this DSE topic operates in low Reynolds numbers. The Reynolds number operating range, the positioning of the propellers near the tip and the morphing of the wing tips made it difficult to calculate the aerodynamic behaviour of the MAV. On top of this, the MAV is also a transitioning vehicle and it is quite hard to calculate the aerodynamic behaviour during all flight conditions. A recommendation is hence to do wind tunnel tests in order to be able to predict the behaviour better and in order to validate numerical calculations. Another recommendation is to look at payload modules. The MAV is designed for endurance, but because of payload integration, the airfoil had to have a certain thickness. This causes the vehicle to fly at a non-optimal C_L/C_D ratio. When implementing payload modules, it might be possible to design a more optimal vehicle.

The structures can also be improved. Because the competition starts half September, there is not much time to produce a swarm of MAV's. This, together with the possibility to integrate the payload, are two of the main reasons why the rapid prototyping technique 3D printing has been chosen as production technique. Because of the minimum printing thickness of 0,7mm, it can be hard to fully make use of the material properties. Using topology optimization, a more optimal design can be made. It will take some time, but it will definitely save some weight. The resulting structure will be more complex, but that is no problem since the structure is 3D printed.

Swarming was also an important part of this DSE topic. Recommendations for swarming are to make the swarm more intelligent and to make it more independent by circumventing the groundstation in the communications.

The ball drop subsystem is a working subsystem right now. Recommendations for the ball drop subsystem are to make the self-designed Printed Circuit Board smaller and to reduce the variation in the response time.

For the propulsion subsystem some recommendations point in the direction of a better estimation of the power consumption at different flight velocities. With this better estimation, better mission planning and battery sizing can be performed.

The QR-code detection subsystem is one of the most important subsystems in the MAV. The way to detect the QR-Codes determines for an important part the way the mission elements are performed and hence what the MAV will look like. In the beginning of the report an estimation has been made about the time spent in hover flight, horizontal flight and at maximum power. During this estimation, it is assumed that the MAV could detect the QR-code in horizontal flight. When this turns out to be different, one can imagine the impact on the MAV design. It is therefore recommended to have an extremely good look at this important estimation and to test as soon as possible the different subsystems that have such an important impact on the final design.

As a general recommendation, performing more iterations according to the N^2 chart will probably also result in a more optimal design. These iterations will continue after the DSE.

Bibliography

- [1] Byte Paradigm, *General Indoor and Outdoor competition rules*, Viewed on 16 June 2013, from http://www.imav2013.org/images/IMAV2013_General_Rules.pdf
- [2] Remes, B., 2013, *Design Synthesis Exercise: Swarm of Hybrid MAV's*, Delft University of Technology, Delft
- [3] Gill, Prof. Dr. E., 2013, *Systems Engineering Methods*, AE3201 Systems Engineering and Aerospace Design, Delft University of Technology, Delft
- [4] Deken, J., Ferrier, Y., Fuchs, M., Goldberg, N., Makus, A., Niessink, M., Pronker, A., Van der Sman, E. & Suiker, R., 2013, *Swarm of Hybrid MAV's Midterm Report*, Version 2.00, Delft University of Technology
- [5] Anderson, J.D. jr., 2007, *Fundamentals of Aerodynamics*, 5th edn., McGraw-Hill, New York
- [6] Lissaman, P.B.S., 1983, *Low-Reynolds-Number Airfoils*, Annual Reviews Inc., Annual Review Fluid Mechanics
- [7] Trips, D., 2010, *Aerodynamic Design and Optimization of a Long Range Mini-UAV*, Faculty of Aerospace Engineering, Delft University of Technonolgy
- [8] L.L.M. Veldhuis. (2004). *Review of Propeller-Wing Aerodynamic Interference*. 24th International Congress of the Aeronautical Sciences.
- [9] S.S. Sathaye. (May 2004). *Lift Distributions on Low Aspect Ratio Wings at Low Reynolds Numbers*. Worcester Polytechnic Institute.
- [10] Roskam, Dr. J. , 1985, *Airplane Design, Part I: Preliminary Sizing of Airplanes*, Roskam Aviation and Engineering Corporation, Ottawa, Kansas
- [11] G. E. Torres, T.J. Mueller . (2004). *Low-Aspect-Ratio Wing Aerodynamics at Low Reynolds Numbers*. AIAA JOURNAL. 42 (5)
- [12] Anderson, J.D. jr, 2008, *Introduction to Flight*, 6th edn., McGraw-Hill, New York
- [13] Mulder, J.A. & Mooij, E., 2013, *Flight Dynamics*, Faculty of Aerospace Engineering, Delft University of Technology, Delft
- [14] R.A.C.M. Slangen, 2009, *Experimental investigation of artificial boundary layer transition*, Faculty of Aerospace Engineering, Delft University of Technology, Delft
- [15] A. Meschini, (2009), *XFLR5 Analysis of foils and wings operating at low Reynolds numbers*
- [16] T. Melin, *Reference manual TORNADO 1.0*, The Royal Institute of Technology (KTH), Sweden
- [17] Norman, S. Nise , 2010, *System Engineering Control*, 6th ed, Wiley
- [18] Gulf Coast Data Concepts, *Top Gun Data Loggers*, viewed on 12 June 2013, from <http://www.gcdatanconcepts.com/airplane.html>
- [19] Bedford, A.M. & Fowler W., (2007), *Engineering Mechanics: Statics*, 5th edn., Prentice Hall, New Jersey
- [20] Megson, T.H.G., (2007), *Aerospace Structures for Engineering Students*, 4th edn., Elsevier, Amsterdam
- [21] R.C. Hibbeler, (2008), *Mechanics of Materials*, 8th edition, Pearson Education Centre
- [22] D. J. Inman, (2008), *Engineering Vibrations*, 3rd edition, Pearson Education
- [23] Amco Polymers LCC, *Elastoblend ®PA12 CL*, Viewed on 23 June 2013, from <http://catalog.ides.com/Datasheet.aspx?l=9451&E=109843>

- [24] EOS, *Material Data Center*, Viewed on 10 June 2013, from <http://eos.materialdatacenter.com/eo/en>
- [25] 3M, *3M Products*, Viewed on 19 June 2013, from http://solutions.3m.com/wps/portal/3M/en_US/WW3/Country/?WT.mc_id=www.3M.com/us
- [26] M. T. Kikuta, (2003), *Mechanical Properties of Candidate Materials for Morphing Wings*, Virginia Polytechnic Institute, Virginia
- [27] H.J. Qi, M.C. Boyce, (2004) *Stress-Strain Behavior of Thermoplastic Polyurethane*, Department of Mechanical Engineering, Massachusetts Institute of Technology, Cambridge
- [28] Bayer MaterialScience, *Thermoplastic Elastomer Films*, Viewed on 19 June 2013, from <http://www.epurex.com/products.html>
- [29] Airtech, *Products*, Viewed on 19 June 2013, from www.airtech.lu
- [30] Lubrizol, *Tecoflex TPU*, Viewed on 19 June 2013, from <http://www.lubrizol.com/Medical/Products/Tecoflex.html>
- [31] Easy Composites, *3mm Carbon Fibre Rod 1m*, Viewed on 23 June 2013, from <http://www.easycomposites.co.uk/products/carbon-fibre-rod/3mm-carbon-fibre-rod.aspx>
- [32] Flight School, *Propeller Aerodynamics*, Viewed on 17 June 2013, from <http://www.free-online-private-pilot-ground-school.com/propeller-aerodynamics.html>
- [33] Sail Plane and electric motors magazine, *Propeller Basics*, Viewed on 17 June 2013, from <http://www.stefanv.com/rcstuff/qf200203.html>
- [34] Dynatic Systems, *Brushed vs Brushless Motors*, viewed on 12 June 2013, from <http://www.dynatic.com/brushless%20vs%20brushed.html>
- [35] Robotica, *Quadcopter liPo battery weight/capacity trade off*, viewed on 27 May 2013, <http://robotics.stackexchange.com/questions/554/quadcopter-lipo-battery-weight-capacity-trade-off>.
- [36] M. Drela, 2006, *QPROP formulation*, viewed on 13 June 2013, from http://web.mit.edu/drela/Public/web/qprop/qprop_theory.pdf
- [37] Winter, M. & Brodd, J., 2004, *What Are Batteries, Fuel Cells, and Supercapacitors?*, Chemical
- [38] Hobby King, *Turnigy 1300mAh 3S 20C Lipo Pack (DE Warehouse)*, Viewed 21 June 2013, from http://www.hobbyking.com/hobbyking/store/uh_viewitem.asp?idproduct=10187
- [39] AA Portable Power Corporation, *Battery Knowledge*, Viewed 22 July 2013, from <http://www.aaportablepower.com/>
- [40] Techlib, *Battery Capacity*, viewed on 22 July 2013, <http://www.techlib.com/reference/batteries.html>
- [41] Electrical Engineering, *How to measure capacity of a Lithium-ion battery*, Viewed 22 July 2013, from <http://electronics.stackexchange.com/questions/18612/how-to-measure-capacity-of-a-lithium-ion-battery>
- [42] Stack Exchange, 2013, *How to Measure Capacity from a Lithium-ion Battery*, Viewed on 14-6-2013, from <http://electronics.stackexchange.com/questions/18612/how-to-measure-capacity-of-a-lithium-ion-battery>
- [43] Paparazzi, *Paparazzi autopilots*, viewed on 27 May 2013, from http://paparazzi.enac.fr/wiki/Main_Page
- [44] CSG Shop, *uBlox NEO-6Q GPS Module with GeoHelix Antenna for UAV, RC, Robots*, Viewed on 13 June 2013, from http://www.csgshop.com/product.php?id_product=106
- [45] Paparazzi, 14 August 2012, *Telemetry*. Viewed on 27 May 2013, from <http://paparazzi.enac.fr/wiki/Telemetry>
- [46] Paparazzi, 10 March 2011, *Messages Format*. Viewed on 27 May 2013, from http://paparazzi.enac.fr/wiki/Messages_Format
- [47] IMAV2013. *Competition Info*. Viewed on 27 May 2013, from <http://www.imav2013.org/index.php/information>
- [48] Digi, 2008, *Demystifying 802.15.4 and ZigBee*
- [49] Digi, 2008, *Wireless Mesh Networking ZigBee vs DigiMesh*
- [50] Digi International Inc, 8 Februari 2012, *XBEE 865/868LP RF Modules. 90002126_A*.

- [51] Digi, 29 August 2008, Hello ZigBee. In: Drew Gislason ZigBee *Wireless Networking*. Newnes. 288.
- [52] R. Roberts. *Introduction to Spread Spectrum*, Viewed on 19 June 2013, from <http://sss-mag.com/ss.html#tutorial>
- [53] Digi International, 2012, *Antenna - 868 MHz, half wave, 2.1 dBi, RPSMA male, articulating*, Viewed on 27 May 2013, from http://store.digi.com/index.cfm?fuseaction=product.display&Product_ID=2597
- [54] Hobby King, *Turnigy 9XR Mode 2*, Viewed on 19 June 2013, from http://www.hobbyking.com/hobbyking/store/___31544__turnigy_9xr_transmitter_mode_2_no_module_.html
- [55] Spektrum, *DSMX*, Viewed on 19 June 2013, from <http://www.spektrumrc.com/Technology/DSMX.aspx>
- [56] Flite Test, *Turnigy 9XR Mode 2*, Viewed on 19 June 2013, from <http://forum.flitetest.com/attachment.php?attachmentid=6786&d=1353698110&thumb=1>
- [57] Hobby King, *OrangeRx R110X Satellite Receiver*, Viewed on 19 June 2013, from <http://www.hobbyking.com/hobbyking/store/catalog/38393.jpg>
- [58] Hobby King, *OrangeRx R110X Satellite Receiver*, Viewed on 20 June 2013, from http://www.hobbyking.com/hobbyking/store/___38393__OrangeRx_R110X_2_4Ghz_DSMX_Satellite_Receiver.html?strSearch=orange%20rx%202.4%20sa
- [59] CMC-12P Mini Color CMOS Camera, 2012, Viewed on 27 May 2013, from http://www.microcameras.com/micro_cameras/mini_color_cmos_camera.htm
- [60] 2.8-5.5 VOLT 125MW TX 2.4GHZ VIDEO TRANSMITTER, Viewed on 27 May 2013, from <http://www.fpvhobby.com/transmitter/15-2-55-volt-500mw-24ghz-video-transmitter.html>
- [61] 5.8 GHz 8 Ch. A/V Receiver, Viewed on 27 May 2013, from <http://www.fpvhobby.com>
- [62] 5.8 GHz 13 dBi Patch Antenna, Viewed on 27 May 2013, from <http://www.fpvhobby.com>
- [63] I. Nikolaidis, K. Wu, (August 20-22, 2010) , *Ad-Hoc, Mobile and Wireless Networks*, 9th International Conference, Edmond, Canada
- [64] Tranzeo, *Wireless Link Budget Analysis*, Viewed on 19 June 2013, from http://www.tranzeo.com/allowed/Tranzeo_Link_Budget_Whitepaper.pdf
- [65] Digi Inc., *Radio Emission Designation And Modulation Type For Digi RF Radios*, Viewed on 19 June 2013, from <http://www.digi.com/support/kbase/kbaseresultdet?id=2148>
- [66] qrcode.com, *QR-Code_History*, Viewed on 18 June 2013, from <http://www.qrcode.com/en/history/>
- [67] Gumstix, *Overo FireSTROM COM*, Viewed on 18 June 2013, from https://www.gumstix.com/store/product_info.php?products_id=267
- [68] Gumstix, *CaspaTMVL*, Viewed on 18 June 2013, from https://www.gumstix.com/store/product_info.php?products_id=260
- [69] J. Brown. (2011). *Zbar decoding*, Viewed on 18 June 2013, from <http://zbar.sourceforge.net/about.html>
- [70] OpenCV, *OpenCV*, Viewed on 18 June 2013, from <https://opencv.org/>
- [71] Paparazzi, *Ground Control Station*, Viewed on 21 June 2013, from <http://paparazzi.enac.fr/wiki/GCS>
- [72] J. Gundlach, 2012, *Designing Unmanned Aircraft Systems - A Comprehensive Approach*, American Institute of Aeronautics and Astronautics
- [73] S. Shkarayev, J. Moschetta and B. Bataille, 2007, *Aerodynamic Design of VTOL Micro Air Vehicles*, EMAV2007, Toulouse
- [74] Paparazzi, 9 February 2013, *Airframe Configuration*, Viewed on 13 June 2013, from http://paparazzi.enac.fr/wiki/Airframe_Configuration
- [75] Paparazzi, 13 March 2013, *Modules*, Viewed on 14 June 2013, from <http://paparazzi.enac.fr/wiki/Modules>
- [76] Paparazzi, 5 March 2013, *GCS*, Viewed on 14 June 2013, from <http://paparazzi.enac.fr/wiki/GCS>

- [77] Paparazzi, 18 May 2012, *Theory of Operation*, Viewed on 13 June 2013, from http://paparazzi.enac.fr/wiki/Theory_of_Operation
- [78] Paparazzi, 25 March 2013, *Flight Plans*, Viewed on 14 June 2013, from http://paparazzi.enac.fr/wiki/Flight_Plans
- [79] Paparazzi, *Pprz communications agents*, Viewed on 21 June 2013, from http://paparazzi.enac.fr/wiki/File:Pprz_communication_agents.gif
- [80] Paparazzi, 31 July 2012, *Control Loops*, Viewed on 13 June 2013, from http://paparazzi.enac.fr/wiki/Control_Loops
- [81] D. Chu, J. Sprinkle, R. Randall and S. Shkarayev, 2009, *Automatic Control of VTOL Micro Air Vehicle During Transition Maneuver*, American Institute of Aeronautics and Astronautics, Chicago
- [82] F. Holzapfel, S. Theil, (2011), *Advances in Aerospace Guidance, Navigation and Control*, Springer, New York
- [83] T. Bailey, 2010, *Communication Protocols*, Institute of Electrical and Electronics Engineering, Mexico
- [84] Motorola, Inc., 2003, *SPI Block Guide V03.06*, Motorola, Schaumburg, Illinois USA
- [85] B. Esme, *Kalman Filter*, viewed on 24 June 2013, from <http://bilgin.esme.org/BitsBytes/KalmanFilterforDummies.aspx>
- [86] Byte Paradigm, *Introduction to I²C and SPI protocols*, Viewed on 16 June 2013, from <http://www.byteparadigm.com/applications/introduction-to-i2c-and-spi-protocols/>
- [87] Rosetta Code, *Permutations*, Viewed on 21 June 2013, from <http://rosettacode.org/wiki/Permutations>
- [88] ssoulsudio, *Test setup for verification*, viewed on 28 May 2013, from <http://ssoulstudio.blogspot.nl/2010/05/w7-cafe-chair-sketch-3.html>
- [89] E. Gill and T. Hovenaars, (2013), *Verification and Validation for the attitude and orbit control system*, Internal Publication Delft University of Technology
- [90] Ublox, *LEA-6T / NEO-6T*, viewed on 28 May 2013, from http://www.u-blox.com/images/downloads/Product_Docs/LEA-NEO-6T_ProductSummary_%28GPS.G6-HW-09020%29.pdf
- [91] R. Curran and W. Verhagen, (2013), *Risk Management and Reliability*, Internal Publication Delft University of Technology
- [92] R. Amini, 2009, *System Engineering and Technical Management Techniques*, Delft University of Technology
- [93] Plascolour, *Nylon 12 - Polyamide or PA 12*, Viewed on 17 June 2013, from <http://www.plascolour.com/material/nylon12.html>
- [94] K. Dotchev and W. Yusoff, 2009, *Recycling of polyamide 12 based powders in the laser sintering process*, Rapid Prototyping Journal, Vol. 15 Issue: 3, pp. 192-203
- [95] Integraal Verantwoord Milieubeheer, *Symbolen op verpakkingen*, Viewed on 17 June 2013, from <http://www.ivmafvalbeheer.be/?Page=itemDetail&Higher=0&Item=70&>
- [96] RedOrbit, *The Dirty Secret of Carbon Fiber*, Viewed on 17 June 2013, from <http://www.redorbit.com/news/science/1112493049/the-dirty-secret-of-carbon-fiber/>
- [97] European commission, *UAS expenditure and market*, viewed on 19 June 2013, from http://www.barnardmicrosystems.com/L4E_uav_market.htm
- [98] Skyward, *UAVs around the world*, viewed on 19 June 2013, from <http://www.theskywardblog.com/2012/06/uavs-world-%E2%80%A6-analysis-growth-3/>
- [99] OREGON UAV Test area, *World UAS production forecast by region*, viewed on 19 June 2013, from <http://oregonuav.blogspot.nl>
- [100] Frost & Sullivan *The Future of the Civil and military UAV market*, viewed 19 June 2013, from <http://www.frost.com/sublib/display-market-insight.do?id=236443867>

Appendix

A Competition Analysis

The IMAV2013 focusses on autonomy and operation of the MAV's. Because of this, the following prices/rewards will be given to the participating teams:

- Outdoor mission *autonomy* and *operation*
- Indoor mission *autonomy* and *operation*
- Special Jury Prize for innovative MAV system (autopilot hardware or software, HMI, payload control, ...)
- Special Jury Prize for innovative MAV design (aerodynamic or mechanical innovation)

The outdoor challenge consists of multiple tasks that have to be performed in a limited time slot. To fulfil all tasks, a swarm of MAV's has to work together and to score well, autonomy is also very important. To win the outdoor challenge, one must obtain the most points. In the two equations below, the formulas for the autonomy and the operation scores are given. These scores determine the ranking and hence determine who wins the competition.

- $Autonomy\ score = Px \sum_{i=1}^{no.MAV's} (MxAxS)_i$
- $Operation\ score = Oxp \sum_{i=1}^{no.MAV's} (MxS)_i$

The letters in the equation stand for:

1. M, sum of successful mission elements
2. A, the level of autonomy
A = 1,2,4,6,10,12, depending on the level of autonomy
3. S, the size of the MAV
S=1/(size of the MAV [m])
4. P, the presentation of the team during the mission
1<P<1.1
5. O, the system operation factor
O = number of MAV / number of mission operators

It can be seen from this that autonomy, operation, size and the succesful elements are very important in the score. The sum of the successful mission elements, M, depend on the number of succesful completions of elements in Table A.1. A picture of the outdoor competition and the location of the different mission elements can be found in Figure A.1.

Table A.1: Point Distribution of the Sperate Mission Elements

Mission Elements	Points	Bonus Points
1. Automatic take off	1 per MAV	-
2. Drop zones	2 /1 per MAV	+2
3. Flight performances	number of laps/8 per MAV	-
4. Target detection and recognition	1/2	-
5. Urban corridor	1/2	1
6. Precision landing	1/2	1

Points

- Automatic take-off points are given as long the safety pilot does not transmit any command, the MAV can be hand-launched and the MAV performs at least one other mission element during its flight(except precision landing).
- Drop zones points can be scored in 4 areas. One point is awarded when the ball is within 10 meters of the QR code and 2 points if it is dropped within 5 meters.
- Flight performance points are awarded if the MAV landed before the time strikes.
- Target detection and recognition gives 2 points when the QR-code is decoded and 1 point when it is clearly seen. It counts only as autonomous when the code is decoded online. And not from screen with mobile phone for example.
- There are two arches where it needs to fly through 2 points are awarded when flying lower than 3 meters and 1 lower than 8 meters.
- Precision landing is divided into field landing, normal landing, and precision landing. For precision 2 points are awarded and for normal 1.

Bonus Points

- For the drop bonus points are awarded when at least one point is scored within each zone.
- For the corridor bonus points are awarded when the borders between the two arches are not crossed.
- Bonus points are awarded when taking off without any operator assistance after 10.

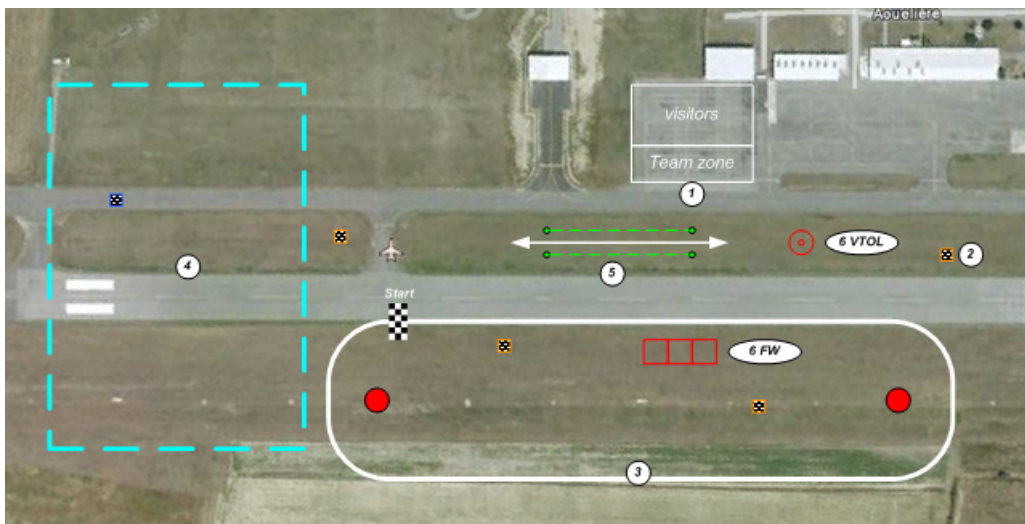


Figure A.1: Overview of the competition and the location of the different mission elements

B Functional Breakdown Structure

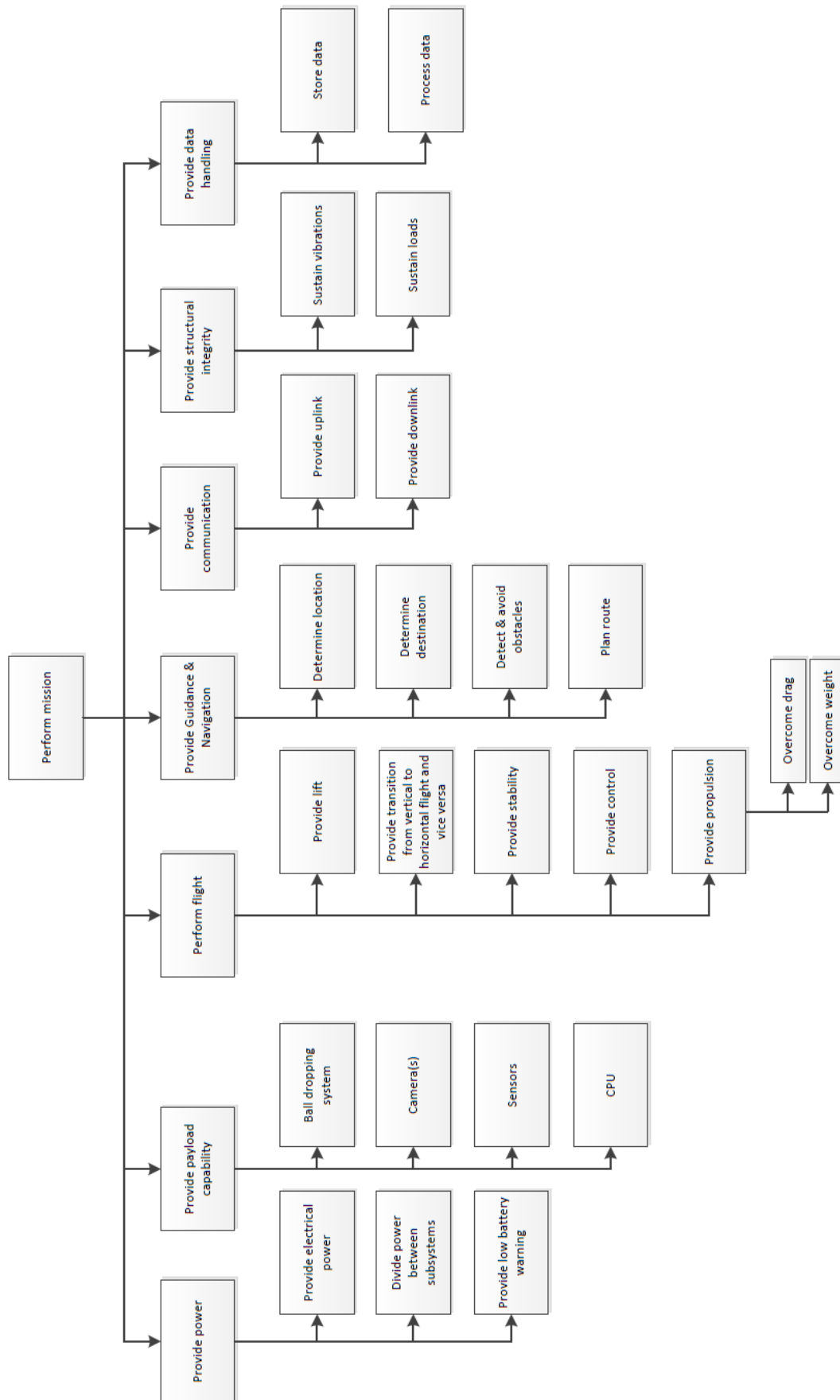
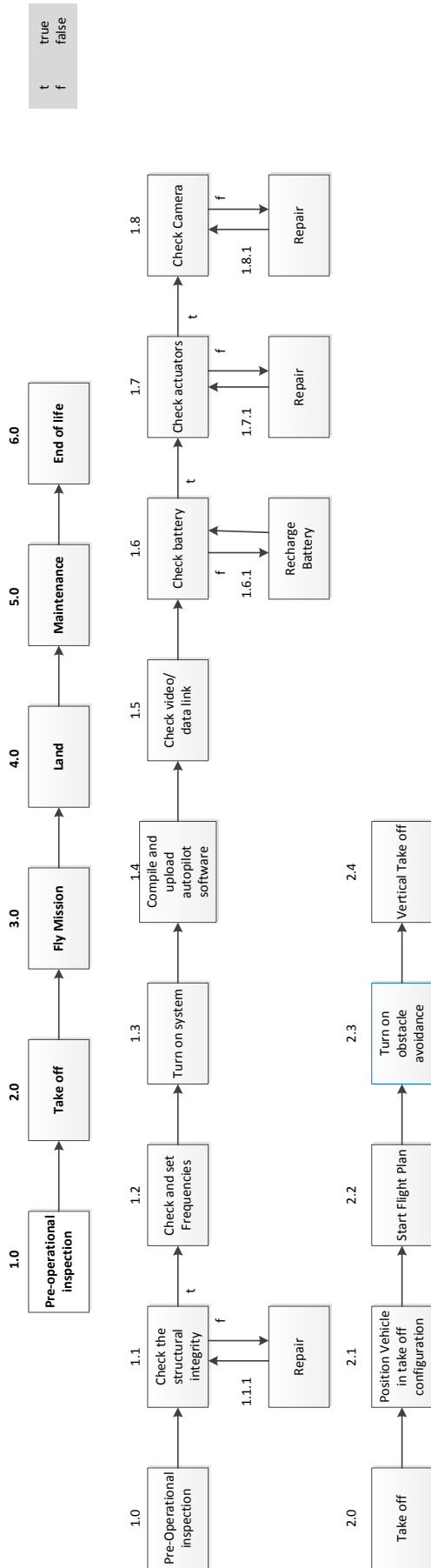
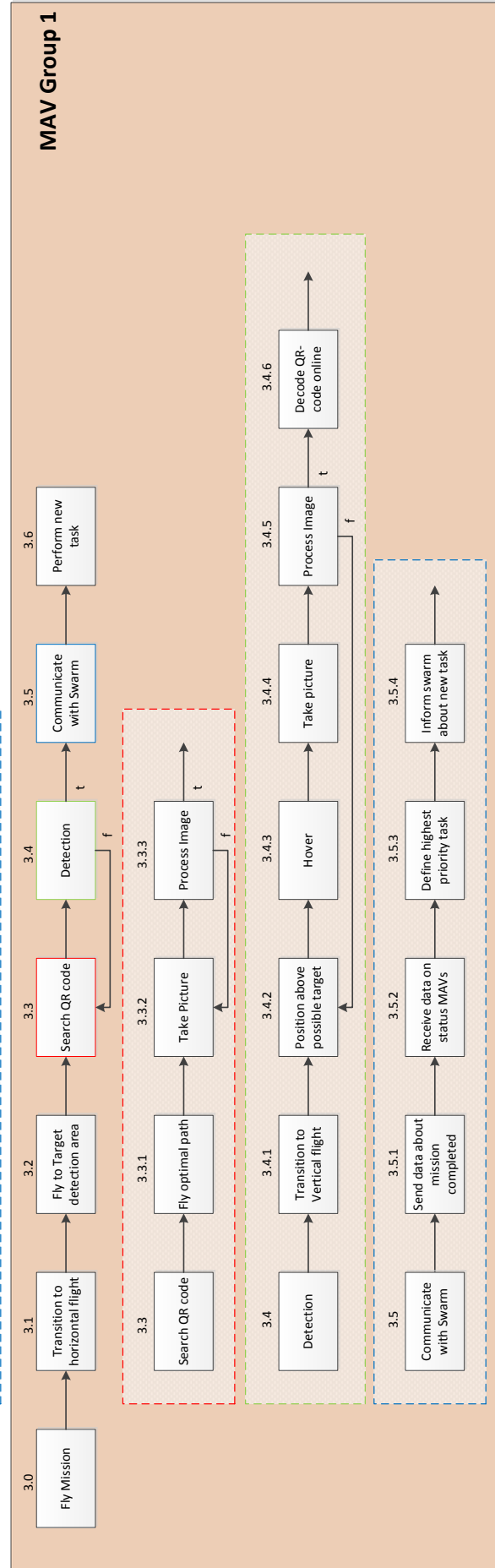


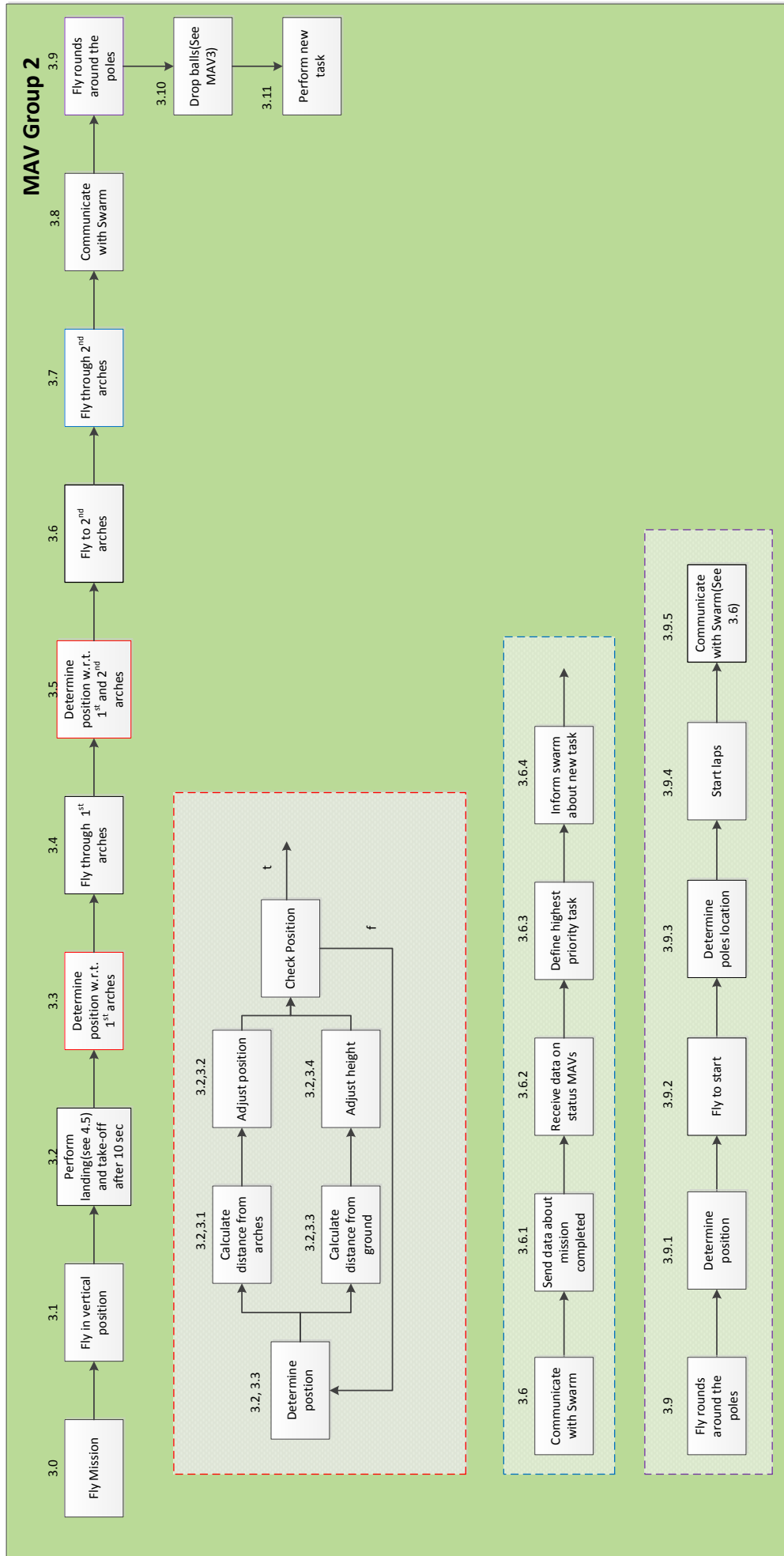
Figure A.2: Functional Breakdown Structure

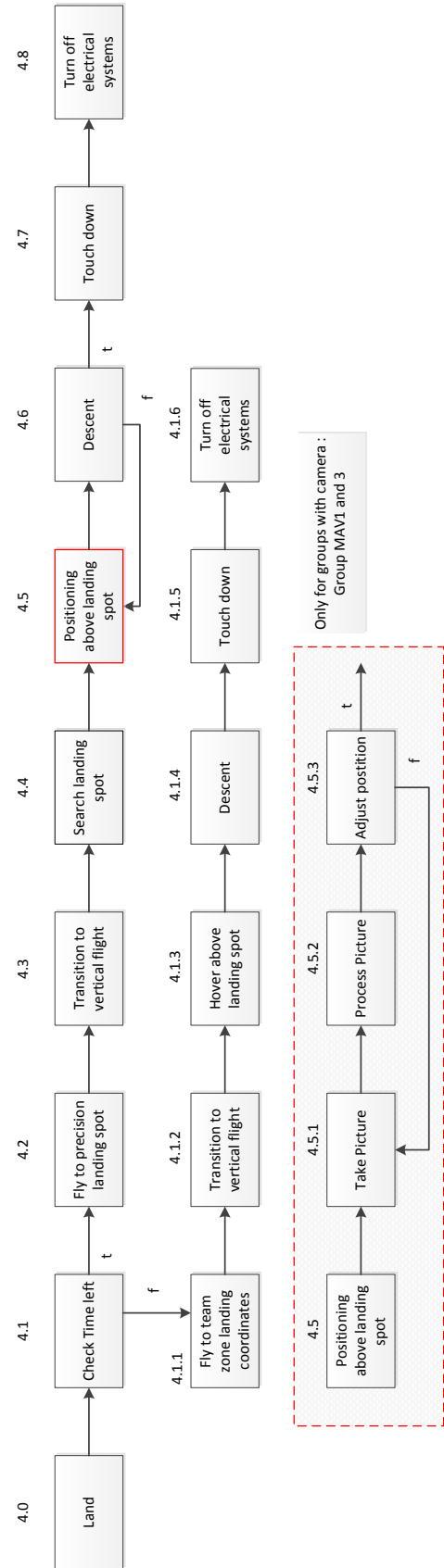
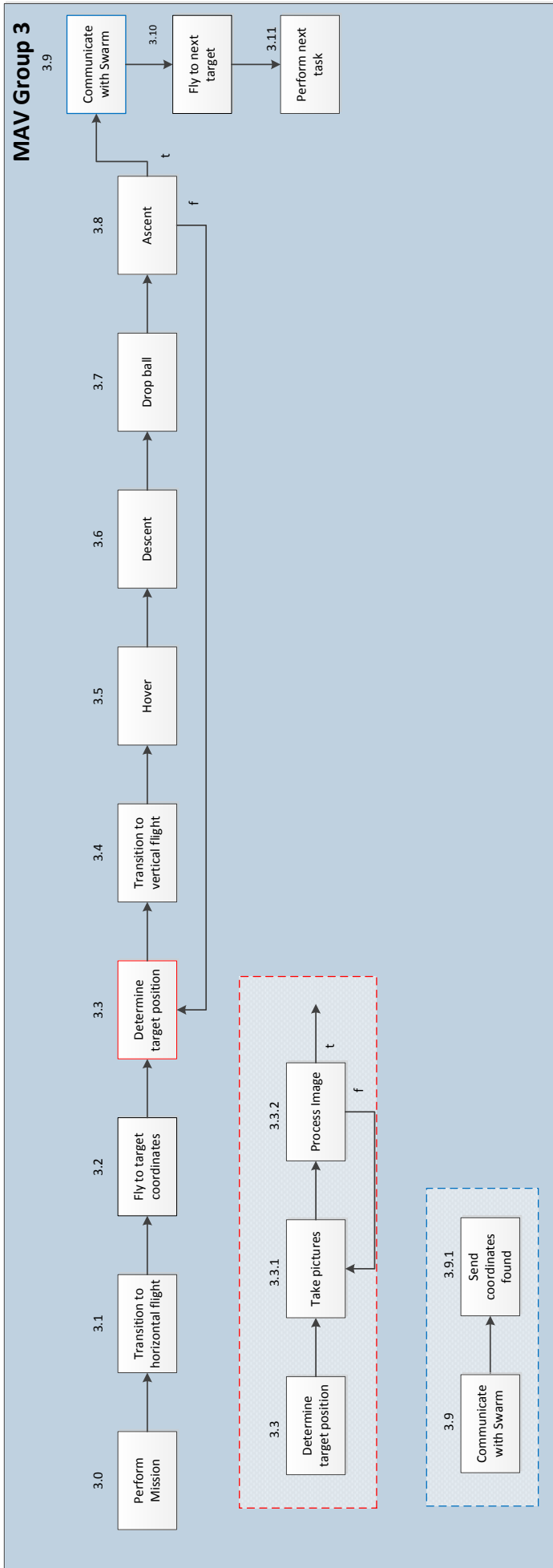
C Functional Flow Diagram

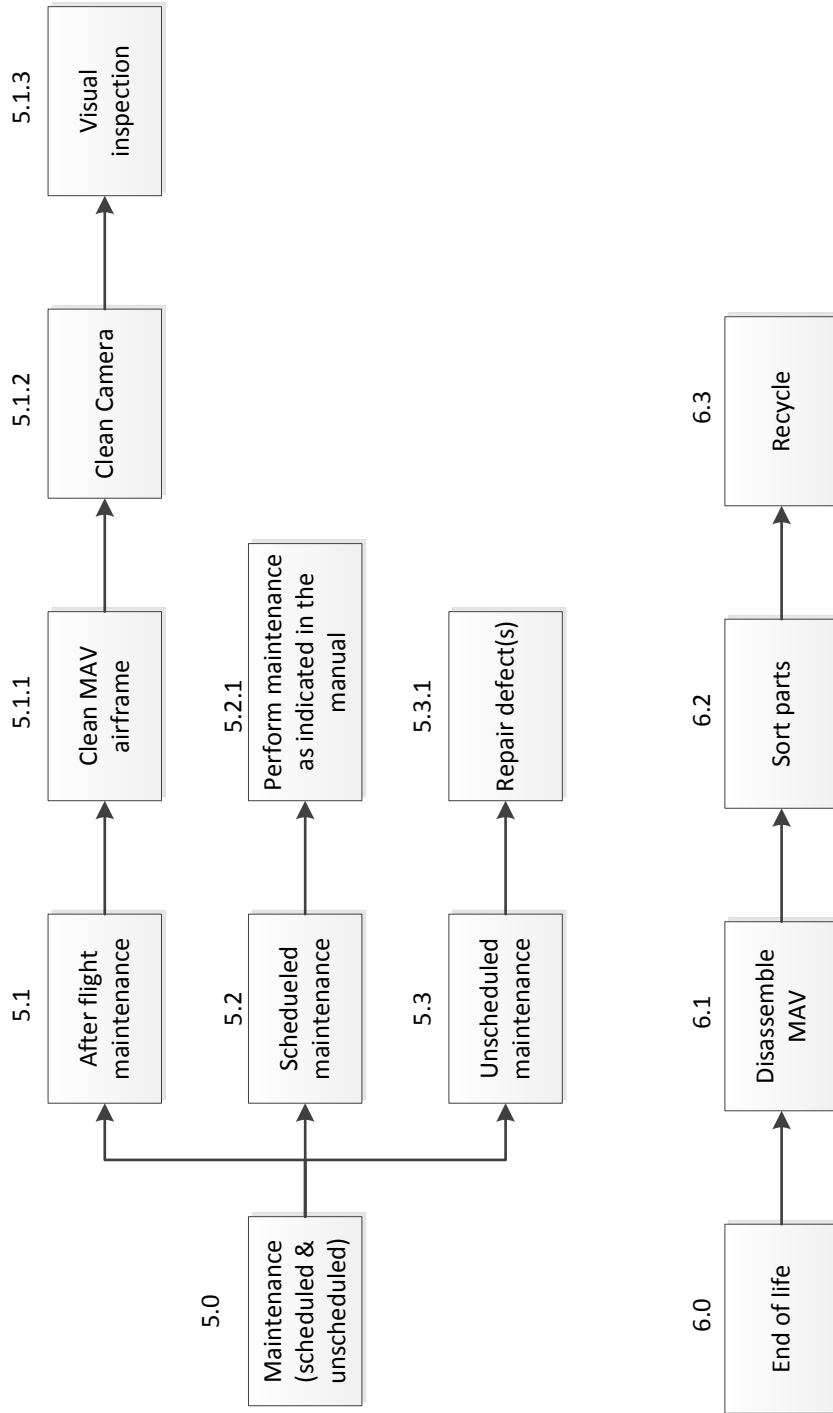


t true
f false









D Drive Calculator

Drive Calculator is a tool that can be used for DC motor analysis and as an aid in the selection of the complete power system for electrically powered model aircraft. The application comes with a database that contains separate tables for motors and drive configurations, batteries, ESCs, gearboxes, propellers and stators.

For each component it knows the maximum load, current, weight etc. With this and general equations it calculates the performances of different combinations. It also gives warnings when for example the motor controller uses too much ampère or when the blade is rotating too slow and it stalls. Finally it plots all the different values at different rpm's like ampères needed, efficiency, thrust and power. The manual can be found on [36] where it can also be downloaded.

The theory behind this program is really complicated due to the non-linear behaviour over the wingspan. In this report [36] an elaborated method is given on how to calculate all the desired variables from a blade element/vortex formulation which calculates the C_l coefficients over the wing span for different rpm's.

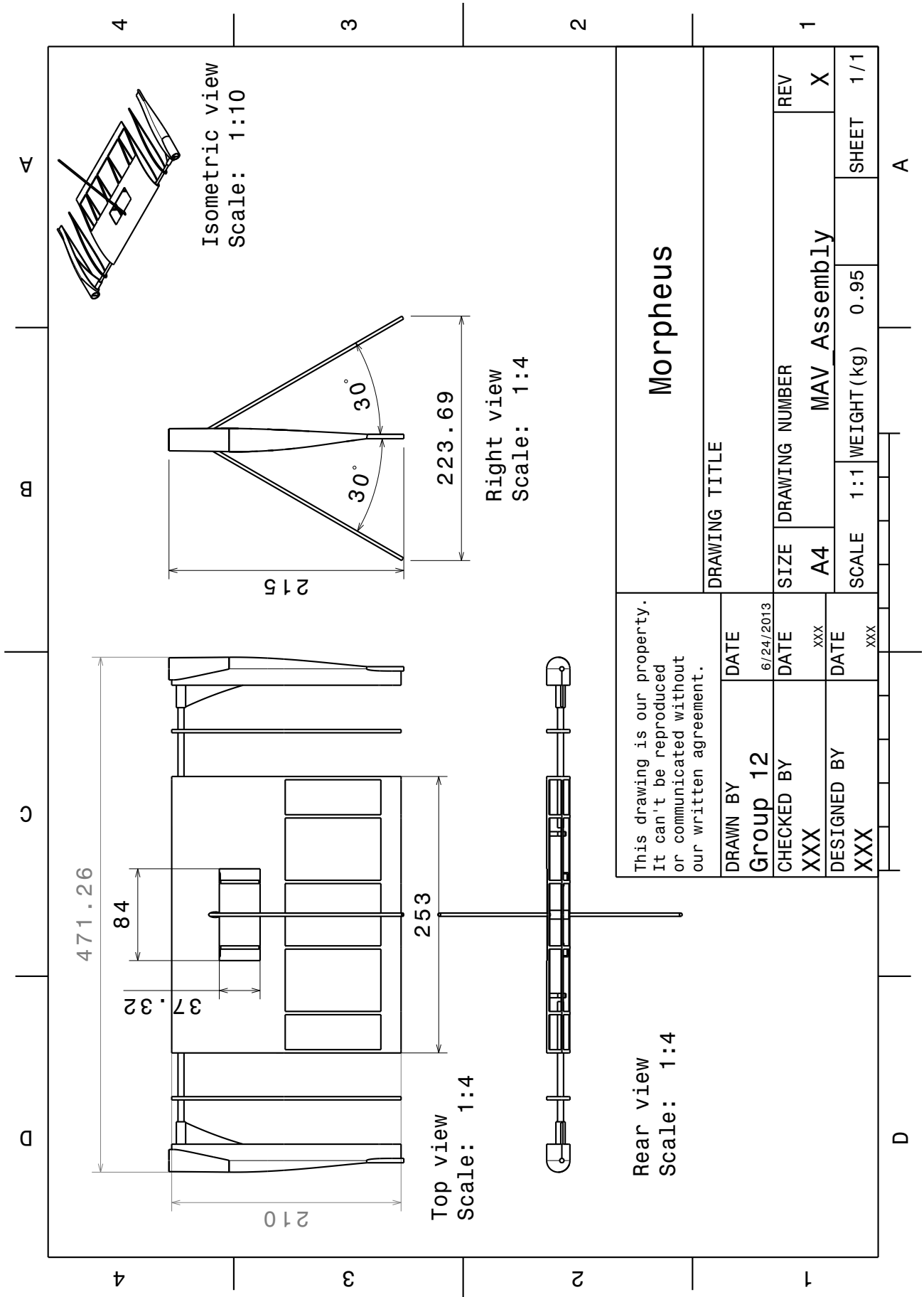
E Telemetry

```
<?xml version="1.0"?>
<!DOCTYPE telemetry SYSTEM "telemetry.dtd">
<telemetry>
  <process name="Main">
    <mode name="default">
      <message name="DL_VALUE" period="1."/>
      <message name="ROTORCRAFT_STATUS" period="1.2"/>
      <message name="ROTORCRAFT_FP" period="0.25"/>
      <message name="ALIVE" period="2.1"/>
      <message name="INS_REF" period="5.1"/>
      <message name="ROTORCRAFT_NAV_STATUS" period="1.6"/>
      <message name="WP_MOVED" period="1.3"/>
      <message name="GPS_INT" period=".25"/>
      <message name="INS" period=".25"/>
    </mode>
  </process>
  <process name="Fbw">
    <mode name="default">
      <message name="FBW_STATUS" period="18." phase="0"/>
    </mode>
  </process>
</telemetry>
```

Message size in bytes:

```
"DL_VALUE" = 5;
"ROTORCRAFT_STATUS" = 231;
"ROTORCRAFT_FP" = 147;
"ALIVE" = 2;
"INS_REF" = 154;
"ROTORCRAFT_NAV_STATUS" = 159;
"WP_MOVED" = 35;
"GPS_INT" = 155;
"INS" = 198;
```

F Technical Drawing Structure



G Flight Plans

File FP_Group12B.xml:

```
<!DOCTYPE flight_plan SYSTEM "flight_plan.dtd">

<flight_plan alt="198" ground_alt="188" lat0="43.449546" lon0="1.263386" max_dist_from_home="500"
name="FP_Group12" qfu="190" security_height="3">
  <header>
    #include "modules/multi/dropball.h"
    #include "subsystems/navigation/nav_line.h"
  </header>
  <waypoints>
    <waypoint name="HOME" x="125.5" y="-5.0"/>
    <waypoint name="STDBY" x="165.3" y="-21.1"/>
    <waypoint name="Arch1" x="129.7" y="-59.1"/>
    <waypoint name="Arch2" x="39.1" y="-11.8"/>
    <waypoint name="VTOL" x="184.8" y="-86.5"/>
    <waypoint alt="193" name="DZ1" x="-71.8" y="54.7"/>
    <waypoint alt="193" name="DZ2" x="-17.2" y="-51.8"/>
    <waypoint alt="193" name="DZ3" x="111.5" y="-139.5"/>
    <waypoint alt="193" name="DZ4" x="281.1" y="-149.5"/>
    <waypoint name="Pole1" x="-97.6" y="-37.2"/>
    <waypoint name="Pole2" x="210.3" y="-200.1"/>
    <waypoint name="Start" x="-69.8" y="-17"/>
    <waypoint name="QR1" x="-170.4" y="-48.1"/>
    <waypoint name="QR2" x="-306.412304237" y="26.0699327476"/>
    <waypoint name="QR4" x="-55.4" y="135.1"/>
    <waypoint name="QR3" x="-190.8" y="208.0"/>
    <waypoint name="TZ1" x="119.6" y="17.8"/>
    <waypoint name="TZ4" x="105.6" y="-6.6"/>
    <waypoint name="TZ2" x="185.3" y="-17.9"/>
    <waypoint name="TZ3" x="171.6" y="-41.5"/>
    <waypoint name="VZ1" x="138.8" y="51.6"/>
    <waypoint name="VZ2" x="202.3" y="16.5"/>
    <waypoint name="FA1" x="-191.1" y="249.1"/>
    <waypoint name="FA2" x="373.9" y="-27.7"/>
    <waypoint name="FA3" x="202.0" y="-305.8"/>
    <waypoint name="FA4" x="-357.8" y="-18.0"/>
    <waypoint alt="188" name="TD" x="5.6" y="-10.9"/>
    <waypoint name="CLIMB" x="167.3" y="-11.1"/>
    <waypoint name="NEXT1" x="184.8" y="-51.8"/>
    <waypoint name="NEXT2" x="184.8" y="-51.8"/>
    <waypoint name="NEXT3" x="184.8" y="-51.8"/>
    <waypoint name="NEXT4" x="184.8" y="-51.8"/>
  </waypoints>

  <sectors>
    <sector color="red" name="QR_Area">
      <corner name="QR1"/>
      <corner name="QR2"/>
      <corner name="QR3"/>
      <corner name="QR4"/>
    </sector>
    <sector color="yellow" name="Team_Zone">
      <corner name="TZ1"/>
      <corner name="TZ2"/>
      <corner name="TZ3"/>
      <corner name="TZ4"/>
    </sector>
    <sector color="blue" name="Visitor_Zone">
      <corner name="VZ1"/>
      <corner name="VZ2"/>
      <corner name="TZ2"/>
      <corner name="TZ1"/>
    </sector>
    <sector color="green" name="Flight_Area">
      <corner name="FA1"/>
      <corner name="FA2"/>
      <corner name="FA3"/>
      <corner name="FA4"/>
    </sector>
  </sectors>

  <!-- stay within flight area:-->
  <exceptions>
    <exception cond="Or(!InsideFlight_Area(GetPosX(),GetPosY()),GetPosAlt())>ground_alt+50)"
deroute="HOME"/>
  </exceptions>

  <blocks>
  <!-- Establish GPS fix-->
    <block name="Wait_GPS">
      <call fun="NavKillThrottle"/>
      <while cond="!GpsFixValid"/>
    </block>
  <!-- Update local waypoints with respect to MAV-->
    <block name="Geo_init">
      <while cond="LessThan(NavBlockTime(),10)"/>
  </blocks>
</flight_plan>
```

```

        <!--<call fun="dropball_WpFound()" />-->
        <call fun="NavSetGroundReferenceHere()" />
    </block>
<!-- Prevent MAV from starting -->
    <block name="Holding_point">
        <call fun="NavKillThrottle()" />
        <attitude pitch="0" roll="0" throttle="0" vmode="throttle" until="FALSE" />
    </block>
<!-- Start engine -->
    <block name="Start_Engine">
        <call fun="NavResurrect()" />
        <attitude pitch="0" roll="0" throttle="0" vmode="throttle" until="FALSE" />
    </block>
<!-- Take off -->
    <block name="Takeoff" strip_button="Takeoff" strip_icon="takeoff.png">
        <!--<exception cond="stateGetPositionEnu_f()->z_u>u3" deroute="Standby" />-->
        <call fun="NavSetWaypointHere(WP_HOME)" />
        <stay vmode="climb" climb="0.5" wp="HOME" />
    </block>
<!-- Standby -->
    <block name="Standby" strip_button="Standby" strip_icon="home.png">
        <stay alt="10" vmode="alt" wp="HOME" />
    </block>
<!-- Fly to precision landing spot -->
    <block name="Go VTOL">
        <go wp="VTOL" hmode="route" />
    </block>
<!-- Set waypoint for precision landing spot -->
    <block name="land_here" strip_button="Land_Here" strip_icon="land-right.png">
        <call fun="NavSetWaypointHere(WP_TD)" />
    </block>
    <block name="land">
        <go wp="TD" />
    </block>
    <block name="flare">
        <exception cond="NavDetectGround()" deroute="Holding_point" />
        <call fun="NavStartDetectGround()" />
        <stay climb="-0.3" vmode="climb" wp="TD" until="FALSE" />
    </block>
<!-- Wait 10 seconds -->
    <block name="Wait">
        <call fun="NavKillThrottle()" />
    </block>
<!-- take-off again -->
    <block name="Start_Engine_2">
        <call fun="NavResurrect()" />
        <attitude pitch="0" roll="0" throttle="0" vmode="throttle" until="FALSE" />
    </block>
    <block name="Takeoff2" strip_button="Takeoff2" strip_icon="takeoff.png">
        <!--<exception cond="stateGetPositionEnu_f()->z_u>u3" deroute="Standby" />-->
        <call fun="NavSetWaypointHere(WP_CLIMB)" />
        <stay vmode="climb" climb="0.5" wp="CLIMB" until="GetPosAlt()>ground_alt+10" />
    </block>
<!-- Fly to corridor -->
    <block name="Go Cor">
        <go from="VTOL" wp="Arch1" hmode="route" />
    </block>
<!-- Fly through corridor -->
    <block name="Corridor">
        <go from="Arch1" wp="Arch2" hmode="route" throttle="0.3" />
        <!-- for testing -->
        <call fun="dropball_WpNew(WP_NEXT1, WP_NEXT2, WP_NEXT3, WP_NEXT4)" />
        <!-->
    </block>
<!-- Fly to dropzone with pre call testing -->
    <block name="Dropzone1">
        <go wp="NEXT1" hmode="route" vmode="glide" />
    </block>
<!-- Fly to dropzone 2 -->
    <block name="Dropzone2">
        <go wp="NEXT2" hmode="route" />
    </block>
<!-- Fly to dropzone 3 -->
    <block name="Dropzone3">
        <go wp="NEXT3" hmode="route" />
    </block>
<!-- Fly to dropzone 4 -->
    <block name="Dropzone4">
        <go wp="NEXT4" hmode="route" />
    </block>
<!-- Fly to start flight performance -->
    <block name="Start_FP">
        <go from="NEXT4" wp="Start" hmode="route" />
    </block>
<!-- Start flight performance element -->
    <block name="Flight_performance">
        <go from="Pole1" wp="Pole2" hmode="route" />
    </block>
</blocks>
</flight_plan>

```

File FP_MAVgroup3.xml:

```
<!DOCTYPE flight_plan SYSTEM "flight_plan.dtd">

<flight_plan alt="198" ground_alt="188" lat0="43.449546" lon0="1.263386" max_dist_from_home="500"
name="FP_MAVGROUP3" qfu="190" security_height="3">
  <header>
    #include "autopilot.h"
    #include "modules/multi/Drop.h"
    #include "modules/multi/dropball.h"
  </header>

  <waypoints>
    <waypoint name="HOME" x="125.5" y="-5.0"/>
    <waypoint name="STDBY" x="165.3" y="-21.1"/>
    <waypoint name="Arch1" x="129.7" y="-59.1" height="2.5"/>
    <waypoint name="Arch2" x="39.1" y="-11.8" height="2.5"/>
    <waypoint name="VTOL" x="184.8" y="-86.5"/>
    <waypoint alt="193" name="DZ1" x="-71.8" y="54.7"/>
    <waypoint alt="193" name="DZ2" x="-17.2" y="-51.8"/>
    <waypoint alt="193" name="DZ3" x="111.5" y="-139.5"/>
    <waypoint alt="193" name="DZ4" x="281.1" y="-149.5"/>
    <waypoint name="Pole1" x="-97.6" y="-37.2"/>
    <waypoint name="Pole2" x="210.3" y="-200.1"/>
    <waypoint name="Start" x="-69.8" y="-17"/>
    <waypoint name="QR1" x="-170.4" y="-48.1"/>
    <waypoint name="QR2" x="-306.412304237" y="26.0699327476"/>
    <waypoint name="QR4" x="-55.4" y="135.1"/>
    <waypoint name="QR3" x="-190.8" y="208.0"/>
    <waypoint name="TZ1" x="119.6" y="17.8"/>
    <waypoint name="TZ4" x="105.6" y="-6.6"/>
    <waypoint name="TZ2" x="185.3" y="-17.9"/>
    <waypoint name="TZ3" x="171.6" y="-41.5"/>
    <waypoint name="VZ1" x="138.8" y="51.6"/>
    <waypoint name="VZ2" x="202.3" y="16.5"/>
    <waypoint name="FA1" x="-191.1" y="249.1"/>
    <waypoint name="FA2" x="373.9" y="-27.7"/>
    <waypoint name="FA3" x="202.0" y="-305.8"/>
    <waypoint name="FA4" x="-357.8" y="-18.0"/>
    <waypoint name="TD" x="125.5" y="-5.0"/>
  </waypoints>

  <sectors>
    <sector color="red" name="QR_Area">
      <corner name="QR1"/>
      <corner name="QR2"/>
      <corner name="QR3"/>
      <corner name="QR4"/>
    </sector>
    <sector color="yellow" name="Team_Zone">
      <corner name="TZ1"/>
      <corner name="TZ2"/>
      <corner name="TZ3"/>
      <corner name="TZ4"/>
    </sector>
    <sector color="blue" name="Visitor_Zone">
      <corner name="VZ1"/>
      <corner name="VZ2"/>
      <corner name="TZ2"/>
      <corner name="TZ1"/>
    </sector>
    <sector color="green" name="Flight_Area">
      <corner name="FA1"/>
      <corner name="FA2"/>
      <corner name="FA3"/>
      <corner name="FA4"/>
    </sector>
  </sectors>

  <!-- stay within flight area:-->
  <exceptions>
    <exception cond="Or(!InsideFlight_Area(GetPosX(),GetPosY()),GetPosAlt())>ground_alt+50"
    deroute="HOME"/>
    <exception cond="(autopilot_flight_time>1200)" deroute="land_here"/>
  </exceptions>

  <blocks>
    <!-- Establish GPS fix-->
    <block name="Wait_GPS">
      <call fun="NavKillThrottle"/>
      <while cond="!GpsFixValid"/>
    </block>
    <!-- Update local waypoints with respect to MAV-->
    <block name="Geo_init">
      <while cond="LessThan(NavBlockTime(),10)"/>
      <call fun="NavSetGroundReferenceHere"/>
      <!--<call fun="NavSetWaypointHere(WP_HOME)"/> for the competition-->
    </block>
    <!-- Prevent MAV from starting-->
    <block name="Holding_point">
```

```

        <call fun="NavKillThrottle()"/>
        <attitude pitch="0" roll="0" throttle="0" vmode="throttle" until="FALSE"/>
    </block>
<block name="Start_Engine">
    <call fun="NavResurrect()"/>
    <attitude pitch="0" roll="0" throttle="0" vmode="throttle" until="TRUE"/>
</block>
<block name="Takeoff" strip_button="Takeoff" strip_icon="takeoff.png">
    <set value="0" var="autopilot_flight_time"/>
    <exception cond="stateGetPositionEnu_f()->z_u>2.0" deroute="Standby"/>
    <call fun="NavSetWaypointHere(WP_HOME)"/>
    <stay vmode="climb" climb="0.5" wp="HOME"/>
</block>
<!--Standby-->
<block name="Standby" strip_button="Standby" strip_icon="home.png">
    <stay alt="10" vmode="alt" wp="HOME"/>
</block>
<!--Transition from vertical to horizontal flight
<block name="Transition1" strip_button="Transition1">
    <call fun= />
</block> -->
<!--Fly to dropzone 1-->
<block name="Go_QR1">
    <go from="HOME" wp="DZ1" hmode="route" vmode="glide"/>
</block>
<!-- Search QR area-->
<block name="searching">
    <for var = "i" from = "0" to = "2">
        <circle wp="DZ1" radius="6+3*$i" alt="6+2*$i" until ="stage_time>15"/>
    </for>
</block>
<!-- Communicate location drop zone 1-->
<block name="Communicate_DZ1">
    <call fun="dropball_WpFound()"/>
</block>
<!--Fly to new dropzone 1-->
<block name="Go_QR1_updated">
    <go wp="DZ1" hmode="route" vmode="glide"/>
</block>
<!-- Drop Ball at QR code 1 -->
<block name="Drop_Ball1">
    <call fun="DropBall_doedrop()"/>
</block>
<!-- Communicate other locations are correct
<block name="Communicate_DZs">
    <call fun="LocationDZs()"/>
</block>-->
<!--Fly to dropzone 2-->
<block name="Go_QR2">
    <go from="DZ1" wp="DZ2" hmode="route"/>
</block>
<!--Check location QR code 2
<block name="Search_QR-code_2">
    <call fun= />
    <stay height="10.0" vmode="alt" wp="DZ2"/>
    <exception cond="DZ2_u=falselocation" deroute="searching" />
</block> -->
<!-- Drop Ball at QR code 2 -->
<block name="Drop_Ball2">
    <call fun="DropBall_doedrop()"/>
</block>
<!-- Communicate location drop zone 2
<block name="Communicate_DZ2">
    <call fun="ParseMovedDropballWP()"/>
</block> -->
<!--Fly to dropzone 3-->
<block name="Go_QR3">
    <go wp="DZ3" hmode="route" vmode="glide"/>
</block>
<!-- Search QR code 3
<block name="Search_QR-code_3">
    <call fun= />
</block> -->
<!-- Drop Ball at QR code 3 -->
<block name="Drop_Ball3">
    <call fun="DropBall_doedrop()"/>
</block>
<!-- Communicate location drop zone 3
<block name="Communicate_DZ3">
    <call fun="ParseMovedDropballWP()"/>
</block> -->
<!--Fly to dropzone 4-->
<block name="Go_QR4">
    <go from="DZ3" wp="DZ4" hmode="route"/>
</block>
<!-- Search QR code 4
<block name="Search_QR-code_4">
    <call fun= />
</block> -->
<!-- Drop Ball at QR code 4 -->
<block name="Drop_Ball4">

```

```

        <call fun="DropBall_drodrop()"/>
    </block>
<!-- Communicate location drop zone 4
    <block name="Communicate_DZ4">
        <call fun="ParseMovedDropballWP()"/>
    </block> -->
<!-- Fly to precision landing spot -->
    <block name="Go VTOL">
        <go from="DZ4" wp="VTOL" hmode="route"/>
    </block>
<!-- Transition from horizontal to vertical flight
    <block name="Transition2" strip_button="Transition2">
        <call fun= />
    </block> -->
<!-- Precision landing
    <block name="Precision_Landing">
        <exception cond="NavDetectGround()" deroute="Holding_point"/>
        <call fun="NavStartDetectGround()"/>
        <stay climb="-0.8" vmode="climb" wp="VTOL"/>
    </block> -->
<!-- Quick Land -->
    <block name="land_here" strip_button="Land_Here" strip_icon="land-right.png">
        <call fun="NavSetWaypointHere(WP_TD)"/>
        <deroute block="land"/>
    </block>
    <block name="land">
        <go wp="TD"/>
        <deroute block="flare"/>
    </block>
    <block name="flare">
        <exception cond="NavDetectGround()" deroute="Holding_point"/>
        <call fun="NavStartDetectGround()"/>
        <stay climb="-0.8" vmode="climb" wp="TD"/>
    </block>
</ blocks >
</flight_plan>

```

H Drop Ball Module

File dropball.h

```

#ifndef DROPBALL_H
#define DROPBALL_H

#include "std.h"

#define NB_DROPBALL_WP      4
struct dropball_waypoint {
    uint8_t wp;
    bool_t detected;
    bool_t dropped;
};

bool_t dropball_WpFound(void);
bool_t dropball_goto_block(void);
bool_t dropball_WpNew(uint8_t wp1, uint8_t wp2, uint8_t wp3, uint8_t wp4);

void on_dropball(void);
void parse_on_dropball_found(uint8_t wp_id);

#endif // DROPBALL

```

File dropball.c

```

#include "multi/dropball.h"

#include "state.h"
#include "generated/airframe.h"
#include "generated/flight_plan.h"
#include "subsystems/ins.h"
#include "subsystems/datalink/downlink.h"
#include "subsystems/datalink/datalink.h"
#include "firmwares/rotorcraft/navigation.h"
#include "math/pprz_geodetic_int.h"

#define DOWNLINK_DEVICE DOWNLINK_AP_DEVICE

/* Make a vector containing only the dropball waypoints and their status */
static struct dropball_waypoint dropball_waypoints[] = {
    {WP_DZ1, TRUE, FALSE},
    {WP_DZ2, FALSE, FALSE},
    {WP_DZ3, TRUE, FALSE},
    {WP_DZ4, TRUE, FALSE},
};

/* find factorial of a number */
uint32_t factorial(uint32_t n) {

```

```

    if (n<=1)
        return (1);
    else
        n=n*factorial(n-1);
    return (n);
}

/* find the next lexicographical permutation */
bool_t next_lex_perm(uint8_t *a, int n) {
#define swap(i, j) {t = a[i]; a[i] = a[j]; a[j] = t;}
    uint8_t k, l, t;

    /* 1. Find the largest index k such that a[k] < a[k + 1]. If no such
       index exists, the permutation is the last permutation. */
    for (k = n - 1; k && a[k - 1] >= a[k]; k--);
    if (!k--) return FALSE;

    /* 2. Find the largest index l such that a[k] < a[l]. Since k + 1 is
       such an index, l is well defined */
    for (l = n - 1; a[l] <= a[k]; l--);

    /* 3. Swap a[k] with a[l] */
    swap(k, l);

    /* 4. Reverse the sequence from a[k + 1] to the end */
    for (k++, l = n - 1; l > k; l--, k++)
        swap(k, l);
    return TRUE;
#undef swap
}

/* Send message */
bool_t dropball_WpFound(void){
    uint8_t move_dropball_ac_id = 10;
    uint8_t move_dropball_wp_id = WP_DZ1;
    struct LlaCoor_i new_cord;
    new_cord.lat = 434505560;
    new_cord.lon = 12640240;
    new_cord.alt = 500;

    DOWNLINK_SEND_FOUND_DROPBALL(DefaultChannel, DefaultDevice, &move_dropball_wp_id,
    &move_dropball_ac_id, &new_cord.lat, &new_cord.lon, &new_cord.alt);
    return FALSE;
}

/* Receive message */

/* parse for the real aircraft */
void on_dropball(void) {
    /*uint8_t ac_id = DL_DROPBALL_FOUND_ac_id(dl_buffer);
    if (ac_id != AC_ID)
        return;*/
    uint8_t wp_id = DL_DROPBALL_FOUND_wp_id(dl_buffer);
    struct LlaCoor_i lla;
    struct EnuCoor_i enu;
    lla.lat = INT32_RAD_OF_DEG(DL_DROPBALL_FOUND_lat(dl_buffer));
    lla.lon = INT32_RAD_OF_DEG(DL_DROPBALL_FOUND_lon(dl_buffer));
    /* WP_alt is in cm, lla.alt in mm */
    lla.alt = DL_DROPBALL_FOUND_alt(dl_buffer)*10 - ins_ltp_def.hmsl + ins_ltp_def.lla.alt;
    enu_of_lla_point_i(&enu, &ins_ltp_def, &lla);
    enu.x = POS_BFP_OF_REAL(enu.x)/100;
    enu.y = POS_BFP_OF_REAL(enu.y)/100;
    enu.z = POS_BFP_OF_REAL(enu.z)/100;
    VECT3_ASSIGN(waypoints[wp_id], enu.x, enu.y, enu.z);
    DOWNLINK_SEND_WP_MOVED_ENU(DefaultChannel, DefaultDevice, &wp_id, &enu.x, &enu.y, &enu.z);
}

/* parse for the simulation */
void parse_on_dropball_found(uint8_t wp_id) {
    /* fill struct */
    uint8_t i = 0;
    for (i = 0; i < NB_DROPBALL_WP; i++) {
        if (dropball_waypoints[i].wp == wp_id)
            dropball_waypoints[i].detected = TRUE;
    }
}

/* Send an urgent go to block */
bool_t dropball_goto_block(void){
    uint8_t block_id = 13;
    uint8_t ac_id = 10;

    DOWNLINK_SEND_GOTOBLOCK(DefaultChannel, DefaultDevice, &block_id, &ac_id);
    return FALSE;
}

/* Find shortest route */
bool_t dropball_WpNew(uint8_t wp1, uint8_t wp2, uint8_t wp3, uint8_t wp4){
    /* just copy the waypoints to a vector for easy use */
    uint8_t dropball_new_waypoints[4] = { wp1, wp2, wp3, wp4 };
}

```

```

/* determine the length of the waypoints and set the initial route */
uint8_t i, j; // Used for several loops
uint8_t wp_skip_count = 0; // Amount of waypoints that aren't found or already dropped
uint8_t length = 0; // Amount of waypoints - wp_skip_count
uint8_t swap_temp[4]; // Without current position and end position

/* Find all dropball points where I could go to */
printf("Initial waypoints:\n");
for (i = 0; i < NB_DROPBALL_WP; i++) {
    // Check if we know where a dropball point is
    if ( dropball_waypoints[i].detected == FALSE || dropball_waypoints[i].dropped == TRUE){
        wp_skip_count++;
    }
    else {
        // Set the initial swap temp
        swap_temp[i-wp_skip_count] = dropball_waypoints[i].wp;
        length++;

        printf("%i\n" , swap_temp[i-wp_skip_count]);
    }
}
/* determine length of the vector */
printf("(length: %i, skipped: %i)\r\n", length, wp_skip_count);

/* determine the distances between the route elements */
uint32_t wp_distances[NB_WAYPOINT][NB_WAYPOINT];
for (i = 0; i < length-1; i++) {
    for (j = i+1; j < length; j++) {
        // Calculate the distance
        struct Int32Vect3 pos_diff;
        VECT3_DIFF(pos_diff, waypoints[swap_temp[i]], waypoints[swap_temp[j]]);
        VECT3_ABS(pos_diff, pos_diff);
        wp_distances[swap_temp[i]][swap_temp[j]] = sqrt(pow(pos_diff.x, 2)
+ pow(pos_diff.y,2) + pow(pos_diff.z,2));
        wp_distances[swap_temp[j]][swap_temp[i]] = wp_distances[swap_temp[i]][swap_temp[j]];

        printf("Calculated distance %i<->%i: %i\r\n", swap_temp[i], swap_temp[j],
wp_distances[swap_temp[i]][swap_temp[j]]);
    }
}

/* determine the distances between the current position and the end position */
uint32_t first_distances[NB_WAYPOINT]; // Distances from current position to waypoints from route
uint32_t last_distances[NB_WAYPOINT]; // Distances from waypoints from route to end position
printf("\ndebug\n");
for (i = 0; i < length; i++) {
    struct Int32Vect3 pos_diff;
    printf("\ndebug\n");
    // Distance from current position
    VECT3_DIFF(pos_diff, *stateGetPositionEnu_i(), waypoints[swap_temp[i]]);
    VECT3_ABS(pos_diff, pos_diff);
    first_distances[swap_temp[i]] = sqrt(pow(pos_diff.x, 2) + pow(pos_diff.y,2) + pow(pos_diff.z,2));
    printf("Calculated distance START->%i: %i\r\n", swap_temp[i], first_distances[swap_temp[i]]);

    // Distance to end position
    VECT3_DIFF(pos_diff, waypoints[swap_temp[i]], waypoints[WP_Start]);
    VECT3_ABS(pos_diff, pos_diff);
    last_distances[swap_temp[i]] = sqrt(pow(pos_diff.x, 2) + pow(pos_diff.y,2) + pow(pos_diff.z,2));
    printf("Calculated distance %i->END(WP_Start): %i\r\n", swap_temp[i],
last_distances[swap_temp[i]]);
}

/* initialize matrix with possible routes */
uint16_t wp_routes_fact = factorial(length); // Factorial of the length
uint32_t wp_route_dist[wp_routes_fact]; // The distances of the routes
uint8_t wp_routes[wp_routes_fact][length]; // All the possible routes TODO: Only save min_route
and not min_route_idx
uint32_t min_distance = 4294967295; // The minimum distance found (set to maximum uint32 at start)
uint8_t min_route_idx = 0; // The index of the minimum distance route

/* find all possible routes */
for (i = 0; i < wp_routes_fact; i++) {
    // Save the route and calculate the distance of the route */
    printf("Route: %i\n", i);

    // Add distance from current position to first of route
    wp_route_dist[i] = first_distances[swap_temp[0]];

    // Add the route and update the distance from the route
    for (j = 0; j < length; j++) {
        wp_routes[i][j] = swap_temp[j];
        // Because distances are calculated between two points
        if (j != length-1)
            wp_route_dist[i] += wp_distances[swap_temp[j]][swap_temp[j+1]];
        printf("%i\n", swap_temp[j]);
    }

    // Add distance from the last of the route to the end point
    wp_route_dist[i] += last_distances[swap_temp[length-1]];
    printf("(distance: %i)\r\n", wp_route_dist[i]);
}

```

```

// When the distance is less than the minimum route
if (wp_route_dist[i] < min_distance) {
    min_route_idx = i;
    min_distance = wp_route_dist[i];
}

/* Calculate the next route */
next_lex_perm(swap_temp, length);
}

/* move waypoints NEXT1, NEXT2, NEXT3 and NEXT4 to the new locations */
printf("Shortest route: \n");
for (i=0; i < length; i++) {
    nav_move_waypoint(dropball_new_waypoints[i], &waypoints[wp_routes[min_route_idx][i]]);
    printf("%d\n", wp_routes[min_route_idx][i]);
}
printf("(distance: %i)\n", min_distance);

return FALSE;
}

```

File dropball.xml

```

<!DOCTYPE module SYSTEM "module.dtd">

<module name="dropball" dir="multi">
  <doc>
    <description>Dropball</description>
  </doc>
  <header>
    <file name="dropball.h"/>
  </header>
  <datalink message="DROPBALL_FOUND" fun="on_dropball()"/>
  <makefile>
    <file name="dropball.c"/>
  </makefile>
</module>

```

I QR-Code Module

\textbf{File Logger.xml}

```

<!DOCTYPE module SYSTEM "module.dtd">

<module name="loggers">
  <doc>
    <description>Connect to external High-Speed SD-logger via SPI</description>
  </doc>
  <header>
    <file name="high_speed_logger_spi_link.h"/>
  </header>
  <init fun="high_speed_logger_spi_link_init()"/>
  <periodic fun="high_speed_logger_spi_link_periodic()" autorun="TRUE"/>
  <makefile>
    <define name="SPI_MASTER" value="1" />
    <define name="USE_SPI1" value="1" />
    <define name="HIGH_SPEED_LOGGER_SPI_LINK_DEVICE" value="spi1" />
    <define name="USE_SPI_SLAVES" value="1" />
    <define name="HIGH_SPEED_LOGGER_SPI_LINK_SLAVE_NUMBER" value="SPI_SLAVE5" />
    <file name="high_speed_logger_spi_link.c"/>
  </makefile>
</module>

```

\textbf{File high_speed_logger_spi_link.h} (adapted from Christophe de Wagter)

```

#ifndef HIGH_SPEED_LOGGER_SPI_LINK_H
#define HIGH_SPEED_LOGGER_SPI_LINK_H

#include "std.h"

extern void high_speed_logger_spi_link_init(void);
extern void high_speed_logger_spi_link_periodic(void);

static int32_t dataFromGumstix.id;
static int32_t dataFromGumstix.lat;
static int32_t dataFromGumstix.lon;

#define PACKED __attribute__((__packed__))

// struct: data of the position of the MAV
struct PACKED high_speed_logger_spi_link_data_tx {
    int32_t gps_mav_lo; // 1
    int32_t gps_mav_la;
    int32_t baro_mav_al;
    // int32_t rotation angle // 4

```

```

};
// struct: data of the position of the QR
struct PACKED high_speed_logger_spi_link_data_rx {
    int32_t id // 1
    int32_t gps_qr_lo;
    int32_t gps_qr_la;
    // int32_t rotation angle // 4
};
#endif /* HIGH_SPEED_LOGGER_SPI_LINK_H_ */

\textbf{File high\_speed\_logger\_spi\_link.c} (adapted from Christophe de Wagter)

#include "high_speed_logger_spi_link.h"

#include "subsystems/imu.h"
#include "mcu_periph/spi.h"

#include "state.h"

#include "pprz_geodetic.int.h"

#include "ins_int.h"

struct high_speed_logger_spi_link_data high_speed_logger_spi_link_data;
struct spi_transaction high_speed_logger_spi_link_transaction;

static volatile bool_t high_speed_logger_spi_link_ready = TRUE;

static void high_speed_logger_spi_link_trans_cb( struct spi_transaction *trans );

uint16_t previous_id = 0;

void high_speed_logger_spi_link_init(void) {
    high_speed_logger_spi_link_data.id = 0;

    high_speed_logger_spi_link_transaction.select = SPISelectUnselect;
    high_speed_logger_spi_link_transaction.cpol = SPICpolIdleHigh;
    high_speed_logger_spi_link_transaction.cpha = SPICphaEdge2;
    high_speed_logger_spi_link_transaction.dss = SPIDss8bit;
    high_speed_logger_spi_link_transaction.bitorder = SPIMSBFirst;
    high_speed_logger_spi_link_transaction.cddiv = SPIDiv64;
    high_speed_logger_spi_link_transaction.slave_idx = HIGH_SPEED_LOGGER_SPI_LINK_SLAVE_NUMBER;
    high_speed_logger_spi_link_transaction.output_length = sizeof(high_speed_logger_spi_link_data_tx);
    high_speed_logger_spi_link_transaction.output_buf = (uint8_t*) &high_speed_logger_spi_link_data_tx;
    high_speed_logger_spi_link_transaction.input_length = sizeof(high_speed_logger_spi_link_data_rx);
    high_speed_logger_spi_link_transaction.input_buf = (uint8_t*) &high_speed_logger_spi_link_data_rx;
    high_speed_logger_spi_link_transaction.after_cb = high_speed_logger_spi_link_trans_cb;
}

stateGetPositionLla_i()

void high_speed_logger_spi_link_periodic(void)
{
    if (high_speed_logger_spi_link_ready)
    {
        high_speed_logger_spi_link_ready = FALSE;
        high_speed_logger_spi_link_data_tx.gps_mav_la = state.lla_pos_i.lat;
        high_speed_logger_spi_link_data_tx.gps_mav_lo = state.lla_pos_i.lon;
        high_speed_logger_spi_link_data_tx.baro_mav_al = ins_ltp_pos.z;
        // high_speed_logger_spi_link_data.rotation_angle = state.;

        spi_submit(&(HIGH_SPEED_LOGGER_SPI_LINK_DEVICE), &high_speed_logger_spi_link_transaction);

        high_speed_logger_spi_link_data_rx.id = dataFromGumstix.id;
        high_speed_logger_spi_link_data_rx.gps_qr_la = dataFromGumstix.lat;
        high_speed_logger_spi_link_data_rx.gps_qr_lo = dataFromGumstix.lon;
    }

    if (previous_id < HannWoeis module_i.id)
    {
        previous_id = HannWoeis module_i.id
    }
}

static void high_speed_logger_spi_link_trans_cb( struct spi_transaction *trans __attribute__((unused)) ) {
    high_speed_logger_spi_link_ready = TRUE;
}

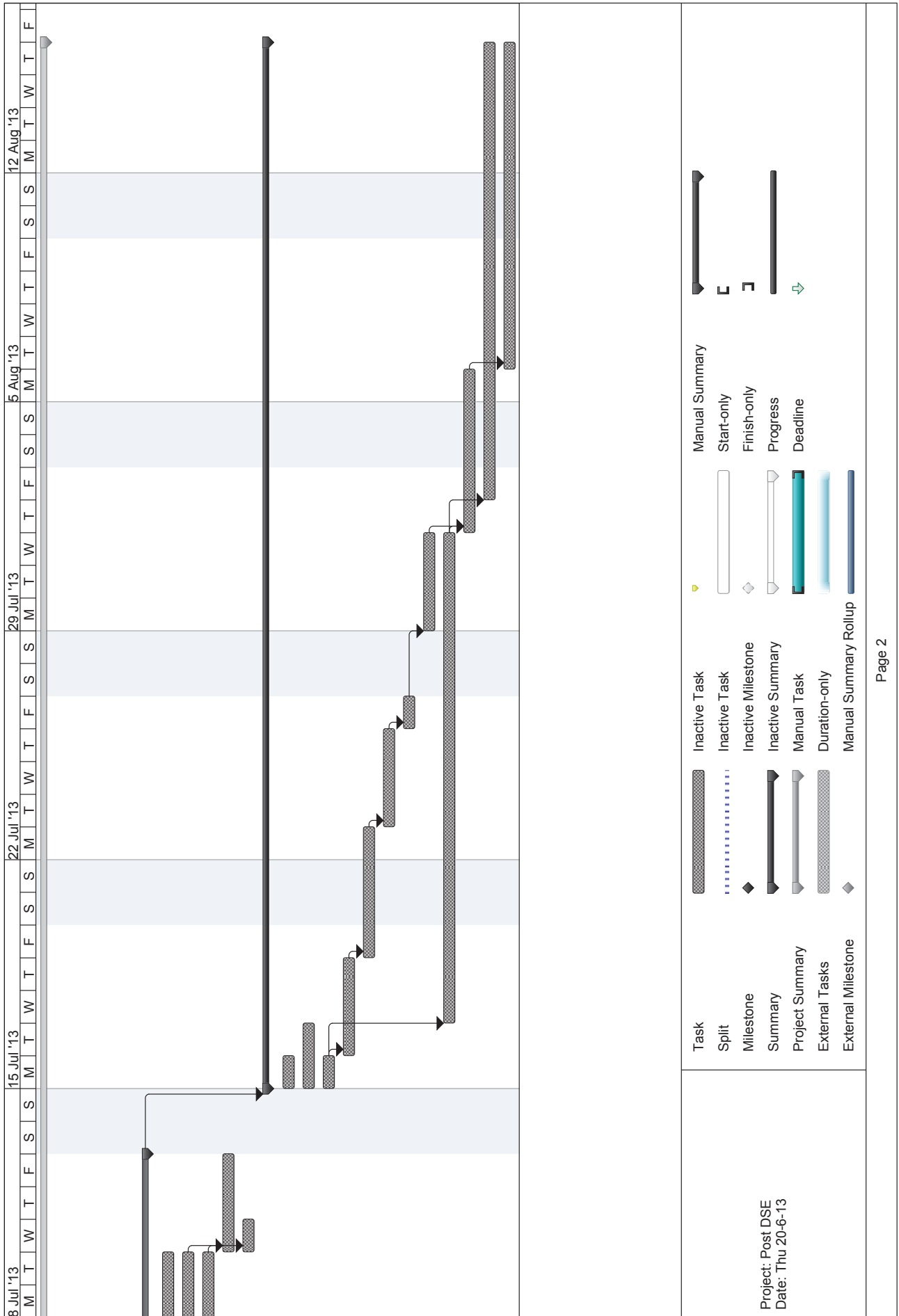
```


K Gant Chart

ID	WBS	Task Name	Work	Duration	Start	Finish	Predecessors
0		0 Post DSE	1.037,2 ...	34 days	Mon 1-7-13	Thu 15-8-13	
1	1	1 Software writing	87,2 hrs	4 days	Mon 1-7-13	Thu 4-7-13	
2	1.1	QR-Code	4 hrs	1 day	Mon 1-7-13	Mon 1-7-13	
3	1.2	Ball Drop System	20 hrs	4 days	Mon 1-7-13	Thu 4-7-13	
4	1.3	Airframe File	60 hrs	4 days	Mon 1-7-13	Thu 4-7-13	
5	2	2 Building	162 hrs	6 days	Fri 5-7-13	Fri 12-7-13	
6	2.1	Airframe	80 hrs	3 days	Fri 5-7-13	Tue 9-7-13	
7	2.2	QR-Code System	24 hrs	3 days	Fri 5-7-13	Tue 9-7-13	
8	2.3	Ball Drop System	24 hrs	3 days	Fri 5-7-13	Tue 9-7-13	
9	2.4	Similar competition elements	24 hrs	3 days	Wed 10-7-13	Fri 12-7-13	
10	2.5	Order parts	10 hrs	1 day	Wed 10-7-13	Wed 10-7-13	
11	3	3 Validation	788 hrs	24 days	Mon 15-7-13	Thu 15-8-13	
12	3.1	Testing QR-code Recognition	4 hrs	1 day	Mon 15-7-13	Mon 15-7-13	
13	3.2	Testing Communication	16 hrs	2 days	Mon 15-7-13	Tue 16-7-13	
14	3.3	GPS Accuracy	8 hrs	1 day	Mon 15-7-13	Mon 15-7-13	
15	3.4	Testing Hover	50 hrs	3 days	Tue 16-7-13	Thu 18-7-13	
16	3.5	Test Take-Off	20 hrs	2 days	Fri 19-7-13	Mon 22-7-13	
17	3.6	Test Landing	40 hrs	3 days	Tue 23-7-13	Thu 25-7-13	
18	3.7	Testing Cruise	20 hrs	1 day	Fri 26-7-13	Fri 26-7-13	
19	3.8	Testing Transition	100 hrs	3 days	Mon 29-7-13	Wed 31-7-13	
20	3.9	Further developing software/system	150 hrs	11 days	Wed 17-7-13	Wed 31-7-13	
21	3.10	Testing the missions separate	80 hrs	3 days	Thu 1-8-13	Mon 5-8-13	20;19
22	3.11	Adjusting software/strategy	200 hrs	10 days	Fri 2-8-13	Thu 15-8-13	20
23	3.12	Test the entire mission	100 hrs	8 days	Tue 6-8-13	Thu 15-8-13	21

Project: Post DSE
Date: Thu 20-6-13

Task		Inactive Task		Manual Summary	
Split		Inactive Task		Start-only	
Milestone		Inactive Milestone		Finish-only	
Summary		Inactive Summary		Progress	
Project Summary		Manual Task		Deadline	
External Tasks		Duration-only			
External Milestone		Manual Summary Rollup			



L Cost Breakdown Structure

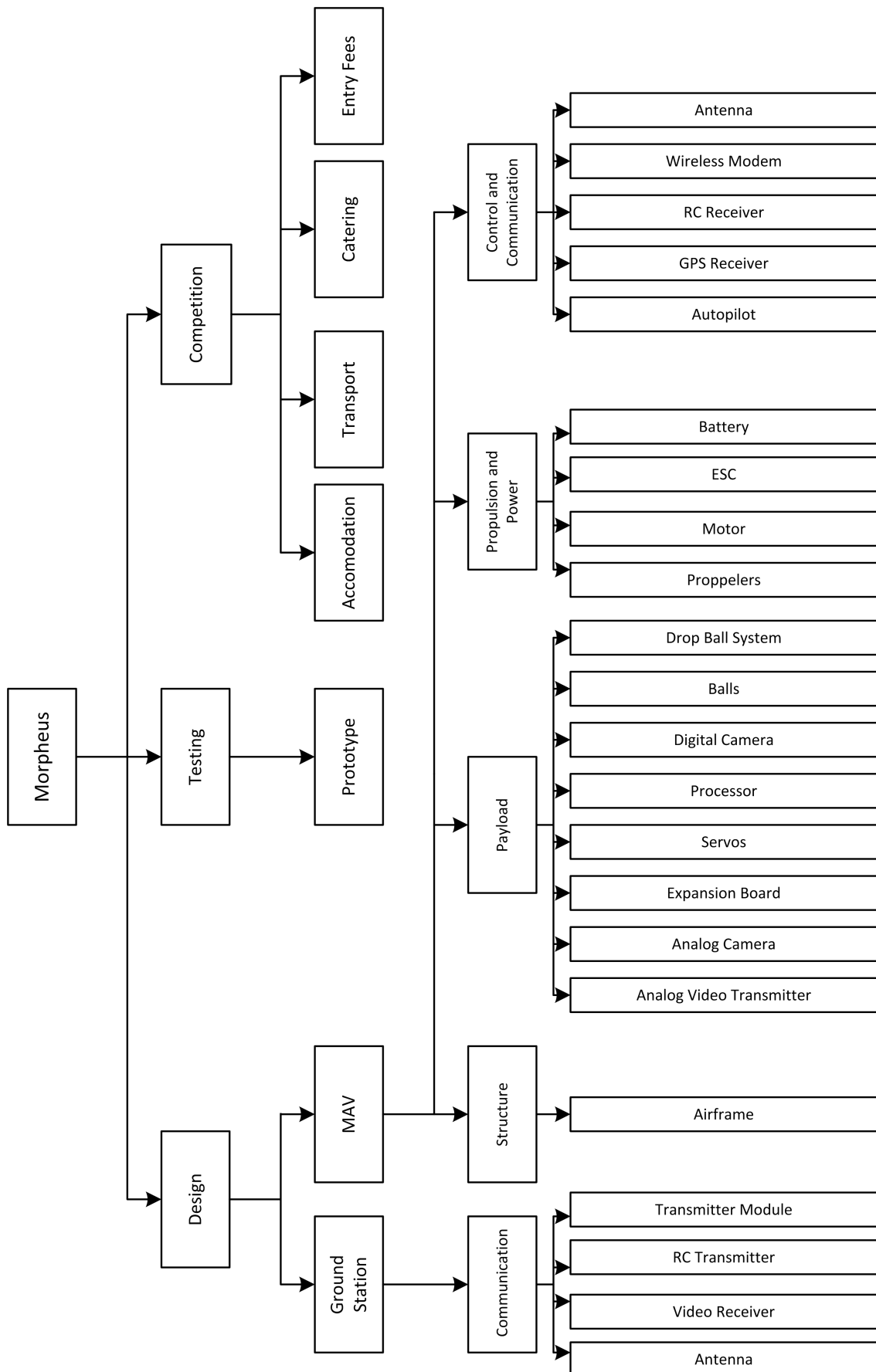


Figure A.5: Cost Breakdown Structure

